Università degli Studi di Genova

Corso di Dottorato in Neuroscienze

Curriculum Neuroscienze e Neurotecnologie

Coordinatore Prof. Angelo Schenone

Ciclo XXXI

Neuromodulated plasticity of the connectivity between the Prefrontal Cortex and the noradrenergic Locus Coeruleus

Author: Andrea Locarno

Supervisor: Raffaella Tonini

ISTITUTO ITALIANO DI TECNOLOGIA

UNIVERSITÀ DEGLI STUDI DI GENOVA

“In the South Seas there is a cargo cult of people. During the war they saw airplanes land with lots of good materials, and they want the same thing to happen now. So they've arranged to imitate things like runways, to put fires along the sides of the runways, to make a wooden hut for a man to sit in, with two wooden pieces on his head like headphones and bars of bamboo sticking out like antennas—he's the controller—and they wait for the airplanes to land. They're doing everything right. The form is perfect. It looks exactly the way it looked before. But it doesn't work. No airplanes land. So I call these things cargo cult science, because they follow all the apparent precepts and forms of scientific investigation, but they're missing something essential, because the planes don't land.”

Richard Feynman

Index

Abstract

Incentive stimuli and environmental stressors are encoded at the level of the prefrontal cortex (PFC) circuits, which send their glutamatergic excitatory projections to several neuromodulatory regions, including the Locus Coeruleus (LC), the major source of noradrenaline (NA) for the entire forebrain. Despite the potential implications for NA-mediated regulation of action control and for the etiology of stress-related neuropsychiatric conditions, it remains to be established how LC neuronal activity is shaped by impinging PFC inputs (PFC→LC) to affect behavior, and whether these inputs are modulated by in-vivo experience.

By combining neurophysiological and optogenetic approaches together with behavioral paradigms in mice, we found that PFC →LC stimulation supports learning and retrieval of contextual memory associations. Consistent with the occurrence of plasticity processes at LC synapses, long-lasting modulation of PFC→LC projections relies on the endocannabinoid (eCB)-mediated signaling capacity, which is dynamically shaped by context adaptations and stress salience experiences. We also found that eCB-plasticity at PFC → LC synapses is regulated during the adolescence to adulthood transition.

In summary, our results not only dissect the behavioral implications of neuromodulated plasticity at PFC inputs to the LC, but also unveil divergent synaptic substrates during postnatal development, which might be relevant to explain some of the different noradrenergic-mediated response in adolescents and adults.

Introduction

The Locus Coeruleus (LC): organization and function

The Locus Coeruleus (LC) is a compact cluster of noradrenergic neurons situated in the pontine region of the brainstem (Amaral and Sinnamon, 1977) (**Figure 1**). In the adult rat brain, the LC contains ≈3000 neurons (Descarries and Saucier, 1972; Aston-Jones, 2004) out of total ≈330,000,000 neurons (Herculano-Houzel and Lent, 2005), and roughly half of the overall number of central noradrenergic neurons; the remaining central noradrenergic neurons are organized in compact nuclei (A1-A7; A stands for Adrenergic (Dahlstroem and Fuxe, 1964)) located in the brainstem. Through their branched axons, LC noradrenergic cells (also called norepinephrine (NE)-LC neurons) project extensively throughout the entire neuroaxis (**Figure 2**). The diffuse and ubiquitous projections of LC have been identified since 1971 (Ungerstedt, 1971). In the light of their widespread projections and postulated synchronous activity, the main physiological role ascribed to LC-NE neurons has been the broad control of arousal levels and brain states, including sleep-wake transitions (Berridge and Waterhouse, 2003; Carter *et al.*, 2010; Lee and Dan, 2012; Sara and Bouret, 2012). It is now well established that LC projections, through NE release, provide fine control of various brain regions, thereby modulating diverse brain functions: noradrenergic action in cortex and thalamus strongly impacts arousal and behavioral state (Berridge and Waterhouse, 2003); LC-NE afferents to thalamic nuclei and sensory cortices provide gating and tuning of sensory processing (Bouret & Sara, 2002; Devilbiss & Waterhouse, 2010; Eckmeier & Shea, 2014; Rodenkirch et al., 2019); LC projections to the hippocampus regulate synaptic plasticity (Dahl and Sarvey, 1989; Maity *et al.*, 2015; Kempadoo *et al.*, 2016); LC projections to the amygdala play an important role in memory consolidation (Schiff *et al.*, 2017; Uematsu *et al.*, 2017); in the frontal cortex, NE is essential for working memory and attention (Rossetti and Carboni, 2005; Hvoslef-Eide *et al.*, 2015). The LC also projects to midbrain neuromodulatory systems such as the Dorsal Raphe Nucleus (DRN) (Kim *et al.*, 2004), the dopaminergic ventral tegmental area (VTA) and substantia nigra pars compacta (SNc) (Mejías-Aponte, Drouin and Aston-Jones, 2009), and to cholinergic nuclei of the brainstem (lateral dorsal tegmental nucleus,

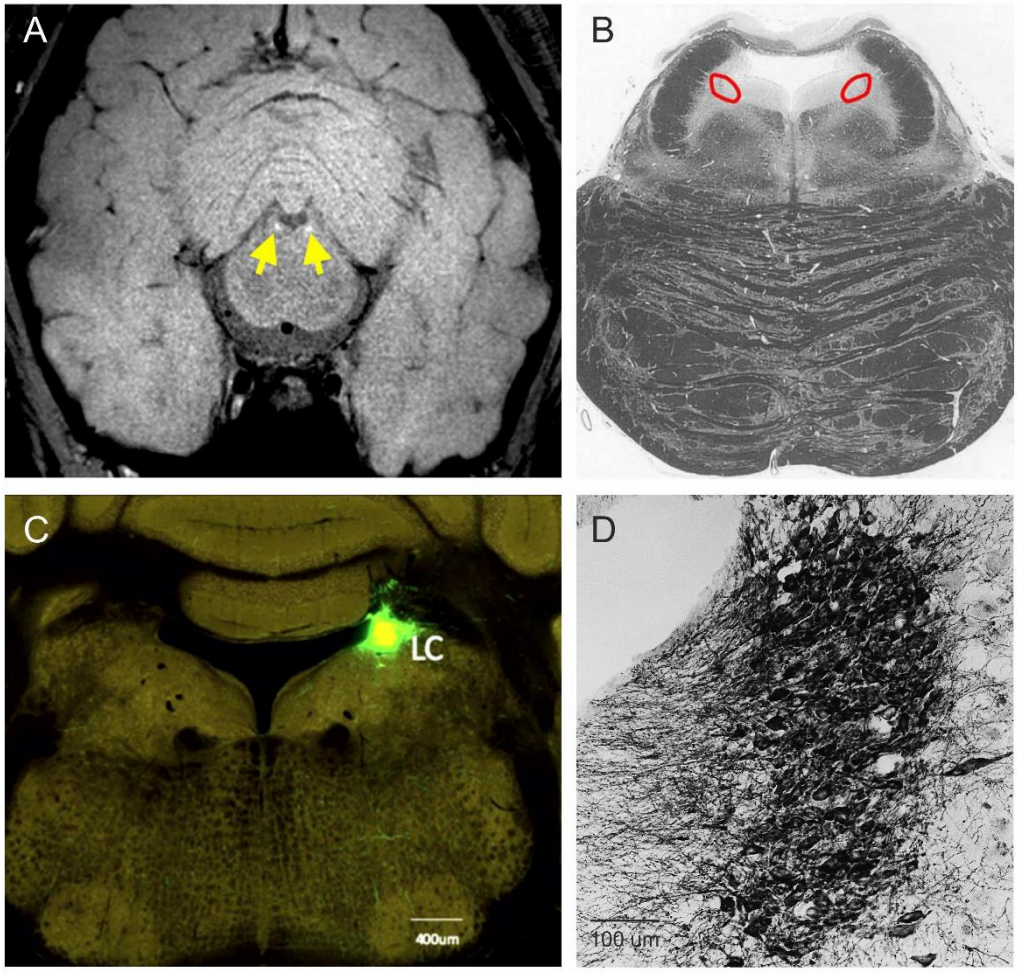

Figure 1 Location of Locus Coeruleus in the brainstem of (A, B Human and (C, D) Rodent brain. (A) Nuclear magnetic resonance image showing the loci coerulei. The loci coerulei are shown by the white areas close to the 4th ventricle (yellow arrows). Neuromelanin-related signal has been used to visualize the LC. (B) Horizontal section of the upper pons. The loci coerulei are circled in red. (C) Expression of fluorophore in the right LC. A Cre-dependent recombinant adeno-associated virus (AAV) expressing a fluorophore was injected into the mouse LC as an anterograde tracer. The mice were from a Cre-driver line in which Cre recombinase is under the tyrosine hydroxylase (TH) promoter (Allen Brain Atlas Connectivity Project Experiment 511971714, TH-Cre_Fl172 mouse). (D) Bright-field photomicrographs of a rat LC section. The section was processed for dopamine β-hydroxylase (DBH) immunohistochemistry to visualize noradrenergic neurons. (A, B) Modified from Szabadi et al. (2013). (C) Modified from Chandler et al. (2019). (D) Modified from Aston-Jones (2004).

pedunculopontine nucleus [LDT/PPN]) (Semba and Fibiger, 1992; Khanday *et al.*, 2016). The role of LC projections towards these neuromodulatory nuclei remains poorly investigated.

Even though the LC is not the only noradrenergic nucleus of the brain, it provides the sole source of NE for the neocortex, hippocampus, cerebellum and most of the thalamus; this highlights its importance in the modulation of higher-order cognitive functions (Sara and Bouret, 2012). Accordingly, dysfunctions in LC-NE system have been observed in neurodegenerative disorders and psychiatric conditions characterized by cognitive deficits.

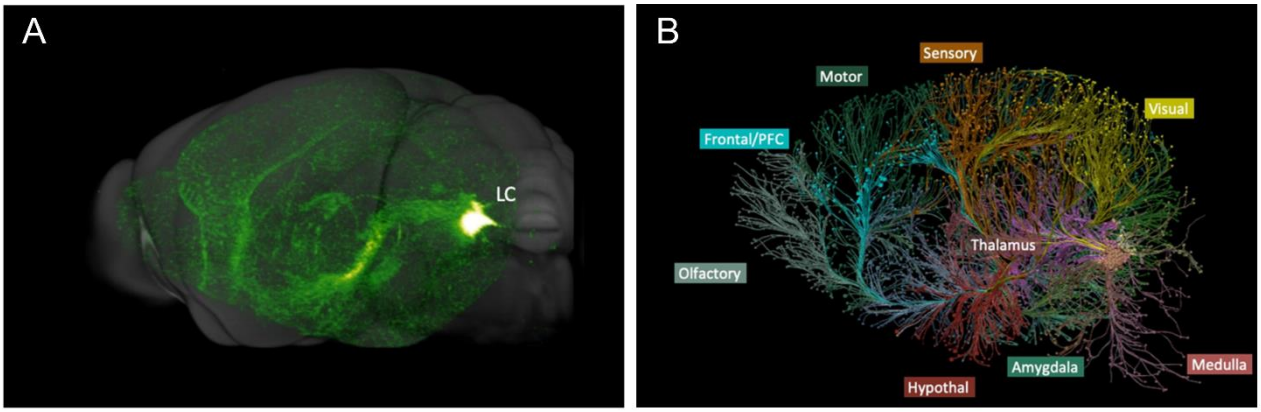

Figure 2 (A) Cre-dependent recombinant adeno-associated virus (AAV) expressing eYFP was injected into the mouse LC as an anterograde tracer. The mice were from a Cre-driver line in which Cre recombinase is under the tyrosine hydroxylase (TH) promoter (Allen Brain Atlas Connectivity Project Experiment 511971714, TH-Cre_Fl172 mouse). After 2-photon serial tomography, the LC axonal projections were reconstructed in 3D. (B) Assignation of projection axons by target region highlights the widespread projection pattern of LC neurons. Modified from Chandler et al. (2019).

LC neuronal degeneration has been observed in both Alzheimer's and Parkinson's disease as well as in other forms of neurodegeneration (for reviews: (Vermeiren and De Deyn, 2017; Weinshenker, 2018). In Alzheimer's disease, the LC shows intraneuronal fibrillary tangles of Tau protein, a hallmark of the pathology, alongside with LC-NE neuronal cell loss (Mann and Yates, 1983). Most importantly, decreased LC neuronal density has been demonstrated to correlate with cognitive decline (Wilson *et al.*, 2013). LC neurons degeneration plays an important role also in the progression of Parkinson's disease. Whilst degeneration of substantia nigra pars compacta (SNc) is the most studied neuropathological trait of the disease, post-mortem studies in human patients demonstrated the presence of α-synuclein aggregates (e.g. Lewy bodies) in LC neurons (Braak *et al.*, 2003), which is associated with a loss of noradrenergic cells (Zarow *et al.*, 2003). Interestingly, degeneration of NE-neurons has been shown to precede SNc dopaminergic cell death, suggesting that LC degeneration is involved in the initial stages of the disease progression (Braak *et al.*, 2003). Collectively, these observations indicate that LC-NE neurons can degenerate both in Parkinson and Alzheimer's disease (Zarow *et al.*, 2003), and this neurodegeneration might lead to depression and vigilance loss associated with the pathologies (Solopchuk *et al.*, 2018). Nevertheless, the causal link between cell loss in LC and specific pathological symptoms has not been fully established yet.

In psychiatric conditions, the LC-NE system might be deregulated, rather than experience cell degeneration. Indeed, many studies point at a hyperactivation of the noradrenergic system in patients with Post-traumatic stress disorder (PTSD) (reviewed in Yamamoto, Shinba and Yoshii, 2014; Hendrickson and Raskind, 2016). The supposedly increased LC activity can induce hyperarousal states, especially following mildly stressful stimuli that strongly characterize and

define this psychiatric disease. The hyperarousal state is correlated with high NE levels in the plasma and in the cerebrospinal fluid (CSF), which are elevated in patients suffering from PTSD. Moreover, the concentration of NE has been shown to positively correlate with the severity of PTSD symptoms (Geracioti *et al.*, 2001, 2008), while adrenergic antagonists are able to ameliorate the disease symptoms (Berardis *et al.*, 2015; Remy Simon and Rousseau, 2017).

In summary, the LC is a small brain structure that can profoundly modulate different aspects of animal behavior. Emerging evidence indicates that the key behavioral role played by the LC is dependent on its connectivity profile and functional properties of its neurons.

Cytoarchitecture and molecular organization

In the rodent brain, the LC nucleus is easily recognizable in stained sections as a densely packed group of cells lying on the ventrolateral side of the 4th ventricle, a region known as the rhomboencephalic tegmentum (Aston-Jones, 2004) (**Figure 1 C-D**). The LC is virtually only composed of noradrenergic neurons, as indicated by immunolabeling for Tyrosine Hydroxylases (TH) or for Dopamine Beta Hydroxylases (DBH), which are two key enzymes for the biosynthesis of Norepinephrine (NE) (Axelrod, 1971). Nevertheless, few findings demonstrated the existence of two pools of inhibitory GABAergic interneurons laying within or in close proximity to the LC. One group of interneurons is intermingled within NE neurons in the LC itself (Ijima and Ohtomo, 1988; Breton-Provencher and Sur, 2019). The second is a large reservoir of grouped inhibitory neurons, called dorsomedial(dm)LC (Jin *et al.*, 2016), which is laying on the medial side of the LC in the mouse brain. These GABAergic cells are morphologically distinguishable from the noradrenergic neurons by their small circular cell bodies. Moreover, LC GABAergic neurons showed electrophysiological characteristics distinguishable from those of LC-NE neurons: high input resistance (≈ 500 MΩ), small membrane capacitance (≈ 20 pF), a prominent sag in response to cell hyperpolarization, and high firing rate (≈ 10 Hz) (Jin *et al.*, 2016). These interneurons could regulate LC-NE neurons activity through feedback and feedforward inhibitory mechanisms (Jin *et al.*, 2016; Breton-Provencher and Sur, 2019).

Using the Golgi staining method, LC-NE neurons have been classified based on their morphology (**Figure 3 A**). Work conducted by different independent groups between the end of the seventies and the beginning of the eighties showed the existence of morphologically distinguishable LC-NE cells: large multipolar neurons (≈ 35µm), medium-sized elongated neurons (≈ 20µm) (Swanson and Hartman, 1975) and ovoid-shaped cells (Cintra, Kemper and Morgane, 1982). The different

shape of these noradrenergic neurons is linked to the orientation of their dendrites; small fusiform cells extend their dendrites along the sagittal and horizontal plane, while multipolar neurons extend their arborization more towards the frontal plane (Sievers *et al.*, 1981).

In addition to the morphological differences, LC-NE neurons are neurochemically diverse regarding their neuropeptide content (Schwarz and Luo, 2015) (**Figure 3 C**). 80% of LC-NE neurons produce the Galanin (Gal) peptide. Gal regulates different behavioral aspects: sleep/wake cycle, nociception, feeding, and parental behavior (Crawley, 1999; Wu *et al.*, 2014; Li *et al.*, 2017; Kroeger *et al.*, 2018). Neurons positive for both NE and Gal are mainly located in the dorsal and central parts of the LC. Another neuropeptide synthesized in a LC subpopulation of cells is the neuropeptide Y. NPY is produced in ≈ 20% of LC cells, which are preferentially distributed in the dorsal part of the LC (for Gal and NPY neurons in the LC see Holets, Hokfelt and Rokaeus, 1988). NPY is a stress-relieving, anxiolytic, orexinergic peptide (Reichmann and Holzer, 2016; Comeras, Herzog and Tasan, 2019). The co-release role of NE with these two different peptides and the distribution of axon-terminals in target brain region positive for NE and Gal or NPY has not been thoroughly investigated so far.

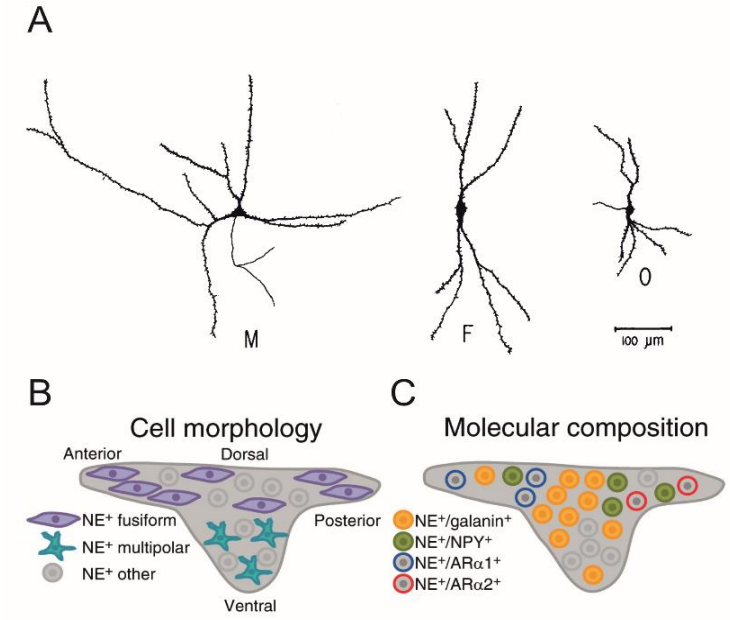

Figure 3 (A) Camera lucida reconstructions of the 3 cell types in the Locus Coeruleus (LC) stained with the Golgi method: multipolar M; fusiform F; ovoid O neurons. (B) Schematic of the biased location of LC neurons along the dorso-ventral axis based on their morphology. (C) Schematic representing the LC molecular composition; although all LC cells produce Norepinephrine (NE), subsets of neurons co-release neuropeptides such as NPY and galanin (Gal). Moreover, subsets of LC neurons express neurotransmitter receptors differentially such as α-adrenergic receptors. (A) Modified from Cintra, Kemper and Morgane, 1982. (B-C) Modified from Schwarz and Luo, 2015.

Another class of molecules that are differentially expressed at the LC level are the adrenergic receptors (AR) (Schwarz and Luo, 2015) (**Figure 3 C**). NE autoreceptors expressed in LC-NE neurons,

for instance, show a rostrocaudal gradient of distribution within the LC. The α2 G-protein coupled receptor (ARα2) is the most abundantly expressed adrenergic receptor in the LC (Young and Kuhar, 1980). α2 receptors are coupled to $G_{i/o}$-protein system, thus their activation inhibits cAMP production, leading to an autoinhibition of LC-NE neurons. α2 receptor distribution follows a rostrocaudal gradient of expression within the LC (Chamba *et al.*, 1991), with higher caudal expression. On the other hand, α1 receptors (ARα1) are coupled to G_q signaling cascade. G_q is a modulatory G protein and induces Ca^{2+} release from the stores. Opposite to α2, α1 receptor is most abundant in the anterior part of the LC (Chamba *et al.*, 1991). This distribution pattern of autoreceptors raises the possibility that NE released from the LC itself, or from other adrenergic nuclei, can induce different responses in different LC cells based on their rostrocaudal position, with stronger autoinhibition of the most caudal part and strong anterior activation. Another example of receptors that show patterned expression within the LC is the ionotropic Nicotinic acetylcholine receptor (nAChRs). Single-cell RT-PCR experiments revealed differential expression of nAChRs in multipolar large cells compared to the medium-sized fusiform ones. The large cells showed α6 and β3 and often α4 mRNAs whereas the elongated fusiform cells showed α3 and β4 mRNAs (but also α6, β3, α5 and α4 mRNAs, although at a lower level). This differential nAChRs mRNAs expression resulted in different sensitivity to nAChRs agonists in large multipolar compared to the smaller fusiform cells, with larger currents observed in the latter (Léna *et al.*, 1999).

LC-NE neurons express many other neurotransmitters and neuropeptide receptors such as GluR, GABA receptors, CRF receptors, orexin receptors, opioid receptors, and endocannabinoid receptors (Luque, Malherbe and Richards, 1994, 1995; Marcus *et al.*, 2001; Reyes *et al.*, 2006; Scavone and Van Bockstaele, 2009; Scavone, Mackie and Van Bockstaele, 2010), but it is not known if they are expressed differentially within the LC.

In light of the aforementioned evidence, the Locus Coeruleus should not be considered only as a homogeneous group of NE producing neurons as initially believed; their morphological and molecular heterogeneity suggests that within the LC itself there are clusters of cells possibly involved in different functions. This hypothesis, however, has not been demonstrated yet (Chandler *et al.*, 2019).

Adrenergic receptors and signaling in the brain

As mentioned in the previous paragraph, the LC is nowadays considered as a complex and differentiated neuromodulatory nucleus. However, the effects of NE on target brain regions

depend largely on the receptor subtype activated, the downstream signaling cascade engaged, and the cell type expressing the NE-receptor. Therefore hereafter, I will briefly discuss Adrenergic receptors, their expression profile in the brain and their functions.

The adrenoceptors are part of the large family of seven transmembrane domain receptors or G-protein coupled receptors. The nine adrenergic receptors identified have been divided into three main groups: α1 adrenergic receptors, α2 adrenergic receptors, and β adrenergic receptors (reviewed in Strosberg, 1993; Insel, 1996) (**Figure 4**).

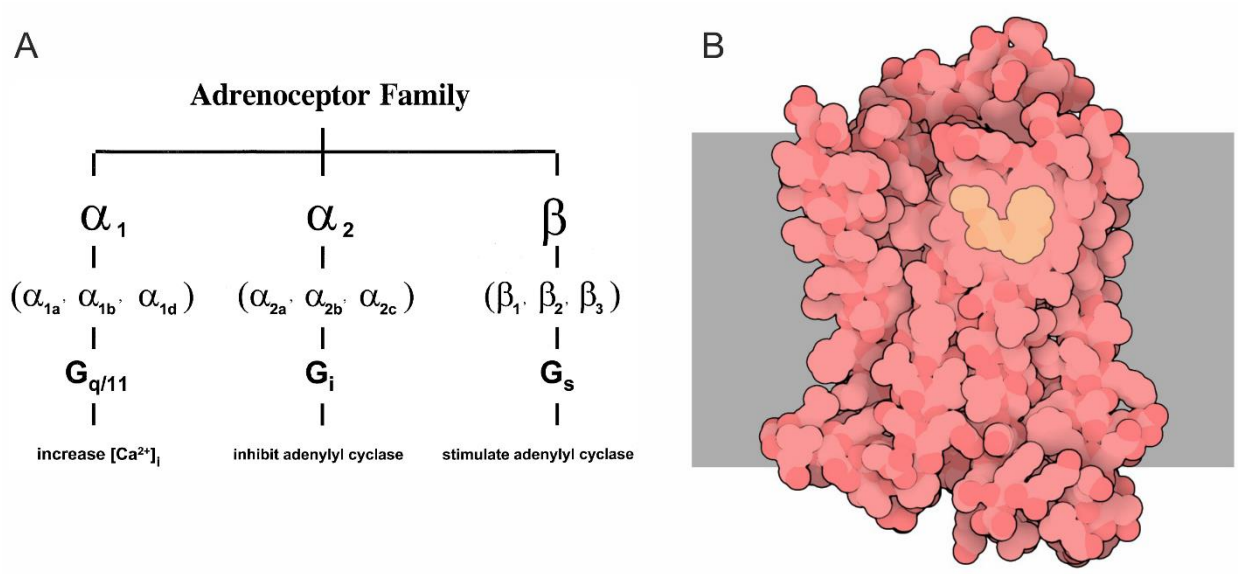

Figure 4 (A) The adrenoceptor family subdivision. The division in subfamilies is based on pharmacological properties and structural homology of the G-protein coupled receptors (GPCR). Some of the adrenoreceptors shown here can be also coupled to different G proteins, for instance, β2 and β3 can be bound to $G_{i/o}$ signaling cascade. (B) β2 adrenoreceptor structure in the presence of the β antagonist carazolol (yellow) bound on its extracellular site. The membrane is shown as a gray stripe. (A) Modified from (Zhong and Minneman, 1999. (B) Adapted from "Protein Data Bank: 2rh1".

α1 adrenergic receptors

Three different α1 adrenoreceptors proteins have been cloned, namely: α1A, α1B, α1D (Zhong and Minneman, 1999). The three α1 are encoded by three different genes and they show a differential distribution in the brain (Scofield, Deupree and Bylund, 2002). In-situ hybridization studies (Day *et al.*, 1997) showed that:

-α1A mRNA is mainly present in the olfactory bulbs, many hypothalamic nuclei, and the brainstem.

-α1B is expressed in the pineal gland, in the thalamus, in the amygdala, and in the raphe nuclei.

-α1D mRNA levels are higher in the olfactory bulb, cortical layers II–V, the hippocampus, the reticular thalamic nucleus, the amygdala and motor nuclei of the brainstem.

All three α1 receptors subtypes are known to be linked to the modulatory $G_{q/11}$ protein that activates phospholipase C (PLC) and phosphatidylinositol signaling, resulting in activation of protein kinase C (PKC) on one side and in the 1,4,5 inositol-triphosphate followed by Ca^{2+} release from the stores on the other (Wu *et al.*, 1992).

The work on recombinant systems showed that the three different α1 receptors have different subcellular localizations and regulatory properties. α1B is mainly localized at the plasma membrane level and it undergoes rapid desensitization and internalization following adrenergic agonist binding. α1A is localized both on plasma membranes and intracellularly and shows a slower internalization rate. Finally, α1D is mainly present on intracellular vesicles, this localization might be due to its continuous internalization (Chalothorn *et al.*, 2002). Since most available drugs are not receptor subtype-specific it is difficult to determine which subtype is involved in modulating a specific behavior *in-vivo*.

More generally, α1 receptors are involved in some symptoms of depression (Stone *et al.*, 2007; Nalepa *et al.*, 2013). It has been shown that antidepressant drugs and treatments increase the α1 receptor mRNA level and density, nonetheless, the mechanism by which α1 receptors mediate antidepressant effects is poorly understood (Deupree, Reed and Bylund, 2007). α1 are also involved in learning and memory although their role is controversial: some studies have shown that their stimulation impairs spatial working memory (Birnbaum et al., 1999), while others point at a facilitating action of α1 in Long term potentiation (LTP) and long-term depression (LTD) induction in the hippocampus (Doze *et al.*, 2011; Dyer-reaves *et al.*, 2019; Scheiderer *et al.*, 2019). In these studies long-term stimulation of α1 improved memory in Morris and T-maze tests, while α1-KO animals displayed worsened cognitive abilities (Spreng, Cotecchia and Schenk, 2001; Doze *et al.*, 2011).

α2 adrenergic receptors

Three different genes have been identified which codify for different α2 receptors: α2A, α2B, α2C (Bylund *et al.*, 1994). They are known to be linked to an inhibitory $G_{i/o}$ signaling cascade, therefore the activation of α2 generally leads to the inhibition of the adenylyl cyclase (Kurose *et al.*, 1991; Remaury *et al.*, 1993). The mRNA of all three subtypes is present at the brain level (Scheinin *et al.*, 1994).

- α2A is widely distributed in the cerebral cortex, LC, amygdala, paraventricular nucleus, nucleus tractus solitarii, reticular formation.

- α2B mRNA has been found almost exclusively in the thalamus.

- α2C is found in the olfactory bulb, cerebral and cerebellar neocortex, hippocampus and basal ganglia.

Amongst α2 adrenergic receptors, α2A and α2C were identified as the main auto-receptors that negatively regulate via a feedback inhibition the release of NE (Starke, 1987; Hein, Altman and Kobilka, 1999; Bücheler, Hadamek and Hein, 2002). Although the main function of the α2 adrenoreceptor was assigned to its presynaptic location, it has been shown that these receptors can also display a postsynaptic localization (Ricardo, 1981). α2 adrenoreceptors are also suited to control the release of other neurotransmitters in addition to NE, it has been shown that these receptors can dampen dopamine (Bücheler, Hadamek and Hein, 2002) and serotonin release acting presynaptically (Scheibner *et al.*, 2001).

α2 receptors are crucial in analgesia and sedation (Hayashi and Maze, 1993; Buerkle and Yaksh, 1998; Giovannoni *et al.*, 2009). α2 agonists are considered strong analgesics since their activation increases the effect of opioids and they are involved in pain perception (Sullivan, Dashwood and Dickenson, 1987; Wilcox *et al.*, 1987; Kawasaki *et al.*, 2003; Sonohata *et al.*, 2004). Other than being potent analgesics, α2 agonists have hypnotic properties, most likely through the inhibition of the LC. α2 agonists reduce LC firing leading to decreased NE levels in target brain regions. In turn, low levels of NE are associated with a decrease in arousal levels (Mizobe *et al.*, 1996; Carter *et al.*, 2010; Giovannitti, Thoms and Crawford, 2015).

β adrenergic receptors

β adrenergic receptors comprise three receptor subtypes each of which is codified by a different gene, the three proteins are named β1, β2, and β3 (Emorine *et al.*, 1987, 1989; Frielle *et al.*, 1987; Machida *et al.*, 1990). The three receptors have been well characterized from a pharmacological point of view; specific agonists and antagonists have been indeed produced and used to determine the presence of specific receptor subtypes in given tissues (reviewed in Minneman, Pittman and Molinofj, 1981; Velmurugan, Baskaran and Huang, 2019).

Most of the cellular effects of β adrenergic receptors activation are mediated by excitatory G_s protein signaling cascade. G_s protein activates the adenylate cyclase that, in turn, brings to an increase of intracellular cyclic adenosine monophosphate (cAMP) and to the activation of protein kinase A (PKA) (Hekman *et al.*, 1984). The binding of agonists to β2 and β3 can also lead to the

activation of a $G_{i/o}$ signaling cascade, inducing inhibition of the adenylate cyclase (Daaka, Luttrell and Lefkowitz, 1997; Soeder *et al.*, 1999; Xiao, 2001).

The mRNA for β1 adrenergic receptor is widely distributed within the rodents' brain, while radioligand assay demonstrated its presence mainly in forebrain structures. β2 adrenoreceptor mRNA is mostly present in the olfactory bulbs, the hippocampus, the piriform cortex, and the cerebellum. However, radioligand assays have shown a dense localization of this receptor subtype especially in the cerebellar cortex (Rainbow, Parsons and Wolfe, 1984; Booze, Crisostomo and Davis, 1989). β3 adrenergic receptor seems to be expressed in the hippocampus, cortex, and striatum (Summers *et al.*, 1995). Interestingly, within the hippocampus, the expression of this adrenoreceptor seems to be restricted in a specific hippocampal neuronal precursor in the subgranular zone (SGZ) of the dentate gyrus (DG), in this region NE acting on β3 increases the number of proliferating cells, *de-facto* activating a niche of self-renewing multipotent cells (Jhaveri *et al.*, 2010).

β adrenergic receptors in the hippocampus are crucial in modulating synaptic plasticity acting on both long term potentiation (LTP) and depression (LTD) (reviewed in Dell *et al.*, 2015; Hagena, Hansen and Manahan-Vaughan, 2016). β adrenergic receptors activation promotes LTP at mossy fibers to CA3 and at CA3 to CA1 synapses (Hopkins and Johnston, 1984, 1988; Thomas *et al.*, 1996; Hagena and Manahan-Vaughan, 2012; Qian *et al.*, 2012). Studies with β receptors agonists in the DG, on the other hand, suggested a dual role of this receptor in this hippocampal region: low concentration of β agonist induces an LTD, while higher concentration of the same agonist is able to induce LTP (Lethbridge, Walling and Harley, 2014).

Since NE, through the activation of β receptors, has such a profound effect on hippocampal plasticity, it is not surprising that it plays a pivotal role in the retrieval of spatial and associative memory. Izquierdo et al. (Izquierdo *et al.*, 1998) showed that the infusion of NE in CA1 improved long term memory in an avoidance task. In the same task, mice KO for DBH, which are unable to produce NE, displayed impaired contextual fear memory retrieval. Memory retrieval could be rescued by injections of NE before the memory testing. Moreover, this restoration was dependent on β adrenergic receptor, since the infusion of isoproterenol (ISO), a strong β receptor agonist was sufficient to recover the retrieval of the memory in DBH-KO animals (Murchison *et al.*, 2004).

Connectivity profile

Classical tract tracing studies have been crucial for the understanding of LC input-output profile (Steindler, 1981; Luppi *et al.*, 1995; Aston-Jones, 2004; Szabadi, 2013). However, these techniques have some limitations: classical tracers cannot be used to target specific neuronal populations and they can be uptaken by *en-passant* fibers (Saleeba *et al.*, 2019). More recent viral tracing techniques allowed for more precise and sophisticated connectivity studies of the LC-NE system. In particular, Schwarz and colleagues' recent work (Schwarz and Luo, 2015; Schwarz *et al.*, 2015) demonstrated that LC output is highly divergent. LC-NE neurons have strong collateralizations, allowing them to project broadly to many brain regions. Nonetheless, this broad collateralization is inhomogeneous; subsets of LC neurons display more biased projections towards selective target areas. In the same study, rabies retrograde tracing revealed that LC receives direct inputs from more than 111 different brain regions, suggesting the strong integrative role of the LC-NE system. Schwarz also introduced a new viral tracing methods, named 'tracing the relationship between input and output' (TRIO) and cell-type-specific TRIO (cTRIO); these techniques allowed to restrict trans-synaptic rabies viruses infection based on the neurons output profile (TRIO), or to their output profile and their cell type (c-TRIO), respectively (**Figure 5**). By using these viral tracing approaches, the authors demonstrated that NE-neurons projecting to different brain regions receive fairly similar inputs. However, subsets of LC-NE neurons showed specific biases in their input-output organization. For instance, LC neurons projecting to the medulla received significantly fewer inputs from the Central Amygdala (CeA) compared to LC neurons projecting anywhere else. This suggests that LC neurons engaged by CeA, involved in anxiety and stress response (McCall *et al.*, 2015), do not directly influence NE-release in the medulla. Altogether these findings provide the anatomical substrate to explain the heavily integrative function of LC-NE neurons and how they broadly modulate many brain regions simultaneously in order to, eventually, regulate brain states. At the same time, this study showed that LC neurons are not completely homogeneous in their connectivity profile; this would ultimately contribute to an ensemble organization within the LC which would allow the generation of the diverse behavioral responses mediated by the LC-NE system.

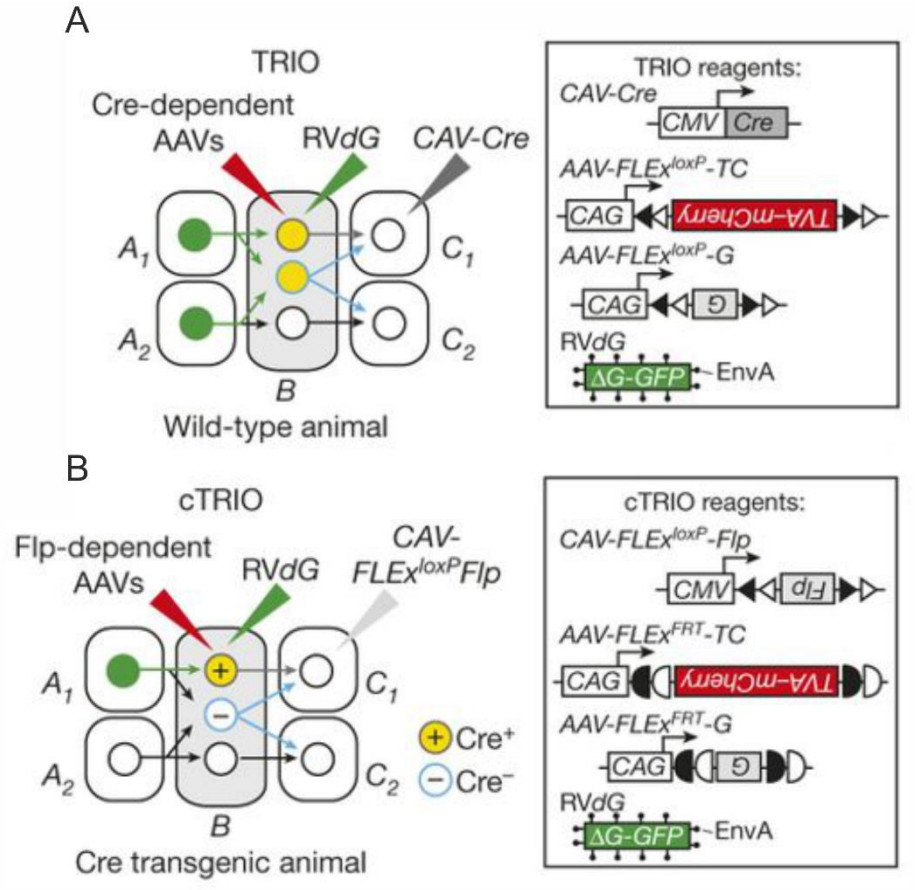

Figure 5 Schematics of TRIO and c-TRIO trans-synaptic viral-genetic tracing techniques. (A) TRIO does not distinguish between region different cell types in region B projecting to the selected C region (grey outlined circles and blue outlined circles in region B represent two different cell types). (B) cTRIO avoids labeling promiscuous projections from Cre– cells (blue). Open and filled triangles, incompatible loxP sites; open and filled half-circles, incompatible FRT sites. Modified from Schwarz et al. 2015.

Efferent projections

NE release in target brain regions can occur via “wiring”- or -“volume” transmission. LC terminal fields can either end in close proximity with single neurons, allowing for NE synaptic release (wiring transmission), or in interstitial spaces, forming varicosities (volume transmission) (Descarries and Mechawar, 2000; Szabadi, 2013).

Nearly all brain regions contain NE positive terminals (Swanson and Hartman, 1975). This finding makes the LC a central neuromodulatory hub for the whole brain.

Olfactory Bulbs

The Olfactory structures receive dense noradrenergic connections. Notably, it has been estimated that a big portion of LC neurons (≈40%) project to the bulbs (Shipley, Halloran and De La Torre, 1985); roughly 10 times more than NE projections to any other cortical areas. The first evidence obtained with retrograde tracing was later confirmed by anterograde tracing methods.

It has been shown that both the main and the accessory olfactory bulb receive LC projections (Mclean *et al.*, 1989). NE-axons are believed to contact mainly granule cells, with minor but important connections with mitral cells (Aston-Jones, 2004). These synaptic connections to both granule and mitral cells allow to finely regulate the olfactory signal to noise (S/N) ratio (Escanilla *et al.*, 2010; Linster, Nai and Ennis, 2011; Linster and Cleland, 2016; Manella, Petersen and Linster, 2017). NE, through modulation of the inhibitory granule cells, helps to reduce the noise in the system (Linster, Nai and Ennis, 2011; Manella, Petersen and Linster, 2017). Moreover, NE modulates the responsiveness of the olfactory bulb by directly increasing the excitability of mitral cells (Jiang *et al.*, 1996; Hayar *et al.*, 2001). This fine regulation of the S/N ratio in the olfactory bulb lowers odor detection threshold and increases the ability to discriminate between similar odors (Linster, Nai and Ennis, 2011).

Neocortex

The LC projects to the cortex through the dorsal noradrenergic bundle, a connection known as the coeruleo-cortical pathway (Szabadi, 2013). Morrison and colleagues proposed that the coeruleo-cortical axons enter the cortex frontally and then they travel caudally towards the occipital lobe, creating a layer of noradrenergic fibers that extends mainly tangentially across the whole cortex (Morrison *et al.*, 1981). The LC projects to all areas and to all layers of the cortex, although not indiscriminately. Layer I contains a meshwork of axons tangential to the cortical surface. Layer II/III is characterized by fibers innervating radially this layer. Layer IV contains convoluted axon fibers. Finally, Layer V and VI contain NE axons arranged along the anteroposterior axis (Morrison *et al.*, 1978). LC neurons project mainly ipsilaterally; it has been indeed estimated that only 5-10% of noradrenergic neurons project to the contralateral cortex (Adèr *et al.*, 1980; Waterhouse *et al.*, 1993; Aston-Jones, 2004). Notably, it has been recently demonstrated how LC neurons projecting to different cortical areas show different electrophysiological characteristics. Single LC neurons project preferentially to either the medial Prefrontal Cortex (mPFC), the Anterior-Cingulate Cortex (ACC), the OrbitoFrontal Cortex (OFC) or the primary motor cortex (M1), with minor overlapping. In other words, virtually no neurons project to more than one of these cortical regions (Waterhouse and Chandler, 2012; Chandler, Gao and Waterhouse, 2014). Remarkably, LC neurons projecting to OFC and mPFC were biochemically and electrophysiologically different from the ones projecting to M1. OFC and mPFC projecting LC-neurons showed higher mRNA levels for synaptic excitability markers (GLUR1 and NMDA R1 subunit), higher spontaneous firing rate and were more responsive to glutamate than neurons

projecting to M1. The increased excitability of these neurons is probably due to the higher requirements for NE in associative cortices related to cognition such as the OFC and the mPFC (Chandler, Gao and Waterhouse, 2014). From a behavioral standpoint, it has been demonstrated that increasing the activation of LC neurons projecting to the PFC through the use of chemogenetics results in an anxiogenic and aversive response (Hirschberg *et al.*, 2017). This finding suggests that the fine regulation of NE concentration at the PFC level is crucial to maintain optimal behavioral responses. Indeed, high NE concentration in the PFC promotes maladaptations and attention impairment (Suto, Eisenach and Hayashida, 2015). Therefore, although virtually all cortical areas receive NE afferents, the functional properties of the LC cells projecting in specific cortical areas are different, making possible a heterogeneous NE release in different cortical areas. This organization, in turn, might support a variety of diverse behavioral functions.

Hippocampus

LC neurons are the sole source of NE for the whole hippocampus (Loughlin, Foote and Grzanna, 1986). The role of adrenergic receptors activation in the hippocampus has been well studied, indeed the LC projections in this region have been implicated in memory consolidation and retrieval (Hansen, 2017). Interestingly, it has been demonstrated that LC terminals in the hippocampus are able to release not only NE but also dopamine (DA) (Kempadoo *et al.*, 2016). However, although it is known that DA has to be synthesized in LC neurons since it is a biochemical precursor of NE (Axelrod, 1971), the mechanism responsible for the co-release NE and DA in LC has not been elucidated yet (Kempadoo *et al.*, 2016). DA released from the LC increased attention, enhanced spatial object recognition and memory persistence acting through the D1/D5 receptor (Kempadoo *et al.*, 2016; Takeuchi *et al.*, 2016).

Thalamus

The LC projects profusely to the thalamus (Lindvall, Bjorklund and Nobin, 1973; Jones and Yang, 1985; Aston-Jones, 2004; Szabadi, 2013). This noradrenergic projection has been involved in sleep/wake cycle regulation, (Mccormick, Pape and Williamson, 1991) and in pain modulation (Westlund *et al.*, 1991; Zhang *et al.*, 1998). The NE modulation of thalamic circuits has been recently re-investigated. Rodenkirch and colleagues (Rodenkirch *et al.*, 2019) studied the role of LC stimulation in thalamus-based sensory processing. LC activation increased thalamic based feature selectivity and improved information transmission acting through an α receptor mediated mechanism. These effects were shown to be mediated by a modulatory effect of NE on both the

ventral posteromedial nucleus (VPm) and on the thalamic reticular nucleus (TRN). Moreover, the LC stimulation led to an increase in the perceptual performance of animals in a tactile discrimination task (Rodenkirch *et al.*, 2019). Since the thalamus is a structure involved in a multitude of brain functions, it is not surprising that LC→Thalamus projections have been also involved in stress responsivity. In this case, LC promotes the enhancing effects on the formation of aversive memories by disinhibiting the midline thalamus. This disinhibition occurs through the activation of D2 receptors by LC-dopamine release (Beas *et al.*, 2018).

Striatum

Most areas of the striatum, especially its dorsal portion, have been considered for a long time to be devoid of NE containing terminals (Berridge and Waterhouse, 2003; Aston-Jones, 2004). Nonetheless, this notion has been recently challenged by a new study in which a retrograde viral tracing approach allowed to unveil LC-NE neurons sparsely projecting to the dorsal striatum (Zerbi *et al.*, 2019). On the other hand, within the ventral striatum, in particular in the nucleus accumbens, there is a considerable noradrenergic innervation (Delfs *et al.*, 1998). This NE containing terminals originates mainly from the A1-noradrenergic nucleus and only a minority of LC cells send projections to the accumbens (Delfs *et al.*, 1998).

Basal Forebrain

The basal forebrain comprises different subcortical nuclei that are known to control arousal, attention and sleep/wake cycle (Ballinger and Ananth, 2016; Mena-Segovia, 2016). Notably, the medial septal area, the medial preoptic area, and the substantia imnominata all receive LC-NE projections (Berridge and Espana, 2006). It has been shown that the LC and Basal Forebrain are intimately linked in the regulation of sleep/wake cycle. Cholinergic neurons of the basal forebrain are known to promote wakefulness, while somatostatin-positive GABAergic interneurons (SOM+) promote non-REM sleep (Xu *et al.*, 2015). The NE released by LC inputs in the nucleus basalis of the substantia imonminata is able to modulate both cholinergic and GABAergic interneurons. In particular, NE positively modulates wakefulness-promoting cholinergic interneurons by an α1 adrenoreceptor mediated mechanism (Fort *et al.*, 1995). At the same time, NE decreases the firing rate of GABAergic interneurons by acting on α2 receptors (Manns *et al.*, 2003). The LC released NE in the basal forebrain, therefore, has a strong wakefulness-promoting effect.

Amygdala

LC projects strongly to the Amygdala. Notably, both the central nucleus (CeA) and the basolateral nucleus (BLA) of the Amygdala are profusely innervated by LC-NE terminals (Asan, 1998; Szabadi, 2013; Zhang, Muller and Mcdonald, 2013). NE released by LC terminals in the BLA promotes anxiety-like behavior. These effects are mediated by β-receptor signaling. Indeed, it has been shown that β-antagonism is sufficient to reduce the anxiety behavior induced by the opto-stimulation of LC fibers in the BLA. Moreover, the optogenetic activation of LC→BLA inputs induced not only a real-time place-aversion but also a conditioned aversion, suggesting a facilitating role for NE released by LC in the formation of new associative memories with a negative valence (McCall *et al.*, 2017). This finding goes in line with the known effect of NE in modulating amygdala plasticity and in promoting amygdala-dependent memory-consolidation (McGaugh, 2002; Tully *et al.*, 2007; Tully and Bolshakov, 2010).

The role of NE in regulating the central Amygdala (CeA) function has been less investigated. Nonetheless, recently it has been hypothesized that LC→CeA projections are required for the expression of defensive responses elicited by conditioned stimuli (Gu *et al.*, 2019).

Hypothalamus and Midbrain

The majority of NE terminals in the hypothalamus derive from the A1/A5 nuclei, however, the LC partially contributes to the noradrenergic innervation of this brain region (Cunningham and Sawchenko, 1988). The role that NE plays in modulating the activity of the hypothalamic neurons is still unclear. The hypothalamic nuclei collectively regulate many behavioral aspects: sleep and circadian rhythm, endocrine system, stress response, autonomic functions, just to cite few of them. Not surprisingly, the LC-NE system is interconnected with the hypothalamus, probably to allow better coordination during their overlapping processes, namely sleep and stress response regulation (Aston-Jones, 2004; Szabadi, 2013; Flak *et al.*, 2014).

LC axons have been found in the periaqueductal gray (PAG) (Fritschy and Grzanna, 1990) and two neuromodulatory structures: the dorsal raphe nucleus (DRN) (Peyron *et al.*, 1996) and the ventral tegmental area (VTA) (Mejías-Aponte, Drouin and Aston-Jones, 2009; Isingrini *et al.*, 2016; Mejias-Aponte, 2016; Park, Bhimani and Park, 2017). The understanding of the mechanisms and functions of the crosstalk between neuromodulatory systems remains fragmented. Pudovkina and colleagues demonstrated that NE activates DRN cells via α1- receptor (Pudovkina, Cremers and Westerink, 2003) but the functions of such connections are unknown. On the other hand, the

mechanism of action of LC→>VTA remains elusive but it has been postulated that NE released in the VTA inhibits dopaminergic neurons. (Isingrini *et al.*, 2016), The LC→VTA projection plays an important role in the behavioral coping strategy adopted by animals previously subjected to repeated/chronic stress (Isingrini *et al.*, 2016). Animals subjected to chronic stress, especially exposed to repeated social defeat, show different anxiety levels (Bosch-Bouju *et al.*, 2016) and can be divided into susceptible and resilient subgroups based on their social avoidance behavior (Golden *et al.*, 2011). In susceptible animals displaying a high level of social avoidance, chronic optogenetic entrainment of LC→VTA projections was sufficient to convert the susceptible phenotype into the resilient one. The direct connection from the LC to DRN and VTA is a piece of important evidence to support the strong integration and inter-dependence between these sub-cortical neuromodulatory nuclei. However, the possible behavioral implications of these pathways activation still need to be investigated.

Cerebellum

The Cerebellum, specifically the cerebellar cortex, receives dense noradrenergic projection from the LC (Olson and Fuxe, 1971). All three types of adrenoreceptors have been found in the cerebellar cortex: α1, α2, and β receptors (Szabadi, 2013). NE, through these different adrenoreceptors, plays an important role in modulating cerebellar synaptic plasticity (Hoxha *et al.*, 2016). From a behavioral standpoint, NE is crucial in orchestrating the cerebellar-mediated acquisition of new motor skills. Animals depleted of NE in the cerebellum showed motor impairments when they had to learn new motor tasks (Watson and Mcelligott, 1984).

Pons and Medulla Oblongata

The entire brainstem receives dense NE containing axons. Notably, LC projects primarily to sensory and associative nuclei of this caudal brain region, while nuclei associated with autonomic and motor nuclei are richly contacted by non-LC NE-fibers (Levitt and Moore, 1979). Suggesting segregating functions for NE coming from different noradrenergic nuclei in this brain area.

Afferent projections

Classic studies aiming at investigating the structures sending projections to the LC were controversial. By injecting retrograde tracing into the LC certain groups reported that several brain regions projects to the LC (Cedarbaum and Aghajanian, 1978; Clavier, 1979), while others claimed that the number of areas projecting to the LC is extremely limited (Aston-Jones *et al.*, 1986). In the first studies (Cedarbaum and Aghajanian, 1978; Clavier, 1979), the unconjugated-HRP technique

allowed to identify as primary forebrain inputs of the LC the central nucleus of the amygdala (CeA), the Bed Nucleus of the Stria Terminalis (BNST), the medial preoptic area, and the dorsomedial and paraventricular nuclei of the hypothalamus. Other relevant inputs were found in the brainstem, including the contralateral LC, midbrain central gray, vestibular nuclei, lateral reticular nucleus, and nucleus tractus solitarius (NTS). Significant inputs were also reported from the fastigial nucleus of the cerebellum. On the other hand, the succeeding Aston-Jones' study (Aston-Jones *et al.*, 1986), using the WGA-HRP iontophoresis technique, identified as the major contributor for the bulk of fibers innervating the LC two medullary nuclei: the nucleus paragigantocellularis (PGi) and the nucleus posterior hypoglossi (PrH). The findings by Aston-Jones (Aston-Jones *et al.*, 1986) were later confirmed by using the cholera toxin (CTb) retrograde tracing technique (Luppi *et al.*, 1995). By using this technique, other regions were found to consistently project to the LC itself: the Kölliker- Fuse nucleus (noradrenergic A7 area), noradrenergic A5 area, median raphe (B9 area), and caudal and lateral hypothalamus. These studies differed in the retrograde labeling technique used. The former studies (Cedarbaum and Aghajanian, 1978; Clavier, 1979) took advantage of the retrograde neuronal transport of the unconjugated horseradish peroxidase (HRP) to mark inputs of the LC, the inputs to the LC were then visualized with diaminobenzidine (DAB). This method, however, presents several limitations: 1) HRP diffuses substantially, allowing labeling of areas projecting adjacently to and not into the LC itself; 2) unconjugated-HRP is uptaken by *en-passant* fibers, possibly leading to the labeling of regions projecting through and not to the LC. Subsequent works (Aston-Jones *et al.*, 1986) used more sensitive and selective techniques: the iontophoretic deposition of wheat germ–agglutinin-conjugated HRP (WGA–HRP) in the LC, revealed by the tetramethylbenzidine (TMB) reaction. This method allowed to obtain restricted injection sites and made the uptake and the transport by neurons more efficient than the transport of unconjugated-HRP. The discrepancies found in these initial studies can be partially due to the anatomical characteristic of the LC. LC neurites broadly extend outside LC borders in a region known as peri-LC (Shipley *et al.*, 1996). Therefore, the diffusion of the retrograde tracers (either unconjugated-HRP, WGA-HRP, or CTb) in the peri-LC not only trace regions directly projecting into the LC but also regions forming synapses at distal dendrites of LC-NE neurons, in the peri-LC region. At the same time, the unspecific diffusion of the tract-tracer outside LC borders represents a major drawback of these techniques since inputs to regions anatomically close to the LC (such as the Barrington's nucleus) can be labeled, leading to possibly misleading results.

Recently, the controversial anatomical characterization of LC afferents has been more definitely addressed thanks to the trans-synaptic rabies viral tracing method (Schwarz and Luo, 2015; Breton-Provencher and Sur, 2019). These studies used a mouse line in which the Cre recombinase is expressed under the Dopamine Beta Hydroxylase promoter (DBH-Cre), to restrict to LC-NE neurons the cells from which the retrograde tracing occurs. Only DBH^+ starter-cells can be virally infected; within these cells then the rabies virions replicate and then spread retrogradely to the mono-synaptically connected pre-synaptic neurons (Saleeba *et al.*, 2019). Contrary to previous

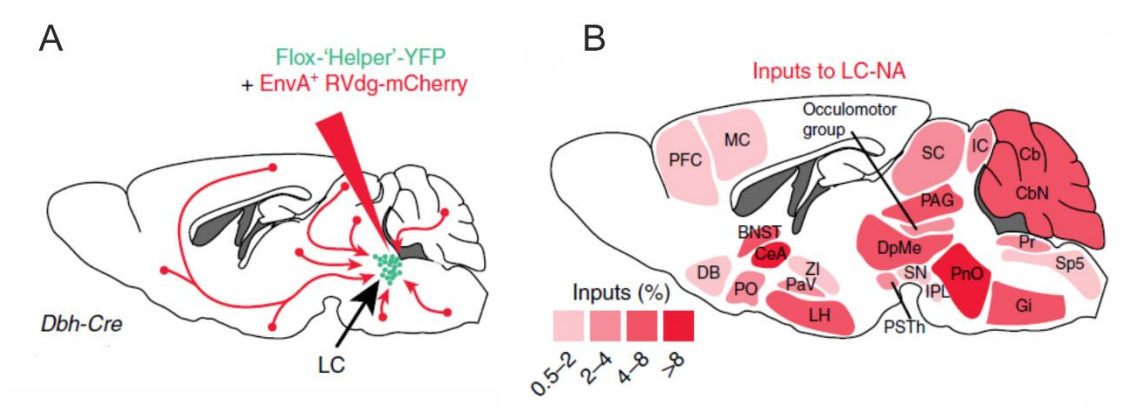

Figure 6 (A) Schematic for targeting delta G-protein Rabies virus (RVdg) to LC-NE neurons (LC-NE). (B) Transynaptically labeled neurons in different brain regions following injection of RVdG in LC of Dbh-Cre mice. LC receives projections from multiple brain regions. BNST, bed nucleus of the stria terminalis; Cb, cerebellum; CbN, cerebellar nuclei; CnF, cuneiform nucleus; DB, diagonal band; DpMe, deep mesencephalic nucleus; Gi, gigantocellular nucleus; IC, inferior colliculus; IPL, interpeduncular nucleus; LH, lateral hypothalamus; LHb, lateral habenular nucleus; MC, motor cortex; PAG, periaqueductal gray; PaV, paraventricular nucleus; PH, posterior hypothalamus; PnO, pontine nucleus; PO, preoptic nucleus; Pr, prepositus nucleus; PSTh, parasubthalamic nucleus; Rt, reticular nucleus; SC, superior colliculus; SN, substantia nigra; Sp5, spinal trigeminal tract; SPF, subparafascicular thalamic nucleus; SuM, supramammillary nucleus; ZI, zona incerta. Modified from Breton-Provencher and Sur, 2019).

techniques, rabies viral tracing allowed to reach neuronal subtype specificity and to label LC input regions regardless of their preference to synapse with LC neurons soma or dendrites. Remarkably, in both studies, an array of different brain regions has been consistently shown to directly synapse to LC-NE neurons (**Figure 6**).

Neocortex

Retrograde studies showed that most areas of the cortex project to the LC (Luppi *et al.*, 1995; Szabadi, 2013; Schwarz *et al.*, 2015; Breton-Provencher and Sur, 2019). Amongst the different cortical areas, the prefrontal cortex (PFC) has one of the strongest connections to the LC. PFC projects mainly to the peri-LC area, where the LC neurons extend their dendritic arborization (Arnsten and Goldman-Rakic, 1984; Luppi *et al.*, 1995). Although the PFC input is relatively sparse, indeed only a limited number of cortical pyramidal neurons are connected to the LC, it exerts a

potent drive on LC-NE neurons (Jodo, Chiang and Aston-Jones, 1998; Sara and Bouret, 2012). Counterintuitively, this connection has been shown to produce both an excitatory and an inhibitory effect on LC (Sara and Hervé-Minvielle, 1995; Jodo, Chiang and Aston-Jones, 1998). This discrepancy might be explained by the technical differences in the anesthesia method used in the two different studies (ketamine, which has been used in Sara and Hervé-Minvielle study, is a known NMDA receptor blocker and it probably affected the glutamatergic connection between the PFC→LC connection). More interestingly, the recent finding by Breton-Provencher (Breton-Provencher and Sur, 2019) demonstrating a direct synaptic connection between the PFC and both the LC-NE neurons and the LC-GABAergic interneurons, can account for the previously observed incongruity on the role of PFC connection to the LC. In this scenario, the PFC can either inhibit LC-NE neurons by activating local LC-GABAergic interneurons or, through a mono-synaptic connection, directly excite LC-NE neurons.

The strong reciprocal connection between PFC and LC activity is further supported by the phase-locking between the LC spiking and the cortical excitability fluctuations. In non-anesthetized rats, during NREM sleep, about 50% of LC units are phase-locked and they fire during the cortical transition from "down" to "up" states (Eschenko *et al.*, 2012; Sara and Bouret, 2012). These findings suggest the involvement of the LC in the cortical state transition and imply an interaction between the PFC and the LC during slow-wave oscillations, moreover, they are compatible with a possible PFC-LC excitatory loop. These results, however, do not rule out whether is the LC that drives PFC oscillations or *vice-versa* if the PFC drives LC firing.

Amygdala

The LC receives a relevant projection from the primary output nucleus of the amygdala: the Central Amygdala (CeA) (Wallace, Magnuson and Gray, 1989; Van Bockstaele, Colago and Valentino, 1998; Reyes, Drolet and Van Bockstaele, 2008; McCall *et al.*, 2015; Schwarz *et al.*, 2015; Breton-Provencher and Sur, 2019). This nucleus sends corticotropin-releasing factor (CRF) projections to the LC (Van Bockstaele, Colago and Valentino, 1998; Reyes, Drolet and Van Bockstaele, 2008; McCall *et al.*, 2015) (see the paragraph in this dissertation: "*LC, stress and the role of Corticotropin-Releasing Factor (CRF): between acute effects and long-lasting adaptations"* for an explanation regarding the CRF effects on LC-NE neurons). Recently it has been shown that CeA terminals projecting to the LC contain the opioid peptide Dynorphin (DYN) in addition to CRF (Reyes, Drolet and Van Bockstaele, 2008). DYN released from CeA neurons promotes anxiety

(Pomrenze *et al.*, 2019), but the exact role of DYN released from the CeA into the LC is not established yet. Interestingly, CeA→LC axon terminals do not release fast neurotransmitters, indeed optogenetic activation of CeA-CRF$^+$ terminals in the LC does not evoke any inhibitory or excitatory postsynaptic current (McCall *et al.*, 2015).

Hypothalamus

Different hypothalamic nuclei involved in sleep/wake regulation project to the LC. These nuclei are known to release different neurotransmitters and/or neuromodulators that ultimately affect LC activity. For instance, the sleep-promoting Ventrolateral preoptic nucleus (VLPO) contains GABAergic projecting neurons that send axons to the LC. This connection, through a GABAergic mediated inhibition of LC-NE neurons, is possibly involved in sleep promotion (Steininger *et al.*, 2001; Szymusiak and McGinty, 2008). Conversely, the wake-promoting Lateral Hypothalamus (LH) and Tuberomammillary nucleus (TMN) send respectively an orexinergic and a histaminergic projection to the LC (Horvath *et al.*, 1999; Korotkova *et al.*, 2005; Lee, Lee and Waterhouse, 2005; Cid-Pellitero and Garzón, 2011). Both neuromodulators activate LC neurons facilitating wakefulness (Horvath *et al.*, 1999; Korotkova *et al.*, 2005).

The LC receives inputs from another hypothalamic structure: the Paraventricular Nucleus (PVN). The PVN is a part of the Hypothalamic–pituitary–adrenal (HPA) axis and it is therefore intimately related to stress response. Corticotropin-releasing factor (CRF) is released from PVN neurons to initiate HPA axis activation, ultimately leading to the secretion of corticosteroids from the adrenal glands (reviewed in Herman *et al.*, 2016). The PVN sends CRF containing terminals to the LC. The PVN→LC terminals form a substantial proportion of asymmetric synapses, suggesting that CRF can be co-released together with glutamate in the Locus Coeruleus (Reyes *et al.*, 2005). Remarkably, Reyes' work supports the existence of two populations of PVN-CRF$^+$ cells with a distinct output profile. One group of neurons projects to the median eminence (ME; the structure, devoid of a blood-brain barrier, where hormones produced by the hypothalamus are collected before entering general circulation) and is, hence, part of the HPA axis; the second non-overlapping population of cells, on the other hand, sends projections to the LC (Reyes *et al.*, 2005). Therefore, stress, through PVN-CRF$^+$ neurons, might differentially affect the HPA axis and LC activation. This can potentially lead to an uncoupling between the central NE response and the rise in blood corticosteroid concentration.

Ventral Tegmental Area (VTA)

The LC receives a connection from the VTA (Beckstead, Domesick and Nauta, 1979; Ornstein *et al.*, 1987). This pathway is comprised mainly of non-dopaminergic (DA) fibers, although a small portion of VTA-DA-fibers is present within the LC (Swanson, 1982). Indirect evidence points at an excitatory drive exerted by the VTA connection on LC neurons. Indeed, local delivery of glutamatergic agonists (kainite) in the VTA increases the levels of the norepinephrine (NE) metabolite 3-methoxy-4-hydroxyphenolglycol (MHPG) in LC target brain regions (Deutch, Goldstein and Roth, 1986).

Dorsal Raphe Nucleus (DRN)

The DRN and the LC are reciprocally connected. The DRN→LC projection comprises both serotonergic and non-serotonergic terminals. Furthermore, DRN→LC has been shown to be more robust than the connection in the opposite direction (LC→DRN) (Segal, 1979; Kim *et al.*, 2004). Serotonin (5-HT) in the LC has been proposed to have an inhibitory role (Segal, 1979), acting primarily *via* 5-HT_{1A} (Pudovkina *et al.*, 2001; Pudovkina, Cremers and Westerink, 2002) and 5-HT_2 (Gorea *et al.*, 1991) receptors. However, a detailed dissection of the behavioral role of this neuromodulatory regulation has not been addressed yet.

Periaqueductal Gray (PAG)

The PAG is a heterogeneous group of cells surrounding the cerebral aqueduct within the midbrain. PAG activity has been associated with a variety of different behavioral functions such as stress response, pain modulation, vocalization and sleep regulation (reviewed in Benarroch, 2012; Keay and Bandler, 2015). A conspicuous number of PAG neurons send projections to the LC (Bajic and Proudfit, 1999; Bockstaele *et al.*, 2001; Schwarz *et al.*, 2015; Kim *et al.*, 2018). PAG terminals within the LC form mainly symmetric synapses; consistently PAG electrical stimulation has an inhibitory effect on LC-NE neurons (Ennis *et al.*, 1991; Bockstaele *et al.*, 2001). It has been recently demonstrated that PAG→LC projection plays an important role in opioid-induced analgesia (Kim *et al.*, 2018).

Lateral Dorsal Tegmental and Pedunculopontine nuclei (LDT/PPN)

LDT/PPN cholinergic neurons project to the LC (Jones and Yang, 1985; Jones, 1990). No studies directly addressed how the activity of LC-NE neurons is modulated by cholinergic afferents, however, acetylcholine is known to exert an excitatory effect on LC neurons acting through both

muscarinic and nicotinic receptors (Engberg and Svensson, 1980; Egan and North, 1985; Léna *et al.*, 1999).

Nucleus Paragigantocellularis (PGi)

The PGi is a nucleus located in the rostral ventrolateral medulla. This nucleus provides an excitatory/glutamatergic input to LC cells (Ennis and Aston-Jones, 1988) and it is one of the strongest projections to the noradrenergic nucleus (Aston-Jones *et al.*, 1986; Aston-Jones, 2004; Schwarz *et al.*, 2015). PGi neurons are involved in the regulation of autonomic functions such as cardiovascular and respiratory control (Van Bockstaele and Aston-Jones, 1995). Consequently, it has been suggested that the LC might broadcast the autonomic information conveyed from the PGi to the rest of the brain thanks to LC- NE neurons' widespread projections.

Nucleus Prepositus Hypoglossi (PrH)

PrH is a nucleus situated in the dorsomedial rostral medulla, it is part of the horizontal gaze holding system, that is involved in the horizontal positioning of the eye in the ocular orbit (Mcfarland and Fuchs, 1992; Kim, Zee and Lac, 2016). GABAergic PrH neurons of the dorsomedial rostral medulla send an inhibitory projection to the LC (Ennis and Aston-Jones, 1989a, 1989b). This inhibitory PrH→LC projection has been involved in the regulation of REM sleep, since stimulation of PrH increased the duration of REM sleep episode in an LC activity-dependent manner (Kaur, Saxena and Mallick, 1997, 2001).

Functional properties of a LC-NE neuron

Typical LC-NE neurons show resting membrane potential ranging between -55 and -65 mV, a fairly high input resistance (≈200 MΩ) and action potential threshold around -55mV (Williams *et al.*, 1984). They display slow and moderately regular spontaneous discharge (≈0.5-10 Hz) (Graham and Aghajanian, 1971) with relatively broad action potentials (≈1-2ms (Williams *et al.*, 1984; Berridge and Waterhouse, 2003)). LC-NE spontaneous discharge has been consistently recorded in *in-vivo* (both in awake and anesthetized animals) (Sugiyama *et al.*, 2012), *ex-vivo* (Williams *et al.*, 1984; Zhang *et al.*, 2010) and in primary cultured LC neurons (Masuko *et al.*, 1986). Because in primary cultured LC neurons synaptic connections with afferent regions are lost, these studies suggest that spontaneous discharge of NE-neurons results from a cell-autonomous peacemaking mechanism. Accordingly, blocking fast excitatory transmission in LC brain slices does not prevent LC tonic discharge (Sanchez-Padilla *et al.*, 2014). LC neuron peacemaking activity relies on a combination of a TTX sensitive Na^+ current, a high TEA-sensitive most likely Ca^{2+} activated K^+

conductance, and a persistent Ca^{2+} current (Williams *et al.*, 1984; Oliveira and Howlett, 2010; Sanchez-Padilla *et al.*, 2014). Moreover, it has been proposed that cAMP might drive or modulate LC tonic firing (Alreja and Aghajanian, 1991).

LC-NE tonic firing is linked to the arousal level and sleep/wake cycle (Hobson, McCarley and Wyzinski, 1975; Foote, Aston-Jones and Bloom, 1980; Carter *et al.*, 2010; Swift *et al.*, 2018; Breton-Provencher and Sur, 2019). Locus Coeruleus neurons fire tonically during wakefulness, their activity strongly decreases during non-Rapid Eye Movement (REM) sleep and they are virtually silent during REM (G. Aston-Jones and Bloom, 1981; Carter *et al.*, 2010; Takahashi *et al.*, 2010). Recent optogenetic studies have demonstrated that neural activity in the LC not only correlates with sleep/wake cycle but it is instrumental to maintain wakefulness. It is sufficient to increase LC activity to promote awakening and to increase locomotor arousal (Carter *et al.*, 2010). During sleep, especially during REM, LC tonic activity is silenced thanks to a mechanism involving an inhibitory GABAergic control exerted by the projections from the nucleus Prepositus Hypoglossi (PrH) (Kaur, Saxena and Mallick, 1997, 2001). The fine regulation of LC tonic activity during sleep and the complete spectrum of neuromodulators that shape LC activity, however, remain to be elucidated.

During wakefulness, the level of LC tonic activity and the performance in a given behavioral task follow an inverted-U relationship (also called Yerkes-Dodson relationship (Yerkes and Dodson, 1908; Teigen, 1994)) (**Figure 7**). For instance, performance in a discrimination task is low at low levels of LC tonic firing. This low level of LC activity is associated with drowsiness and non-alertness. On the opposite side of the spectrum, a very high level of LC tonic activity is related to poor performance; subjects show a labile attentiveness that doesn't allow them to focus optimally in a given task. At the same time, high tonic firing is linked with increased behavioral flexibility that might be required when animals are exposed to a new environment. To ensure optimal performance under stable conditions subjects must be attentive and focused this condition correlates with a moderate level of LC tonic firing. LC activity is therefore crucial in finely regulating the trade-off between focused-optimal and flexible behavior (Aston-Jones, Rajkowski and Cohen, 1999; Aston-Jones and J. D. Cohen, 2005) (**Figure 7**).

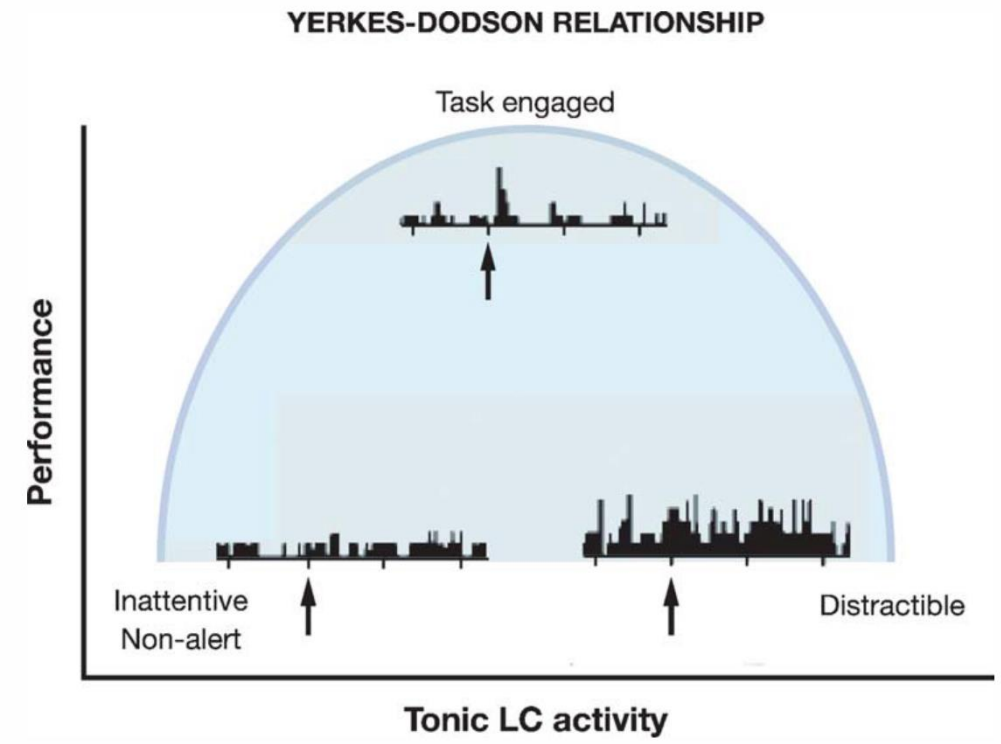

Figure 7 Inverted U-shape relationship between Locus Coeruleus (LC) activity and performance on a task that requires focused attention. Performance is poor at very low levels of LC tonic discharge (depicted by the peri-stimulus histogram (PSTH) in black). Performance is optimal with moderate LC tonic activity and prominent phasic LC activation when exposed to salient stimuli (black arrow). Adapted from Aston-Jones and J. D. Cohen, 2005.

While the tonic activity of LC neurons results from the intrinsic properties of its neurons, LC phasic activity results from the integration of sensory inputs of different modalities. Novel or salient multimodal-stimuli, as well as top-down decision-making processes, are able to elicit phasic discharge of LC-NE neurons (Foote, Aston-Jones and Bloom, 1980; Gary Aston-Jones and Bloom, 1981; Berridge and Waterhouse, 2003; Clayton *et al.*, 2004). These bursts of activity, superimposed to the tonic firing, are composed of few action potentials, usually 2-3, at 10-20 Hz. Often, these phasic bursts are followed by a suppression of the firing rate lasting 300-700ms (Berridge and Waterhouse, 2003; Devilbiss and Waterhouse, 2010). Phasic and tonic discharge modalities are interdependent in that phasic responses are correlated with the underlying tonic activity. Moderate tonic discharge allows optimal phasic responses when a salient stimulus is presented to the subject. In-contrast, phasic responses are weaker when tonic firing is too low for instance during drowsiness, or when tonic firing is too high, as in stressful situations (Valentino and Foote, 1987; Berridge and Waterhouse, 2003; Aston-Jones and J. D. Cohen, 2005).

The LC neurons post-activation inhibition is, at least partially, dependent on autocrine and paracrine NE release. The autoreceptor α2 is thought to play a primary role in this auto-inhibitory effect. Accordingly, iontophoretic local application of NE causes inhibition of LC firing, which is

prevented by the antagonism of the α2 receptor (Kimura and Nakamura, 1987). Moreover, the α2-receptor agonist clonidine suppresses LC-NE firing (Svensson, Bunney and Aghajanian, 1975; Svensson and Usdin, 1978).

From a network perspective, the LC has been long considered to be an undifferentiated "state controller" of the brain as for many other neuromodulatory nuclei (Lee and Dan, 2012). Supporting this view, extracellular recordings of spiking and field potentials indirectly suggested widespread network synchronicity within the LC (Gary Aston-Jones and Bloom, 1981; Akaike, 1982; Sakaguchi and Nakamura, 1987; Ishimatsu and Williams, 1996; Alvarez *et al.*, 2002). Recent evidence, however, supports an ensemble-based organization of the noradrenergic nucleus. This new model envisages that subsets of LC-neurons are not necessarily firing synchronously. This would allow for more fine control of NE release in different brain regions targeted by different ensembles (Chandler, Gao and Waterhouse, 2014; Schwarz *et al.*, 2015; Hirschberg *et al.*, 2017; Uematsu *et al.*, 2017; Totah *et al.*, 2018). Consistently with this view, single-unit large-scale population recordings of the LC demonstrated the existence of an ensemble code in this brain region (Totah *et al.*, 2018). In anesthetized rats, LC population activity was not characterized by correlations amongst all the single units. However, sparse and everchanging correlations among networks of LC cells were found on a broad range of timescales amongst different subsets of single-units. Moreover, spiking was not found to be a population event involving the whole LC structure even when nociceptive stimuli, which are thought to evoked synchronous discharge in many LC cells (Gary Aston-Jones and Bloom, 1981), were delivered to the animal. In this context, the reported presence of gap-junctions amongst neurons in the developing and adult LC (Christie and Jelinek, 1993; Travagli, Dunwiddie and Williams, 1995; Ishimatsu and Williams, 1996; Bockstaele *et al.*, 2004; Rash *et al.*, 2007) might be possibly involved in the sharp sub-milliseconds correlations that were found between small neural-networks. This type of sharp synchronicity was found only in neuronal pairs, suggesting that this form of activity-correlation is limited and spatially confined (Totah *et al.*, 2018). Correlations over longer time scales (up to tens of milliseconds), on the other hand, are possibly caused by shared synaptic inputs among LC neurons and modulation of the synchrony timing by lateral inhibition (Totah *et al.*, 2018). These findings advocate against LC as an undifferentiated state controller of the brain and suggest that LC is a complex nucleus with heterogeneous network dynamics among different ensembles.

The understanding of the functional properties of LC neurons was -and still is- essential to postulate hypotheses regarding the potential behavioral functions of this important neuromodulatory hub. Recent findings point to a new scenario in which the diversity in functional and physiological properties of LC-NE neurons allows for a nuanced and finely tuned neuromodulation. Nonetheless, these studies are not in opposition to the notion of LC-mediated global neuromodulatory changes in brain states (i.e. regulation of arousal or sleep/wake cycle) but they rather contribute to its refinement.

Plasticity in the LC

In the previous paragraphs, I described some of the "steady-state" properties of LC-NE neurons. However, the brain can rapidly adapt to changes in the environment by virtue of its plastic properties (Kandel, Dudai and Mayford, 2014). Although the effects of NE in gating and modulating plasticity in numerous LC target brain regions is well established, very few studies have been performed trying to address whether and how plasticity occurs in the LC itself.

LC developmental plasticity

Nakamura and Sakaguchi (Nakamura and Sakaguchi, 1990) have systematically recorded the *in-vivo* tonic and sensory-evoked responses in rat LC neurons at different developmental stages. In their pioneering studies, they have shown a dramatic change in the spontaneous activity of LC neurons extracellularly recorded activity from the prenatal period to adulthood. Conversely to what has been shown in adults, most LC cells in fetal and neonatal rats show no spontaneous activity, the fewer LC neurons showing tonic firing displayed sporadic discharge spaced by periods of long-lasting inactivity. During development, the firing pattern became more regular, with rats at postnatal day 20 (P20) showing tonic firing in most LC cells.

Given their higher chance of being silent, one can speculate that LC neurons during perinatal development are not functional yet. As a matter of fact, even at prenatal stages, LC neurons responded strongly to tactile stimulations like air-puffs (Sakaguchi and Nakamura, 1987), suggesting that they are already functional but still undergoing a maturation process. LC neurons of adult awake animals are able to respond to multimodal sensory stimulation, this feature, however, is lost in adult anesthetized animals. In this condition, only noxious stimuli are able to phasically entrain the noradrenergic cells (Korf, S. Bunney and K. Aghajanian, 1974), while non-noxious and non-tactile stimuli are ineffective. Surprisingly, in LC cells of neonatal rats, tactile

noxious and non-noxious stimuli but also visual and auditory ones were effective in activating noradrenergic neurons. This suggests that in younger rats LC evoked activity is more tightly linked to the peripheral sensory system compared to adult subjects. Moreover, the response latency to sensory stimulation was shown to decrease along different developmental stages, underlining how LC neurons are still under development at the different time-points inspected.

Sakaguchi also estimated the conduction velocity of LC-NE axons by using the antidromic stimulation technique at different developmental stages. In his studies, he showed how LC axons are able to conduct action potential in cortical areas already at prenatal stages. To evaluate possible developmental changes in the conduction efficiency of LC neurons, Sakaguchi measured the latency between the stimulation in the frontal cortex and the antidromic spikes recorded in the LC demonstrating a strong consistency of the antidromic latency amongst different developmental stages (≈40ms). On the other hand, the estimated mean conduction velocity has been shown to increase to keep up with the increase in brain size, which allows the maintenance of constant conduction time in an expanding brain. It is worth noting that the conduction time from the LC to the frontal cortex has been shown to be similar not only amongst different ages but also amongst different animal models, such as in rodents and monkeys (Aston-Jones, Foote and Segal, 1985; Nakamura, Kimura and Sakaguchi, 1987). This evidence suggests that the conduction time from the LC to target brain regions is a crucial feature for the correct physiological function of the noradrenergic nucleus.

The pioneering studies of Nakamura and Sakaguchi first showed how LC neurons undergo profound developmental plastic changes. Up to now, it is not yet understood which internal and external factors shape this developmental trajectory and how the observed differences in the LC tonic firing pattern and in the sensory-evoked responses shape animal behavior.

LC, stress and the role of Corticotropin-Releasing Factor (CRF): between acute effects and long-lasting adaptations

During stress exposure, Corticotropin-Releasing Factor (CRF) is released into the LC by different stress-responsive brain regions: the Paraventricular Nucleus (PVN), the Central Nucleus of the Amygdala (CeA), the Bed Nucleus of the Stria Terminalis (BNST) and the Barrington's nucleus (Valentino *et al.*, 1992; Valentino, Bockstaele and Van Bockstaele, 2008; McCall *et al.*, 2015). CRF, through the activation of CRF1R (Jedema and Grace, 2004; Reyes *et al.*, 2006), a G_s-coupled receptor, increases LC tonic discharge rate (Valentino, Foote and Aston-Jones, 1983). The

increased tonic firing of LC-NE neurons is associated with impairments in sensory signal discrimination, cognitive impairments and increased levels of anxiety (Aston-Jones and Jonathan D. Cohen, 2005). At first sight, this might seem a maladaptive response. However, it has been hypothesized that an increased LC tonic discharge, therefore high NE level, promotes vigilance and facilitates an escape response from threatening situations (Valentino, Bockstaele and Van Bockstaele, 2008; Borodovitsyna, Joshi and Chandler, 2018) by dampening top-down inhibition from the prefrontal cortex (PFC) to subcortical structures (Birnbaum *et al.*, 1999; Ramos and Arnsten, 2007). It is worth noting, however, that the modulatory effect of specific CRF containing inputs onto LC neurons might induce more subtle changes that the ones described so far. McCall and colleagues (McCall *et al.*, 2015) showed that when CRF^{+} terminals from the CeA are optogenetically activated, roughly half of the responsive LC units increased their firing and the other half was significantly inhibited. Although the effect on LC neuron firing rate was not homogeneous, this optogenetic stimulation was sufficient to induce an aversive and anxiogenic behavioral response (**Figure 8**). The effects of the photostimulation were rescued by the antagonism of CRF1R, demonstrating a direct involvement of CRF.

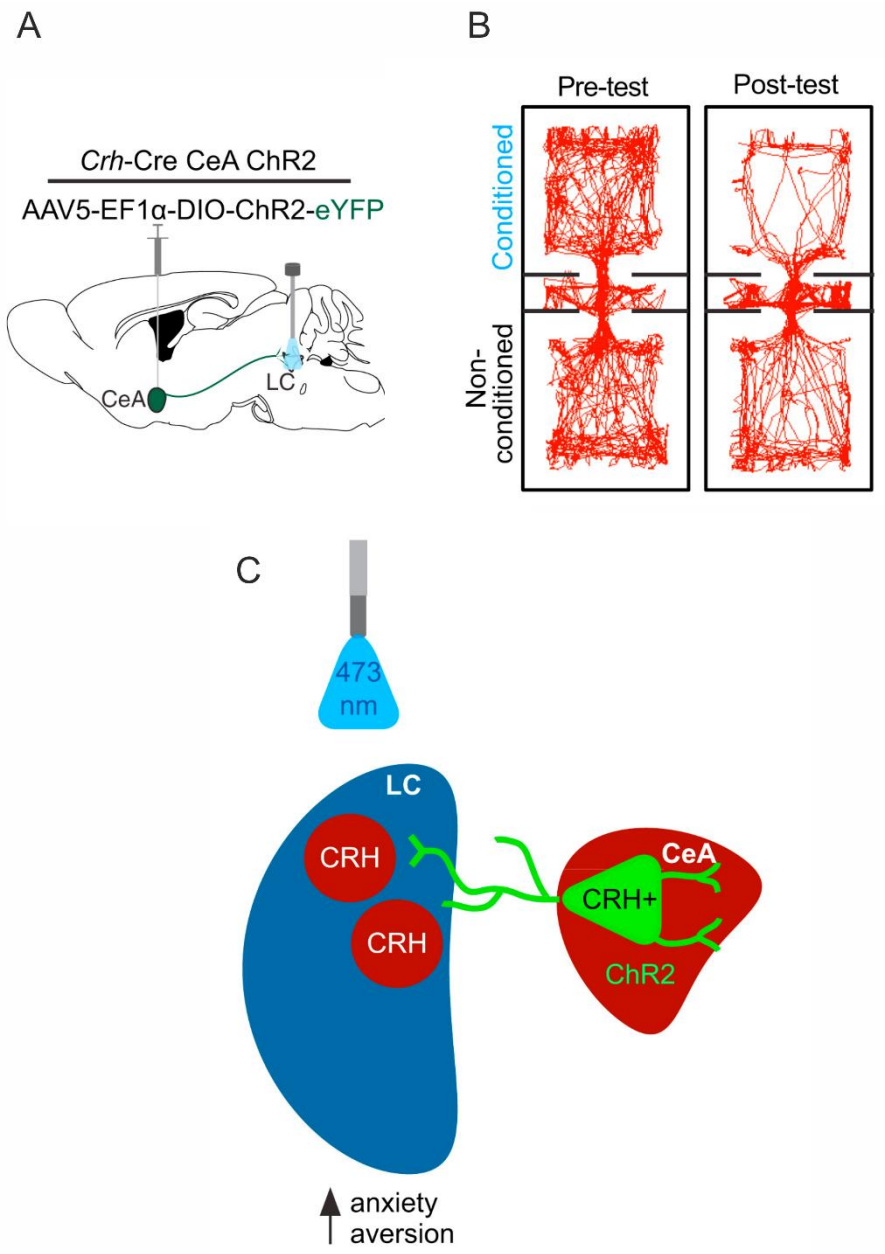

Figure 8 (A) Schematic showing the viral-genetic strategy used to obtain specific expression of ChR2 in Central Amygdala (CeA) CRF^{+} neurons and the optic fiber implant in the Locus Coeruleus (LC). A CRH-Cre driver mouse line has been used for this purpose. (B) Mice injected with ChR2 show a significant Conditioned place aversion compared to mice injected with an eYFP control virus. (C) As depicted in the schematic selective illumination of CeA-CRF containing terminals in the LC increases anxiety behavior and is aversive. Modified from McCall et al. 2015.

Acutely, CRF increases LC tonic firing signaling through a cAMP-dependent mechanism, an intracellular increase of cAMP leads to an inhibition of a K^{+} conductance and hence to a depolarization of the noradrenergic neurons (Jedema and Grace, 2004). Moreover, the acute application of CRF on brain slices induces a dose-dependent effect on excitatory spontaneous transmission. Lower concentration of CRF1R agonist (50µM CRF) increases the amplitude and charge transfer of spontaneous Excitatory Postsynaptic Currents (sEPSCs), while higher

concentration of CRF (200µM) leads to a significant decrease in excitatory synaptic transmission (Prouty, Waterhouse and Chandler, 2016). Similarly to what has been observed upon bath applying CRF on LC brain slices, a single exposure to a combination of stressors (restraint stress coupled to predator odor exposure) decreased synaptic transmission efficacy with a reduction in sEPSC amplitude and charge transfer. Furthermore, the LC spontaneous discharge rate was higher in stressed compared to control subjects. The observed excitability change was not accompanied by a change in the neuronal input resistance (Borodovitsyna, Flamini and Chandler, 2018). Interestingly, in 5-6 weeks old rats, a single stressor exposure was not only able to induce short term modification but also long-lasting effects on LC-NE neurons: a form of experience-dependent plasticity. When tested one week after the stressful experience, sEPSCs amplitude -but not frequency- was still lower in LC neurons of stressed animals. This points at a long-lasting adaptation occurring at glutamatergic synapses upon a single exposure to stress. The effect on synaptic transmission was co-occurring together with neuroplastic changes in neuronal excitability: similarly to what was observed immediately after stress exposure, spontaneous LC-NE neuron discharge rate was higher upon stress exposure. Contrary to the acute study, the input resistance and the action potential threshold of LC-NE neurons were affected by a single stress-exposure when probed one week later, indicating a possible re-arrangement of the cells' conductances that takes time to be established (Borodovitsyna, Flamini and Chandler, 2018). These findings suggest that even short and acute exposure to stressors chronically increase LC-NE firing. This would likely lead to changes in the level of NE released in target brain regions which is ultimately crucial in the fine modulation and regulation of a variety of behavioral tasks.

CRF, possibly released in the LC upon stress exposure, is not only able to shape excitatory transmission, but it also induces strong morphological changes in noradrenergic neurons by acting on the cells' cytoskeleton (Cibelli *et al.*, 2001; Swinny and Valentino, 2006; Bangasser *et al.*, 2012). In immortalized neurons derived from LC neurons, CRF triggers the formation of long and thin neurites, which is dependent on cAMP production and ERK signaling cascade (Cibelli *et al.*, 2001). A similar effect has also been observed in organotypic slices containing LC cells (Swinny and Valentino, 2006). In this study, 12h exposure to CRF induced an increase in the number of LC-NE primary processes, in the number of branching points and in the length of the processes. These effects were mediated by CRF1R since the application of a non-selective CRF1/CRF2R antagonist (Astressin 10µM) prevented the effects on processes morphology, while CRF2R specific antagonism (antisauvagine-30, 1µM) was ineffective. Not surprisingly, the cytoskeleton

rearrangements were mediated by the activation of the Rho GTPase Rac1. Rac1 is known to promote neurite outgrowth and morphology (Ruchhoeft *et al.*, 1999; Woo and Gomez, 2006). As expected, the inhibition of Rac1 prevented the stimulatory effect of CRF on neurites outgrowth and morphology. In line with these findings, overexpressing CRF neuropeptide increased significantly the complexity of LC-NE neuron dendritic arborization (Bangasser *et al.*, 2012).

In summary, these studies suggest that stress, most likely through CRF release in the LC, induces an immediate response and profound long-lasting adaptations in noradrenergic neurons. Overall it has been shown that CRF alters synaptic transmission and neuronal excitability, moreover, it induces morphological and dendritic rearrangements. These effects are mediated by the activation of CRF1R and its downstream signaling cascades, which include cAMP/PKA and MAPK/ERK activation. The plastic changes in activity and morphology of LC neurons can profoundly affect target brain regions that receive profuse noradrenergic innervation. Changes in NE levels, in turn, could promote a "neuroadaptation cascade" in areas crucially regulated by norepinephrine signaling, such as the hippocampus (Doze *et al.*, 2011; Kempadoo *et al.*, 2016), the amygdala (Kravets *et al.*, 2015; Schiff *et al.*, 2017) and the frontal cortex (Birnbaum *et al.*, 1999; Arnsten, 2000; Ramos and Arnsten, 2007; Wang *et al.*, 2007).

Synaptic plasticity in the LC: a field yet to explore

Albeit the amount of research conducted in the last four decades, few studies on the LC have been focused on the plastic properties of its synapses. Recent evidence (including the studied reported in the previous paragraph showing how acute stress persistently modulates synaptic transmission (Borodovitsyna, Flamini and Chandler, 2018)) suggests that LC synapses can undergo different forms of plasticity following diverse stimuli. Synaptic plasticity in LC neurons might be instrumental to finely set the gain of LC evoked responses, making more efficient the selection process of salient stimuli. At the same time, drugs of abuse can induce maladaptive forms of plasticity that can contribute to withdrawal and reinstatement of drug-seeking. Although limited in number, these studies demonstrate how flexible and adaptable is the LC system. Nevertheless, the fine molecular mechanisms involved in these forms of plasticity and their functional implication are far from being clearly elucidated.

Hereafter I reported two different case studies in which synaptic plasticity has been shown to occur in LC-NE cells.

LC plasticity driven by auditory stimuli

To address whether LC neuronal activity is affected by auditory experiences, Martins and Froemke (Martins and Froemke, 2015) performed patch-clamp recordings of LC neurons while assessing their responsiveness to auditory stimulation. As previously described (see: "LC developmental plasticity"), in adult rats pure tones did not evoke any responses in LC cells. Nonetheless, following a repetitive pairing of the auditory stimulus with a nociceptive stimulation (foot-shock), LC neurons became specifically responsive to the paired tone. Moreover, substituting foot-shock stimulation with LC electrical stimulation was enough to induce responses to auditory-stimuli in previously unresponsive LC cells. This form of long-lasting auditory driven plasticity was dependent on NMDA receptors. Indeed, the antagonism of this glutamatergic receptor with AP-V was sufficient to prevent the observed plastic change. This form of plasticity was similar to the potentiation previously described in silent synapses of other brain regions (Montgomery, Pavlidis and Madison, 2001).

Martins and Froemke, additionally, assessed the role of LC-NE stimulation in modulating the cortical sensory representation of auditory stimuli. By performing electrophysiological recordings of neurons in the primary auditory cortex (AI), they quantified the tuning curves of AI cells. They measured AI tuning curves before and after a pairing protocol in which a defined pure tone was paired to electrical or optogenetic stimulation of the LC-NE neurons (LC-tone pairing). The LC-tone pairing induced: 1) an initial increase in cortical responses to all tone frequencies lasting 5-10 minutes or, in other words, a broadened tuning curve; 2) a shift of the best-frequency to the paired one; 3) a subsequent return of the tuning curve width to baseline condition, with a maintained preference for the paired tone lasting for the whole duration of the recording. At the same time, the LC pairing induced a significant increase in both, tone evoked EPSCs and IPSCs in AI cortical cells. This was co-occurring with a decrease in spontaneous inhibition without affecting excitatory synaptic transmission. The described decrease in spontaneous inhibition, together with an unaffected evoked transmission, would act as a simple gain enhancer for all the incoming inputs regardless of whether they were precedently paired or not. The authors then aimed at understanding whether the observed disinhibition of spontaneous transmission could, on its own, account for the tuning-shift observed during the LC-tone pairing. To address this question, they measured the responses of AI cortical while antagonizing the GABA-A receptor. The disinhibition caused by the GABA-A antagonism was sufficient to progressively tune the synaptic responses to a repeated tone and not to other frequency tones. Furthermore, this effect was dependent on

NMDA receptor activation in AI cells. Therefore, disinhibition coupled with a repeated tone is sufficient to induce long-lasting enhancement of the AI neurons responses to a selective tone frequency. NE, consequently, might tune the best-frequency by decreasing the spontaneous inhibitory tone in the AI cortex.

NE in the cortex activates α-adrenergic receptors. These receptors are necessary for the induction and maintenance of the best-frequency shift induced by LC-tone pairing: the antagonism of these receptors prevented the tuning shift induced by pairing. The authors, thus, hypothesized a scenario in which modifications induced in the LC are required for AI cortical plasticity. In this way, after the pairing protocol, every other paired tone would induce NE release in the cortex, and this would, in turn, be necessary to maintain reliable changes in cortical representations. If this holds true, the antagonism of NMDA receptors confined in the LC would prevent subsequent long-lasting shifts in the AI neurons tuning curves upon pairing. Accordingly, when AP-V (that has already been shown to be necessary for plastic changes in LC) was applied locally in the LC, the enduring effect of LC-pairing on AI tuning-shifts was dramatically decreased.

The authors then tested whether the LC pairing was able to affect auditory perception and discrimination. In a cued operant conditioning task, rats had to nose-spoke for food reward in response to a specific target tone stimulus, while refraining from responding to foil tones. When the target tone was paired to a short-term optogenetic LC-stimulation, the animal's ability to detect auditory stimuli and, therefore, to respond correctly in the behavioral task, was greatly increased. In particular: 1) the likelihood of responding to low-intensity stimuli at a given frequency, previously unable to be detected, increased; 2) the ability to detect spectrally similar tones, initially decreased for the first hours, then gradually increased to reach an above-baseline level at 12h after training. This mirrored the effects of LC-tone pairing on the AI cortex: an initial broadening of the tuning curve, with a subsequent re-sharpening of the curve to the new best-frequency. The effect on animals' performance lasted for days after training and it was prevented by AP-V infusion in the LC, strongly supporting the importance of LC plastic changes induced by NMDA receptor activation. Finally, LC pairing was able to improve behavioral performance in a reversal-learning task. Animals first trained to respond to a specific pure tone had to switch to a new rewarded frequency tone in a subsequent training session. When animals received a pairing between the LC opto-stimulation and the "reversal-tone" on the day of reversal they more readily learned the new association between the stimulus and the reward.

Martins and Froemke first showed that context associations can be formed in the LC, thanks to long-lasting plasticity mechanisms happening in this region. Moreover, the LC NMDA-dependent form of plasticity that they described is instrumental for downstream plastic adaptations happening in the AI cortex. This "plasticity cascade" ultimately influences behavioral responses, shaping the animal's ability to discriminate and perceive auditory stimuli.

Martins and Froemke's study, hence, represents the first step in answering whether and how LC plasticity occurs and the molecular mechanisms underlying these plastic phenomena.

A single exposure to drugs of abuse induces plastic changes in LC-NE neurons

In their recent study, Zhu and colleagues (Zhu *et al.*, 2017) tested the effect of a single administration of cocaine on LC glutamatergic transmission. In brain regions containing catecholaminergic neurons like the Ventral Tegmental area (VTA), a single cocaine exposure has been shown to cause synaptic plastic changes (Ungless *et al.*, 2001; Sarti *et al.*, 2007; Arora *et al.*, 2011). Cocaine has a high affinity for the norepinephrine transporter (NET) (Trendelenburg, 1991; Torres, Gainetdinov and Caron, 2003; Zhou, 2004). NE might, therefore, play an important role in cocaine addiction, especially when considering that the administration of α1-adrenergic receptors antagonist reduces the hyperlocomotion and the drug-seeking behavior induced by drugs of abuse (Wellman *et al.*, 2002; Zhang and Kosten, 2005).

Zhu and colleagues demonstrated that a single cocaine administration increased the AMPA/NMDA ratio in LC excitatory synapses. In cocaine treated animals, but not in vehicle-treated animals, the amplitude of EPSC recorded at -70mV (AMPA component) was decreased upon application of a selective Ca^{2+}-permeable AMPA receptor blocker. This suggests that cocaine leads to the insertion of new Ca^{2+} permeable AMPARs, similarly to what has been previously described in the VTA (Bellone and Lüscher, 2006; Argilli *et al.*, 2008). Accordingly, the AMPAR current measured in the LC neurons of cocaine treated animals showed a stronger inward rectification compared to control animals; the rectification index (RI; $\frac{AMPA\ current-70mV}{AMPA\ current+40mV}$) was higher in cocaine treated animals, further supporting a cocaine-induced insertion on the post-synaptic membrane of GluR2 lacking Ca^{2+} permeable AMPA receptors. The authors ruled out the involvement of pre-synaptic adaptations caused by cocaine by measuring the presynaptic quantal glutamatergic release (mEPSC) and the paired-pulse ratio (PPR) of the glutamatergic responses, an index of the release probability of the pre-synaptic site. These two parameters were unchanged supporting a post- and not pre-synaptic functional remodeling of LC excitatory synapses upon cocaine treatment. Finally,

to assess whether α1-adrenergic receptors could mediate the effect of cocaine on LC synaptic plastic changes, Zhu and colleagues antagonized this class of receptors by *in-vivo* treating the animals with prazosin before cocaine administration. This pharmacological treatment abolished the effect of cocaine on both AMPA/NMDA ratio and RI. This suggests that α1 receptors mediate the insertion of new GluR2 lacking AMPA receptors, causing the observed potentiation of synaptic transmission.

Zhu's study points to a synaptic substrate potentially important for the maladaptive adaptations induced by cocaine. Moreover, it further supports the plastic properties of LC glutamatergic synapses.

Taken together, the two studies described above show how LC neurons can undergo heterogeneous forms of synaptic plasticity. These changes in synaptic strength, that are intimately related to experience, can eventually be instrumental for the animal's behavior or, conversely, under adverse circumstances can potentially be detrimental and, thus, be considered maladaptive. Although the evidence supporting the importance of LC synaptic plasticity is still scattered, this emerging research topic might be important to better understand LC physiology. Neuroplastic and, in particular, synaptic plastic changes happening at the level of LC neurons might ultimately affect NE release in LC target regions. Changes in NE release can, in turn, modulate plasticity in the multiple LC target brain regions.

Cannabinoid role in regulating LC physiology

Neuromodulators play a pivotal role across the brain in shaping and/or gating plasticity (Hardingham *et al.*, 2013; Blackwell and Jadrzejewska-Szmek, 2014; Nadim and Bucher, 2014; Pedrosa, Clopath and Zhang, 2017; Foncelle *et al.*, 2018; Gerstner *et al.*, 2018; Brzosko, Mierau and Paulsen, 2019). Neuromodulators released by afferent pathways (i.e. NE, serotonin, dopamine, acetylcholine) and locally released signaling molecules (i.e. endocannabinoids, nitric oxide) are both able to influence plasticity (Gu, 2002; Reynolds and Wickens, 2002; Sjöström, Turrigiano and Nelson, 2003; Tzounopoulos *et al.*, 2007; Cui *et al.*, 2015, 2016). In particular, the endoCannabinoid (eCB) system is involved in many forms of transient (i.e. short-term depression, depolarization-induced suppression of inhibition/excitation) and long-lasting plasticity (mainly Long-Term Depression), both at excitatory and inhibitory synapses (Gerdeman and Lovinger, 2003; Chevaleyre, Takahashi and Castillo, 2006; Castillo *et al.*, 2012). Cannabinoids are known to modulate the activity of NE neurons (Gobbi *et al.*, 2005; Muntoni *et al.*, 2006).However, the role

of these signaling pathways in regulating LC synaptic plasticity as well as the functional and behavioral implication of this modulation remains to be explored.

Already at the beginning of the nineties, Cannabinoid receptor 1 (CB1r) mRNA and protein were found in the LC region (Herkenham *et al.*, 1991; Matsuda, Bonner and Lolait, 1993). More recently, immunofluorescence and electron microscopy studies have shown that the CB1r is presynaptically located on both glutamatergic and GABAergic terminals that synapse onto NE cells. Interestingly, the distribution of CB1r is not exclusively presynaptic; indeed this cannabinoid receptor is also present in the somatodendritic compartment of LC-NE cells (Scavone, Mackie and Van Bockstaele, 2010). In other brain regions such as the cerebral cortex, activation of postsynaptic CB1 auto-receptors induces auto-inhibition of a subset of interneurons (Bacci, Huguenard and Prince, 2004; Marinelli *et al.*, 2008), hence one may speculate that the same self-inhibition might happen in LC neurons. Alternatively, postsynaptic CB1r could be optimally located to regulate glutamatergic synaptic transmission without affecting the presynaptic release probability.

Recently, CB1r has been also found on CRF^+ terminals within the LC region. Using Phaseolus Vulgaris Leucoagglutinin (PHAL) as an anterograde tracer, Wyrofsky and colleagues demonstrated the presence of CB1r on amygdala afferents (R. Wyrofsky, Reyes and van Bockstaele, 2017). The release of CRF release is associated with stress response and it induces LC increased excitability and firing activity, therefore, CB1r on CRF^+ is placed in a critical spot to finely regulate NE release following stress exposure. However, the anatomical evidence showing CB1R on CRF^+ terminals are not flanked by findings revealing the role of the cannabinoid receptor in this location.

The presence of cannabinoid receptors in the LC is in line with findings showing how cannabinoids can profoundly shape LC-NE cells' activity (for reviews: Carvalho & Van Bockstaele, 2013; Wyrofsky et al., 2019). Agonists of the cannabinoid receptors administered systemically or centrally increase LC tonic firing rate in anesthetized rats. This effect has been shown to be blocked by the selective CB1r antagonist SR 141716A (Mendiguren and Pineda, 2006; Muntoni *et al.*, 2006). Furthermore, inhibiting the enzyme fatty acid amide hydrolase (FAAH), the enzyme responsible for the hydrolysis of the eCB anandamide (AEA) with its selective blocker URB597, induces an increase in the spontaneous firing of LC-NE neurons (Gobbi *et al.*, 2005; Muntoni *et al.*, 2006). Therefore, both exogenous cannabinoids and endocannabinoids (eCBs) modulate LC-NE neural activity. Moreover, the LC is under tonic eCBs regulation: application of cannabinoid antagonist can slightly but significantly decrease LC activity. eCBs play a role in modulating specific inputs, indeed Muntoni

(Muntoni *et al.*, 2006) and colleagues showed that the application of CB1r agonists: WIN55212-2 or tetrahydrocannabinol (Δ^9THC) attenuates the inhibition on LC tonic discharged induced by the electrical stimulation of the GABAergic nucleus prepositus hypoglossi (PrH). Since the PrH provides strong inhibitory innervation to the LC (Aston-Jones *et al.*, 1986; Ennis and Aston-Jones, 1989; Kaur, Saxena and Mallick, 2001), it has been hypothesized that the counterintuitive positive effect of cannabinoid agonists on the LC-NE firing activity might be due to a "suppression of inhibition" effect (Muntoni *et al.*, 2006). This suppression of inhibition might be involved in LC neuron disinhibition from its tonic GABAergic control of firing discharge, demonstrated in various studies (Cherubini, North and Williams, 1988; Shefner and Osmanovic, 1991; Aston-Jones, Zhu and Card, 2004; Jin *et al.*, 2016; Breton-Provencher and Sur, 2019). This evidence, however, does not rule out the possibility that the eCB system in the LC plays an important role in shaping and modulating glutamatergic inputs or in the direct modulation of LC-NE neurons excitability acting post-synaptically.

Aims and Relevance

The LC is a highly integrative neuromodulatory nucleus. Therefore, investigating the synaptic physiology of noradrenergic neurons by focusing on how impinging inputs shape LC-NE neuronal activity is crucial to better characterize the behavioral importance of this small brainstem region. Anatomical evidence highlights how hundreds of brain regions send direct monosynaptic inputs to the LC (Schwarz *et al.*, 2015; Breton-Provencher and Sur, 2019). Nevertheless, it remains to be established how impinging inputs are integrated and modulated by local neuromodulators at the synaptic level. As shown in Martins' study (Martins and Froemke, 2015), unveiling the experience-driven synaptic adaptations occurring in a neuromodulatory nucleus such as the LC might shed light on a "synaptic plasticity cascade" induced by the release of NE in target brain regions. Amongst the brain areas sending projections to the LC, the Prefrontal Cortex (PFC) is considered to be one of the major glutamatergic cortical drive for NE neurons (Sara and Hervé-Minvielle, 1995; Jodo, Chiang and Aston-Jones, 1998). Whilst anatomical observations indicate direct monosynaptic projections from the PFC to LC (PFC→LC), functional evidence for this connectivity is still sparse. PFC→LC inputs might convey cognitive and affective information while providing "top-down" – or "executive" – control over LC activity. In this context, PFC projection might instruct the LC about general features of the environment to guide behavior in previously unseen circumstances. Hypothetically, the PFC could entrain LC neurons during goal-directed behavior to increase NE release upon the presentation of targets that have been pre-identified by PFC-dependent cognitive processes. Hence, PFC→LC projections might play an important role in preparatory attention and during complex cognitive tasks (Alnæs *et al.*, 2014; Unsworth and Robison, 2017). To fully elucidate the functional role of PFC→LC projections, it would be key considering not only the properties of the hardwired connections between these two regions but also plasticity mechanisms, which can modulate synaptic efficacy. These plasticity mechanisms can ultimately lead to changes in postsynaptic firing output upon exposure to relevant salient experiences, such as stress exposure, or during postnatal development when PFC complete maturation (Van Eden, Kros and Uylings, 1991; Caballero, Granberg and Tseng, 2016; Hodel, 2018). Notably, plasticity mechanisms occurring in the LC might be shaped by local neuromodulators, such as endocannabinoids (eCBs), and/or by neuromodulators released by long-range impinging inputs (long-range neuromodulators), such as Corticotropin-releasing factor (CRF) and Serotonin (5-HT), which are known to modulate LC-NE neuronal excitability (see: "*Cannabinoid role in*

regulating LC physiology" and "*LC, stress and the role of Corticotropin-Releasing Factor (CRF): between acute effects and long-lasting adaptations*").

To dissect the behavioral role of long-range neuromodulators, perturbing neuronal activity in neuromodulatory nuclei is key. Genetically encoded inhibitory optogenetic proteins are useful tools to dissect neural circuits without imposing artificial firing patterns. Currently available inhibitory optogenetic tools allow short and transient silencing of neurons, but they do not achieve long-lasting inhibition. Thus, there is the need for developing and validating novel optogenetic tools to provide sustained and reliable silencing of neural networks (Wiegert *et al.*, 2017).

In my PhD project, I have been testing the ***hypothesis*** that experience-dependent plasticity at PFC→LC inputs modulates action control, and that this modulation is shaped by the activity of local LC neuromodulators as well as by neuromodulators *via* long-range projections.

To test this hypothesis, I have been developing the following aims:

1. To define the direct PFC→LC connectivity by providing anatomical, functional and behavioral evidence.
2. To investigate synaptic mechanisms of plasticity at glutamatergic LC synapses, with a special focus on PFC→LC synapses.
3. To elucidate how these mechanisms of plasticity are modified in response to different forms of experience (e.g. plasticity induced by context adaptations/salient experiences and postnatal developmental plasticity). This will be instrumental in understanding how experience-dependent plasticity in the LC affects its NE output, goal-directed control of behavior, and the development of stress-related neuropsychiatric conditions in adulthood.

To develop the project, I combined neurophysiological, pharmacological and optogenetic approaches with behavioral paradigms. Furthermore, I validated a newly engineered genetically encoded light-activated potassium channels for long-lasting neuronal silencing of neuromodulatory brain nuclei (Alberio & Locarno *et al.*, 2018).

Results

Defining the PFC→LC input: in-vivo dissection

By using *in-vivo* electrophysiology in anesthetized adult mice [C57BL/6J mice; postnatal day (P) 60-75], we first investigated whether LC neurons were controlled by PFC projections at the single-cell level. To this purpose, I trained for few months at the laboratory of François Georges, Institut des maladies neurodégénératives (IMN), University of Bordeaux, where I performed single-unit recordings of firing evoked responses in LC neurons upon stimulation of the PFC (100 stimuli @0.5Hz 0.5-1.5 mA-500 µs) (**Figure 9 A, D**). Putative LC neurons were selected based on their single-unit wave-form duration (>1 ms; 1.06 ms-2.40 ms), slow tonic firing rate (0.75 Hz-3.55 Hz) (**Figure 9 B-C**), and by their response to nociceptive stimulation (contralateral paw-electrical stimulation - foot shock; 100 stimuli @0.5Hz 1-2 mA-500 µs), as previously described (Muntoni *et al.*, 2006) (**Figure 9 E**). In response to PFC electrical stimulation, we found that 44% of LC cells (11/25 single units) were orthodromically activated (**Figure 9 B**) with a short and reliable excitation latency (16.15 ms ± 1.62 ms), as expected for of a direct monosynaptic connection and consistent with previous observations in rats (Jodo, Chiang and Aston-Jones, 1998).

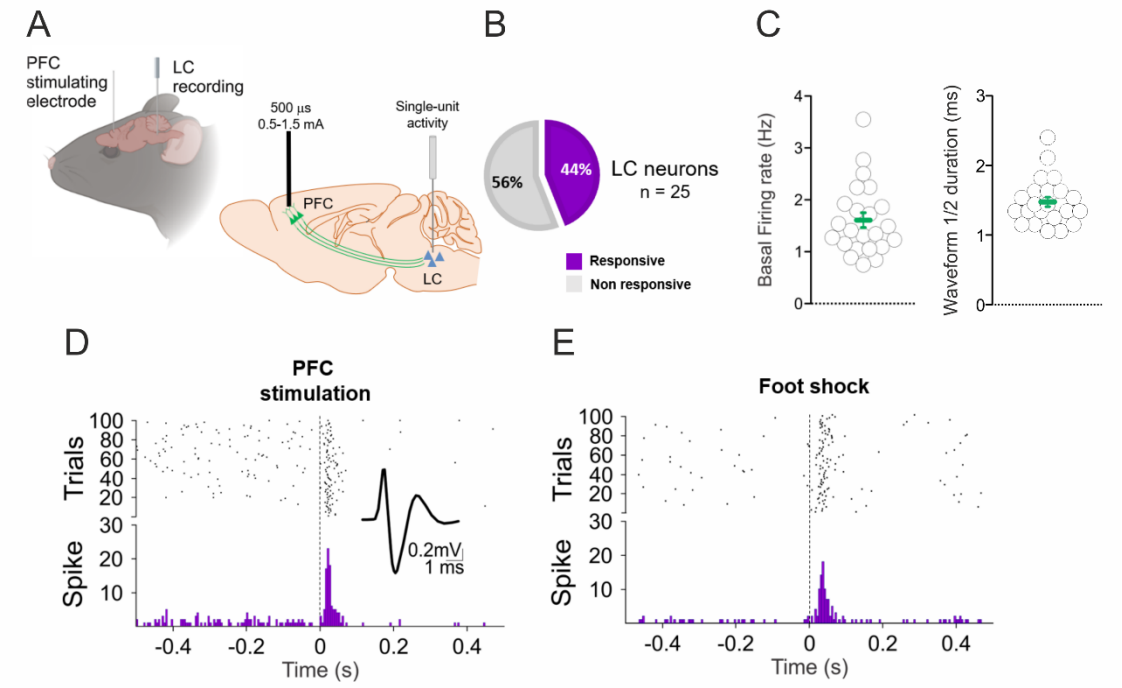

Figure 9 (A) Schematics illustrating the concomitant LC recording and PFC stimulation sites. (B) Pie-chart showing the percentage of LC neurons responding to PFC stimulation. (C, left) Scatter-plot of the basal firing rate of LC neurons (1.61 Hz ± 0.14 Hz, n=25). (right) Scatter-plot showing the distribution of waveform ½ duration (1.48 ms ± 0.07 ms, n=25). (D) Representative peri- stimulus histogram (PSTH) and raster-plot of a LC neuron activated by PFC stimulation. (inset) representative LC spike. (E) Representative PSTH and raster-plot of a LC neuron activated by Foot shock.

PFC→LC optogenetic activation drives Real-Time- and Conditioned-Place Preference

Next, we sought to assess the behavioral implications of PFC→LC connectivity. In collaboration with Dan Covey and Joseph Cheer (University of Maryland), we tested whether activation of this specific input has a positive or negative valence by combining optogenetic with the real-time place preference paradigm (Stamatakis and Stuber, 2013; Qi *et al.*, 2014).

P30-35 C57BL/6J mice were injected with a channelrhodopsin (ChR2) expressing virus combination [AAV1/2-CaMKIIa-Cre + AAV5-EF1a-DIO-ChR2(H134R)-eYFP] in the PFC while implanted with optical fibers in the LC, to deliver light stimulation (**Figure 10 A**). 6 weeks after viral injection, we detected a strong expression of the reporter-gene eYFP in the injection site as well as in the PFC terminals within the LC and peri-LC regions (**Figure 10 B**). To asses valence in response to stimulation of PFC→LC, animals were then tested in a 3 chambers real-time place-preference apparatus (3C-RTPP), in which they received trains of either 10Hz or 30 Hz (10 ms) light stimulation when they entered the laser-paired chambers; stimulation was stopped upon animal entry in the 0Hz chamber. This multifrequency design evaluates the bias for photostimulation and it allows comparing the effect of two different photostimulation frequencies at a time (Prus, James and Rosecrans, 2009; Qi *et al.*, 2014; Root *et al.*, 2014).

During day1-habituation session (Pre; 15 min), ChR2-expressing animals did not show preference for any of the three chambers ($\frac{time\ spent\ in\ one\ chamber}{total\ time} * 100$; 0Hz = 30% ± 1% versus 10Hz = 31% ± 1% versus 30 Hz = 34 ± 2% n=7; Tukey $p > 0.05$). Day2-photostimulation session (Stim1; 30 min) significantly increased the time spent in the 10 Hz light-paired chamber (0Hz = 26% ± 3% versus 10Hz = 37% ± 4% versus 30Hz = 32 ± 3% n=7; $p < 0.05$). Day3-photostimulation session (Stim 2; 30 min) resulted in mice exhibiting significant preference for both light-paired chambers (10 and 30 Hz) (0Hz = 20% ± 1% versus 10Hz = 42% ± 2% versus 30Hz = 33 ± 2% n=7; $p < 0.05$), although they still showed stronger preference for the 10Hz light-paired chamber (n=7; $p = 0.02$). Thus, stimulation of PFC→LC projections induces acute place preference. Furthermore, when tested in day4-post-test session (Post; 15 min), during which no photostimulation occurred, mice were still biased towards the previously light-paired chambers (0Hz = 22% ± 2% versus 10Hz = 44% ± 3% versus 30Hz = 32 ± 2% n=7; $p_s < 0.05$). This suggests that the activation of PFC→LC pathway produces a learned change in behavior (**Figure 10 C-D**). Locomotor activity did not differ among either stimulation frequencies or sessions (2Way ANOVA, n=7, $p>0.05$) (**Figure 10 E**).

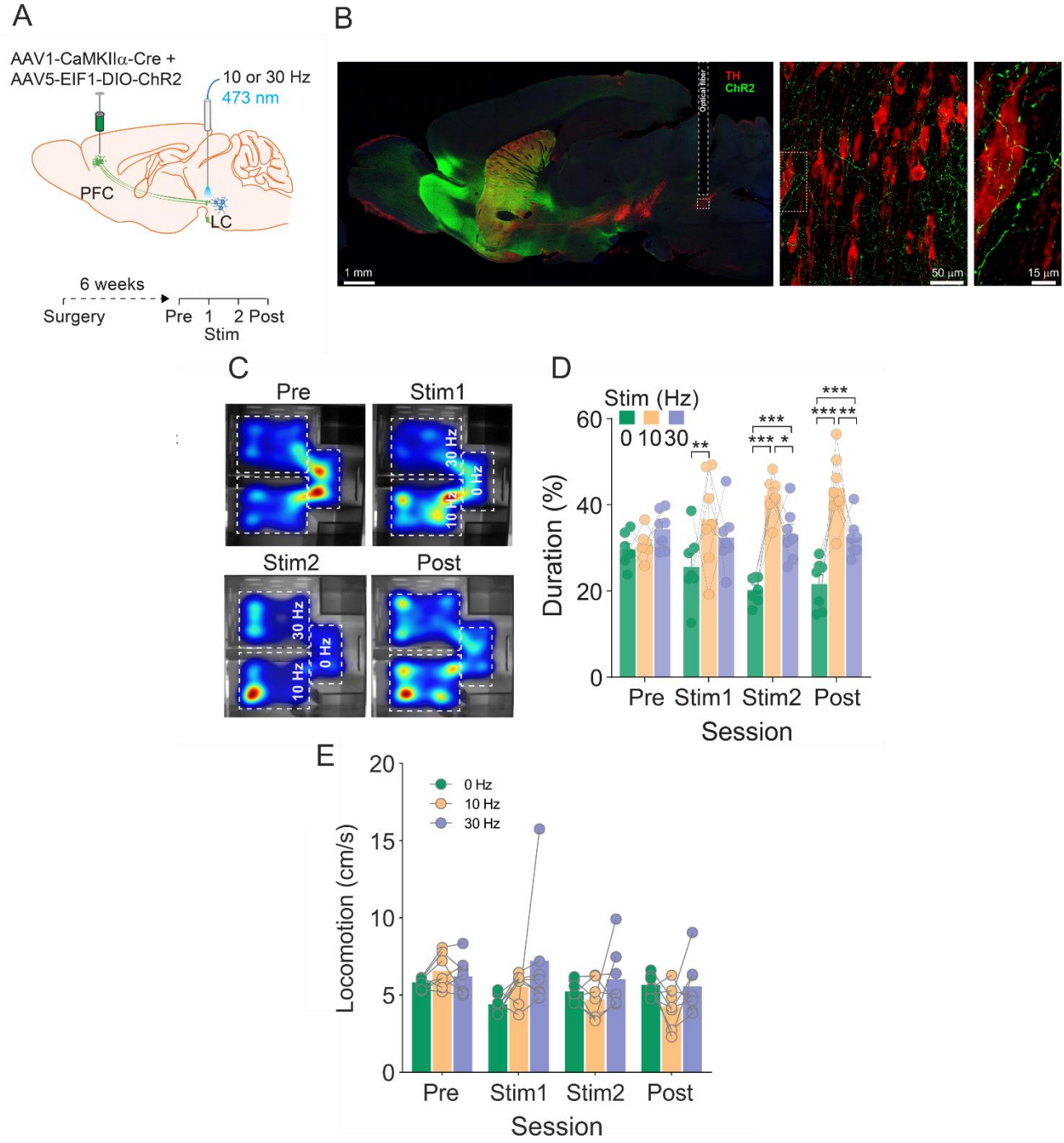

Figure 10 (A, top) Schematic of the viral injection in the PFC and the optic fiber implantation. (A, bottom) Time course of the experiment. Animals were injected with AAV1/2-CaMKIIa-Cre + AAV5-EF1a-DIOChR2(H134R)-eYFP and implanted with an optic fiber in the LC. 6 weeks after the surgery animal underwent 3chambers real-time place preference (3C-RTPP). (B) Representative immunofluorescent staining at different magnifications of a brain sagittal session showing the expression of Chr2-eYFP in the PFC (green) and the TH positive neurons (red). The dashed line represents the optic fiber track placed above the LC. (C) Representative heatmaps across the 4 different sessions. (D) Animals showed preference for the laser-paired chambers (2-Way ANOVA; n=7; Stim Frequency main effect, $F_{2,18}$= 20, p<0.0001). In the Pre-session animals did not show any preference for any of the three chambers (2-Way ANOVA; n=7; 0Hz vs 10Hz p=0.9; 0Hz vs 30Hz p=0.3; 10Hz vs 30Hz p=0.6; Tukey). During Stim1 animals increased the relative time exploring the 10Hz paired chamber compared to the others (2-Way ANOVA; n=7; 0Hz vs 10Hz p=0.004; 0Hz vs 30Hz p=0.1; 10Hz vs 30Hz p=0.4; Tukey). During Stim2, mice spent more time in the 2 laser-paired chambers (10-30Hz) (2-Way ANOVA; n=7; 0Hz vs 10Hz p<0.0001; 0Hz vs 30Hz p=0.0007; 10Hz vs 30Hz p=0.02; Tukey). During Post, animals maintained their preference for the photostimulated chambers (2-Way ANOVA; n=7; 0Hz vs 10Hz p<0.0001; 0Hz vs 30Hz p=0.006; 10Hz vs 30Hz p=0.003; Tukey). (E) Photostimulation did not affect the locomotor velocity at any stimulation frequency across different sessions (2-Way ANOVA; n=7, Stim Frequency main effect, $F_{2,18}$=2, p=0.1).

The 3C-RTPP results indicate that PFC→LC optogenetic activation induces both acute- and conditioned place preference, suggesting possible rewarding effect. Next, we asked whether this effect was sufficient to drive operant reinforcement in an optogenetic intracranial self-stimulation paradigm (o-ICSS) (**Figure 11 A**) (Lippert *et al.*, 2018; Covey and Cheer, 2019).

Mice that received the ChR2-viral infusion and optical implantation (**Figure 10 A**) were trained for 12 sessions to lever press for laser stimulation [2 sessions x day; Fixed Ratio-1 (FR1)] (**Figure 11 A**). During 30-minute sessions, both levers of the ICSS apparatus remained extended and no other cues were presented. Presses on one lever (active) produced immediate laser stimulation (1s, 10 or 30 Hz), while presses on the other lever (inactive) were collected but had no consequence. We found that training of optogenetic stimulation of PFC→LC connection was not sufficient to sustain operant reinforcement (< 10 active lever presses per 30 min sessions, n=7; Average responses across different sessions: $Active_{10Hz}$ = 3.4 ± 0.5; $Active_{30Hz}$ = 5.1 ± 0.7; $Inactive_{10Hz}$ = 0.9 ± 0.2; $Inactive_{30Hz}$ = 2.1 ± 0.3) (**Figure 11 B-C**). Mice showed a slight but significant higher number of active than inactive lever presses (3-Way ANOVA; n=7, p<0.0001), which might result from a cue effect provided by the photostimulation *per se.* To rule out this possibility, we are currently running o-ICSS and RTPP experiments in mice injected with the control [AAV1/2-CaMKIIa-Cre + AAV5-EF1a-DIO-eYFP] virus.

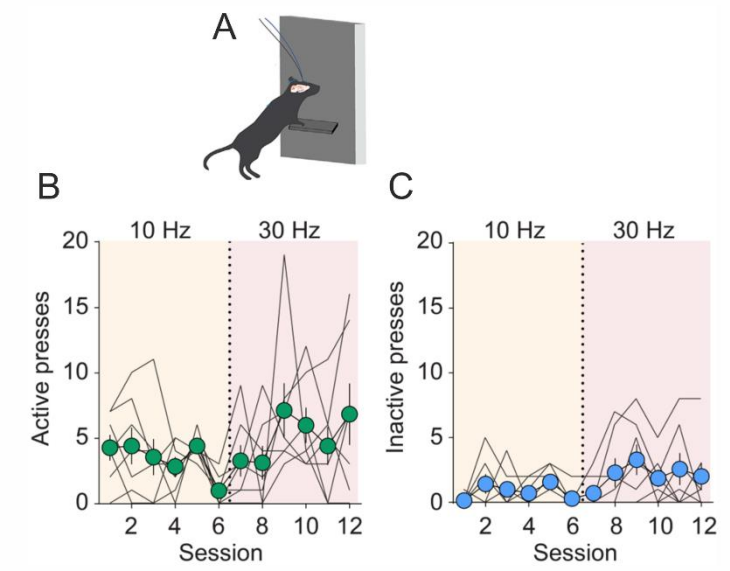

Figure 11 (A) Schematic representing the opto-Intracranial Self Stimulation paradigm (ICSS). Mice have to lever press in order to have LC→PFC opto-activation (1s, 10Hz or 30Hz). (B) Time-course of the active lever presses at 10Hz and 30 Hz across 12 sessions lasting 30min each (green dots). (C) Time-course of the inactive lever presses at 10Hz and 30 Hz across 12 sessions lasting 30min each. (B-C) Animals show a bias towards the active lever press, but performance did not change across sessions (3-Way ANOVA, n=7; lever main effect, $F_{1,5}$=37, p<0.0001; session main effect, $F_{5,5}$=1, p=0.4). Black traces represent the performance of each mouse.

Altogether these experiments suggest that PFC→LC inputs biases mice behavior. Upon PFC→LC input activation mice not only learn context associations but they can also recall this association. These effects point at long-term plasticity processes at this specific input.

Synaptic mechanisms of plasticity at LC glutamatergic synapses: ex-vivo brain slice recordings

The synaptic mechanisms of long-term plasticity in the LC are still largely unexplored. With the ultimate goal of dissecting plasticity at PFC→LC synapses, we specifically focused on timing-dependent plasticity, and in particular on t-LTD (Long-Term-Depression). This form of plasticity can be studied on *ex-vivo* brain slice preparations by applying a post-pre STDP paradigm, in which the postsynaptic spike precedes the presynaptic stimulation of a critical time window (Caporale and Dan, 2008; Feldman, 2012) (**Figure 12 A**). We targeted t-LTD as at several glutamatergic synapses the occurrence of t-LTD depends on the retrograde endocannabinoid (eCB) signaling and activation of the presynaptic cannabinoid 1 receptor (CB1), thereby on decreased release probability of glutamate (Gerdeman, Ronesi and Lovinger, 2002; Chevaleyre and Castillo, 2003; Chevaleyre, Takahashi and Castillo, 2006; Soler-Llavina and Sabatini, 2006; Chevaleyre *et al.*, 2007; Lafourcade *et al.*, 2007; Nazzaro *et al.*, 2012) (**Figure 12 B**). eCB-mediated plasticity is a fundamental means by which post-synaptic neuronal activity fine-tunes the synaptic gain at cortical afferents (Melis *et al.*, 2004; Gremel *et al.*, 2016; Mateo *et al.*, 2017), thus influencing the transmission of information relevant to behavior, including learning and retrieval of contextual memory associations (Zanettini *et al.*, 2011; Maroso *et al.*, 2016; Kruk-Slomka *et al.*, 2017).

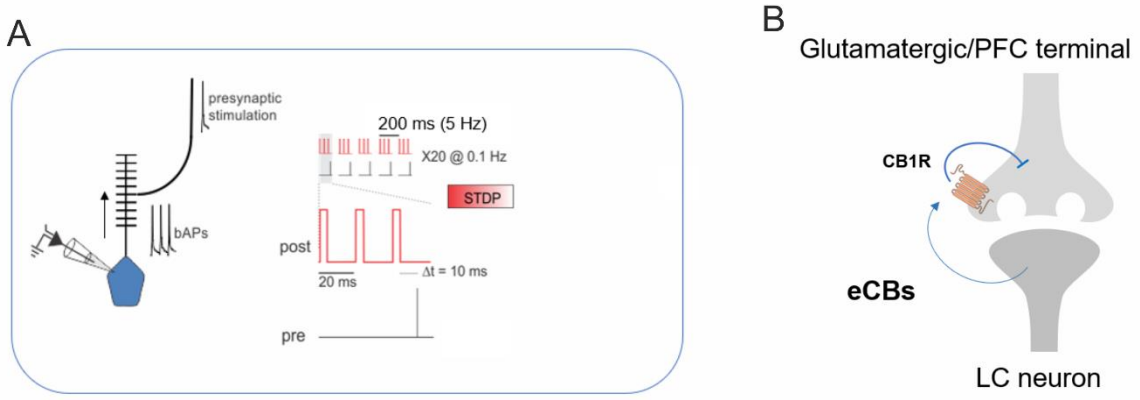

Figure 12 (A) Burst pairing protocol for the induction of the negative-STDP. The protocol consists of 20 bouts of EPSPs paired with action potentials, delivered 10 s apart. Each bout consists of five bursts (200 ms apart) each composed of three action potentials at 50 Hz followed by one EPSP (negative timing) (see also: "Materials and methods"). (B) Schematic representation of the eCB signaling. eCBs are produced postsynaptically then they travel retrogradely to decrease the presynaptic release of neurotransmitters acting on CB1R.

We initially measured plasticity at non-dissected glutamatergic-LC synapses, which include inputs from cortical regions and subcortical regions (e.g. Nucleus Paragigantocellularis, Paraventricular Nucleus). Norepinephrine (NE) containing neurons of the LC (NE-LC) were identified by their positions - near the IV ventricle-, their soma morphology (20-30µm along their major axis), and their tonic firing activity (Williams *et al.*, 1984; Sanchez-Padilla *et al.*, 2014) (**Figure 13 B**). After recording, LC cell identity was confirmed by immunostaining for the marker Tyrosine Hydroxylase (TH), a key enzyme for the biosynthesis of catecholamines, including NE (Axelrod, 1971) (**Figure 13 A**).

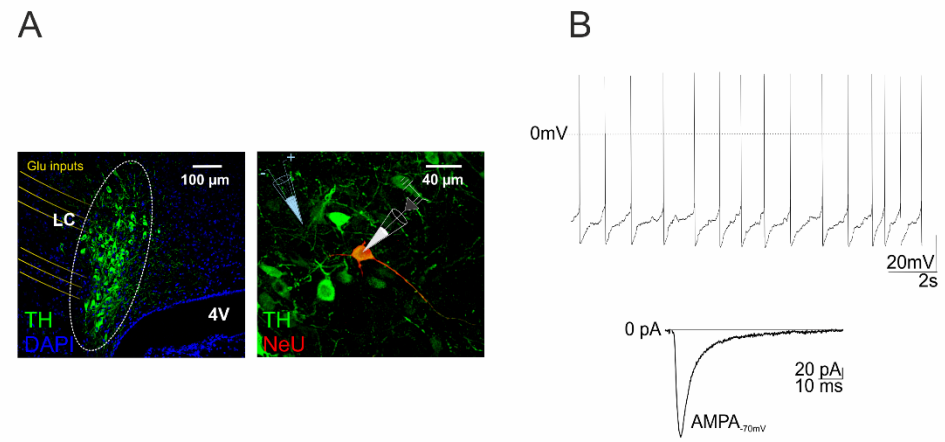

Figure 13 (A, left) Representative immunofluorescent staining of LC containing slice, in yellow are depicted the glutamatergic afferents to the LC. Tyrosine Hydroxylase (TH) in green and DAPI in blue. (A, right) TH staining in green and patched cell filled with Neurobiotin in red. A patch pipette is depicted in white, while a bipolar stimulator is represented in blue. Locus Coeruleus (LC). Fourth ventricle (4V). (B, top) Representative trace of a LC neuron tonic firing. (B, bottom) AMPA component of a representative electrically evoked EPSC.

On ex-vivo brain slices from P60-75 C57BL/6J mice, we recorded excitatory synaptic currents (EPSCs) in LC neurons upon the delivery of twin intra-LC stimuli, and in the presence of the GABAergic blocker gabazine (10 µM). The post-pre STDP protocol (**Figure 12 A**) resulted in LTD of postsynaptic currents (measured at the peak of the first response; 78% ± 6% of baseline n=7; $p < 0.05$; Tukey) (**Figure 14**). We found that t-LTD at glutamatergic-LC synapses is dependent on eCB-mediated signaling since it was blocked by the CB1R antagonist AM251 (4 µM) (119% ± 8% of baseline n=9; $p > 0.05$; Tukey) (**Figure 14 B**), as expected (Gerdeman, Ronesi and Lovinger, 2002; Chevaleyre and Castillo, 2003; Chevaleyre, Takahashi and Castillo, 2006; Soler-Llavina and Sabatini, 2006; Chevaleyre *et al.*, 2007; Lafourcade *et al.*, 2007; Nazzaro *et al.*, 2012). We also investigated the locus of plasticity expression by measuring paired-pulse ratio (PPR) of the twin synaptic responses, before and after the STDP protocol. t-LTD was associated with slight, but significant, increase in PPR, a hallmark of presynaptic plasticity ($^{5\text{-}10min}$Pre-STDP = 1.37 ± 0.16 versus $^{20\text{-}}$

^{25min}Post-STDP = 1.47 ± 0.17 ; $p < 0.05$; **Figure 14 C**). No changes in PPR were observed in the presence of AM251 ($^{5\text{-}10min}$Pre-STDP = 1.57 ± 0.16 versus $^{20\text{-}25min}$Post-STDP = 1.41 ± 0.10; $p<0.05$; **Figure 14 D**). Thus, these results suggest a presynaptic locus of plasticity expression, which is consistent with a canonical form of eCB-mediated t-LTD.

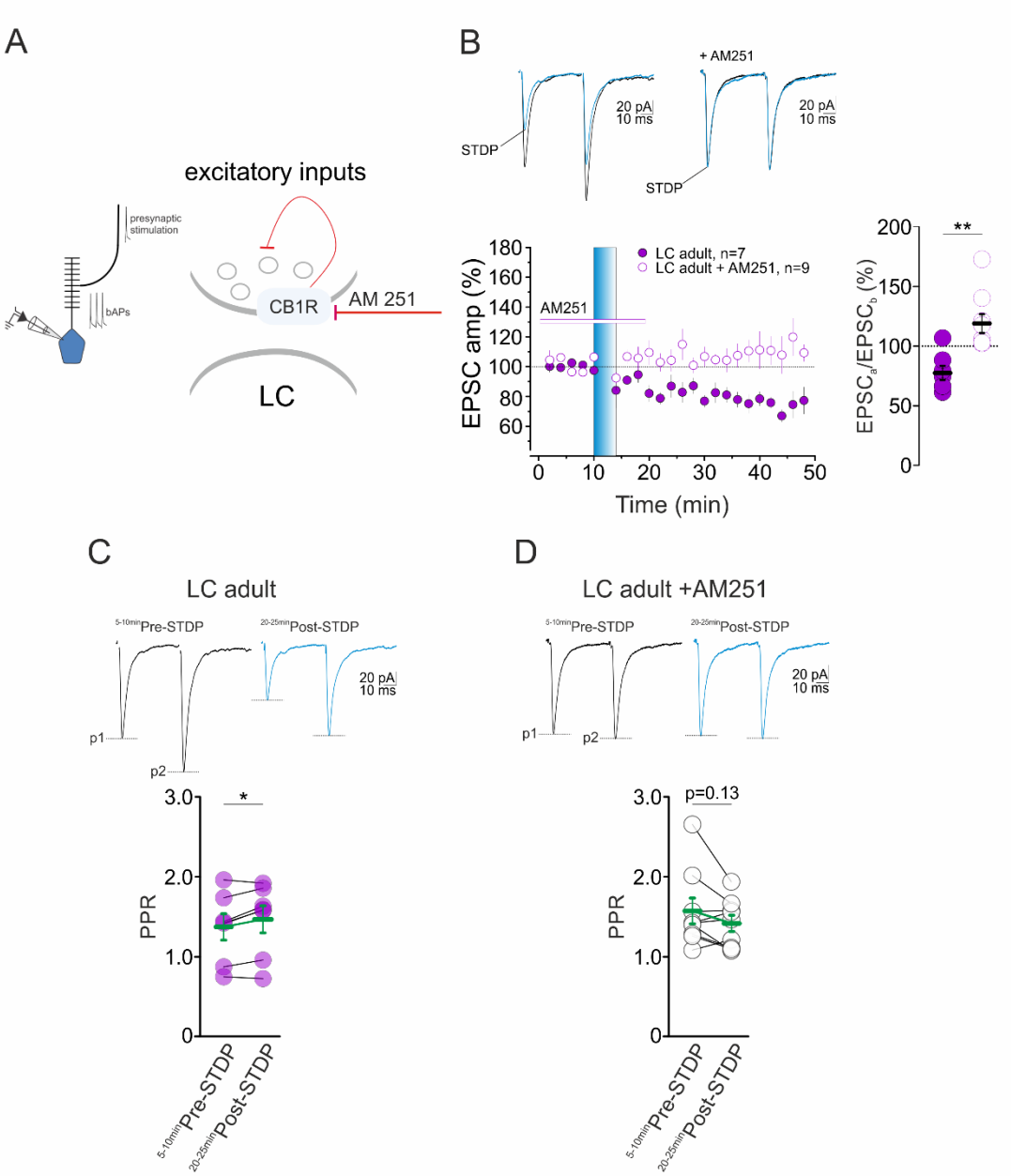

Figure 14 (A, left) Schematic of the experimental setting used to record EPSCs in LC-NE neurons. (A, right) Representation of the AM251-mediated CB1R antagonism. (B) In LC-NE cells, t-LTD was induced by the post-pre timing pairing (solid circles). In these neurons, bath perfusion of AM251 (4µM; empty horizontal bar) during the STDP was sufficient to prevent the t-LTD (empty circles) (LC adult; n=7 versus LC adult + AM251; n=9, p=0.03; Mann-Whitney test). (C) Scatter plot indicating the paired-pulse ratios of the last 5 min of baseline and 20-25 min after STDP. PPR was expressed as the ratio between the amplitude of the second (p2) and the first averaged EPSCs (p1) ($^{5\text{-}10min}$Pre-STDP versus $^{20\text{-}25min}$Post-STDP, p=0.04; 2tailed paired t-test). (D) AM251 Scatter plot indicating the paired-pulse ratios of the last 5 min of baseline and 20-25 min after STDP ($^{5\text{-}10min}$Pre-STDP versus $^{20\text{-}25min}$Post-STDP, p=0.13; 2tailed paired t-test). (C-D) Insets represent averaged recordings (30 traces) before (black) and after (blue) the delivery of the STDP protocol (blue vertical bar). Dots represent single paired values. The average value ± s.e.m. is represented by the green symbols.

(B) In these figures, and in the analogous plots that follow throughout the manuscript, data are presented as a time course (mean ± SEM) of normalized EPSC amplitudes. The EPSC time courses were obtained in presence of 10 µM gabazine, and in whole cell configuration. Scatter plot summarizes the ratios of synaptic responses 20-25min after (a) and 5-10min before (b) the STDP. Insets represent superimposed averaged recordings (30 traces) before (black) and after (blue) the delivery of the STDP protocol (blue vertical bar).

For synaptic plasticity to have functional consequences, it must ultimately influence firing activity in the postsynaptic neuron. To test whether eCB-tLTD affects the LC-NE neuronal output, we recorded excitatory evoked postsynaptic potentials (EPSPs). We delivered trains of ten stimuli (20 Hz) and set the stimulation intensity so that ~ 50% of EPSPs would result in action potentials (APs) (**Figure 15 A**). Change in the amplitude of the first EPSP positively correlated with the STDP-induced change in APs number (**Figure 15 B**), thus indicating that variation in synaptic strength translates into changes in output-firing in the post-synaptic NE neurons.

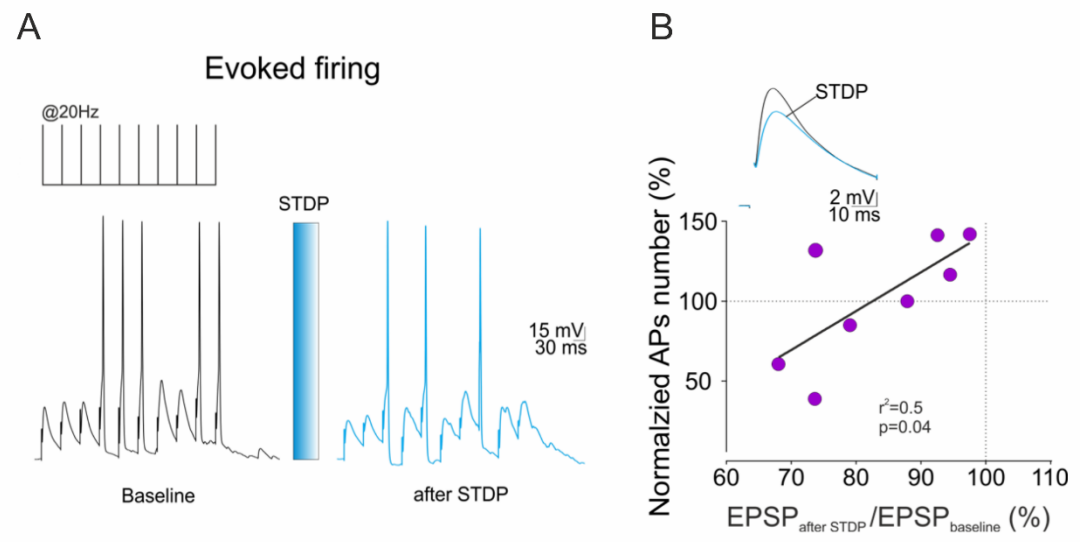

Figure 15 (A) Schematic represents the ten stimuli provided at a frequency of 20Hz. Sample traces showing a decrease in the APs number upon the delivery of the post-pre STDP. (B) Sample traces before (black) and after (blue) the post-pre STDP. Graph showing the correlation between normalized synaptically-driven firing and normalized EPSP peak (Pearson correlation, r = 0.71; p =0.04). Insets represent superimposed averaged recordings (30 traces) before (black) and after(blue) the delivery of the STDP protocol (blue vertical bar).

eCBs regulate synaptic plasticity at Prefrontal Cortex (PFC) inputs

So far, we provided evidence that eCB signaling, through the activation of CB1R, is involved in the induction of t-LTD at glutamatergic input to the LC. To dissect whether this plasticity mechanism occurs at PFC→LC synapses, we probed the LC-NE circuit with optogenetics. We bilaterally injected an adeno-associated viral (AAV) vector encoding ChR2-eYFP under the control of the CaMKIIa promoter [AAV5-CaMKIIa-ChR2(H134R)-eYFP] into the PFC of P30-35 C57BL/6J mice (**Figure 16 A**). 5-7 weeks after the injection, we obtained strong expression of the reporter fluorophore eYFP in the injection site as well as in PFC terminals in LC and peri-LC regions. On *ex-vivo* LC slices, short blue light pulses through the microscope objective (1 ms at 470 nm) elicited EPSCs (EPSCs-Opto$_{PFC}$) in NE-neurons. We investigated post-pre STDP at PFC→LC synapses by

monitoring EPSCs-Opto$_{PFC}$ before and after the induction protocol. During the post-pre pairing paradigm, the pre-synaptic EPSP was obtained by optogenetic stimulation of cortical terminals. In this experimental setting, the Opto$_{PFC}$-STDP induced a t-LTD of PFC→LC synapses (65 % ± 7 % of baseline n=7; $p < 0.05$; Tukey), thus recapitulating the LTD obtained at non-dissected glutamatergic synapses upon electrical stimulation (**Figure 16 B**). Consistent with this, $_{PFC}$t-LTD was dependent on eCB signaling since it was prevented in the presence of the CB1R antagonist AM251 (91 % ± 8 % of baseline n=9; $p > 0.05$; Tukey) (**Figure 16 B**).

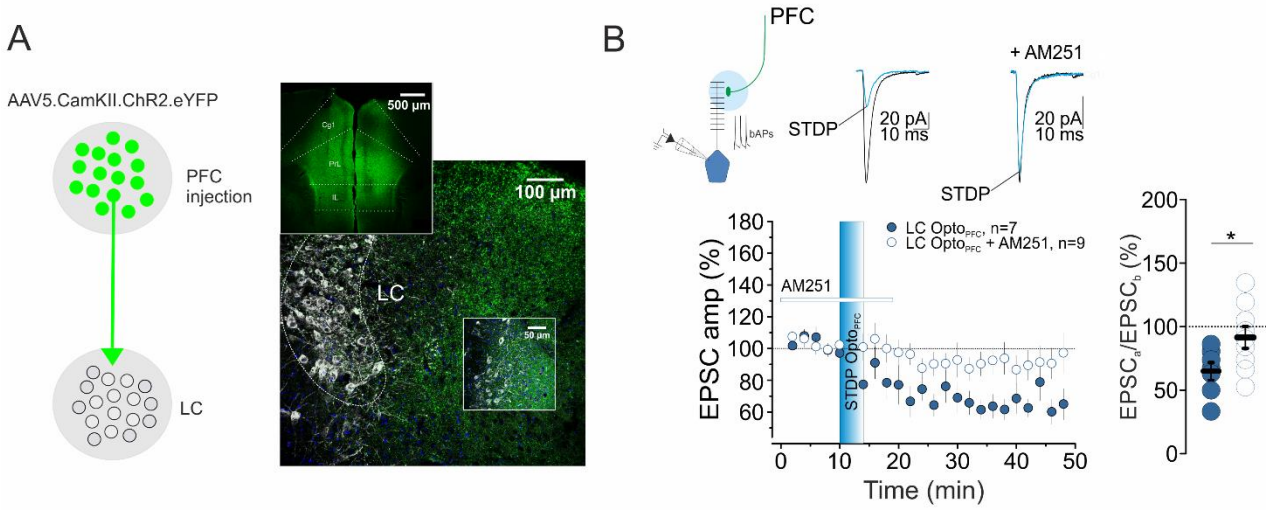

Figure 16 (A, left) Schematic of the injection site and (right) AAV5-CaMKIIa-ChR2(H134R)-eYFP expression targeting the PFC (inset), the LC and the peri-LC region. eYFP(green), TH (grey). (B, top, left) Schematic of the recording configuration in LC-NE neurons. (B, bottom, left) Time course and (B, bottom, right) scatter plot showing the LTD induced by the Post-pre pairing (solid circles), and (B, top, right) representative current traces. The CB1R antagonism by AM25 (4µM; empty horizontal bar) blunted the LTD elicited by the Opto$_{PFC}$-STDP (empty circles) (LC adult; n=7 versus LC adult + AM251; n=9, p=0.04; Mann-Whitney test).

Modulation of synaptic plasticity at PFC→LC inputs

We demonstrated that the eCB signaling is required for the induction of LC t-LTD in response to either electrical or optogenetic STDP paradigms, on *ex-vivo* brain slices. We next assessed the engagement of this plasticity mechanism *in-vivo*. To this purpose, we investigated how eCB-LTD is modified in response to two different forms of in-vivo experience: (I) exposure to context adaptations and salience experiences; (II) postnatal development, specifically the adolescence to adulthood transition.

(I) Experience salience modulates t-LTD at PFC → LC synapses

The PFC mediates behavioral responses to environmental changes (Fogelson *et al.*, 2009; Lenartowicz, Escobedo-quiroz and Cohen, 2010; Waskom and Wagner, 2017; Werchan and Amso, 2017). Also, in brain regions other than the LC, the eCB system acts as a dynamic regulator of adaptations to the environmental context and changes in CB1R function correlate with the salience of an experience (Wamsteeker, Kuzmiski and Bains, 2010; Cusulin *et al.*, 2014). We therefore assessed how t-LTD at PFC → LC is modulated by context habituation and by exposure to a novel, salient stressor.

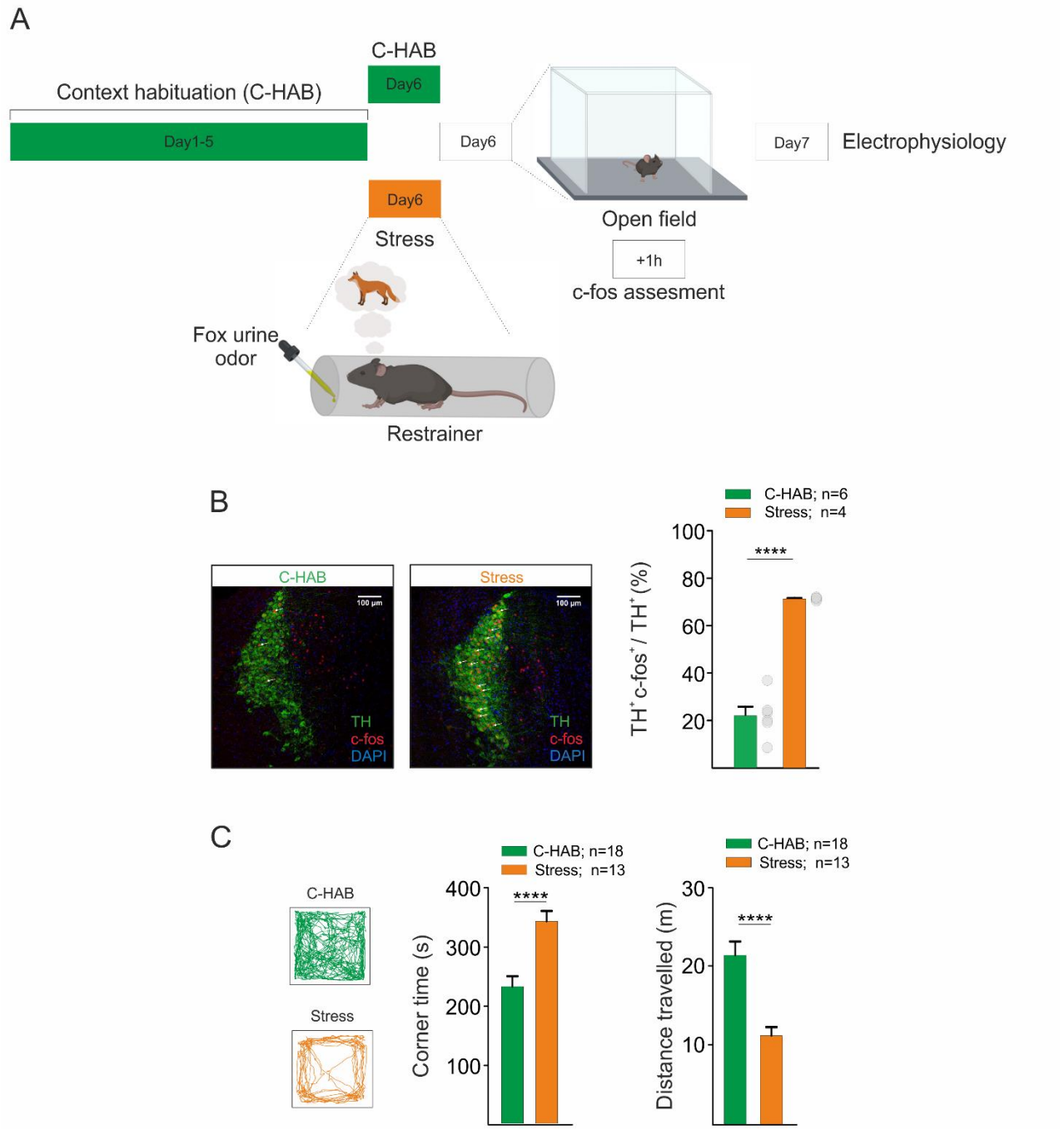

Figure 17 (A) Schematic showing the behavioral protocol used. Following 5 days of context habituation (C-HAB), animals underwent either an extra session of C-HAB or a novel stress exposure (Stress; restraint stress coupled to fox urine odor). Anxiety levels were scored in an open-field arena, then animals were sacrificed to evaluate c-fos activation in the LC. (B, left) Representative immunofluorescent c-fos staining of LC obtained by animals that underwent C-HAB or Stress. TH (green), c-fos (red), DAPI (blue), the arrows indicate c-fos$^+$-TH$^+$ neurons. (B, right) Percentage of TH$^+$-c-fos$^+$ neurons in C-HAB and Stressed animals (C-HAB n= 6 versus Stress n=4; p<0.0001; 2sided unpaired t-test). (C, left) Representative traces show motor behavior in C-HAB and Stressed animals. (C, middle) Scoring of the corner time (C-HAB, n= 18 versus Stress, n= 13; p<0.0001, 2sided unpaired t-test). (C, right) Scoring of the distance travelled (C-HAB, n= 18 versus Stress, n= 13; p<0.0001, 2sided unpaired t-test).

We subjected mice expressing ChR2 in the PFC→LC terminals (**Figure 16 A**) to either 6 days of context habituation (c-HAB group) or to 5 days of context habituation followed by simultaneous exposure to physical restraint and predator odor (Stress group; day 6; **Figure 17 A**) (Borodovitsyna, Flamini and Chandler, 2018; Borodovitsyna, Joshi and Chandler, 2018). 24 later, both groups underwent behavioral testing in an open-field arena (OFT) to measure anxiety-like behavior (Tye *et al.*, 2011; Seibenhener and Wooten, 2015; Borodovitsyna, Flamini and Chandler, 2018). To confirm the activation of LC neurons by stress compared to control conditions, a subset of mice from each cohort was sacrificed 1 hr. after the OFT. Brain sections containing the LC were prepared and co-immunostained for TH, while the expression of c-Fos was used as a proxy for neuronal activation (Bullitt, 1990; Perrin-Terrin *et al.*, 2016). Compared to C-HAB, we found that stress exposure significantly reduced the total distance traveled (C-HAB = 21.5 m ± 1.7 m, n= 18 versus Stress = 11.3 m ± 1.1 m, n=13; $p < 0.0001$) and increased the time spent in the corners (C-HAB = 233 s ± 17 s, n= 18 versus Stress = 343 s ± 18 s, n= 13; $p<0.0001$), indicative of anxiety-like behavior (**Figure 17 C**). This occurred in parallel to higher expression of c-Fos in the Stress group compared to C-HAB, as indicated by the significant difference in percentage of $c\text{-}fos^{+}/Th^{+}$ cells between the two cohorts (C-HAB = 22.1 % ± 3.75 %, n = 6 versus Stress = 70.5 % ± 0.3 % n = 4; $p < 0.0001$)(**Figure 17 B**).

Finally, we investigated the modulation of t-LTD at PFC→LC synapses in a second subset of C-HAB or Stress mice, 1 day after OFT. We found that $Opto_{PFC}$-STDP was impaired by context habituation (90 % ± 7 % of baseline, n=13; $p > 0.05$; Tukey) and restored upon stress salience (61 % ± 6 % of baseline n=6; $p < 0.05$; Tukey) (**Figure 18**). Together, these results indicate that, in the LC, changes in CB-mediated signaling capacity reflect experience-dependent modulation of PFC→LC synapses.

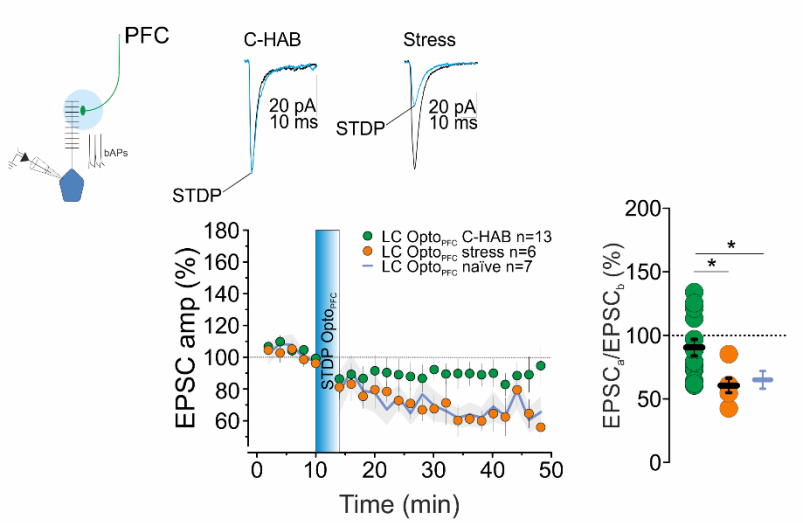

Figure 18 Schematic of the experimental setting used to record EPSCs-Opto$_{PFC}$ in LC-NE neurons. Time course and scatter plot showing that C-HAB (green dots) impairs t-LTD at PFC→LC synapses. Stress (orange dots) restores the t-LTD. The shadowed line shows the time course of plasticity from the LC Opto$_{PFC}$ group (Figure 15) (1WA; $F_{2,23}$=5.1; p=0.015; LC OPTO$_{PFC}$ C-HAB versus LC OPTO$_{PFC}$ Stress, p=0.023; LC OPTO$_{PFC}$ C-HAB versus LC OPTO$_{PFC}$ naïve, p=0.037; Dunnet). Insets represent superimposed averaged recordings (30 traces) before (black) and after (blue) the delivery of the STDP protocol (blue vertical bar).

(II) eCB-mediated plasticity at LC glutamatergic synapses is developmental regulated during the adolescent to adulthood transition.

Not only the eCB system shapes excitatory synaptic plasticity in LC neurons of adult mice (this study) but it plays a key role in modulating the developmental trajectories of the PFC during adolescent brain maturation (Ellgren *et al.*, 2008; Heng *et al.*, 2012; Meyer, Lee and Gee, 2018). This raises the possibility that eCB-mediated plasticity at PFC→LC synapses is developmentally regulated during the adolescent to adulthood transition. As an initial step to test this hypothesis, we investigated t-LTD at non-dissected glutamatergic synapses in the LC of young (P23-P28) mice in response to intra-LC electrical stimulation (Laviola *et al.*, 2003; Brust, Schindler and Lewejohann, 2015). Differently from adult mice (**Figure 14 D**), the post-pre STDP protocol resulted in LTP of postsynaptic currents (148 ± 17% of baseline; n=7; $p < 0.05$; Tukey) (**Figure 19 B**). Notably, this form of plasticity was still dependent on eCB signaling as it was sensitive to CB1R antagonism (AM251, 4 µM; 98 ± 10% of baseline n = 8; $p > 0.05$; Tukey) (**Figure 19 B**). Although no significant changes in PPR were associated with LTP induction ($^{5\text{-}10min}$Pre-STDP = 1.76 ± 0.16 versus $^{20\text{-}25min}$Post-STDP = 1.45 ± 0.11; p = 0.058) (**Figure 19 C**), we observed a trend towards a decreased in PPR, which would be consistent with increased glutamate release, thereby with LTP.

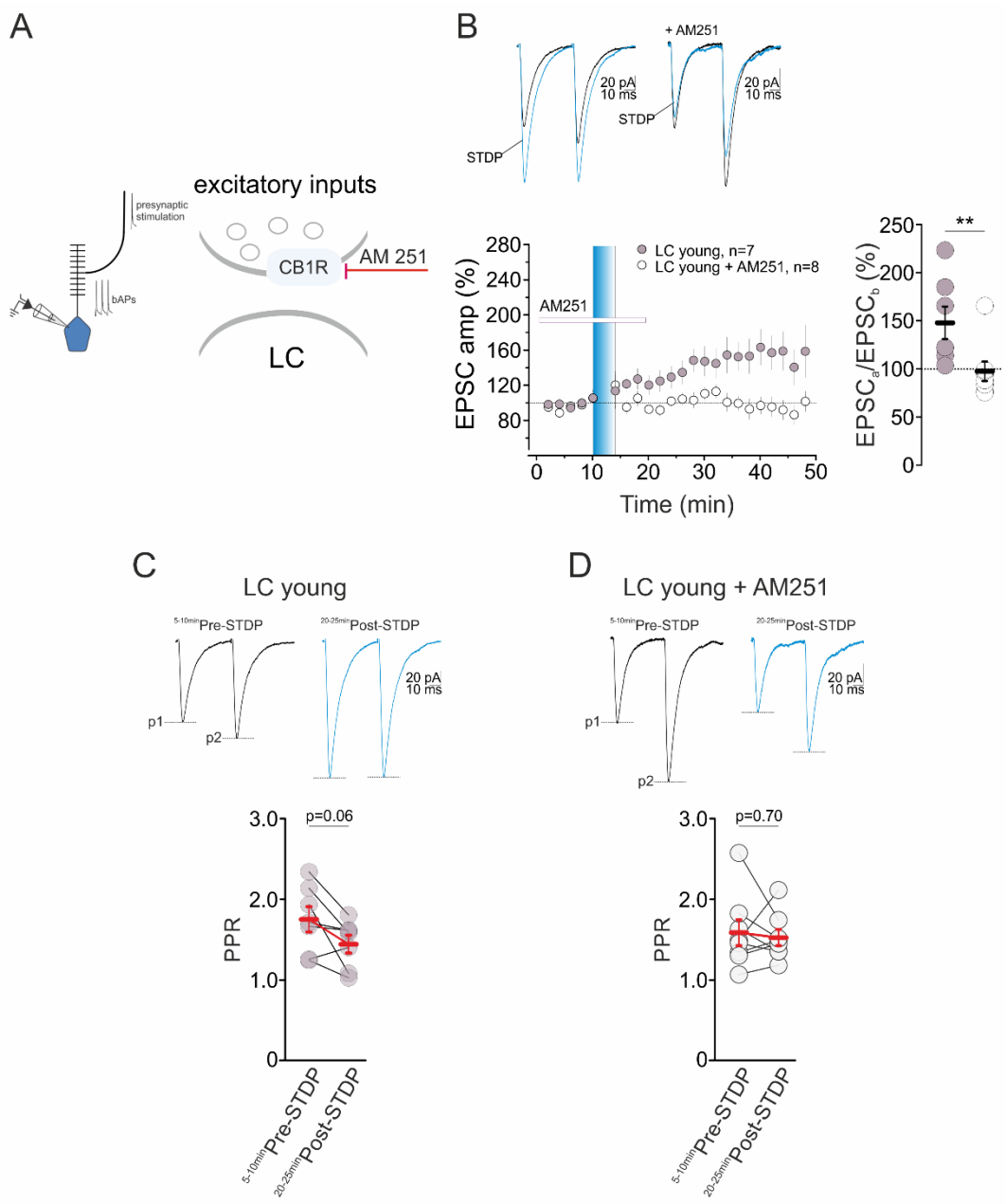

Figure 19 (A, left) Schematic of the experimental setting used to record EPSCs in LC-NE neurons. (A, right) Representation of the AM251-mediated CB1R antagonism. (B) In LC-NE neurons of young animals, t-LTP was induced by the post-pre timing pairing (solid circles). In these neurons, bath perfusion of AM251 (4µM; empty horizontal bar) during the STDP was sufficient to prevent the t-LTP (empty circles) (LC young; n=7 versus LC young + AM251; n=8, p=0.006; Mann-Whitney test). (C) Scatter plot indicating the paired-pulse ratios of the last 5 min of baseline and 20-25 min after STDP. PPR was expressed as the ratio between the amplitude of the second (p2) and the first averaged EPSCs (p1) ($^{5\text{-}10min}$Pre-STDP versus $^{20\text{-}25min}$Post-STDP, p=0.058; 2tailed paired t-test). (D) AM251 Scatter plot indicating the paired-pulse ratios of the last 5 min of baseline and 20-25 min after STDP ($^{5\text{-}10min}$Pre-STDP versus $^{20\text{-}25min}$Post-STDP, p=0.70; 2tailed paired t-test). (C-D) Insets represent averaged recordings (30 traces) before (black) and after (blue) the delivery of the STDP protocol (blue vertical bar). Dots represent single paired values. The average value ± s.e.m. is represented by the red symbols.

Previous studies described uncanonical forms of eCB-mediated LTP (Cachope *et al.*, 2007; Lin *et al.*, 2011; Xu, Zhang and Chen, 2012; Cui *et al.*, 2016; Wang *et al.*, 2016; Maglio *et al.*, 2017; Cui, Perez and Venance, 2018; Xu *et al.*, 2018). Nevertheless, the majority of these plastic phenomena rely upon GABAergic disinhibition mechanism (Carlson, Wang and Alger, 2002; Chevaleyre and Castillo, 2004; Lin *et al.*, 2011; Xu, Zhang and Chen, 2012; Silva-Cruz *et al.*, 2017). This is not the case in our experimental settings, as recordings were performed in the presence of a $GABA_A$ receptor antagonist (Gabazine 10 µM). Change in synaptic plasticity rules (i.e. the switch between t-LTD and t-LTP in response to the same stimulating protocol) may also depend upon the activity of long-range neuromodulators (Cachope *et al.*, 2007; Yang and Dani, 2014; Brzosko *et al.*, 2017; Xu *et al.*, 2018; Brzosko, Mierau and Paulsen, 2019), which might differ between young and adult mice. In the LC, intra-LC electrical stimulation is likely to recruit projections from the Central Nucleus of the Amygdala (CeA), which releases Corticotropin-releasing factor (CRF) (Van Bockstaele, Colago and Valentino, 1998; McCall *et al.*, 2015). In the LC-NE neurons, CFR binds the CRF1 receptor (CRF1R) (Jedema and Grace, 2004; Reyes *et al.*, 2006), which is coupled to Gs-signaling pathways. Activation of CRF1R has been shown triggering synaptic potentiation in other brain regions (Blank *et al.*, 2002; Pollandt *et al.*, 2006; Krishnan *et al.*, 2010). We, therefore, reasoned that the functional interplay between CRF release and eCB mobilization in response to

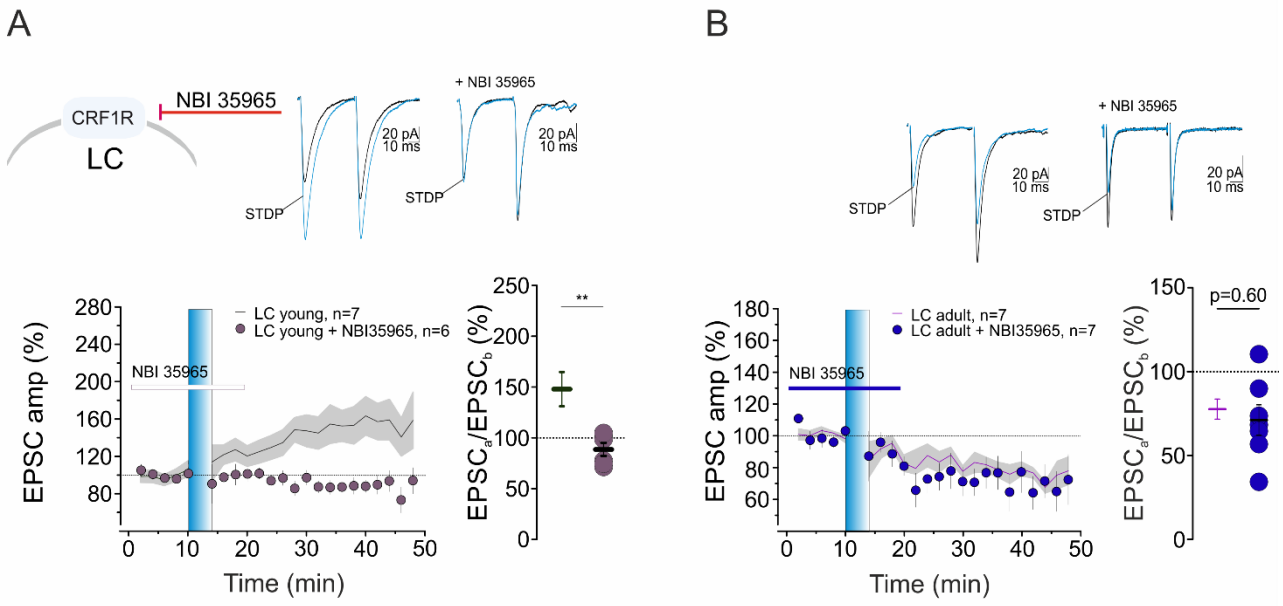

Figure 20 (A, left) Representation of the NBI 35965-mediated CRF1R. (A, bottom) antagonism Perfusion of the CRF1R selective antagonist NBI 35965 (1 µM; empty horizontal bar) prevented the STDP-LTP in young animals (LC young; n=7 versus LC young + NBI 35965; n=6, p=0.005; Mann-Whitney test). (B) NBI 35965 (1 µM; solid horizontal bar) was unaffecting on the adult animal LTD (LC adult; n=7 versus LC adult + NBI 35965; n=7, p=0.60; Mann-Whitney test). (A-B) The shadowed line shows the time course of plasticity from the young animal group of Figure 19 (B) and the adult animal group of Figure 14 (B).

presynaptic activity could be developmentally regulated in the LC. To test this, we blocked the activity of CRF1R during the post-pre STDP protocol by using the selective antagonist NBI 35965 (Million *et al.*, 2003; Kosoyan, Grigoriadis and Tache, 2005) (**Figure 20**). CRF1R antagonism was sufficient to impair t-LTP induction (NBI 35965, 1 µM (Ma *et al.*, 2013); 89% ± 6% of baseline; n=6; $p > 0.05$; Tukey) (**Figure 20 A**) in young mice whereas it had no effects on t-LTD induced in adult animals (71% ± 9% of baseline; n=7; $p < 0.05$; Tukey) (**Figure 20 B**).

Opto$_{PFC}$-STDP induces eCB-LTD at PFC→LC synapses of young animals

In young animals, to investigate whether the LTP observed at non-dissected excitatory LC synapses also occurs at dissected PFC→LC synapses, we injected an adeno-associated viral (AAV) vector encoding ChR2-eYFP under the control of the CaMKIIa promoter [AAV9-CaMKIIa-ChR2(H134R)-eYFP] into the PFC of P0-3 C57BL/6J mice; we opted to the AAV serotype 9 for infection of mouse pups as we observed that this virus type has a higher infection yield compared to AAV serotype 5 at this post-natal age. (Passini *et al.*, 2003) (data not shown). At P23-28, we detected eYFP expression in the PFC injection, in the peri-LC area, and in the LC (**Figure 21 A**). Differently from electrical STDP that resulted in LTP of synaptic responses (**Figure 19 B**), the Opto$_{PFC}$-STDP induced t-LTD at PFC→LC projections of young mice (61% ± 7% of baseline; n=8; $p < 0.05$; Tukey) (**Figure 21 B**). On-going experiments are investigating the role of eCBs in this form $_{PFC}$t-LTD as well as the mechanisms underlying the dichotomous behavior of non-dissected and dissected PFC→LC synapses in response to electrical and opto-STDP paradigms, respectively (see Project implementation and Discussion).

Collectively, this evidence suggests that eCB-mediated plasticity is developmentally regulated during the adolescent to adulthood transition, thus further supporting the engagement of this plasticity mechanism *in-vivo*.

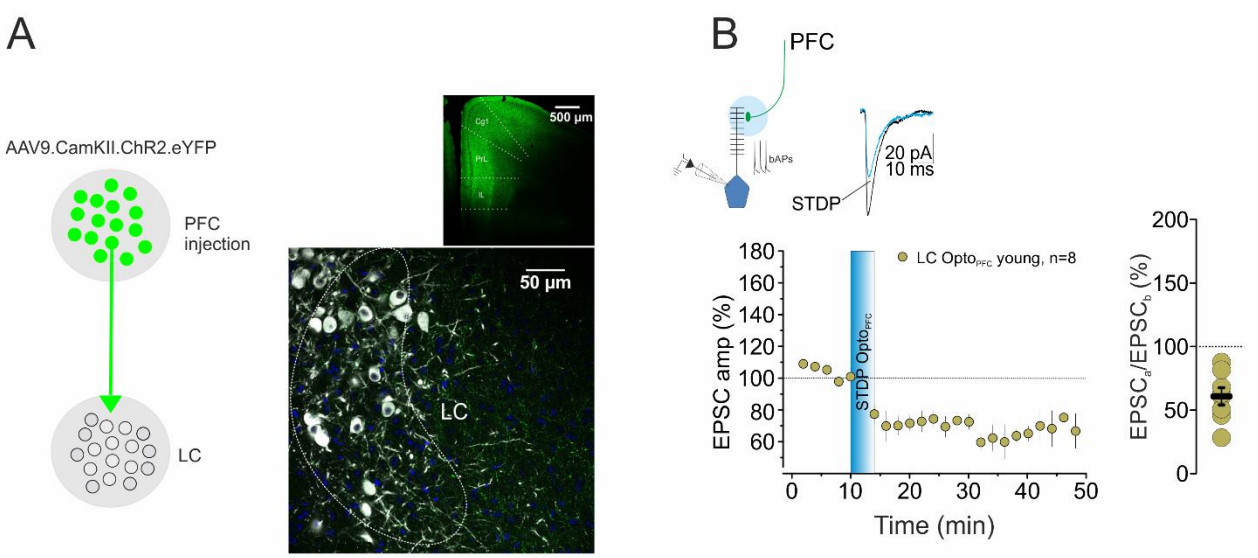

Figure 21 (A, left) Schematic of the injection site and (right) AAV9-CaMKIIa-ChR2(H134R)-eYFP expression targeting the PFC (inset), the LC and the peri-LC region. eYFP (green), TH (grey). (B, top, left) Schematic of the recording configuration in LC-NE neurons. (B, bottom, left) Time course and (B, bottom, right) scatter plot showing the LTD induced by the Post-pre pairing (solid circles) (RM1WA; $F_{7,20} = 1.66$; $p = 0.047$; $n = 8$; Tukey), and (B, top, right) representative current traces.

Project Implementation

The main findings of our study can be summarized as

1) Optogenetic activation of PFC→LC inputs supports the expression of place preference together with learning and retrieval of context associations (**Figure 10**).
2) Plasticity at PFC → LC projections relies on eCB-mediated signaling capacity (**Figure 16**), which is dynamically regulated by context adaptations and salience experiences (**Figure 18**; **Figure 21**).

Project implementation requires establishing synaptic causalities between eCB-mediated modulation of PFC→LC inputs and place conditioning as well as elucidating how this modulation affects the LC noradrenergic output during naturalistic forms of behavior that are dependent on the PFC (i.e. working memory, social interaction, task switching, etc.).

Establishing a direct role of CB1R at PFC→LC synapses in the expression and acquisition of place preference

- To establish the involvement of eCB-mediated modulation of PFC→LC inputs in the expression of real-time place preference and/or in the learning conditioned place preference (3C-RTPP test), we are currently applying an "occlusion" strategy. Specifically, if eCBs/CB1R-mediated signaling is engaged during the place preference paradigm the subsequent *ex-vivo* induction of eCB-LTD at PFC→LC synapses will be disfavored, at least immediately after the behavioral testing. The occurrence of eCB-LTD will be evaluated either upon the Stim1 session, for assessing the contribution of eCB signaling in the expression of real-time place preference or following the post-stimulus session for testing its contribution in learning or retrieving of contextual memory associations.

- To test whether it is sufficient to block the function of CB1R to prevent the expression and/or acquisition of place preference induced by stimulation of PFC→LC synapses during the 3C-RTPP paradigm, we will delete CB1R in the PFC by using a conditional approach. The PFC-CB1R deletion will be obtained by injecting the CRE and ChR2 virus combination [AAV1/2-CaMKIIa-Cre + AAV5-EF1a-DIOChR2(H134R)-eYFP] in the PFC of homozygous CB1 floxed animals (CB1 Flox/Flox; $Cnr1^{tm1Ltz}$) (Marsicano *et al.*, 2002) implanted with optical fibers in the LC, as before (**Figure 10 A**). This viral approach will allow deleting CBR1 in the PFC, thus also at PFC→LC projections. Although this viral strategy will result in CB1R deletion in all PFC target regions, by optogenetic stimulating

PFC→LC terminals during 3C-RTPP paradigm we will gain behavioral insights into the role of CB1R expressed at this specific input.

Investigating the role of CB1R at PFC→LC inputs in a PFC-dependent naturalistic behavior: the 5-choice serial reaction time task

While the 3C-RTPP is an effective behavioral paradigm to evaluate the positive or negative valence associated with the activation the PFC→LC inputs, it implies the artificial optogenetic stimulation of these projections, possibly enforcing eCB-release from LC neurons. To get insights on the physiological role of eCB-mediated modulation of PFC→LC inputs we will test how deletion of CB1R at this input will affect a behavioral task that relies on PFC activation. To achieve CB1R deletion the PFC→LC projections we will implement an intersectional viral approach (Kakava-Georgiadou *et al.*, 2019) in which CB1R deletion is dependent on a retrograde CRE-expressing FLP-dependent virus injected in the LC (retroAAV-EF1a-FRT-CRE) and a Flp recombinase expressing virus injected in the PFC of CB1 Flox/Flox mice. CB1R PFC→LC-deleted mice (PFC→LC-CB1R-KO) will be tested in the 5-choice serial reaction time task (5-CSRTT), which involves PFC functional activity and noradrenergic signaling (Liu *et al.*, 2009; Economidou *et al.*, 2012; Fitzpatrick *et al.*, 2018).

Collectively, these experiments will stride towards a better understanding of the behavioral role of the eCB system at the PFC→LC inputs, thus overcoming inferences associated with optogenetic stimulation of this pathway.

Exploring NE dynamics upon CB1R deletion

Our data indicate the eCB system modulates PFC→LC synapses (**Figure 16**; **Figure 21**). We hypothesize that eCB-mediated LTD at PFC to LC inputs represents a key a feedback mechanism to regulate the reciprocal connectivity between the PFC and the LC, as this plasticity mechanism would limit the cortical drive of the LC, ultimately shaping the spatial and temporal dynamic profile of NE release in the cortex. This type of regulation might be critical in the trade-off between exploration and exploitation (Aston-Jones and J. D. Cohen, 2005; Jepma *et al.*, 2010), for example upon stress exposure, or for tuning the behavioral responses to salience experiences.

To assess how CB1R expressed at PFC→LC inputs shape NE release in LC target regions, we will image the signal dynamic of a genetically encoded NE sensor ($GRAB_{NE}$; Feng *et al.*, 2019) by using fiber photometry in freely-moving mice. Our findings indicate that photoactivation of the PFC→LC pathway sustains learning and retrieval of contextual associations (**Figure 10**). Therefore, we will

image NE signal not only in the PFC but also in the Hippocampus (Preston and Eichenbaum, 2013), because of its role in contextual memory (Smith and Bulkin, 2014). We expect to observe deregulation of NE levels in target regions upon the deletion of CB1R at PFC→LC connection. Since eCB signaling modulates neuronal activity *on-demand*, we expect to find deregulation of NE levels together with impairment in behavioral performances only when PFC→LC-CB1R-KO mice are engaged in a task that strongly requires PFC→LC connection activation. Therefore, we will test how the eCB system finely tunes LC activity during the 5-CSRTT, which requires frontal-cortex entrainment (Robbins, 2002; Benn and Robinson, 2014).

Validation of a novel optogenetic tools to manipulate neuromodulatory projections to the LC: the genetically encoded light-activated K^+ channel (BLINK2)

Results obtained during project development indicate that experience-dependent plasticity at PFC→LC inputs is shaped by the activity of local LC neuromodulators (i.e. eCB) as well as by neuromodulators via long-range projections (i.e. CRF). With the ultimate goal of resolving the behavioral function of long-range neuromodulatory projecting to the LC at cellular resolution, I devoted part of my PhD to validate novel optogenetic tools for sustained neuronal silencing. In collaboration with Anna Moroni (Department of Biosciences, University of Milano, Italy), we developed a viral-based strategy for the neuron-specific expression of a newly engineered, genetically encoded light-activated K^+ channel (BLINK2).

In Alberio & Locarno et al., (2018), by means of electrophysiological and optogenetic approaches (ex-vivo and in-vivo) we have tested the ability of BLIN2 of silencing neurons in different neuronal subtypes (Alberio & Locarno, et al., Nature Methods, 2019; see also Appendix). The combination of large unitary conductance and prolonged light-off activity of BLINK2 allows cellular inhibition in a time range inaccessible to other inhibitory tools, such as eNpHR3.0 (Wiegert *et al.*, 2017).

BLINK2 in brief

Given the universal role of K^+ conductances in the termination of action potentials and their major contribution to the resting potential, there is interest in engineering light-gated K^+ channels. The Laboratory of Anna Moroni previously engineered BLINK version 1 (BLINK1) (Cosentino *et al.*, 2015), in which a LOV2 photoreceptor domain (Christie, 2007; Christie *et al.*, 2012) reversibly controls a K^+ channel (KcvPBCV1) (Plugge *et al.*, 2000) in response to blue light (455 nm) (Cosentino *et al.*, 2015). BLINK1 has favorable properties for optogenetics: a low light requirement that avoids tissue heating and damage, a large unitary conductance (>100 pS) to counteract excitatory currents, and a lack of inactivation during prolonged illumination. In vivo experiments with zebrafish embryos highlighted the use of BLINK1 as an inhibitory tool. However, BLINK1 has low surface expression, especially in mammalian neurons, which hampers its wider use. To improve the surface expression of BLINK, signal sequences that promote forward trafficking in eukaryotic K^+ channels (Gradinaru *et al.*, 2010) have been added to the BLINK1 C-terminal. Specifically, BLINK2 has the same topology as BLINK1 and the C terminus of the KAT1 sequence that ends with the binding motif ^{673}YFSDN^{677} for 14-3-3 proteins, a class of adaptors that promote KAT1 surface expression (Saponaro *et al.*, 2017).

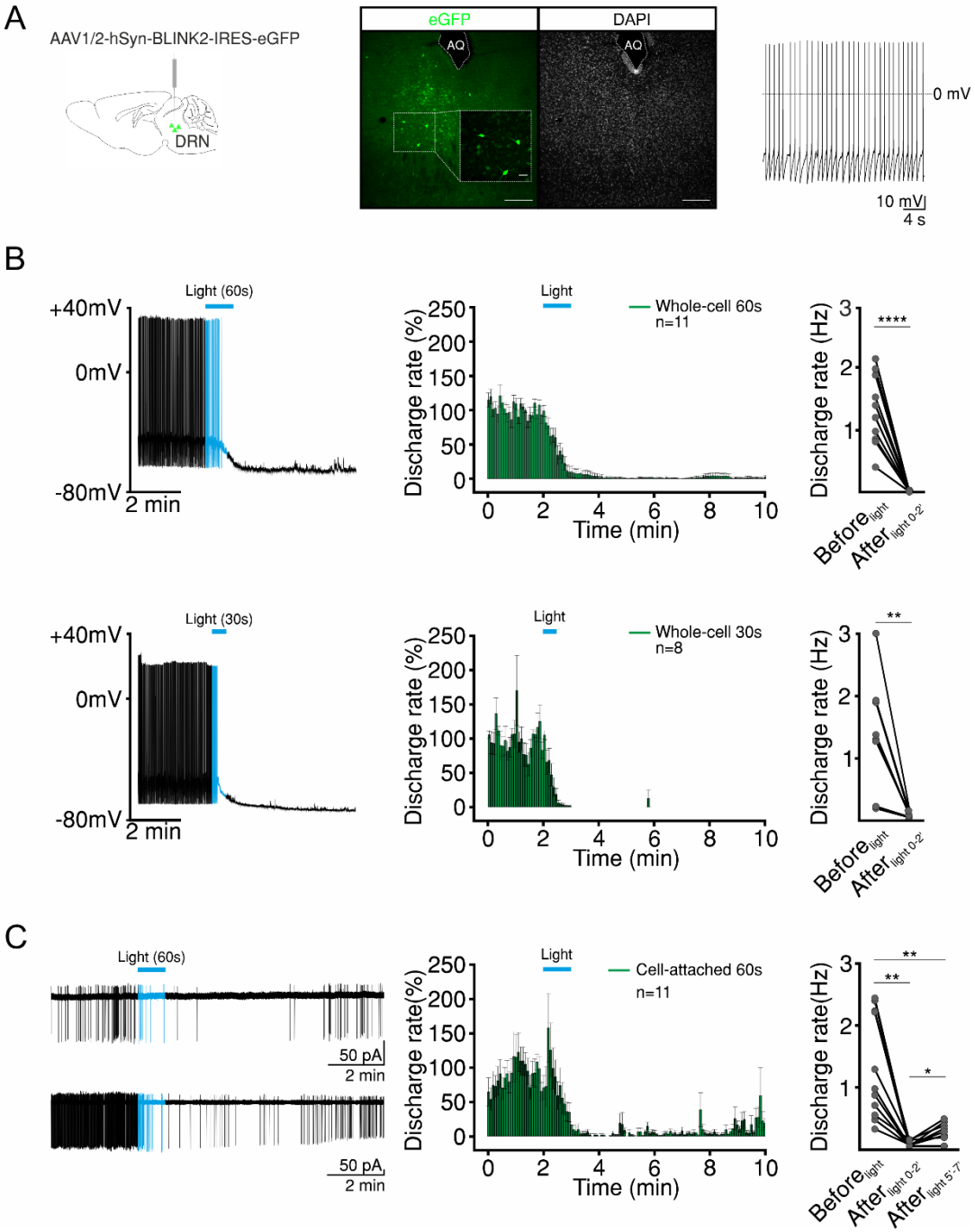

Figure 22 (A, left) Diagram indicating the virus injection site. (middle) sample confocal image showing expression of the AAV1/2-hSyn-BLINK2-IRES-eGFP virus in the mouse DRN (green, GFP; gray, DAPI). Scale bars, 200 µm or 40 µm (inset). AQ, aqueduct. Right, representative current-clamp recording of tonic firing activity in DRN GFP$^+$ neurons. (B, left) representative whole-cell current-clamp recordings of the firing response before and after 60 s (top) and 30 s (bottom) of blue light stimulation (top, n = 11; bottom, n = 8). (middle) Effect of 60 s (top) and 30 s (bottom) of blue light stimulation (blue bar) on the firing rate (5-s binning). (right) summary plots indicating the mean firing discharge rate 2 min before light (Before$_{light}$; baseline) and 2 min after light-off (After$_{light\ 0–2'}$) (60 s, Before$_{light}$ versus After$_{light\ 0–2'}$, n = 11, p < 0.0001, 2sided paired t-test; 30 s, Before$_{light}$ versus After$_{light\ 0–2'}$, n = 8, p = 0.004, 2sided paired t-test). c, Left, representative cell-attached voltage-clamp recordings of firing responses before and after 60 s of blue light stimulation (blue bar) (n = 11 independent recordings). (middle) Time course of the effect of 60 s of blue light stimulation (blue bar) on the firing rate (5-s binning). Right, summary plot indicating the mean discharge rate 2 min before light (Before$_{light}$) and at 2 (After$_{light\ 0–2'}$) and 5 (After$_{light\ 5'–7'}$) min after the end of light exposure (n = 11; RM1WA, $F_{10,2} = 22$, p = 0.0007; Before$_{light}$ versus After$_{light\ 0–2'}$, p = 0.002; Before$_{light}$ versus After$_{light\ 5'–7'}$, p = 0.003; After$_{light\ 0–2'}$ versus After$_{light\ 5'–7'}$, p = 0.02; Tukey). Blue light (470 nm, 8.7 mW/mm^2).

BLINK2 validation on ex-vivo brain slices

To test neuronal silencing by BLINK2 in brain slices, we injected the AAV-hSyn-BLINK2- IRES-eGFP virus in the dorsal raphe nucleus (DRN) of the midbrain (**Figure 22 A**). We selected the DRN for the tonic activity of its neurons and for the known neuromodulatory projections to the Locus Coeruleus (LC) (Segal, 1979; Kim *et al.*, 2004). BLINK2-expressing neurons (GFP^+) recorded at the soma in the dark showed basal tonic firing (0.2–7 Hz, **Figure 22 A**), similar to the activity in untransfected acute DRN slices (Mlinar *et al.*, 2016; Giorgi *et al.*, 2017). After transfection with a control GFP-expressing virus (AAV1/2-hSyn-eGFP), none of the recorded cells (n=7) showed inhibition of firing activity (**Figure 23**).

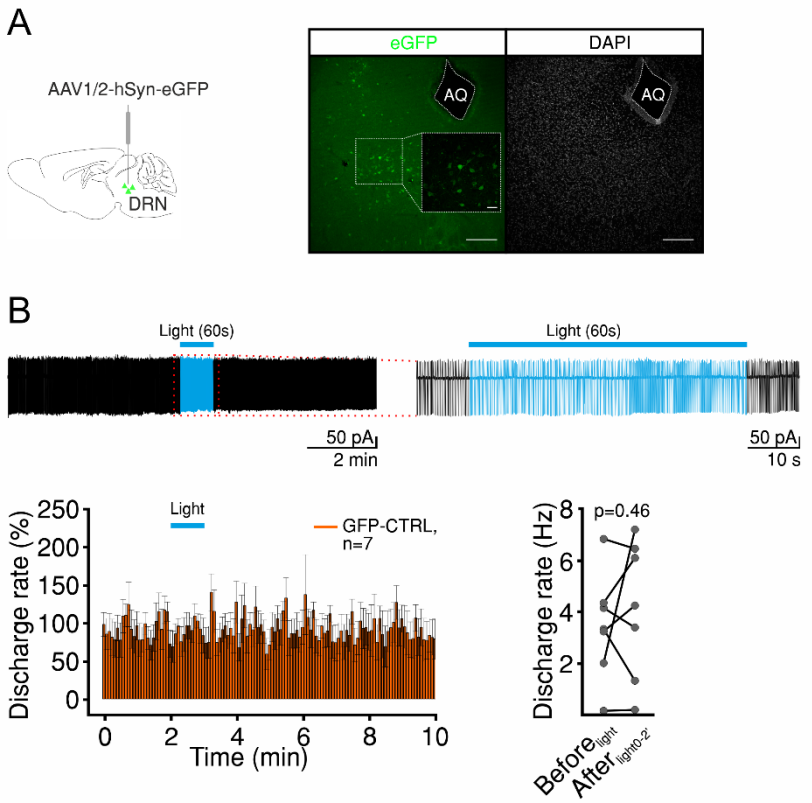

Figure 23 (A, left) Diagram of injection site in the DRN. (right) Sample confocal image showing expression of the AAV1/2-hSyn-eGFP virus in the DRN (green, GFP; gray, DAPI). Scale bars, 200 µm or 40 µm (inset). AQ, aqueduct. (B, top, left) Representative cell-attached voltage clamp recording of firing response before and after 60-s blue light illumination (blue bar) (n = 7). (B, top, right) Expanded view of the recording period defined by the red dotted box. (B, bottom, left) Time course of the effect of 60-s blue light stimulation (blue bar) on discharge firing rate (5-s binning). (B, bottom, right) Summary plots indicate mean firing discharge rate 2 min prior to light ($Before_{light}$) and 2 min after lights-off ($After_{light\ 0\text{-}2'}$) ($Before_{light}$, 3.4 ± 0.8 Hz; $After_{light\ 0\text{-}2'}$, 4.1 ± 1.0 Hz n = 7, 2sided paired t-test)

Passive and active properties of BLINK2-expressing cells were indistinguishable from those of controls in the dark (**Figure 24**), which indicates that the channel is closed in the dark. After exposure to 60 s or 30 s of blue light (470 nm, 8.7 mW/mm^2), light-responsive neurons hyperpolarized and stopped firing within 2 min after the light was switched off (for 60-s exposure (n = 11), 1.32 ± 0.17 Hz Before$_{light}$ and 0.005 ± 0.003 Hz After$_{light\ 0\text{-}2'}$; for 30-s exposure (n = 8), 1.39 ± 0.2 Hz Before$_{light}$ and 0.016 ± 0.007 Hz After$_{light\ 0\text{-}2'}$) (**Figure 22 A**). The firing did not recover for at least 20–30 min after stimulation (data not shown). We reasoned that dialysis of intracellular constituents during whole-cell recordings might represent a caveat, and therefore we analyzed the discharge rate of tonically active GFP$^+$ neurons in a cell-attached configuration. Although light stimulation (60 s) substantially reduced the firing discharge rate (Before$_{light}$, 1.3 ± 0.3 Hz; After$_{light\ 0\text{-}2'}$, 0.03 ± 0.01 Hz), we observed a slight recovery of activity (After$_{light\ 5'\text{-}7'}$, 0.18 ± 0.05 Hz) in 7 out of 11 cells in the dark (n = 11; repeated measures one-way ANOVA, F10,2 = 22, p = 0.0007; post hoc, Before$_{light}$ versus After$_{light\ 0\text{-}2'}$, p = 0.002; Before$_{light}$ versus After$_{light\ 5'\text{-}7'}$, p = 0.003; After$_{light\ 0\text{-}2'}$ versus After$_{light\ 5'\text{-}7'}$, p = 0.02; multiple comparison and Tukey's p-value correction) (**Figure 22 C**).

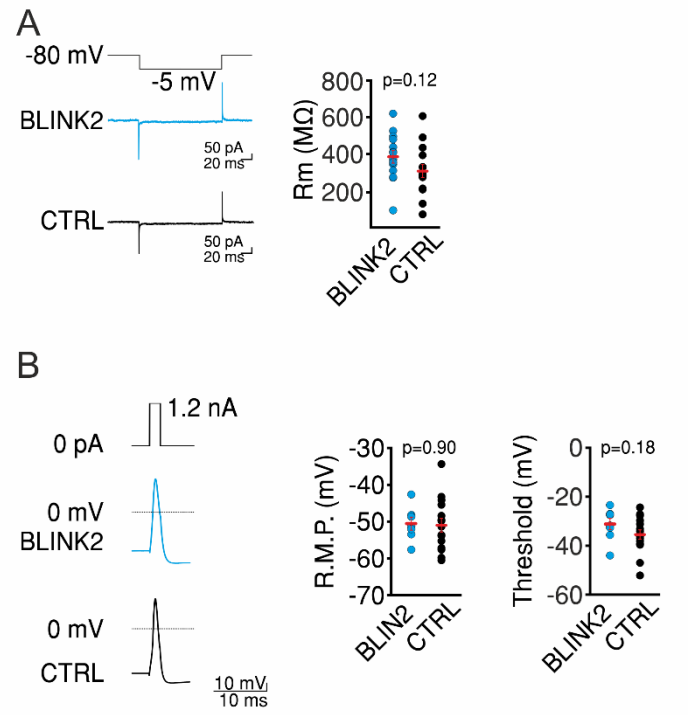

Figure 24 (A, left) Representative current traces. (A, right) Membrane resistance (Rm) was measured in response to –5mV steps in voltage clamp configuration and did not significantly change between BLINK2 and CTRL group (Rm, BLINK2 386 ± 35 MΩ, n = 14; CTRL, 308 ± 35 MΩ, n = 15; p = 0.12, 2sided unpaired t-test). (B, left) Representative current clamp traces in response to fixed current injections. Action potential firing was generated by 2-ms current pulses at 1.2 nA. (right) resting membrane potential (R.M.P.) and action potential threshold did not differ between BLINK2 and CTRL groups (R.M.P.: BLINK2, –50.6 ± 1.8 mV n = 7; CTRL, –50.9 ± 1,8 mV, n = 15, p = 0.90, 2sided unpaired t-test; Threshold: BLINK2, –31.1 ± 2.3 mV, n = 8; CTRL, –35.4 ± 1.9 mV, n = 15, p = 0.18, 2sided unpaired t-test). Action potential threshold was determined from the second derivative of the spike waveform.

To compare BLINK2 to the opsin-based chloride pump eNphR3.0, we coinjected AAV1-hsyn-Cre and AAV5-EF1α-DIO-eNpHR3.0-eYFP viruses into the DRN (**Figure 25 A**). In YFP^+ cells, 60 s of yellow light (585 nm, 17 mW/mm^2) induced rapid (<5 s) silencing of firing activity (**Figure 25 B)**; this inhibitory effect faded within the illumination period. The firing rate returned to control levels within 2 min of dark onset ($Before_{light}$, 2.7 ± 0.8 Hz; Light, 1.3 ± 0.7 Hz; $After_{light\ 0\text{-}2'}$, 2.3 ± 0.9 Hz) (**Figure 25 C**). To provide a quantitative comparison between the eNpHR3.0-mediated and BLINK2-

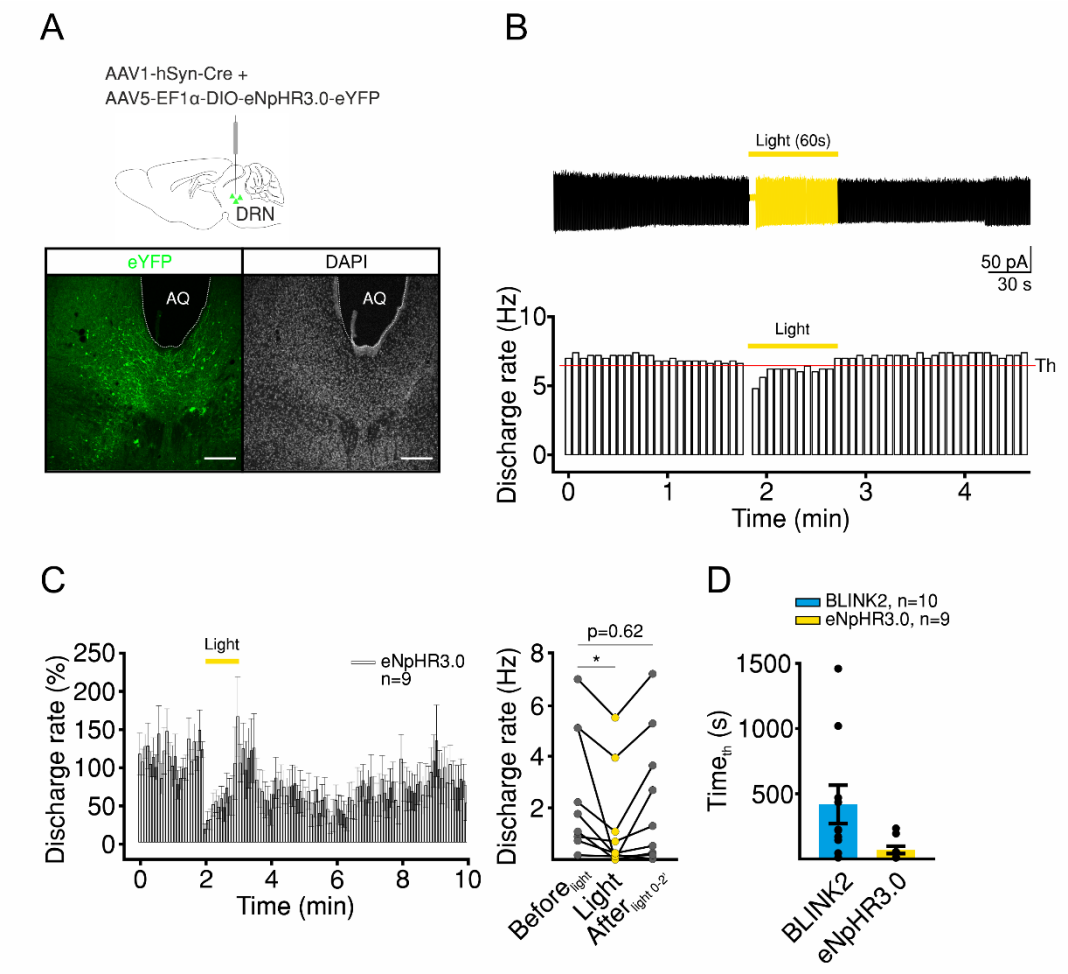

Figure 25 (A, top) Diagram represents virus injection site (AAV1-hSyn-Cre + AAV5-EF1α-DIO-eNpHR3.0-eYFP). (A, bottom) Confocal image showing expression of eNpHR3.0-eYFP in the mouse DRN (green, YFP; gray, DAPI; scale bar, 200 µm; AQ, aqueduct). (B, top) Representative cell-attached voltage clamp recording of firing response before and after 60 s of yellow light illumination (yellow bar). (B, bottom) Time course of the effect on the discharge rate of 60 s of yellow light stimulation (yellow bar) on this representative recording; red horizontal bar represents the threshold (Th) defined as the mean discharge rate minus two times the s.d.; mean firing rate is calculated on values (5-s binning) computed over 1 min prior to light illumination (see also "Materials and method"). (C, left) Average time course of the effect of 60 s of yellow light stimulation (yellow bar) on firing discharge rate (5-s binning). (C, right) Summary plots indicate mean firing discharge rate 2 min prior to light ($Before_{light}$), during 1 min of light (Light) and 2 min after light ($After_{light\ 0\text{-}2'}$) (n = 9; RM1WA, $F_{8,2} = 6$, p = 0.019; $Before_{light}$ versus Light, p = 0.047; $Before_{light}$ versus $After_{light\ 0\text{-}2'}$, p = 0.62; with multiple comparison and Dunnett). (D) Bar graph indicating the duration of neuronal silencing (time below threshold; $Time_{th}$) induced by eNpHR3.0 or BLINK2 activation ($Time_{th}$: BLINK2 versus eNpHR3.0, p = 0.03, 2sided Mann–Whitney test). The $Time_{th}$ of BLINK2 has been calculated from the dataset included in Figure 22. Data are presented as mean ± s.e.m.

mediated effects, we calculated the duration of firing inhibition as the 'time below threshold' (see also "*Materials and methods*"), which was 71 ± 28 s for eNpHR3.0 (n = 9) and 420 ± 148 s for BLINK2 (n = 10) (**Figure 25 D**). Thus eNpHR3.0-induced inhibition was faster than that of BLINK2 and did not persist in the dark.

Target manipulation of long-range neuromodulatory projections to the LC

We have previously shown that BLINK2 is suitable for somatic neuronal inhibition (Alberio & Locarno *et al.*, 2018). We are currently validating this tool for synaptic silencing, in order to manipulate neuromodulatory projections to the LC originating from the Central Amygdala and from the Dorsal Raphe Nucleus.

1) Central Amygdala:

We will investigate the involvement of CRF released by Central Amygdala (CeA) projections to the LC (CRF-CeA→LC) in the induction of t-LTP occurring at non-dissected glutamatergic synapses of young animals in response to electrical STDP (**Figure 19**). We have shown that this form of LTP is sensitive to pharmacological antagonism of CRF1R (**Figure 20**). This raises the possibility that the electrical STDP obtained by intra-LC stimulation results in CRF release from CFR-containing fibers impinging on the LC, this would promote LTP by activating the Gs-coupled CRF1R. Many brain regions targeting the LC (e.g. BNST, CeA, PVN) can be the source of CRF required for LTP. Amongst those regions, the CeA provides a strong and dense input to the LC (Schwarz *et al.*, 2015; Breton-Provencher and Sur, 2019). By using BLINK2, we will test whether inhibiting CeA-CRF^{+} neurons, thereby CRF release in the LC, is sufficient to prevent LTP observed at glutamatergic synapses of young animals upon electrical STDP. To this purpose, we will inject in the CeA of P 0-3 CRF-Cre mice (B6(Cg)-Crh$^{tm1(cre)Zjh}$/J), a DIO (double-inverted-floxed) AAV vector coding for BLINK2 (AAV-hSyn-DIO-BLINK2-IRES-eGFP; currently under production). *Ex-vivo* electrophysiological experiments will be performed in which the electrical post-pre STDP will be coupled to optogenetic inhibition of CRF-CeA→LC terminals. We expect optogenetic inhibition of CRF release to recapitulate the effect of pharmacological inhibition of CRF1R.

2) Dorsal-Raphe Nucleus (DRN)

We have shown that BLINK2 is suitable for inhibition of DRN neurons (Alberio & Locarno *et al.*, 2018)(**Figure 22**). We will therefore exploit this optogenetic tool to explore the role of serotonergic regulation of LC-NE neurons. While anatomical evidence supports a connection between DRN and LC (Segal, 1979; Kim *et al.*, 2004), how these inputs shape LC activity is still unaddressed. Furthermore, it is not clear whether tonic release of serotonin (5-HT) in the LC modulates NE-neurons firing.

First, we will investigate how tonic release of 5-HT from DRN projections affects LC-NE discharge rate. To this purpose, we will take advantage of a TpH2-Cre driver mouse line (Tg(Tph2-icre/ERT2)6Gloss/J; Bartsch, Weber and Scho, 2011) to achieve BLINK2 expression specifically in 5HT-DRN neurons by injecting the AAV-hSyn-DIO-BLINK2-IRES-eGFP virus (currently under production) in the DRN of adult mice. We will then perform *ex-vivo* electrophysiology experiments in which we will record tonic firing activity of LC-NE neurons upon local photoinhibition of DRN-5HT terminal fields.

Not only these experiments will help to understand how CRF released by the CeA or 5-HT released by the DRN modulates the physiology of LC-NE neurons, but they will pave the way for future investigations regarding the role of DRN→LC projection in major depression or the role of CeA→LC projection in stress-induced maladaptations. In this context, BLINK2 would be useful to circumvent the paradoxical effects arising from the activation of commonly used inhibitory opsins (Wiegert *et al.*, 2017).

Discussion

Although the role of Norepinephrine (NE) in Locus Coeruleus (LC) target regions has been extensively investigated (reviewd by Sara, 2009), it is still unclear how impinging inputs dynamically shape Locus Coeruleus neuronal activity to affect NE release. In the light of anatomical evidence supporting the highly integrative nature of LC-NE neurons (Szabadi, 2013; Schwarz *et al.*, 2015; Breton-Provencher and Sur, 2019), studying synaptic physiology of these cells could provide useful insights for the understanding of how NE neurons affect behavior. Amongst the numerous brain regions projecting to the LC, the Prefrontal Cortex (PFC) is of particular interest, first because it bears a strong cortical drive to this noradrenergic nucleus (Jodo, Chiang and Aston-Jones, 1998) and secondly as it might provide top-down control over the sub-cortical LC during cognition and stress response (Sara and Bouret, 2012).

In-vivo and ex-vivo dissection of PFC→LC connectivity

By performing *in-vivo* electrophysiological recordings in mice, we demonstrated that pulse stimulation of the PFC generates orthodromic spikes in 44% of LC neurons. Similar excitatory influence of PFC stimulation on LC neurons has been previously described in rats (Jodo, Chiang and Aston-Jones, 1998). In contrast, other studies suggested an inhibitory influence of the PFC on LC neurons (Sara and Hervé-Minvielle, 1995; Breton-Provencher and Sur, 2019). In Sara and Hervé-Minvielle's study (Sara and Hervé-Minvielle, 1995), local inactivation of the PFC resulted in increased LC tonic activity. The authors suggested that PFC provides inhibitory control over LC neurons by activating local GABAergic interneurons. However, the authors did not directly assess the effect of PFC stimulation on LC activity. Accordingly, Breton-Provencher and Sur (Breton-Provencher and Sur, 2019) demonstrated that activating PFC terminals in the LC region induces pupillary constriction, which can be used as a readout of LC activity (Joshi *et al.*, 2016; Zerbi *et al.*, 2019). Nonetheless, pupil size is regulated also by other neuromodulators such as acetylcholine (Larsen and Waters, 2018) and dopamine (Van Slooten *et al.*, 2018).

In-vivo, we found latency of LC responses to PFC stimulation (≈ 15 ms), which is consistent with direct monosynaptic connectivity between these two regions. *Ex-vivo*, we demonstrated that shedding light on PFC-ChR2-expressing terminals resulted in optogenetically evoked excitatory postsynaptic currents in LC-NE neurons. Our work, together with previous anatomical evidence (Breton-Provencher and Sur, 2019), supports a direct PFC→LC monosynaptic connection. Further

experiments are needed to conclusively demonstrate the direct synaptic connectivity between these two brain areas. To this purpose, we are currently testing whether opto-induced depolarization of PFC terminal fields in the LC region results in EPSCs even when neuronal firing is pharmacologically blocked by Tetrodotoxin (TTX) (Yamawaki *et al.*, 2016).

Behavioral relevance of PFC→LC projections

Our results suggest that activation of PFC→LC projections results in mice acquiring place conditioning, indicative of appetitive learning and retrieval of contextual memory associations. To the best of our knowledge, this is the first evidence showing behavioral implications of PFC→LC input activation.

Previous studies have demonstrated that LC neurons are responsive to appetitive as well as to aversive stimuli (Foote, Aston-Jones and Bloom, 1980; Gary Aston-Jones and Bloom, 1981). However, optogenetic/chemogenetic activation of LC-NE neurons (McCall *et al.*, 2015; Zerbi *et al.*, 2019), or activation of CRF^{+} Central Amygdala (CeA)→LC projections (McCall *et al.*, 2015), promotes anxiety-like behavior (e.g. more time spent in the corners of an open field, more time spent in the closed arms of an elevated plus-maze), and induces strong and reliable aversion. Therefore, optogenetic excitation of the LC as a whole, or activation of CRF^{+} terminals impinging on the LC, is sufficient to recapitulate the stress-induced increase in anxiety levels (e.g. decreased animal's exploratory behavior, increased freezing). Contrary to what it has been previously shown, we did not find any aversive effect of PFC→LC projections stimulation. The different impact of neuromodulatory CRF^{+}-CeA→LC stimulation versus glutamatergic PFC→LC-(see: "*Results*") activation in generating aversive state may reside in the level and mode of excitation exerted by these two inputs on LC neurons. LC firing responses evoked by CRF show lower maximum magnitude of activation (measured as the increase in discharge rate frequency), slower onset, and longer duration than glutamate-induced ones (Jedema and Grace, 2004; Valentino, Bockstaele and Van Bockstaele, 2008). Furthermore, CRF biases LC activity towards high tonic firing mode, whereas glutamate release induces phasic LC activation (Valentino, Bockstaele and Van Bockstaele, 2008). While CRF, and CRF-mediated stress stimuli, have been shown to activate the overall LC neuronal population (see: "*Results",* and Rassnick *et al.*, 1998; McDevitt *et al.*, 2009; McCall *et al.*, 2015; Borodovitsyna, Flamini and Chandler, 2018), we found that PFC stimulation orthodromically activated only 44% of LC neurons. Also, our *in-vivo* results show an increase in LC spike probability upon PFC pulse stimulation with short onset. Contrary to CRF-CeA→LC

projections activation (McCall *et al.*, 2015), PFC pulse stimulation did not result in long-lasting tonic entrainment of NE-neurons (see: "*Results*"). Taken together, the behavioral differences observed upon activating CRF-CeA→LC projections or the PFC→LC terminals could be explained by a different spatio-temporal dynamic of NE signal in LC target regions in the two different experimental settings. Indeed, while high NE levels are associated with stressful situations (Finlay, Zigmond and Abercrombie, 1995; Morilak *et al.*, 2005), moderate concentrations of NE favors behavioral performance in tasks requiring focused attention by decreasing distractibility (Arnsten and Contant, 1992; Aston-Jones and J. D. Cohen, 2005). Levels of NE in the brain and behavioral performance accuracy are known to follow an inverted-U shape relationship [or Yerkes-Dodson relationship (Yerkes and Dodson, 1908; Teigen, 1994)]. Specifically low levels of NE, corresponding to low arousal, correlate to drowsiness and non-alertness. Performances are optimal with moderate levels of NE, which favors the exploitation of task-related sources of reward; this condition might be recapitulated by the activation of PFC→LC connection, which may engage only a minority of LC neurons, and for a shorter period of time. On the other side of the spectrum, high levels of LC activity, as induced by stressors or CRF, deteriorate cognitive performances and allow exploration of the environment to escape potentially dangerous situations (Aston-Jones and J. D. Cohen, 2005; Luksys, Gerstner and Sandi, 2009). This view can be complemented when considering that LC neurons receiving input from the PFC might have a distinct output-projection pattern compared to the rest of LC cells. The LC might be divided into functional subpopulations playing divergent behavioral roles accordingly to their input-output profile. Supporting this view, in other brain regions involved in emotional processing, such as the Amygdala, a "minority population" of neurons could support the opposite behavioral phenotype from the structure as a whole, based on by their output-profile (Tye *et al.*, 2011; Tye, 2018). Accordingly, previous studies showed a functional dichotomy between LC neurons with distinct projection pathways. LC efferent ascending pathway is able to exacerbate spontaneous pain while LC efferent descending pathway positively modulates analgesia (Hirschberg *et al.*, 2017). Future studies are needed to address the output pathway of LC neurons receiving projections from the PFC.

In the RTPP testing, we found that optogenetic stimulation of the PFC→LC inputs is sufficient to learn conditioned place preference, thus suggesting that activation of this input has a positive valence. Nevertheless, stimulation of the PFC→LC projections does not support operant reinforcement when assessed in an opto-ICSS paradigm (o-ICSS); this speaks against a rewarding effect of PFC→LC input activation. Although during o-ICSS mice showed preference for the lever

paired with light stimulation of PFC→LC terminals (active lever) over the inactive lever, the number of responses on the active lever were very low, especially when compared to response rates observed during o-ICSS of structures belonging to the reward system (Mateo *et al.*, 2017; Brocka *et al.*, 2018; Covey and Cheer, 2019). It is therefore possible that other factors, rather than PFC→LC stimulation, may shape preference for the active lever. Since we have not performed yet control experiments in animals that do not express ChR2, we cannot exclude that mice were pressing for unspecific effects induced by photostimulation. Current experiments in mice injected with a control virus are on-going to validate our findings.

To explain why activation of PFC→LC inputs results in conditioned place preference without being rewarding, one might consider that the role of NE in valence processing is controversial (Tye, 2018). The LC is believed to encode for the salience of an event more than for its valence (Berridge and Waterhouse, 2003; Vazey, Moorman and Aston-Jones, 2018). Hence, we can speculate that mice showed place preference during the RTPP paradigm because of perceiving novelty, or increased saliency, associated with photostimulation rather than for the positive valence of this experience. Consistent with this, rodents display a tendency to explore novel environments (Bardo, Neisewander and Pierce, 1989; Bevins and Besheer, 2005) and to interact with novel objects (Bevins *et al.*, 2002; Kennedy *et al.*, 2016). This suggests that novel environments/objects can be perceived as appetitive. Indeed, the appetitive qualities of novelty can induce conditioned place preference; animals repeatedly exposed to novel objects in the same environment display learned preference for the environmental cues previously paired with the novel objects (Bevins, 2001; Bevins and Besheer, 2005). Therefore, the formation of place preference upon PFC→LC input stimulation might be reminiscent of novelty-induced conditioned place preference.

NE has been recently suggested to boost incidental memory (Hauser *et al.*, 2019). Incidental memory - or non-intentional memory- is the formation of memory when subjects are not asked to remember. In behavioral paradigms assessing incidental memory, subjects are engaged in a specific task when non-task-relevant information is presented. It follows that subjects menage to recall the non-task-relevant information without prior effort made to memorize it (Kontaxopoulou *et al.*, 2017). Photoactivation of PFC→LC input during the RTPP might support the formation of incidental memories by increasing the arousal state of the animal and increasing the awareness of environmental cues. Therefore, PFC→LC activation might facilitate the encoding and/or retrieval of contextual memories.

Behavioral relevance of long-term synaptic plasticity at PFC→LC projections

The evidence that mice form contextual associations upon PFC→LC input stimulation and can recall the experience of this association points at long-term plasticity processes occurring at this specific input. It is worth noting that mechanisms of synaptic plasticity at PFC→LC synapses, or more in general in the LC, have not been explored so far.

In this study, we assessed long-term synaptic plasticity *ex-vivo* in the LC by applying a post-pre STDP paradigm, which resulted in eCB-mediated t-LTD of PFC→LC inputs, consistent with a wealth of experimental evidence obtained in other brain regions (Crozier *et al.*, 2007; Heifets and Castillo, 2009; Li and Burrell, 2011; Cui *et al.*, 2015; Bosch-Bouju *et al.*, 2016; Cavaccini *et al.*, 2018; Cui, Perez and Venance, 2018; Foncelle *et al.*, 2018; Xu *et al.*, 2018). As already introduced in the "Project Implementation" paragraph, we targeted this form of plasticity because retrograde eCB signaling at PFC→LC synapses may represent a key feedback mechanism to regulate the connectivity between the PFC and the LC, ultimately shaping the spatial and temporal dynamic profile of NE release in target brain regions, thereby affecting action control.

We also found that the eCB-mediated signaling capacity in the LC reflects experience-dependent plasticity at PFC→LC synapses. Indeed, while repeated exposure to the same context impairs $_{PFC}$LTD, a single exposure to a novel salient stressor is able to re-open this form of plasticity. Our result goes in line with what has been previously observed in other stress-responsive brain regions (Cusulin *et al.*, 2014). We still need to provide evidence that $_{PFC}$LTD re-opened by stress salience is eCB-mediated. Whether and how other salient events, such as positive experiences, are able to re-open LTD at LC→PFC synapses is a matter of future investigation.

As a further demonstration of LC synapses' plastic properties, we found that postnatal development plays a crucial role in determining the post-pre STDP outcome. The same electrical post-pre STDP protocol that induces eCB-LTD at adult non-dissected glutamatergic synapses resulted in eCB-mediated LTP at excitatory synapses of young animals. This form of synaptic potentiation requires activation of CRF1R-mediated signaling, which has been shown to modulate post-synaptically the biosynthesis of eCB (Megan Gray *et al.*, 2015; Natividad *et al.*, 2017). Thus, eCBs and CRF appear acting in concert to regulate synaptic plasticity at LC glutamatergic synapses of young animals. This is in line with the evidence that our optogenetic post-pre STDP paradigm, which does not engage neuromodulatory afferent fibers, including CRF-releasing projections to the LC, results in LTD at dissected LC→PFC inputs of young mice. Reminiscent of higher synaptic strength of CRF-releasing afferents in young compared to adult LC, we hypothesize that activation

of CRF^+-containing terminals arising from CeA during the electrical STDP might lead to potentiation of PFC→LC synapses. To demonstrate our hypothesis, in young animals we will either chemogenetically activate CeA-CRF^+ terminals during the opto-STDP or we will optogenetically suppress (for instance by using BLINK2) CeA-CRF release during the electrical STDP. In the first case, we expect to induce potentiation of PFC→LC synapses, while in the latter we should prevent the LTP at non-dissected glutamatergic synapses. Additionally, future experiments will aim at better characterizing the molecular interplay between CRF1R and eCB system in young mice's LC neurons. Finally, we will try to address whether the divergent LC synaptic substrates between young and adult animals play a role in determining different stress susceptibility observed during adolescence (Casey, Jones and Hare, 2008).

In summary, we found that PFC→LC stimulation supports learning and/or retrieval of contextual memory associations. Consistent with the occurrence of plasticity processes at LC synapses, long-lasting modulation of PFC→LC projections relies on eCB-mediated signaling capacity, which is dynamically shaped by context adaptations and stress salience experiences. We also found that eCB-mediated plasticity at PFC → LC synapses is regulated during postnatal development, thus unveiling divergent synaptic substrates that might be relevant to explain some of the different noradrenergic-mediated response in adolescents and adults.

Materials and methods

Animals

Male C57BL/6J [postnatal day 23-28 (young) or postnatal day 60-75 (adult)] were used in this study. Male mice were kept in standard cages with food and water ad libitum at 22 ± 1 °C under artificial 12/12-h light (7-19) /dark cycle.

In-vivo electrophysiology

Stereotaxic surgeries for electrophysiology were performed under 1.0–1.2% isoflurane (in 50% air/50% O2; 1 L/min) anesthesia. Stimulation and recording electrodes were, respectively, stereotaxically placed into the LC (AP -5.4 mm/bregma; ML 0.8 mm/midline; DV (-2.6)-(-3.5) mm/brain surface) and in the the PFC (AP 1.8 mm/bregma; ML 0.5 mm/bregma; DV -1.25 mm/brain surface).

A glass micropipette (1–2 µm, 10–12 mΩ) filled with 2.0% pontamine sky blue in 0.5 m sodium acetate was used for recording. The extracellular potential was recorded with an Axoclamp-2B amplifier and filter (300/0.5 Hz). Single-neuron spikes were collected on-line (CED 1401, SPIKE 2, Cambridge Electronic Design).

Bipolar electrical stimulation of the PFC was conducted with a concentric electrode (Phymep, France) and a stimulus isolator (500 µs duration, 0.5–1.5 mA; Digitimer, UK). Electrical Footshock stimulation was conducted with silver wires connected to the hindlimb footpad (500 µs duration, 0.5–2 mA; Digitimer, UK). During electrical stimulation of the PFC or Foot shock stimulation, cumulative peristimulus time histograms (PSTH, 100 stimuli @ 0.5Hz, 5 ms bin width) of LC activity were generated for each neuron recorded. Cells were considered responsive to the stimulation when in at least 2 consecutive bins after the stimulation the spike count was higher than the average baseline spike count ± 2.5 standard deviations.

At the end of each recording, the recording pipette placement was marked with an iontophoretic deposit of pontamine sky blue dye (−20 µA, 30 min). To mark the electrical stimulation site, +50 µA was passed through the stimulation electrode for 90 s. Afterward, brains were removed and snap-frozen in a solution of isopentane stored at −80 °C. Brains were then coronally sliced and mounted on glass slides. The recording and electrical stimulation locations were verified under a transmitted light stereo-microscope.

Ex-vivo Electrophysiology

Slice preparation

Mice were anesthetized under isoflurane, intracardially perfused with a dissecting artificial cerebrospinal fluid (aCSF) solution containing: 87mM NaCl, 2.5mM KCl, 1,25mM NaH_2PO_4, 7Mm $MgCl_2$, 75mM Sucrose, 25mM $NaHCO_3$, 25mM D-glucose, 0,5mM $CaCl_2$, saturated with a carbogen mix 95%O_2 5%CO_2. Mice were subsequently decapitated; their brains were kept in the same ice-cold dissecting aCSF used during cutting for the successive vibratome slicing procedure. Horizontal slices containing pons sections (200 µm thickness) or coronal slices containing the DRN (250 µm thickness) were obtained using a Vibratome 1000S (Leica) then transferred to aCSF containing: 115 mM NaCl, 3.5 mM KCl, 1.2 mM NaH_2PO_4, 1.3 mM $MgCl_2$, 2 mM $CaCl_2$, 25 mM $NaHCO_3$ and 25 mM D-glucose, aerated with 95% O*2* and 5% CO_2. Slices were incubated for 20 min at 32°C, then kept at 22-24 °C. During electrophysiological experiments, slices were continuously superfused with aCSF at a rate of 2mL/min at 28-30°C.

LC recordings

Whole-cell patch-clamp recordings were performed on LC-NE neurons in horizontal slices. Neurons were visualized under IR-DIC (infrared differential interference contrast) and selected by their anatomical location, their morphology and, after patching, by their electrophysiological properties (Zhang *et al.*, 2010). The intracellular solution contained: 130 mM KMeSO4, 5 mM KCl, 5 mM NaCl, 10 mM HEPES, 0.1 mM EGTA, 2 mM MgCl2, 0.05 mM CaCl2, 2 mM Na2-ATP and 0.4 mM Na3-GTP (pH 7.2-7.3, 280-290 mOsm/kg). The excitatory postsynaptic currents (EPSPs) were induced at 0.1 Hz in the presence of the GABAA receptor antagonist gabazine (10 mM) by local electrical stimulation using a theta electrode connected to a constant current insulator unit (Digitimer Ltd.) or by optogenetic stimulation of prefrontal cortex afferents using short blue light pulses (1 ms at 470 nm) of LED light delivered through the microscope objective (CoolLED, pE-100, Andover, Hampshire, United Kingdom). To induce plasticity a negative STDP paradigm was used: 20 EPSPs bouts paired with bAPs, delivered 10 s apart. Each bout consisted of five bursts (200 ms apart), each composed of three bAPs at 50 Hz followed by one EPSP (negative timing). The onset of the EPSPs followed the peak of the last postsynaptic action potential in the burst by 10 ms (Δt =-10 ms). During plasticity induction, the postsynaptic neuron was held at -70mV in between bAPs. Data were excluded when the access resistance (Ra) changed > 20%. Data are reported without corrections for liquid junction potentials. Data were acquired using a Multiclamp 700B amplifier

controlled by pClamp 10 software (Molecular Device), filtered at 2.4 kHz and sampled at 10 kHz (voltage clamp), or filtered at 10 kHz and sampled at 20 kHz (current clamp) with a (Digidata 1322, Molecular Device).

Data analysis

The occurrence and magnitude of synaptic plasticity were evaluated by comparing EPSC normalized amplitudes from the last 5 min of baseline recordings with the values between 20–25 min after conditioning. The plasticity loci (pre- vs postsynaptic) were deduced from the change in the paired-pulse ratio (PPR) after the delivery of the stimulation protocol in the same time periods.

DRN recordings

Electrophysiology recordings were performed on coronal brain slices containing the DRN. The DRN was first visualized under infrared differential interference contrast to allow for subsequent identification of GFP^+ or YFP^+ neurons by epifluorescence microscopy. Patch pipettes (4–6 MΩ) were filled with a solution containing 135 mM NaCl, 10 mM HEPES, pH 7.2–7.3, for cell-attached recording or 130 mM KMeSO4, 5 mM KCl, 5 mM NaCl, 10 mM HEPES, 2 mM MgCl2, 0.1 mM EGTA, 0.05 mM CaCl2 , 2 mM Na2ATP and 0.4 mM Na3GTP, pH 7.2–7.3 (280–290 mOsm/kg), for whole-cell recordings. Cell-attached experiments were performed in the voltage-clamp configuration with GFP+ or YFP+ neurons held at the potential that gave a holding current of 0pA, whereas whole-cell experiments were performed in the current-clamp configuration, without current injection. Light (470 nm for BLINK2 activation, 8.7 mW/mm^2; 585 nm for eNpHR3.0 activation, 17 mW/mm^2) emitted by an LED (CoolLED) was delivered to the specimen through the microscope objective (IR-ACHROPLAN 40× /0.8-NA (numerical aperture); Zeiss). Data were acquired with a Multiclamp 700B amplifier controlled by pClamp 10 software (Molecular Devices) filtered at 10 kHz and sampled at 50 kHz (current clamp and voltage clamp) (Digidata 1322; Molecular Devices). We generated time-course plots by averaging the discharge firing rate every 5 s; values were normalized to 1 min of baseline recording before light illumination. All data are reported without corrections for liquid junction potentials. Data where the access resistance (Ra) changed by > 20%, were excluded from further analyses. To identify light-responsive cells, we applied a threshold-based criterion: the threshold (Th) was set as the mean discharge rate minus 2 standard deviations, and the mean firing rate was calculated on values (5-s binning) computed over 1 min prior to light illumination. Cells were considered light-responsive when their mean discharge rate fell below Th, or to zero, in at least two consecutive 5-s bins. 'Time below threshold' ($Time_{th}$) was measured as

the interval between the time point at which the discharge rate fell below Th in at least two consecutive 5-s bins and the time point at which the discharge rate increased above Th in at least two consecutive 5-s bins.

Substances

Triton-X, NaCl, KCl, NaH_2PO_4, $MgCl_2$, $CaCl_2$, $NaHCO_3$, D-glucose, Sucrose, $KMeSO_4$, HEPES, $MgCl_2$, Na_2-ATP, Na_3-GTP, 2,4,5-trimethylthiazole (TMT), Paraformaldehyde (PFA), were purchased from Sigma Aldrich. Gabazine (SR 95531 hydrobromide), AM251 were purchased from HelloBio. NBI 35965 was purchased from Tocris Bioscience. TH-antibody was purchased from Merck-Millipore. GFP-antibody was purchased from AbCam. C-fos antibody was purchased from Cell Signaling Technology, Inc. Neurobiotin was purchased from (DBA, Italy). DAPI and Streptavidin conjugated with Alexa 568 (Termofisher Scientific).

Animal surgeries

Adult viral injections

C57BL/6J mice (postnatal day 30-45) were anesthetized with isoflurane (4-5% for induction, 1-2% for maintenance) and O_2 mix. Subsequently, mice were mounted on a stereotaxic frame (Stoelting). To target the PFC 0.5-0.6 µL of AAV5.CamKII.hChR2.EYFP (AddGene, viral prep #26969-AAV5) or a combination of AAV1.hSyn.Cre (AddGene, viral prep #105553-AAV5) and AAV5.Ef1α.DIO.hChR2.EYFP (AddGene, viral prep # 20298-AAV5) was delivered at the following stereotaxic coordinates from bregma: AP +1.94; ML ±0.4; DV -2.4., the virus volume was delivered at a 0.1 µL/min rate using a syringe (WPI, Nanofil 10µL) connected to a Micro Pump (WPI, UMP3 UltraMicroPump). Electrophysiological recordings were performed at least 5 weeks after the surgery. To deliver BLINK2 or eNpHR3.0 to the DRN, we injected 0.5 µ l (titer 10^{13} GC/mL) of AAV1/2-hSyn-Blink2-IRES-eGFP, AAV1/2-hSyn-eGFP or a 1:1 mixture of AAV1-hsyn-Cre (pENN.AAV.hSyn.Cre.WPRE.hGH, a gift from James M. Wilson (Perelman School of Medicine, University of Pennsylvania); Addgene viral prep # 105553-AAV1) and AAV5-EF1α -DIO-eNpHR3.0-eYFP (Stanford Virus Core) into the DRN (mediolateral, + 1.15 mm, anteroposterior, –4.4 mm, dorsoventral, –3.6 mm under an angle of 20° from bregma; or mediolateral, + 0.5 mm, anteroposterior, –4.36 mm, dorsoventral, –3 mm from bregma). *Ex-vivo* electrophysiology was performed at least 2 weeks after surgeries.

P0-P3 viral injections

C57BL/6J mice (postnatal day 0-3) were anesthetized through hypothermia and mounted on a stereotaxic apparatus (Stoelting). A small AAV9.CamKII.hChR2.EYFP volume (0.25 µL) was injected into the PFC (stereotaxic coordinates from bregma: AP +0.5; ML ±0.1; DV-0.9) at a 0.1 µL/min rate using a syringe (WPI, Nanofil 10µL) connected to a Micro Pump (WPI, UMP3 UltraMicroPump). Electrophysiological recordings were performed between postnatal day 23 and 28.

Optical ferrules implantation

Animals that were injected AAV1.hSyn.Cre (AddGene, viral prep #105553-AAV5) and AAV5.Ef1α.DIO.hChR2.EYFP (AddGene, viral prep # 20298-AAV5) underwent, during the same surgical procedure, optic fiber implantation in the LC. Briefly, an optical fiber (200 um core, 0.48 NA, Thorlabs) was implanted bilaterally above the LC injection site (AP -5.45, ML 1.0, DV -3.65, from bregma with a 6° ML angle). Optic fiber ferrules were then permanently affixed with dental cement (Metabond, Parkell, Inc). Mice were allowed 6 weeks to recover from surgery and to allow viral expression.

Behavioral paradigms

Real-Time -and conditioned- Place Preference

A three-chamber conditioned place preference apparatus was used for the real-time place preference test (Anymaze, Stoelting). The apparatus consisted of three chambers (20 × 18 × 35 cm) with distinct walls patterns and floors. The animal's position was monitored via a CCD camera. Mice expressing ChR2 at the PFC level and with optic fibers implanted in the LC area were used for real-time place preference. On each of the four days, mice were connected to an optical fiber and allowed to access the three chambers of the apparatus freely. On Pre-session, mice were connected to an optical fiber with no laser (15-min session). Mice showing side preference were excluded. On Stim1 and Stim2 (30-min session), two chambers were assigned as the stimulation chambers (counterbalanced across all mice). Whenever the mouse was within the stimulation chambers the laser was on (473 nm, 1 mW, 10 ms pulse length duration at 10 Hz and 30Hz in different chambers) (**Figure 26**). On Post-session (15-min session), the mice were allowed to freely explore the three chambers without optical stimulation.

IntraCranial Self Stimulation (ICSS)

Mice expressing ChR2 at the PFC level and with optic fibers implantation in the LC were used for ICSS. Animals were placed into the operant chamber featured with two levers. They were trained

on a fixed ratio (FR1) reinforcement schedule; each time the mouse pressed the active response lever, the computer delivered a 1-s 10 Hz or a 1-s 30Hz pulse of light stimulation (473 nm, 1 mW, 10 ms pulse length duration)(**Figure 26**). The inactive lever presses were not associated with any consequence. Animals underwent 2 training sessions per day, each session lasted 30 min. Six ICSS training sessions were associated with 10Hz opto-stimulation, the remaining 6 were associated with 30Hz opto-stimulation. We recorded both active and inactive lever presses during the 6 days.

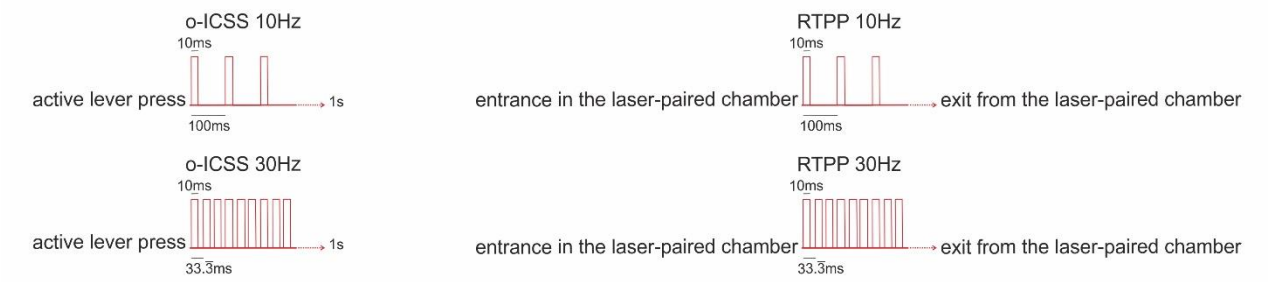

Figure 26 Schematics of the optogenetic stimulation protocols used for the ICSS and Place Preference paradigms.

Context habituation and stress exposure

Mice were habituated to the context and handled by the experimenter for 5-10 min per day for 5 days prior to experimentation. Mice were also habituated to a plastic chamber where stress or control conditions took place. To induce acute stress, mice were placed in a rodent restrainer for 15 min, the restrainer was then placed inside a sealed anesthesia induction chamber. A piece of filter paper was placed inside the chamber and saturated with 100 µL predator odor (2,4,5-trimethylthiazole, TMT, Sigma-Aldrich).

Open Field Test

Immediately after the last context habituation session (C-HAB) or the stress exposure (Stress), animals were tested for their anxiety levels in an open field test (OFT). The OFT apparatus consisted in a 30cmx30cmx40xm dark plastic box. Mice were allowed to freely explore the apparatus for 10 minutes, during which their activity was filmed with an infrared camera situated above the maze. 1h after the conclusion of each test, mice were sacrificed for c-fos staining. Alternatively, mice used for electrophysiology were sacrificed 24h after the test. Behavior was scored using AnyMaze behavioral tracking software (Stoelting).

Immunofluorescence

Tyrosine Hydroxylase (TH) immunostaining

To confirm the LC-NE identity of the recorded neurons, the patched cells were filled with Neurobiotin (0.3mg/mL, DBA Italia) and processed post-hoc for their immunoreactivity for the TH

marker. Following the electrophysiological recordings, brain slices were kept for 24-48h in 4% paraformaldehyde in 0.1M Phosphate Buffer 7.4pH (PB). Brain slices were then rinsed 3 times in PB saline (PBS) for 15min and then permeabilized and blocked (PBS containing 3% Bovine serum albumin (BSA) [w/v]; 0.3% Triton-X [v/v]). Slices were then incubated at 4°C overnight in the same permeabilization and blocking medium containing the anti-TH rabbit polyclonal antibody (1:500, Merk-Millipore). Brain sections were then rinsed 3x15min in PBS and incubated 4h RT in the permeabilization and blocking buffer containing Alexa568-streptavidin (1:1000, Thermofisher) to label the Neurobiotin filled patched cells. Subsequently, slices were rinsed 3x15min in PBS and incubated 2h RT in the permeabilization and blocking medium containing Alexa488 conjugated secondary antibody (1:500, Thermofisher). After rinsing the slices 3x15 min, the nuclei were stained with DAPI solution (1:500 in PBS, Sigma-Aldrich), rinsed again, mounted on glass slides, and coverslipped with ProLong Gold antifade reagent (Invitrogen).

C-fos immunostaining

Briefly, mice were transcardially perfused with 25mL Phosphate Buffer Saline (PBS) and 25mL 4% paraformaldehyde in 0.1M phosphate buffer (PFA). Brains were extracted, post-fixed in PFA 4%, cryoprotected (sucrose 20%), and sliced in the coronal plane to generate brain sections containing LC. Free-floating sections were rinsed in 0.1M PBS three times, blocked in 4% bovine serum albumin (BSA), incubated in anti-TH chicken polyclonal antibody (1:500, Merk-Millipore) and rabbit anti-c-Fos (1:500, Cell Signaling Technology) @ 4°C overnight, rinsed again 3 times in 0.1M PBS, incubated in AlexaFluor 568 goat anti-chicken (1:500, Invitrogen) and AlexaFluor 488 goat anti-rabbit (1:500, Invitrogen) secondary antibodies, washed in 0.1M PBS, and incubated. After rinsing the slices 3x15 min, the nuclei were stained with DAPI solution (1:500 in PBS, Sigma-Aldrich), rinsed again, mounted on glass slides, and coverslipped with ProLong Gold antifade reagent (Invitrogen). From each brain, 5 images of LC-containing slices were acquired with an inverted Leica TCS SP5 confocal microscope. Th^+ cells and Th^+ $c\text{-}fos^+$ were counted using ImageJ software.

Statistics

Appropriate parametric statistics were used to test our hypothesis unless data did not meet the assumptions of the intended parametric test (normality test). In that case, appropriate nonparametric tests were used. Power analysis assumptions were as follows: power, 0.9; alpha, 0.5; two-tailed and expected difference 50% greater than the observed s.d. Data were analyzed by one-way repeated measures ANOVA for comparisons within a group, by one-way ANOVA for

between-group comparisons. Two-way and three-way- ANOVA were used in case we compared respectively two or three independent factors (GraphPad Prism 7 software). Post hoc analysis (Tukey or Dunnet, as indicated) was performed only when ANOVA yielded a significant main effect. Two groups were tested for statistical significance by two-population t-test and Mann–Whitney U nonparametric test (GraphPad Prism 7 software). Statistical details of experiments are shown in the results, figures and figure legends. Data are reported as mean ± s.e.m. *$p<0.05$, **$p<0.01$, ***$p<0.001$, ****$p<0.0001$.

Bibliography

Adèr, J. P. *et al.* (1980) 'Bilaterally diverging axon collaterals and contralateral projections from rat locus coeruleus neurons, demonstrated by fluorescent retrograde double labeling and norepinephrine metabolism', *Journal of Neural Transmission*, 49, pp. 207–218. doi: 10.1007/BF01252126.

Akaike, T. (1982) 'Periodic bursting activities of locus coeruleus neurons in the rat', *Brain Research*, 239, pp. 629–633. doi: 10.1016/0006-8993(82)90540-6.

Alberio, L. *et al.* (2018) 'A light-gated potassium channel for sustained neuronal inhibition', *Nature Methods*, 15, pp. 969–976. doi: 10.1038/s41592-018-0186-9.

Alnæs, D. *et al.* (2014) 'Pupil size signals mental effort deployed during multiple object tracking and predicts brain activity in the dorsal attention network and the locus coeruleus', *Journal of Vision*, 14, pp. 1–20. doi: 10.1167/14.4.1.

Alreja, M. and Aghajanian, G. K. (1991) 'Pacemaker activity of locus coeruleus neurons : whole-cell recordings in brain slices show dependence on cAMP and protein kinase A', *Brain Research*, 556, pp. 339–343. doi: 10.1016/0006-8993(91)90327-R.

Alvarez, V. A. *et al.* (2002) 'Frequency-dependent synchrony in locus ceruleus : Role of electrotonic coupling', *Proceedings of the National Academy of Sciences*, 99(6), pp. 4032–4036. doi: 10.1073/pnas.062716299.

Amaral, D. G. and Sinnamon, H. M. (1977) 'The Locus Coeruleus: Neurobiology of a Central Noradrenergic Nucleus', *Progress in Neurobiology*, 9, pp. 147–196. doi: 10.1016/0301-0082(77)90016-8.

Argilli, E. *et al.* (2008) 'Mechanism and time course of cocaine-induced long-term potentiation in the ventral tegmental area', *Journal of Neuroscience*, 28(37), pp. 9092–9100. doi: 10.1523/JNEUROSCI.1001-08.2008.

Arnsten, A. F. T. (2000) 'Through the Looking Glass: Differential Noradenergic Modulation of Prefrontal Cortical Function', *Neural Plasticity*, 7, pp. 133–147. doi: 10.1155/NP.2000.133.

Arnsten, A. F. T. and Contant, T. A. (1992) 'Alpha-2 adrenergic agonists decrease distractibility in aged monkeys performing the delayed response task', *Psychopharmacology*, 108, pp. 159–169. doi: 10.1007/bf02245302.

Arnsten, A. F. T. and Goldman-Rakic, P. S. (1984) 'Selective prefrontal cortical projections to the region of the locus coeruleus and raphe nuclei in the rhesus monkey', *Brain Research*, 306(1–2), pp. 9–18. doi: 10.1016/0006-8993(84)90351-2.

Arora, D. *et al.* (2011) 'Acute cocaine exposure weakens GABAB receptor-dependent G-protein-gated inwardly rectifying K+ signaling in dopamine neurons of the ventral tegmental area', *Journal of Neuroscience*, 31(34), pp. 12251–12257. doi: 10.1523/JNEUROSCI.0494-11.2011.

Asan, E. (1998) 'The catecholaminergic innervation of the rat amygdala.', *Advances in anatomy, embryology, and cell biology*, 142, pp. 1–118. doi: 10.1007/978-3-642-72085-7.

Aston-Jones, G. *et al.* (1986) 'The Brain Nucleus Locus Coeruleus : Restricted Afferent Control of a Broad Efferent Network', *Science*, 234, pp. 734–737. doi: 10.1126/science.3775363.

Aston-Jones, G. (2004) 'Locus Coeruleus, A5 and A7 Noradrenergic Cell Groups', pp. 259–294. doi: 10.1016/B978-012547638-6/50012-2.

Aston-Jones, G. and Bloom, F. E. (1981) 'Activity of norepinephrine-containing Locus Coeruleu Neurons in Behaving Rats Anticipates Fluctuations In the Sleep-Waking Cycle', *The Journal of Neuroscience*, 1(8), pp. 876–886. doi: 10.1523/JNEUROSCI.01-08-

00876.1981.

Aston-Jones, Gary and Bloom, F. E. (1981) 'Norepinephrine-containing Locus coeruleus Neurons in Behaving Rats exhibit pronounced responses to non-noxious environmental stimuli', *The Journal of Neuroscience*, 1(8), pp. 887–900. doi: 10.1523/JNEUROSCI.01-08-00887.1981.

Aston-Jones, G. and Cohen, Jonathan D. (2005) 'Adaptive gain and the role of the locus coeruleus-norepinephrine system in optimal performance', *Journal of Comparative Neurology*, 493(1), pp. 99–110. doi: 10.1002/cne.20723.

Aston-Jones, G. and Cohen, J. D. (2005) 'An integrative theory of locus coeruleus-norepinephrine function: adaptive gain and optimal performance.', *Annual review of neuroscience*, 28, pp. 403–450. doi: 10.1146/annurev.neuro.28.061604.135709.

Aston-Jones, G., Foote, S. L. and Segal, M. (1985) 'Impulse conduction properties of noradrenergic locus coeruleus axons projecting to monkey cerebrocortex', *Neuroscience*, 15(3). doi: 10.1016/0306-4522(85)90077-6.

Aston-Jones, G., Rajkowski, J. and Cohen, J. (1999) 'Role of locus coeruleus in attention and behavioral flexibility', *Biological Psychiatry*, 46(9), pp. 1309–1320. doi: 10.1016/S0006-3223(99)00140-7.

Aston-Jones, G., Zhu, Y. and Card, J. P. (2004) 'Numerous GABAergic Afferents to Locus Ceruleus in the Pericerulear Dendritic Zone : Possible Interneuronal Pool', 24(9), pp. 2313–2321. doi: 10.1523/JNEUROSCI.5339-03.2004.

Axelrod, J. (1971) 'Noradrenaline: Fate and control of its biosynthesis', *Science*, 173(3997), pp. 598–606. doi: 10.1126/science.173.3997.598.

Bacci, A., Huguenard, J. R. and Prince, D. A. (2004) 'Long-lasting self-inhibition of neocortical interneurons mediated by endocannabinoids', *Nature*, 431, pp. 1–5. doi: 10.1038/nature02782.1.

Bajic, D. and Proudfit, H. K. (1999) 'Projections of Neurons in the Periaqueductal Gray to Pontine and Medullary Catecholamine Cell Groups Involved in the Modulation of Nociception', 379, pp. 359–379. doi: 10.1002/(SICI)1096-9861(19990315)405:3<359::AID-CNE6>3.0.CO;2-W.

Ballinger, E. and Ananth, M. (2016) 'Basal Forebrain Cholinergic Circuits and Signaling in Cognition and Cognitive Decline', *Neuron*, 91(6), pp. 1199–1218. doi: 10.1016/j.neuron.2016.09.006.Basal.

Bangasser, D. A. *et al.* (2012) 'Increased vulnerability of the brain norepinephrine system of females to corticotropin-releasing factor overexpression', *Molecular Psychiatry*. Nature Publishing Group, 18(2), pp. 166–173. doi: 10.1038/mp.2012.24.

Bardo, M. T., Neisewander, J. L. and Pierce, R. C. (1989) 'Novelty-induced place preference behavior in rats: Effects of opiate and dopaminergic drugs', *Pharmacology, Biochemistry and Behavior*, 32(3), pp. 683–689. doi: 10.1016/0091-3057(89)90018-X.

Beas, B. S. *et al.* (2018) 'The locus coeruleus drives disinhibition in the midline thalamus via a dopaminergic mechanism', *Nature Neuroscience*, 21, pp. 963–973. doi: 10.1038/s41593-018-0167-4.

Beckstead, R. M., Domesick, V. B. and Nauta, W. J. H. (1979) 'Efferent connections of the substantia nigra and ventral tegmental area in the rat', *Brain Research*, 175(2), pp. 191–217. doi: 10.1016/0006-8993(79)91001-1.

Bellone, C. and Lüscher, C. (2006) 'Cocaine triggered AMPA receptor redistribution is reversed in vivo by mGluR-dependent long-term depression', *Nature Neuroscience*, 9, pp. 636–641. doi: 10.1038/nn1682.

Benarroch, E. E. (2012) 'Periaqueductal gray: An interface for behavioral control', *Neurology*, 78, pp. 210–217. doi: 10.1212/WNL.0b013e31823fcdee.

Benn, A. and Robinson, E. S. J. (2014) 'Investigating Glutamatergic Mechanism in Attention and Impulse Control Using Rats in a Modified 5-Choice Serial Reaction Time Task', *PLoS ONE*, 9, pp. 1–22. doi: 10.1371/journal.pone.0115374.

Berardis, D. *et al.* (2015) 'Targeting the Noradrenergic System in Posttraumatic Stress Disorder: A Systematic Review and Meta-Analysis of Prazosin Trials', *Current Drug Targets*, 16, pp. 1094–1106. doi: 10.2174/1389450116666150506114108.

Berridge, C. W. and Espana, R. A. (2006) 'Organization of Noradrenergic Efferents to Arousal-Related Basal Forebrain', *THe Journal of Comparative Neurology*, 683, pp. 668–683. doi: 10.1002/cne.

Berridge, C. W. and Waterhouse, B. D. (2003) 'The locus coeruleus-noradrenergic system: Modulation of behavioral state and state-dependent cognitive processes', *Brain Research Reviews*, pp. 33–84. doi: 10.1016/S0165-0173(03)00143-7.

Bevins, R. A. (2001) 'Novelty Seeking and Reward : Implications for the Study of High-Risk Behaviors', *Current Directions in Psychological Science*, 10, pp. 189–193. doi: 10.1111/1467-8721.00146.

Bevins, R. A. *et al.* (2002) 'Novel-object place conditioning: Behavioral and dopaminergic processes in expression of novelty reward', *Behavioural Brain Research*, 129(1–2), pp. 41–50. doi: 10.1016/S0166-4328(01)00326-6.

Bevins, R. A. and Besheer, J. (2005) 'Novelty reward as a measure of anhedonia', *Neuroscience and Biobehavioral Reviews*, 29(4–5), pp. 707–714. doi: 10.1016/j.neubiorev.2005.03.013.

Birnbaum, S. *et al.* (1999) 'A Role for Norepinephrine in Stress-Induced Cognitive Deficits : alpha-1-Adrenoceptor Mediation in the Prefrontal Cortex', *Biological Psychiatry*, 3223(99), pp. 1266–1274. doi: 10.1016/S0006-3223(99)00138-9.

Blackwell, K. and Jadrzejewska-Szmek, J. (2014) 'Molecular mechanisms underlying neuronal synaptic plasticity: systems biology meets computational neuroscience in the wilds of synaptic plasticity', *Wiley Interdisciplinary Reviews: Systems Biology and Medicine*, 5(6), pp. 717–731. doi: 10.1002/wsbm.1240.Molecular.

Blank, T. *et al.* (2002) 'Priming of long-term potentiation in mouse hippocampus by corticotropin-releasing factor and acute stress: implications for hippocampus-dependent learning', *J Neurosci*, 22(9), pp. 3788–3794. doi: 10.1523/JNEUROSCI.22-09-03788.2002.

Bockstaele, E. J. Van *et al.* (2001) 'Topographic architecture of stress-related pathways targeting the noradrenergic locus coeruleus', *Physiology & Behavior*, 73, pp. 273–283. doi: 10.1016/s0031-9384(01)00448-6.

Bockstaele, E. J. Van *et al.* (2004) 'Expression of connexins during development and following manipulation of afferent input in the rat locus coeruleus', *Neurochemistry International*, 45, pp. 421–428. doi: 10.1016/j.neuint.2003.08.019.

Van Bockstaele, E. J. and Aston-Jones, G. (1995) 'Integration in the Ventral Medulla and coordination of sympathetic, pain and arousal functions', *Clinical and Experimental Hypertension*, 17, pp. 153–165. doi: 10.3109/10641969509087062.

Van Bockstaele, E. J., Colago, E. E. O. and Valentino, R. J. (1998) 'Amygdaloid corticotropin-releasing factor targets locus coeruleus dendrites: Substrate for the co-ordination of emotional and cognitive limbs of the stress response', *Journal of Neuroendocrinology*, 10(10), pp. 743–757. doi: 10.1046/j.1365-2826.1998.00254.x.

Booze, R. M., Crisostomo, E. A. and Davis, J. N. (1989) 'Species differences in the localization and number of CNS beta adrenergic receptors: Rat versus guinea pig', *Journal of Pharmacology and Experimental Therapeutics*, 249, pp. 911–920. Available at: http://jpet.aspetjournals.org/content/249/3/911.

Borodovitsyna, O., Flamini, M. D. and Chandler, D. J. (2018) 'Acute Stress Persistently Alters Locus Coeruleus Function and Anxiety-like Behavior in Adolescent Rats', *Neuroscience*, 373, pp. 7–19. doi: 10.1016/j.neuroscience.2018.01.020.

Borodovitsyna, O., Joshi, N. and Chandler, D. (2018) 'Persistent stress-induced neuroplastic changes in the locus coeruleus/norepinephrine system', *Neural Plasticity*, 2018. doi: 10.1155/2018/1892570.

Bosch-Bouju, C. *et al.* (2016) 'Endocannabinoid-Mediated Plasticity in Nucleus Accumbens Controls Vulnerability to Anxiety after Social Defeat Stress', *Cell Reports*, 16(5), pp. 1237–1242. doi: 10.1016/j.celrep.2016.06.082.

Bouret, S. and Sara, S. J. (2002) 'Locus coeruleus activation modulates firing rate and temporal organization of odour-induced single-cell responses in rat piriform cortex', *European Journal of Neuroscience*, 16(12), pp. 2371–2382. doi: 10.1046/j.1460-9568.2002.02413.x.

Braak, H. *et al.* (2003) 'Staging of brain pathology related to sporadic Parkinson's disease', *Neurobiology of Aging*, 24(2), pp. 197–211. doi: 10.1016/S0197-4580(02)00065-9.

Breton-Provencher, V. and Sur, M. (2019) 'Active control of arousal by a locus coeruleus GABAergic circuit.', *Nature neuroscience*, 22, pp. 218–228. doi: 10.1038/s41593-018-0305-z.

Brocka, M. *et al.* (2018) 'Contributions of dopaminergic and non-dopaminergic neurons to VTA-stimulation induced neurovascular responses in brain reward circuits', *NeuroImage*. Elsevier Ltd, 177, pp. 88–97. doi: 10.1016/j.neuroimage.2018.04.059.

Brust, V., Schindler, P. M. and Lewejohann, L. (2015) 'Lifetime development of behavioural phenotype in the house mouse (Mus musculus)', *Frontiers in Zoology*, 12(1), pp. 1–14. doi: 10.1186/1742-9994-12-S1-S17.

Brzosko, Z. *et al.* (2017) 'Sequential neuromodulation of hebbian plasticity offers mechanism for effective reward-based navigation', *eLife*, 6, pp. 1–18. doi: 10.7554/eLife.27756.

Brzosko, Z., Mierau, S. B. and Paulsen, O. (2019) 'Neuromodulation of Spike-Timing-Dependent Plasticity: Past, Present, and Future', *Neuron*. Elsevier Inc., 103(4), pp. 563–581. doi: 10.1016/j.neuron.2019.05.041.

Bücheler, M. M., Hadamek, K. and Hein, L. (2002) 'Two α2-adrenergic receptor subtypes, α2A and α2C, inhibit transmitter release in the brain of gene-targeted mice', *Neuroscience*, 109, pp. 819–826. doi: 10.1016/S0306-4522(01)00531-0.

Buerkle, H. and Yaksh, T. L. (1998) 'Pharmacological evidence for different alpha2-adrenergic receptor sites mediating analgesia and sedation in the rat', *British Journal of Anaesthesia*, 81, pp. 208–215. doi: 10.1093/bja/81.2.208.

Bullitt, E. (1990) 'Expression of C-fos-like protein as a marker for neuronal activity following noxious stimulation in the rat', *Journal of Comparative Neurology*, 296, pp. 517–530. doi: 10.1002/cne.902960402.

Bylund, D. B. *et al.* (1994) 'IV. International union of pharmacology nomenclature of adrenoceptors', *Pharmacological Reviews*, pp. 121–136. Available at: http://pharmrev.aspetjournals.org/content/46/2/121.long.

Caballero, A., Granberg, R. and Tseng, K. Y. (2016) 'Mechanisms contributing to Prefrontal Cortex Maturation during Adolescence', *Neuroscience & Biobehavioral Reviews*, 176(10), pp. 139–148. doi: 10.1016/j.physbeh.2017.03.040.

Cachope, R. *et al.* (2007) 'Potentiation of Electrical and Chemical Synaptic Transmission Mediated by Endocannabinoids', *Neuron*, 56(6), pp. 1034–1047. doi: 10.1016/j.neuron.2007.11.014.

Caporale, N. and Dan, Y. (2008) 'Spike timing-dependent plasticity: a Hebbian learning rule.', *Annual review of neuroscience*, 31, pp. 25–46. doi: 10.1146/annurev.neuro.31.060407.125639.

Carlson, G., Wang, Y. and Alger, B. E. (2002) 'Endocannabinoids facilitate the induction of LTP in the hippocampus', *Nature Neuroscience*, 5(8), pp. 723–724. doi: 10.1038/nn879.

Carter, M. E. *et al.* (2010) 'Tuning arousal with optogenetic modulation of locus coeruleus neurons.', *Nature neuroscience*. Nature Publishing Group, 13(12), pp. 1526–1533. doi: 10.1038/nn.2682.

Carvalho, F. A. and Van Bockstaele, E. J. (2013) 'Cannabinoid modulation of noradrenergic circuits: implication for psychiatric disorders', *Progress in Neuro-Psychopharmacology and Biological Psychiatry*, 38, pp. 59–67. doi: 10.1016/j.pnpbp.2012.01.008.Cannabinoid.

Casey, B. J., Jones, R. M. and Hare, T. A. (2008) 'The adolescent brain', *Annals of the New York Academy of Sciences*, 1124, pp. 111–126. doi: 10.1196/annals.1440.010.

Castillo, P. E. *et al.* (2012) 'Endocannabinoid signaling and synaptic function', *Neuron*, 76(1), pp. 70–81. doi: S0896-6273(12)00855-0 [pii]\r10.1016/j.neuron.2012.09.020.

Cavaccini, A. *et al.* (2018) 'Serotonergic Signaling Controls Input-Specific Synaptic Plasticity at Striatal Circuits', *Neuron*, 98(4), pp. 801–816. doi: 10.1016/j.neuron.2018.04.008.

Cedarbaum, J. M. and Aghajanian, G. K. (1978) 'Afferent projections to the rat locus coeruleus as determined by a retrograde tracing technique', *Journal of Comparative Neurology*, 178, pp. 1–16. doi: 10.1002/cne.901780102.

Chalothorn, D. *et al.* (2002) 'Differences in the cellular localization and agonist-mediated internalization properties of the α1-adrenoceptor subtypes', *Molecular Pharmacology*, 61, pp. 1008–1016. doi: 10.1124/mol.61.5.1008.

Chamba, G. *et al.* (1991) 'Distribution of Alpha-l and Alpha-2 Binding Sites in the Rat Locus Coeruleus', *Brain Research Bulletin*, 76, pp. 185–193. doi: 10.1016/0361-9230(91)90225-9.

Chandler, D. J. *et al.* (2019) 'Redefining Noradrenergic Neuromodulation of Behavior : Impacts of a Modular Locus Coeruleus Architecture', *Journal of Neuroscience*, 39(42), pp. 8239–8249. doi: 10.1523/JNEUROSCI.1164-19.2019.

Chandler, D. J., Gao, W. J. and Waterhouse, B. D. (2014) 'Heterogeneous organization of the locus coeruleus projections to prefrontal and motor cortices', *Proceedings of the National Academy of Sciences of the United States of America*, 111(18), pp. 6816–6821. doi: 10.1073/pnas.1320827111.

Cherubini, B. Y. E., North, R. A. and Williams, J. T. (1988) 'Synaptic Potential in Rat Locus Coeruleus Neuornes', *The Journal of Physiology*, 406, pp. 431–442. doi: 10.1113/jphysiol.1988.sp017389.

Chevaleyre, V. *et al.* (2007) 'Endocannabinoid-Mediated Long-Term Plasticity Requires cAMP/PKA Signaling and RIM1α', *Neuron*, 54, pp. 801–812. doi: 10.1016/j.neuron.2007.05.020.

Chevaleyre, V. and Castillo, P. E. (2003) 'Heterosynaptic LTD of hippocampal GABAergic synapses: A novel role of endocannabinoids in regulating excitability', *Neuron*, 38, pp. 461–472. doi: 10.1016/S0896-6273(03)00235-6.

Chevaleyre, V. and Castillo, P. E. (2004) 'Endocannabinoid-mediated metaplasticity in the hippocampus', *Neuron*, 43(6), pp. 871–881. doi: 10.1016/j.neuron.2004.08.036.

Chevaleyre, V., Takahashi, K. A. and Castillo, P. E. (2006) 'Endocannabinoid-mediated synaptic plasticity in the CNS.', *Annual review of neuroscience*, 29, pp. 37–76. doi: 10.1146/annurev.neuro.29.051605.112834.

Christie, J. M. (2007) 'Phototropin Blue-Light Receptors', *Annual Review of Plant Biology*, 58(1), pp. 21–45. doi: 10.1146/annurev.arplant.58.032806.103951.

Christie, J. M. *et al.* (2012) 'LOV to BLUF: Flavoprotein contributions to the optogenetic toolkit', *Molecular Plant*, 5(3), pp. 533–544.

doi: 10.1093/mp/sss020.

Christie, M. J. and Jelinek, H. F. (1993) 'Dye-coupling among neurons of the Rat Locus Coeruleus during postnatal development', *Neuroscience*, 56(1), pp. 129–137. doi: 10.1016/0306-4522(93)90568-Z.

Cibelli, G. *et al.* (2001) 'Corticotropin-releasing factor triggers neurite outgrowth of a catecholaminergic immortalized neuron via cAMP and MAP kinase signalling pathways', *European Journal of Neuroscience*, 13, pp. 1339–1348. doi: 10.1046/j.0953-816x.2001.01510.x.

Cid-Pellitero, E. Del and Garzón, M. (2011) 'Hypocretin1/OrexinA-containing axons innervate locus coeruleus neurons that project to the Rat medial prefrontal cortex. Implication in the sleep-wakefulness cycle and cortical activation', *Synapse*, 65(9), pp. 843–857. doi: 10.1002/syn.20912.

Cintra, L., Kemper, T. and Morgane, P. J. (1982) 'Nucleus Locus Coeruleus : A Morphometric Golgi Study in Rats of Three Age Groups', *Brain Research*, 247, pp. 17–28. doi: 10.1016/0006-8993(82)91023-x.

Clavier, R. M. (1979) 'Afferent projections to the self-stimulation regions of the dorsal pons, including the locus coeruleus, in the rat as demonstrated by the horseradish peroxidase technique', *Brain Research Bulletin*, 4, pp. 497–504. doi: 10.1016/0361-9230(79)90034-0.

Clayton, E. C. *et al.* (2004) 'Phasic Activation of Monkey Locus Ceruleus Neurons by Simple Decisions in a Forced-Choice Task', *The Journal of Neuroscience*, 24(44), pp. 9914–9920. doi: 10.1523/JNEUROSCI.2446-04.2004.

Comeras, L. B., Herzog, H. and Tasan, R. O. (2019) 'Neuropeptides at the crossroad of fear and hunger: a special focus on neuropeptide Y', *Annals of the New York Academy of Sciences*, 1455, pp. 59–80. doi: 10.1111/nyas.14179.

Cosentino, C. *et al.* (2015) 'Engineering of a light-gated potassium channel', *Science*, 648(6235), pp. 707–710. doi: 10.1126/science.aaa2787.

Covey, D. P. and Cheer, J. F. (2019) 'Accumbal Dopamine Release Tracks the Expectation of Dopamine Neuron-Mediated Reinforcement', *Cell Reports*. ElsevierCompany., 27(2), pp. 481-490.e3. doi: 10.1016/j.celrep.2019.03.055.

Crawley, J. N. (1999) 'The role of galanin in feeding behavior', *Neuropeptides*, 33(5), pp. 369–375. doi: 10.1054/npep.1999.0049.

Crozier, R. A. *et al.* (2007) 'Deprivation-induced synaptic depression by distinct mechanisms in different layers of mouse visual cortex', *Proceedings of the National Academy of Sciences of the United States of America*, 104(4), pp. 1383–1388. doi: 10.1073/pnas.0609596104.

Cui, Y. *et al.* (2015) 'Endocannabinoids mediate bidirectional striatal spike-timing-dependent plasticity', *The Journal of Physiology*, 593(13), pp. 2833–2849. doi: 10.1113/JP270324.

Cui, Y. *et al.* (2016) 'Endocannabinoid dynamics gate spike- timing dependent depression and potentiation', *eLife*, 5, pp. 1–32. doi: 10.7554/eLife.13185.

Cui, Y., Perez, S. and Venance, L. (2018) 'Endocannabinoid-LTP mediated by CB1 and TRPV1 receptors encodes for limited occurrences of coincident activity in neocortex', *Frontiers in Cellular Neuroscience*, 12, pp. 1–14. doi: 10.3389/fncel.2018.00182.

Cunningham, E. T. and Sawchenko, P. E. (1988) 'Anatomical specificity of noradrenergic inputs to the paraventricular and supraoptic nuclei of the rat hypothalamus', *Journal of Comparative Neurology*, 274, pp. 60–76. doi: 10.1002/cne.902740107.

Cusulin, J. I. W. *et al.* (2014) 'Experience salience gates endocannabinoid signaling at hypothalamic synapses', *Journal of*

Neuroscience, 34(18), pp. 6177–6181. doi: 10.1523/JNEUROSCI.0163-14.2014.

Daaka, Y., Luttrell, L. M. and Lefkowitz, R. J. (1997) 'Switching of the coupling of the β2-adrenergic receptor to different g proteins by protein kinase A', *Nature*, 390, pp. 88–91. doi: 10.1038/36362.

Dahl, D. and Sarvey, J. M. (1989) 'Norepinephrine induces pathway-specific long-lasting potentiation and depression in the hippocampal dentate gyrus', *Proceedings of the National Academy of Sciences*, 86, pp. 4776–4780. doi: 10.1073/pnas.86.12.4776.

Dahlstroem, A. and Fuxe, K. (1964) 'EVIDENCE FOR THE EXISTENCE OF MONOAMINE-CONTAINING NEURONS IN THE CENTRAL NERVOUS SYSTEM. I. DEMONSTRATION OF MONOAMINES IN THE CELL BODIES OF BRAIN STEM NEURONS.', *Acta physiologica Scandinavica. Supplementum*, 65, pp. 573–596. doi: 10.1007/BF00337069.

Day, H. E. *et al.* (1997) 'Distribution of alpha 1a-, alpha 1b- and alpha 1d-adrenergic receptor mRNA in the rat brain and spinal cord.', *Journal of chemical neuroanatomy*, 13(2), pp. 115–139. doi: 10.1016/s0891-0618(97)00042-2.

Delfs, J. M. *et al.* (1998) 'Origin of noradrenergic afferents to the shell subregion of the nucleus accumbens : anterograde and retrograde tract-tracing studies in the rat', *Brain Research*, 806, pp. 127–140. doi: 10.1016/s0006-8993(98)00672-6.

Dell, T. J. O. *et al.* (2015) 'B -Adrenergic receptor signaling and modulation of long-term potentiation in the mammalian hippocampus', *Learning & Memory*, 22, pp. 461–471. doi: 10.1101/lm.031088.113.

Descarries, L. and Mechawar, N. (2000) 'Ultrastructural evidence for diffuse transmission by monoamine and acetylcholine neurons of the central nervous system', *Progress in Brain Research*, 125, pp. 27–47. doi: 10.1016/S0079-6123(00)25005-X.

Descarries, L. and Saucier, G. (1972) 'Disappearance of the locus coeruleus in the rat after intraventricular 6-hydroxydopamine', *Brain Research*, 37(2), pp. 310–316. doi: 10.1016/0006-8993(72)90676-2.

Deupree, J. D., Reed, A. L. and Bylund, D. B. (2007) 'Differential Effects of the Tricyclic Antidepressant Desipramine on the Density of Adrenergic Receptors in Juvenile and Adult Rats', *The Journal of Pharmacology and Experimental Therapeutics*, 321(2), pp. 770–776. doi: 10.1124/jpet.106.118935.nervous.

Deutch, A. Y., Goldstein, M. and Roth, R. H. (1986) 'Activation of the locus coeruleus induced by selective stimulation of the ventral tegmental area', *Brain Research*, 363(2), pp. 307–314. doi: 10.1016/0006-8993(86)91016-4.

Devilbiss, D. M. and Waterhouse, B. D. (2010) 'Phasic and Tonic Patterns of Locus Coeruleus Output Differentially Modulate Sensory Network Function in the Awake Rat', *Journal of Neurophysiology*, 105, pp. 69–87. doi: 10.1152/jn.00445.2010.

Doze, V. A. *et al.* (2011) 'Long-Term alpha-1A -Adrenergic Receptor Stimulation Improves Synaptic Plasticity , Cognitive Function , Mood , and Longevity', *Molecular Pharmacology*, 80(4), pp. 747–758. doi: 10.1124/mol.111.073734.Norepinephrine.

Dyer-reaves, K. *et al.* (2019) 'Alpha1-Adrenergic Receptor Mediated Long-Term Depression at CA3-CA1 Synapses Can Be Induced via Accumulation of Endogenous Norepinephrine and Is Preserved Following Noradrenergic Denervation', *Frontiers in Synaptic Neuroscience*, 11, pp. 1–10. doi: 10.3389/fnsyn.2019.00027.

Eckmeier, D. and Shea, S. D. (2014) 'Noradrenergic plasticity of olfactory sensory neuron inputs to the main olfactory bulb', *Journal of Neuroscience*, 34(46), pp. 15234–15243. doi: 10.1523/JNEUROSCI.0551-14.2014.

Economidou, D. *et al.* (2012) 'Norepinephrine and Dopamine Modulate Impulsivity on the Five-Choice Serial Reaction Time Task Through Opponent Actions in the Shell and Core Sub-Regions of the Nucleus Accumbens', *Neuropsychopharmacology*. Nature Publishing Group, 37(9), pp. 2057–2066. doi: 10.1038/npp.2012.53.

Van Eden, C. G., Kros, J. M. and Uylings, H. B. M. (1991) 'The development of the rat prefrontal cortex: Its size and development of connections with thalamus, spinal cord and other cortical areas', *Progress in Brain Research*, 85, pp. 169–183. doi: 10.1016/S0079-6123(08)62680-1.

Egan, T. M. and North, R. A. (1985) 'Acetylcholine acts on m2-muscarinic receptors to excite rat locus coeruleus neurones', *British Journal of Pharmacology*, 85(4), pp. 733–735. doi: 10.1111/j.1476-5381.1985.tb11070.x.

Ellgren, M. *et al.* (2008) 'Dynamic changes of the endogenous cannabinoid and opioid mesocorticolimbic systems during adolescence : THC effects', *European Neuropsychopharmacology*, 18, pp. 826–834. doi: 10.1016/j.euroneuro.2008.06.009.

Emorine, L. J. *et al.* (1987) 'Structure of the gene for human β2-adrenergic receptor: Expression and promoter characterization', *Proceedings of the National Academy of Sciences of the United States of America*, 84, pp. 6995–6999. doi: 10.1073/pnas.84.20.6995.

Emorine, L. J. *et al.* (1989) 'Molecular characterization of the human B3-Adrenergic receptor', *Science*, 54(1), pp. 279–280. doi: 10.1016/0167-0115(94)90498-7.

Engberg, G. and Svensson, T. H. (1980) 'Pharmacological analysis of a cholinergic receptor mediated regulation of brain norepinephrine neurons', *Journal of Neural Transmission*, 49(3), pp. 137–150. doi: 10.1007/BF01245220.

Ennis, M. *et al.* (1991) 'Projections From the Periaqueductal Gray to the Rostromedial Pericoerulear Region and Nucleus Locus Coeruleus : Anatomic and Physiologic Studies', *The Journal of Comparative Neurology*, 306, pp. 480–494.

Ennis, M. and Aston-Jones, G. (1988) 'Activation of locus coeruleus from nucleus paragigantocellularis: A new excitatory amino acid pathway in brain', *Journal of Neuroscience*, 8(10), pp. 3644–3657. doi: 10.1523/jneurosci.08-10-03644.1988.

Ennis, M. and Aston-Jones, G. (1989a) 'GABA-Mediated Inhibition of Locus Coeruleus from the Dorsomedial Rostral Medulla', *The Journal of Neuroscience*, pp. 2973–2981. doi: 10.1523/JNEUROSCI.09-08-02973.1989.

Ennis, M. and Aston-Jones, G. (1989b) 'Potent inhibitory input to locus coeruleus from the nucleus prepositus hypoglossi', *Brain Research Bulletin*, 22, pp. 793–803. doi: 10.1016/0361-9230(89)90022-1.

Escanilla, O. *et al.* (2010) 'Noradrenergic modulation of behavioral odor detection and discrimination thresholds in the olfactory bulb', *European Journal of Neuroscience*, 32(3), pp. 458–468. doi: 10.1111/j.1460-9568.2010.07297.x.

Eschenko, O. *et al.* (2012) 'Noradrenergic neurons of the locus coeruleus are phase locked to cortical up-down states during sleep', *Cerebral Cortex*, 22(2), pp. 426–435. doi: 10.1093/cercor/bhr121.

Feldman, D. E. (2012) 'The spike time dependence of plasticity', *Neuron*, 75(4), pp. 556–571. doi: 10.1016/j.neuron.2012.08.001.

Feng, J. *et al.* (2019) 'A Genetically Encoded Fluorescent Sensor for Rapid and Specific In Vivo Detection of Norepinephrine A Genetically Encoded Fluorescent Sensor for Rapid and Specific In Vivo Detection of Norepinephrine', *Neuron*. Elsevier Inc., 102(4), pp. 745-761.e8. doi: 10.1016/j.neuron.2019.02.037.

Finlay, J. M., Zigmond, M. J. and Abercrombie, E. D. (1995) 'INCREASED DOPAMINE AND NOREPINEPHRINE RELEASE IN MEDIAL PREFRONTAL CORTEX INDUCED BY ACUTE AND CHRONIC STRESS: EFFECTS OF DIAZEPAM', *Neruoscience*, 64, pp. 619–628. doi: 10.1016/0306-4522(94)00331-x.

Fitzpatrick, C. M. *et al.* (2018) 'Differential effects of chemogenetic inhibition on dopamine and norepinephrine neurons in the mouse 5-choice serial reaction time task', *Progress in Neuropsychopharmacology & Biological Psychiatry*, 90, pp. 264–276. doi: 10.1016/j.pnpbp.2018.12.004.

Flak, J. N. *et al.* (2014) 'Role of Paraventricular Nucleus-projecting Norepinephrine/ Epinephrine Neurons in Acute and Chronic Stress', *European Journal of Neuroscience*, 176(5), pp. 139–148. doi: 10.1016/j.physbeh.2017.03.040.

Fogelson, N. *et al.* (2009) 'Prefrontal cortex is critical for contextual processing : evidence from brain lesions', *Brain a Journal of Neurology*, 132, pp. 3002–3010. doi: 10.1093/brain/awp230.

Foncelle, A. *et al.* (2018) 'Modulation of Spike-Timing Dependent Plasticity : Towards the Inclusion of a Third Factor in Computational Models', *Frontiers in Computational Neuroscience*, 12, pp. 1–21. doi: 10.3389/fncom.2018.00049.

Foote, S. ., Aston-Jones, G. and Bloom, F. E. (1980) 'Impulse activity of locus coeruleus neurons in awake rats and monkeys is a function of sensory stimulation and arousal Neurobiology ':, *Proceedings of the National Academy of Sciences*, 77(5), pp. 3033–3037. doi: 10.1073/pnas.77.5.3033.

Fort, P. *et al.* (1995) 'Noradrenergic Modulation of Cholinergic Nucleus Basalis Neurons Demonstrated by in vitro Pharmacological and lmmunohistochemical Evidence in the Guinea-pig Brain', *European Journal of Neuroscience*, 7, pp. 1502–1511. doi: 10.1111/j.1460-9568.1995.tb01145.x.

Frielle, T. *et al.* (1987) 'Cloning of the cDNA for the human β1-adrenergic receptor', *Proceedings of the National Academy of Sciences of the United States of America*, 84, pp. 7920–7924. doi: 10.1073/pnas.84.22.7920.

Fritschy, J. -M and Grzanna, R. (1990) 'Distribution of locus coeruleus axons within the rat brainstem demonstrated by Phaseolus vulgaris leucoagglutinin anterograde tracing in combination with dopamine-β-hydroxylase immunofluorescence', *Journal of Comparative Neurology*, 293, pp. 616–631. doi: 10.1002/cne.902930407.

Geracioti, T. D. *et al.* (2001) 'CNS Norepinephrine in Posttraumatic Stress Disorder', *American Journal of Psychiatry*, 158(8), pp. 1227–1230. doi: 10.1176/appi.ajp.158.8.1227.

Geracioti, T. D. *et al.* (2008) 'Effects of trauma-related audiovisual stimulation on cerebrospinal fluid norepinephrine and corticotropin-releasing hormone concentrations in post-traumatic stress disorder', *Psychoneuroendocrinology*, 33, pp. 416–424. doi: 10.1016/j.psyneuen.2007.12.012.

Gerdeman, G. L. and Lovinger, D. M. (2003) 'Emerging roles for endocannabinoids in long-term synaptic plasticity', *British journal of pharmacology*, 140, pp. 781–789. doi: 10.1038/sj.bjp.0705466.

Gerdeman, G. L., Ronesi, J. and Lovinger, D. M. (2002) 'Postsynaptic endocannabinoid release is critical to long-term depression in the striatum', *Nature Neuroscience*, 5(5), pp. 446–451. doi: 10.1038/nn832.

Gerstner, W. *et al.* (2018) 'Eligibility Traces and Plasticity on Behavioral Time Scales : Experimental Support of NeoHebbian Three-Factor Learning Rules', *Frontiers in neural circuits*, 12(July), pp. 1–16. doi: 10.3389/fncir.2018.00053.

Giorgi, A. *et al.* (2017) 'Brain-wide Mapping of Endogenous Serotonergic Transmission via Chemogenetic fMRI', *Cell Reports*. ElsevierCompany., 21(4), pp. 910–918. doi: 10.1016/j.celrep.2017.09.087.

Giovannitti, J. A., Thoms, S. M. and Crawford, J. J. (2015) 'Alpha-2 adrenergic receptor agonists: A review of current clinical applications', *Anesthesia Progress*, 62, pp. 31–39. doi: 10.2344/0003-3006-62.1.31.

Giovannoni, M. P. *et al.* (2009) 'α2-agonists as analgesic agents', *Medicinal Research Reviews*, pp. 339–368. doi: 10.1002/med.20134.

Gobbi, G. *et al.* (2005) 'Antidepressant-like activity and modulation of brain monoaminergic transmission by blockade of anandamide hydrolysis', *Proceedings of the National Academy of Sciences*. National Academy of Sciences, 102(51), pp. 18620–

18625. doi: 10.1073/PNAS.0509591102.

Golden, S. A. *et al.* (2011) 'A standardized protocol for repeated social defeat stress in mice.', *Nature protocols*, 6(8), pp. 1183–91. doi: 10.1038/nprot.2011.361.

Gorea, E. *et al.* (1991) 'Regulation of Noradrenergic Coerulean Neuronal Firing mediated by 5-HT2 receptors: Involvment of the prepositus Hypoglossal Nucleus', *Neuropharmacology*, 30, pp. 1309–1318. doi: 10.1016/0028-3908(91)90028-a.

Gradinaru, V. *et al.* (2010) 'Molecular and Cellular Approaches for Diversifying and Extending Optogenetics', *Cell*. Elsevier Ltd, 141(1), pp. 154–165. doi: 10.1016/j.cell.2010.02.037.

Graham, A. W. and Aghajanian, G. K. (1971) 'Effects of Amphetamine on Single Cell Activity in a Catecholamine Nucleus, the Locus Coeruleus', *Nature*, 234, pp. 100–102. doi: 10.1038/234100b0.

Gremel, C. M. *et al.* (2016) 'Endocannabinoid Modulation of Orbitostriatal Circuits Gates Habit Formation', *Neuron*. Elsevier Inc., 90(6), pp. 1312–1324. doi: 10.1016/j.neuron.2016.04.043.

Gu, Q. (2002) 'Neuromodulatory transmitter systems in the cortex and their role in cortical plasticity', *Neuroscience*, 111, pp. 815–835. doi: 10.1016/S0306-4522(02)00026-X.

Gu, Y. *et al.* (2019) 'A brainstem-central amygdala circuit underlies defensive responses to learned threats', *bioRxiv*. doi: 10.1101/519249.

Hagena, H., Hansen, N. and Manahan-Vaughan, D. (2016) 'β-Adrenergic Control of Hippocampal Function: Subserving the Choreography of Synaptic Information Storage and Memory', *Cerebral Cortex*, 26(4), pp. 1349–1364. doi: 10.1093/cercor/bhv330.

Hagena, H. and Manahan-Vaughan, D. (2012) 'Learning-facilitated long-term depression and long-term potentiation at mossy fiber-CA3 synapses requires activation of β-adrenergic receptors', *Frontiers in Integrative Neuroscience*, 6, pp. 1–11. doi: 10.3389/fnint.2012.00023.

Hansen, N. (2017) 'The Longevity of Hippocampus-Dependent Memory Is Orchestrated by the Locus Coeruleus-Noradrenergic System', *Neural Plasticity*, 2017, pp. 1–9. doi: 10.1155/2017/2727602.

Hardingham, N. *et al.* (2013) 'The role of nitric oxide in pre-synaptic plasticity and homeostasis', *Frontieris in cellular neuroscience*, 7, pp. 1–19. doi: 10.3389/fncel.2013.00190.

Hauser, T. U. *et al.* (2019) 'Distinct Roles of Dopamine and Noradrenaline in Incidental Memory', *The Journal of neuroscience : the official journal of the Society for Neuroscience*, 39(39), pp. 7715–7721. doi: 10.1523/JNEUROSCI.0401-19.2019.

Hayar, A. *et al.* (2001) 'Direct excitation of mitral cells via activation of α1-noradrenergic receptors in rat olfactory bulb slices', *Journal of Neurophysiology*, 86(5), pp. 2173–2182. doi: 10.1152/jn.2001.86.5.2173.

Hayashi, Y. and Maze, M. (1993) 'Alpha2 adrenoceptor agonists and anaesthesia', *British Journal of Anaesthesia*, 71, pp. 108–118. doi: 10.1093/bja/71.1.108.

Heifets, B. D. and Castillo, P. E. (2009) 'Endocannabinoid Signaling and Long-term Synaptic Plasticity', *Annual Reviews of Physiology*, 71, pp. 283–306. doi: 10.1146/annurev.physiol.010908.163149.Endocannabinoid.

Hein, L., Altman, J. D. and Kobilka, B. K. (1999) 'Two functionally distinct α2-adrenergic receptors regulate sympathetic neurotransmission', *Nature*, 402, pp. 481–484. doi: 10.1038/46040.

Hekman, M. *et al.* (1984) 'Reconstitution of beta-adrenergic receptor with components of adenylate cyclase.', *The EMBO Journal*,

3, pp. 3339–3345. doi: 10.1002/j.1460-2075.1984.tb02301.x.

Hendrickson, R. C. and Raskind, M. A. (2016) 'Noradrenergic dysregulation in the pathophysiology of PTSD', *Experimental Neurology*, 284, pp. 181–195. doi: 10.1016/j.expneurol.2016.05.014.

Heng, L. *et al.* (2012) 'Differential developmental trajectories for CB1 cannabinoid receptor expression in limbic/associative and sensorimotor cortical areas', *Synapse*, 65(4), pp. 278–286. doi: 10.1002/syn.20844.Differential.

Herculano-Houzel, S. and Lent, R. (2005) 'Isotropic fractionator: A simple, rapid method for the quantification of total cell and neuron numbers in the brain', *Journal of Neuroscience*, 25(10), pp. 2518–2521. doi: 10.1523/JNEUROSCI.4526-04.2005.

Herkenham, M. *et al.* (1991) 'Characterization and Localization of Cannabinoid Receptors Brain : A Quantitative in vitro Autoradiographic Study in Rat', *The Journal of Neuroscience*, 7, pp. 563–583. doi: 10.1523/JNEUROSCI.11-02-00563.1991.

Herman, J. P. *et al.* (2016) 'Regulation of the hypothalamic-pituitary-adrenocortical stress response', *Comprehensive Physiology*, 6(2), pp. 603–621. doi: 10.1002/cphy.c150015.Regulation.

Hirschberg, S. *et al.* (2017) 'Functional dichotomy in spinal-vs prefrontal-projecting locus coeruleus modules splits descending noradrenergic analgesia from ascending aversion and anxiety in rats', *eLife*, 6, pp. 1–26. doi: 10.7554/eLife.29808.001.

Hobson, A. J., McCarley, R. W. and Wyzinski, P. W. (1975) 'Sleep Cycle Oscillation : Reciprocal Discharge by Two Brainstem Neuronal Groups', *Science*, 189, pp. 55–58. doi: 10.1126/science.1094539.

Hodel, A. S. (2018) 'Rapid infant prefrontal cortex development and sensitivity to early environmental experience', *Developmental Review*. Elsevier, 48(March), pp. 113–144. doi: 10.1016/j.dr.2018.02.003.

Holets, V. R., Hokfelt, A. and Rokaeus, A. (1988) 'LOCUS COERULEUS NEURONS IN THE RAT CONTAINING NEUROPEPTIDE Y, TYROSINE HYDROXYLASE OR GALANIN AND THEIR EFFERENT PROJECTIONS TO THE SPINAL CORD , CEREBRAL CORTEX AND HYPOTHALAMUS', *Neuroscience*, 24(3), pp. 893–906. doi: 10.1016/0306-4522(88)90076-0.

Hopkins, W. F. and Johnston, D. (1984) 'Frequency-dependent noradrenergic modulation of long-term potentiation in the hippocampus', *Science*, 226, pp. 350–352. doi: 10.1126/science.6091272.

Hopkins, W. F. and Johnston, D. (1988) 'Noradrenergic enhancement of long-term potentiation at mossy fiber synapses in the hippocampus', *Journal of Neurophysiology*, 59(2), pp. 667–687. doi: 10.1152/jn.1988.59.2.667.

Horvath, T. L. *et al.* (1999) 'Hypocretin (orexin) activation and synaptic innervation of the locus coeruleus noradrenergic system', *Journal of Comparative Neurology*, 415(2), pp. 145–159. doi: 10.1002/(SICI)1096-9861(19991213)415:2<145::AID-CNE1>3.0.CO;2-2.

Hoxha, E. *et al.* (2016) 'Modulation , Plasticity and Pathophysiology of the Parallel Fiber-Purkinje Cell Synapse', *Frontiers in Synaptic Neuroscience*, 8(November), pp. 1–16. doi: 10.3389/fnsyn.2016.00035.

Hvoslef-Eide, M. *et al.* (2015) 'Facilitation of spatial working memory performance following intra-prefrontal cortical administration of the adrenergic alpha1 agonist phenylephrine', *Psychopharmacology*, 232(21–22), pp. 4005–4016. doi: 10.1007/s00213-015-4038-3.

Ijima, K. and Ohtomo, K. (1988) 'Immunocytochemical Study Using a GABA Antiserum for the Demonstration of Inhibitory Neurons in the Rat Locus Ceruleus', *The American Journal of Anatomy*, 52, pp. 43–52. doi: 10.1002/aja.1001810106.

Insel, P. A. (1996) 'Adrenergic Receptors-evolving concepts and clinical implications', *The New England Journal of Medicine*, 334,

pp. 580–585. doi: 10.1056/NEJM199602293340907.

Ishimatsu, M. and Williams, J. T. (1996) 'Synchronous Activity in Locus Coeruleus Results from Dendritic Interactions in Pericoerulear Regions', *The Journal of Neuroscience*, 16(16), pp. 5196–5204. doi: 10.1523/JNEUROSCI.16-16-05196.1996.

Isingrini, E. *et al.* (2016) 'Resilience to chronic stress is mediated by noradrenergic regulation of dopamine neurons', *Nature Neuroscience*, 19(4), pp. 560–563. doi: 10.1038/nn.4245.

Izquierdo, I. *et al.* (1998) 'Short- and long-term memory are differentially regulated by monoaminergic systems in the rat brain', *Neurobiology of Learning and Memory*, 69, pp. 219–224. doi: 10.1006/nlme.1998.3825.

Jedema, H. P. and Grace, A. A. (2004) 'Corticotropin-releasing hormone directly activates noradrenergic neurons of the locus ceruleus recorded in vitro', *Journal of Neuroscience*, 24, pp. 9703–9713. doi: 10.1523/JNEUROSCI.2830-04.2004.

Jepma, M. *et al.* (2010) 'The role of the noradrenergic system in the exploration – exploitation trade-off : a psychopharmacological study', *Frontiers in Human Neuroscience*, 4(August), pp. 1–13. doi: 10.3389/fnhum.2010.00170.

Jhaveri, D. J. *et al.* (2010) 'Norepinephrine directly activates adult hippocampal precursors via β3-adrenergic receptors', *Journal of Neuroscience*, 30(7), pp. 2995–2806. doi: 10.1523/JNEUROSCI.3780-09.2010.

Jiang, M. *et al.* (1996) 'Activation of locus coeruleus enhances the responses of olfactory bulb mitral cells to weak olfactory nerve input', *Journal of Neuroscience*, 16(19), pp. 6319–6329. doi: 10.1523/jneurosci.16-19-06319.1996.

Jin, X. *et al.* (2016) 'Identification of a Group of GABAergic Neurons in the Dorsomedial Area of the Locus Coeruleus', *PLoS ONE*, pp. 1–13. doi: 10.1371/journal.pone.0146470.

Jodo, E., Chiang, C. and Aston-Jones, G. (1998) 'Potent excitatory influence of prefrontal cortex activity on noradrenergic locus coeruleus neurons', *Neuroscience*, 83(1), pp. 63–79. doi: 10.1016/S0306-4522(97)00372-2.

Jones, B. E. (1990) 'Immunohistochemical study of choline acetyltransferase-immunoreactive processes and cells innervating the pontomedullary reticular formation in the rat', *Journal of Comparative Neurology*, 295(3), pp. 485–514. doi: 10.1002/cne.902950311.

Jones, B. E. and Yang, T. (1985) 'The Efferent Projections From the Reticular Formation and the Locus Coeruleus Studied by Anterograde and Retrograde Axonal Transport in the Rat', *The Journal of Comparative Neurology*, 92, pp. 56–92. doi: 10.1002/cne.902420105.

Joshi, S. *et al.* (2016) 'Relationships between pupil diameter and neuronal activity in the locus coeruleus, colliculi, and cingulate cortex', *Neuron*, 89(1), pp. 221–234. doi: 10.1016/j.neuron.2015.11.028.Relationships.

Kakava-Georgiadou, N. *et al.* (2019) 'An Intersectional Approach to Target Neural Circuits With Cell- and Projection-Type Specificity : Validation in the Mesolimbic Dopamine System', *Frontiers in Molecular Neuroscience*, 12(February), pp. 1–9. doi: 10.3389/fnmol.2019.00049.

Kandel, E. R., Dudai, Y. and Mayford, M. R. (2014) 'Review The Molecular and Systems Biology of Memory', *Cell*. Elsevier Inc., 157(1), pp. 163–186. doi: 10.1016/j.cell.2014.03.001.

Kaur, S., Saxena, R. N. and Mallick, B. N. (1997) 'GABA in locus coeruleus regulates spontaneous rapid eye movement sleep by acting on GABAA receptors in freely moving rats', *Neuroscience Letters*, 3940(May 2018), pp. 3–7. doi: 10.1016/S0304-3940(97)13410-3.

Kaur, S., Saxena, R. N. and Mallick, B. N. (2001) 'GABAergic Neurons in Prepositus Hypoglossi Regulate REM Sleep by Its Action on

Locus Coeruleus in Freely Moving Rats', *Synapse*, 150(November 2000), pp. 141–150. doi: 10.1002/syn.1109.

Kawasaki, Y. *et al.* (2003) 'a2 adrenoceptor-mediated presynaptic inhibition of primary afferent glutamatergic transmission in rat substantia gelatinosa neurons', *Anesthesiology*, 98, pp. 682–689. doi: 10.1097/00000542-200303000-00016.

Keay, K. A. and Bandler, R. (2015) 'Periaqueductal Gray', *The Rat Nervous System, IV edition*, pp. 207–221. doi: 10.1016/B978-0-12-374245-2.00010-3.

Kempadoo, K. A. *et al.* (2016) 'Dopamine release from the locus coeruleus to the dorsal hippocampus promotes spatial learning and memory', *Proceedings of the National Academy of Sciences*, 113(51), pp. 14835–14840. doi: 10.1073/pnas.1616515114.

Kennedy, B. C. *et al.* (2016) 'Conditioned object preference: An alternative approach to measuring reward learning in rats', *Learning and Memory*, 23(11), pp. 623–630. doi: 10.1101/lm.042598.116.

Khanday, M. A. *et al.* (2016) 'Noradrenaline from locus coeruleus neurons acts on pedunculo-pontine neurons to prevent rem sleep and induces its loss-associated effects in rats', *eNeuro*, 3(6), pp. 1–19. doi: 10.1523/ENEURO.0108-16.2016.

Kim, J. *et al.* (2018) 'Yin-and-yang bifurcation of opioidergic circuits for descending analgesia at the midbrain of the mouse', *Proceedings of the National Academy of Sciences of the United States of America*, 115(43), pp. 11078–11083. doi: 10.1073/pnas.1806082115.

Kim, M. A. *et al.* (2004) 'Reciprocal connections between subdivisions of the dorsal raphe and the nuclear core of the locus coeruleus in the rat', *Brain Research*, 1026(1), pp. 56–67. doi: 10.1016/j.brainres.2004.08.022.

Kim, S., Zee, D. S. and Lac, S. (2016) 'Nucleus prepositus hypoglossi lesions produce a unique ocular motor syndrome', *Neurology*, 87(19), pp. 2026–2033. doi: 10.1212/WNL.0000000000003316.

Kimura, F. and Nakamura, S. (1987) 'Postnatal development of alpha-adrenoceptor-mediated autoinhibition in the locus coeruleus.', *Brain research*, 432(1), pp. 21–26. doi: 10.1016/0165-3806(87)90004-6.

Kontaxopoulou, D. *et al.* (2017) 'Incidental and Intentional Memory: Their Relation with Attention and Executive Functions', *Archives of Clinical Neuropsychology*, 32(5), pp. 519–532. doi: 10.1093/arclin/acx027.

Korf, J., S. Bunney, B. and K. Aghajanian, G. (1974) 'Noradrenergic Neurons: Morphine inhibition of spontaneous activity', *European Journal of Pharmacology*, 25(2), pp. 165–169. doi: 10.1016/0014-2999(74)90045-4.

Korotkova, T. M. *et al.* (2005) 'Histamine excites noradrenergic neurons in locus coeruleus in rats', *Neuropharmacology*, 49(1), pp. 129–134. doi: 10.1016/j.neuropharm.2005.03.001.

Kosoyan, H. P., Grigoriadis, D. E. and Tache, Y. (2005) 'The CRF 1 receptor antagonist , NBI-35965 , abolished the activation of locus coeruleus neurons induced by colorectal distension and intracisternal CRF in rats', 1056, pp. 85–96. doi: 10.1016/j.brainres.2005.07.010.

Kravets, J. L. *et al.* (2015) 'Direct targeting of peptidergic amygdalar neurons by noradrenergic afferents: linking stress-integrative circuitry', *Brain structure & function*, 220(1), pp. 541–558. doi: 10.1007/s00429-013-0674-8.

Krishnan, B. *et al.* (2010) 'Dopamine receptor mechanisms mediate corticotropin-releasing factor-induced long-term potentiation in the rat amygdala following cocaine withdrawal', *European Journal of Neuroscience*, 31(6), pp. 1027–1042. doi: 10.1111/j.1460-9568.2010.07148.x.

Kroeger, D. *et al.* (2018) 'Galanin neurons in the ventrolateral preoptic area promote sleep and heat loss in mice', *Nature*

Communications, 9, pp. 1–14. doi: 10.1038/s41467-018-06590-7.

Kruk-Slomka, M. *et al.* (2017) 'Endocannabinoid System: the Direct and Indirect Involvement in the Memory and Learning Processes—a Short Review', *Molecular Neurobiology*. Molecular Neurobiology, 54(10), pp. 8332–8347. doi: 10.1007/s12035-016-0313-5.

Kurose, H. *et al.* (1991) 'Functional Interactions of Recombinant a2 Adrenergic Receptor Subtypes and G Proteins in Reconstituted Phospholipid Vesicles', *Biochemistry*, 30, pp. 3335–3341. doi: 10.1021/bi00227a024.

Lafourcade, M. *et al.* (2007) 'Molecular Components and Functions of the Endocannabinoid System in Mouse Prefrontal Cortex', *PLoS ONE*, 2(8), pp. 1–11. doi: 10.1371/journal.pone.0000709.

Larsen, R. S. and Waters, J. (2018) 'Neuromodulatory correlates of pupil dilation', *Frontiers in Neural Circuits*, 12(March), pp. 1–9. doi: 10.3389/fncir.2018.00021.

Laviola, G. *et al.* (2003) 'Risk-taking behavior in adolescent mice: Psychobiological determinants and early epigenetic influence', *Neuroscience and Biobehavioral Reviews*, 27(1–2), pp. 19–31. doi: 10.1016/S0149-7634(03)00006-X.

Lee, H. S., Lee, B. Y. and Waterhouse, B. D. (2005) 'Retrograde study of projections from the tuberomammillary nucleus to the dorsal raphe and the locus coeruleus in the rat', *Brain Research*, 1043(1–2), pp. 65–75. doi: 10.1016/j.brainres.2005.02.050.

Lee, S. H. and Dan, Y. (2012) 'Neuromodulation of Brain States', *Neuron*, 76(1), pp. 209–222. doi: 10.1016/j.neuron.2012.09.012.

Léna, C. *et al.* (1999) 'Diversity and distribution of nicotinic acetylcholine receptors in the locus ceruleus neurons', *Proceedings of the National Academy of Sciences*, 96(21), pp. 12126–12131. doi: 10.1073/pnas.96.21.12126.

Lenartowicz, A., Escobedo-quiroz, R. and Cohen, J. D. (2010) 'Updating of context in working memory: An event related potential', *Cognitive, Affective, & Behavioral Neuroscience*, 10(2), pp. 298–315. doi: 10.3758/CABN.10.2.298.Updating.

Lethbridge, R. L., Walling, S. G. and Harley, C. W. (2014) 'Modulation of the perforant path-evoked potential in dentate gyrus as a function of intrahippocampal β-adrenoceptor agonist concentration in urethane-anesthetized rat', *Brain and Behavior*, 4(1), pp. 95–103. doi: 10.1002/brb3.199.

Levitt, P. A. T. and Moore, R. Y. (1979) 'Origin and Organization of Brainstem Catecholamine Innervation in the Rat', *Journal of Comparative Neurology*, 186, pp. 505–528. doi: 10.1002/cne.901860402.

Li, Q. and Burrell, B. D. (2011) 'Associative , bidirectional changes in neural signaling utilizing NMDA receptor- and endocannabinoid-dependent mechanisms', *Learning & Memory*, 18(9), pp. 545–553. doi: 10.1101/lm.2252511.

Li, S. Y. *et al.* (2017) 'Involvement of galanin and galanin receptor 1 in nociceptive modulation in the central nucleus of amygdala in normal and neuropathic rats', *Scientific Reports*. Springer US, 7(1), pp. 1–10. doi: 10.1038/s41598-017-13944-6.

Lin, Q.-S. *et al.* (2011) 'Hippocampal endocannabinoids play an important role in induction of long-term potentiation and regulation of contextual fear memory formation', *Brain Research Bulletin*, 86(3–4), pp. 139–145. doi: 10.1016/j.brainresbull.2011.07.011.

Lindvall, O., Bjorklund, A. and Nobin, A. (1973) 'The Adrenergic Innervation of the Rat Thalamus as Revealed by the Glyoxylic Acid Fluorescence Method '', *Journal of Comparative Neurology*, 154(3), pp. 317–348. doi: 10.1002/cne.901540307.

Linster, C. and Cleland, T. A. (2016) 'Neuromodulation of olfactory transformations', *Current Opinion in Neurobiology*. Elsevier Ltd, 40, pp. 170–177. doi: 10.1016/j.conb.2016.07.006.

Linster, C., Nai, Q. and Ennis, M. (2011) 'Nonlinear effects of noradrenergic modulation of olfactory bulb function in adult rodents',

Journal of Neurophysiology, 105(4), pp. 1432–1443. doi: 10.1152/jn.00960.2010.

Lippert, M. T. *et al.* (2018) 'Optogenetic Intracranial Self-Stimulation as a Method to Study the Plasticity-Inducing Effects of Dopamine', *Handbook of Behavioral Neuroscience*, 28, pp. 311–326. doi: 10.1016/B978-0-12-812028-6.00017-3.

Liu, Y. *et al.* (2009) 'Alpha adrenergic modulation on effects of norepinephrine transporter inhibitor reboxetine in five-choice serial reaction time task', *Journal of Biomediacal Science*, 12, pp. 1–12. doi: 10.1186/1423-0127-16-72.

Loughlin, S. E., Foote, S. L. and Grzanna, R. (1986) 'Efferent projections of nucleus locus coeruleus: Morphologic subpopulations have different efferent targets', *Neuroscience*, 18(2), pp. 307–319. doi: 10.1016/0306-4522(86)90156-9.

Luksys, G., Gerstner, W. and Sandi, C. (2009) 'Stress , genotype and norepinephrine in the prediction of mouse behavior using reinforcement learning', *Nature Neuroscience*, 12(9), pp. 1180–1188. doi: 10.1038/nn.2374.

Luppi, P. H. *et al.* (1995) 'Afferent projections to the rat locus coeruleus demonstrated by retrograde and anterograde tracing with cholera-toxin B subunit and Phaseolus vulgaris leucoagglutinin', *Neuroscience*, 65(1), pp. 119–160. doi: 10.1016/0306-4522(94)00481-J.

Luque, J. M., Malherbe, P. and Richards, J. G. (1994) 'Localization of GABA-A receptor subunit mRNA s in the rat locus coeruleus', *Molecular Brain Research*, 24, pp. 219–226. doi: 10.1016/0169-328X(94)90135-X.

Luque, J. M., Malherbe, P. and Richards, J. G. (1995) 'Localization of NMDA receptor subunit mRNAs in the rat locus coeruleus', *Molecular Brain Research*, 29(2), pp. 224–232. doi: 10.1016/0169-328X(94)00253-B.

Ma, S. *et al.* (2013) 'The Journal of Physiology Heterogeneous responses of nucleus incertus neurons to corticotrophin-releasing factor and coherent activity with hippocampal theta rhythm in the rat', 16, pp. 3981–4001. doi: 10.1113/jphysiol.2013.254300.

Machida, C. A. *et al.* (1990) 'Molecular cloning and expression of the rat β1-adrenergic receptor gene', *Journal of Biological Chemistry*, 265(22), pp. 12960–12965. Available at: http://www.jbc.org/content/265/22/12960.long.

Maglio, L. E. *et al.* (2017) 'Endocannabinoid-Dependent Long-Term Potentiation of Synaptic Transmission at Rat Barrel Cortex', *Cerebral Cortex*, 28(5), pp. 1568–1581. doi: 10.1093/cercor/bhx053.

Maity, S. *et al.* (2015) 'Norepinephrine triggers metaplasticity of LTP by increasing translation of specific mRNAs', *Learning & Memory*, 22, pp. 499–508. doi: 10.1101/lm.039222.115.

Manella, L. C., Petersen, N. and Linster, C. (2017) 'Stimulation of the locus ceruleus modulates signal-to-noise ratio in the olfactory bulb', *Journal of Neuroscience*, 37(48), pp. 11605–11615. doi: 10.1523/JNEUROSCI.2026-17.2017.

Mann, D. M. A. and Yates, P. O. (1983) 'Pathological basis for neurotransmitter changes in Parkinson's disease', *Neuropathology and Applied Neurobiology*, 9, pp. 3–19. doi: 10.1111/j.1365-2990.1983.tb00320.x.

Manns, I. D. *et al.* (2003) 'Alpha 2 adrenergic receptors on GABAergic , putative sleep-promoting basal forebrain neurons', *European Journal of Neuroscience*, 18(May), pp. 723–727. doi: 10.1046/j.1460-9568.2003.02788.x.

Marcus, J. N. *et al.* (2001) 'Differential expression of Orexin receptors 1 and 2 in the rat brain', *Journal of Comparative Neurology*, 435(1), pp. 6–25. doi: 10.1002/cne.1190.

Marinelli, S. *et al.* (2008) 'The Endocannabinoid 2-Arachidonoylglycerol Is Responsible for the Slow Self-Inhibition in Neocortical Interneurons', *The Journal of Neuroscience*, 28(50), pp. 13532–13541. doi: 10.1523/JNEUROSCI.0847-08.2008.

Maroso, M. *et al.* (2016) 'Cannabinoid Control of Learning and Memory through HCN Channels', *Neuron*. Elsevier Inc., 89(5), pp.

1059–1073. doi: 10.1016/j.neuron.2016.01.023.

Marsicano, G. *et al.* (2002) 'The endogenous cannabinoid system controls extinction of aversive memories', *Nature*, 418, pp. 557–560. doi: 10.1038/nature00839.

Martins, A. R. O. and Froemke, R. C. (2015) 'Coordinated forms of noradrenergic plasticity in the locus coeruleu and primary auditory cortex', *Nature Neuroscience*, 18(10), pp. 1483–1492. doi: 10.1038/nn.4090.Coordinated.

Masuko, S. *et al.* (1986) 'Noradrenergic Neurons from the Locus Ceruleus in Dissociated Culture : Culture Methods , Morphology , and Electrophysiology', *The Journal of Neuroscience*, 6, pp. 3229–3241. doi: 10.1523/JNEUROSCI.06-11-03229.1986.

Mateo, Y. *et al.* (2017) 'Endocannabinoid Actions on Cortical Terminals Orchestrate Local Modulation of Dopamine Release in the Nucleus Accumbens', *Neuron*, 96(5), pp. 1112-1126.e5. doi: 10.1016/j.neuron.2017.11.012.

Matsuda, L. A., Bonner, T. O. M. I. and Lolait, S. J. (1993) 'Localization of Cannabinoid Receptor mRNA in Rat Brain', *The Journal of Comparative Neurology*, 550, pp. 535–550. doi: 10.1002/cne.903270406.

McCall, J. G. *et al.* (2015) 'CRH Engagement of the Locus Coeruleus Noradrenergic System Mediates Stress-Induced Anxiety', *Neuron*. Elsevier Inc., 87(3), pp. 605–620. doi: 10.1016/j.neuron.2015.07.002.

McCall, J. G. *et al.* (2017) 'Locus coeruleus to basolateral amygdala noradrenergic projections promote anxiety-like behavior', *eLife*, 6, pp. 1–23. doi: 10.7554/eLife.18247.

Mccormick, D. A., Pape, H. and Williamson, A. (1991) 'Actions of norepinephrine in the cerebral cortex and thalamus : implications for function of the central noradrenergic system', *Progress in Brain Research*, 88, pp. 293–305. doi: 10.1016/s0079-6123(08)63817-0.

McDevitt, R. A. *et al.* (2009) 'Stress-induced activity in the locus coeruleus is not sensitive to stressor controllability', *Brain Research*, 1285, pp. 109–118. doi: 10.1016/j.brainres.2009.06.017.Stress-induced.

Mcfarland, J. L. and Fuchs, A. F. (1992) 'Discharge Patterns in Nucleus Prepositus Hypoglossi and Adjacent Medial Vestibular Nucleus During Horizontal Eye Movement in Behaving Macaques', *Journal of Neurophysiology*, 68(1), pp. 319–332. doi: 10.1152/jn.1992.68.1.319.

McGaugh, J. L. (2002) 'Memory consolidation and the amygdala: A systems perspective', *Trends in Neurosciences*, 25(9), pp. 456–461. doi: 10.1016/S0166-2236(02)02211-7.

Mclean, J. H. *et al.* (1989) 'Chemoanatomical Organization of the Noradrenergic Input From Locus Coeruleus to the Olfactory Bulb of the Adult Rat', *THe Journal of Comparative Neurology*, 285, pp. 339–349. doi: 10.1002/cne.902850305.

Megan Gray, J. *et al.* (2015) 'Corticotropin-releasing hormone drives anandamide hydrolysis in the amygdala to promote anxiety', *Journal of Neuroscience*, 35(9), pp. 3879–3892. doi: 10.1523/JNEUROSCI.2737-14.2015.

Mejias-Aponte, C. A. (2016) 'Specificity and impact of adrenergic projections to the midbrain dopamine system', *Brain Research*, 176(3), pp. 139–148. doi: 10.1016/j.physbeh.2017.03.040.

Mejías-Aponte, C. A., Drouin, C. and Aston-Jones, G. (2009) 'Adrenergic and noradrenergic innervation of the midbrain ventral tegmental area and retrorubral field: Prominent inputs from medullary homeostatic centers', *Journal of Neuroscience*, 29(11), pp. 3613–3626. doi: 10.1523/JNEUROSCI.4632-08.2009.

Melis, M. *et al.* (2004) 'Prefrontal cortex stimulation induces 2-arachidonoyl-glycerol-mediated suppression of excitation in

dopamine neurons', *Journal of Neuroscience*, 24(47), pp. 10707–10715. doi: 10.1523/JNEUROSCI.3502-04.2004.

Mena-Segovia, J. (2016) 'Structural and functional considerations of the cholinergic brainstem', *Journal of Neural Transmission*. Springer Vienna, 123(7), pp. 731–736. doi: 10.1007/s00702-016-1530-9.

Mendiguren, A. and Pineda, J. (2006) 'Systemic effect of cannabinoids on the spontaneous firing rate of locus coeruleus neurons in rats', *European Journal of Pharmacology*, 534, pp. 83–88. doi: 10.1016/j.ejphar.2006.01.002.

Meyer, H. C., Lee, F. S. and Gee, D. G. (2018) 'The Role of the Endocannabinoid System and Genetic Variation in Adolescent Brain Development', *Neuropsychopharmacology*. Nature Publishing Group, 43(1), pp. 21–33. doi: 10.1038/npp.2017.143.

Million, M. *et al.* (2003) 'A novel water-soluble selective CRF1 receptor antagonist, NBI 35965, blunts stress-induced visceral hyperalgesia and colonic motor function in rats', *Brain Research*, 985(1), pp. 32–42. doi: 10.1016/S0006-8993(03)03027-0.

Minneman, K. P., Pittman, R. N. and Molinofj, P. B. (1981) 'Beta-Adrenergic receptor subtypes: properties, distribution, and regulation', *Annual Review of Neuroscience*, 4, pp. 419–461. doi: 10.1146/annurev.ne.04.030181.002223.

Mizobe, T. *et al.* (1996) 'Antisense technology reveals the α(2A) adrenoceptor to be the subtype mediating the hypnotic response to the highly selective agonist, dexmedetomidine, in the locus coeruleus of the rat', *Journal of Clinical Investigation*, 98(5), pp. 1076–1080. doi: 10.1172/JCI118887.

Mlinar, B. *et al.* (2016) 'Firing properties of genetically identified dorsal raphe serotonergic neurons in brain slices', *Frontiers in Cellular Neuroscience*, 10, pp. 1–17. doi: 10.3389/fncel.2016.00195.

Montgomery, J. M., Pavlidis, P. and Madison, D. V. (2001) 'Pair recordings reveal all-silent synaptic connections and the postsynaptic expression of long-term potentiation', *Neuron*, 29(3), pp. 691–701. doi: 10.1016/S0896-6273(01)00244-6.

Morilak, D. A. *et al.* (2005) 'Role of brain norepinephrine in the behavioral response to stress', *Progress in Neuro-Psychopharmacology and Biological Psychiatry*, 29, pp. 1214–1224. doi: 10.1016/j.pnpbp.2005.08.007.

Morrison, J. H. *et al.* (1978) 'The distribution and orientation of noradrenergic fibers in neocortex of the rat: An immunofluorescence study', *Journal of Comparative Neurology*, 181(1), pp. 17–39. doi: 10.1002/cne.901810103.

Morrison, J. H. *et al.* (1981) 'The intra-cortical trajectory of the coeruleo-cortical projection in the rat: A tangentially organized cortical afferent', *Neuroscience*, 6(2), pp. 139–158. doi: 10.1016/0306-4522(81)90051-8.

Muntoni, A. L. *et al.* (2006) 'Cannabinoids modulate spontaneous neuronal activity and evoked inhibition of locus coeruleus noradrenergic neurons', *European Journal of Neuroscience*, 23(9), pp. 2385–2394. doi: 10.1111/j.1460-9568.2006.04759.x.

Murchison, C. F. *et al.* (2004) 'A distinct role for norepinephrine in memory retrieval', *Cell*, 117(1), pp. 131–143. doi: 10.1016/S0092-8674(04)00259-4.

Nadim, F. and Bucher, D. (2014) 'Neuromodulation of Neurons and Synapses', *Current Opinion in Neurobiology*, 29, pp. 48–56. doi: 10.1016/j.conb.2014.05.003.Neuromodulation.

Nakamura, S., Kimura, F. and Sakaguchi, T. (1987) 'Postnatal development of electrical activity in the locus ceruleus', *Journal of Neurophysiology*, 58(3), pp. 510–524. doi: 10.1152/jn.1987.58.3.510.

Nakamura, S. and Sakaguchi, T. (1990) 'Development and plasticity of the locus coeruleus: A review of recent physiological and pharmacological experimentation', *Progress in Neurobiology*, 34(6), pp. 505–526. doi: 10.1016/0301-0082(90)90018-C.

Nalepa, I. *et al.* (2013) 'a 1 -Adrenergic receptor subtypes in the central nervous system: insights from genetically engineered mouse

models', *Pharmacological Reports*, 65(6), pp. 1489–1497. Available at: http://www.if-pan.krakow.pl/pjp/pdf/2013/6_1489.pdf.

Natividad, L. A. *et al.* (2017) 'Constitutive Increases in Amygdalar Corticotropin-Releasing Factor and Fatty Acid Amide Hydrolase Drive an Anxious Phenotype', *Biological Psychiatry*, 82(7), pp. 500–510. doi: 10.1016/j.biopsych.2017.01.005.

Nazzaro, C. *et al.* (2012) 'SK channel modulation rescues striatal plasticity and control over habit in cannabinoid tolerance', *Nature Neuroscience*. Nature Publishing Group, 15(2), pp. 284–293. doi: 10.1038/nn.3022.

Oliveira, R. B. D. E. and Howlett, M. C. H. (2010) 'Pacemaker currents in mouse locus coeruleus neurons', *Neuroscience*. Elsevier Inc., 170(1), pp. 166–177. doi: 10.1016/j.neuroscience.2010.06.028.

Olson, L. and Fuxe, K. (1971) 'On the projections from the locus coieruleus noradrenaline neurons : The cerebellar innervation', *Brain Research*, 28, pp. 165–171. doi: 10.1016/0006-8993(71)90533-6.

Ornstein, K. *et al.* (1987) 'Biochemical and radioautographic evidence for dopaminergic afferents of the locus coeruleus originating in the ventral tegmental area', *Journal of Neural Transmission*, 70(3–4), pp. 183–191. doi: 10.1007/BF01253597.

Park, J. W., Bhimani, R. V. and Park, J. (2017) 'Noradrenergic Modulation of Dopamine Transmission Evoked by Electrical Stimulation of the Locus Coeruleus in the Rat Brain', *ACS Chemical Neuroscience*, 8(9), pp. 1913–1924. doi: 10.1021/acschemneuro.7b00078.

Passini, M. A. *et al.* (2003) 'Intraventricular brain injection of adeno-associated virus type 1 (AAV1) in neonatal mice results in complementary patterns of neuronal transduction to AAV2 and total', *Journal of Virology*, 77(12), pp. 7034–7040. doi: 10.1128/JVI.77.12.7034.

Pedrosa, V., Clopath, C. and Zhang, B. (2017) 'The Role of Neuromodulators in Cortical Plasticity . A Computational Perspective', *Frontiers in Synaptic Neuroscience*, 8(January), pp. 1–9. doi: 10.3389/fnsyn.2016.00038.

Perrin-Terrin, A. S. *et al.* (2016) 'The c-FOS protein immunohistological detection: A useful tool as a marker of central pathways involved in specific physiological responses in vivo and ex vivo', *Journal of Visualized Experiments*, 110, pp. 1–9. doi: 10.3791/53613.

Peyron, C. *et al.* (1996) 'Lower brainstem catecholamine afferents to the rat dorsal raphe nucleus', *Journal of Comparative Neurology*, 364(3), pp. 402–413. doi: 10.1002/(SICI)1096-9861(19960115)364:3<402::AID-CNE2>3.0.CO;2-8.

Plugge, B. *et al.* (2000) 'A potassium channel protein encoded by chlorella virus PBCV-1', *Science*, 287(5458), pp. 1641–1644. doi: 10.1126/science.287.5458.1641.

Pollandt, S. *et al.* (2006) 'Cocaine withdrawal enhances long-term potentiation induced by corticotropin-releasing factor at central amygdala glutamatergic synapses via CRF1, NMDA receptors and PKA', *European Journal of Neuroscience*, 24(6), pp. 1733–1743. doi: 10.1111/j.1460-9568.2006.05049.x.

Pomrenze, M. B. *et al.* (2019) 'Dissecting the Roles of GABA and Neuropeptides from Rat Central Amygdala CRF Neurons in Anxiety and Fear Learning', *Cell Reports*, 29(1), pp. 13–21. doi: 10.1016/j.celrep.2019.08.083.

Preston, A. R. and Eichenbaum, H. (2013) 'Interplay of hippocampus and prefrontal cortex in memory', *Current Biology*, 23(17), pp. 1–21. doi: 10.1016/j.cub.2013.05.041.Interplay.

Prouty, E. W., Waterhouse, B. D. and Chandler, D. J. (2016) 'Corticotropin releasing factor dose-dependently modulates excitatory synaptic transmission in the noradrenergic nucleus locus coeruleus', *European Journal of Neuroscience*, 45(5), pp. 712–722. doi: 10.1111/ejn.13501.

Prus, A. J., James, J. R. and Rosecrans, J. A. (2009) 'D 4. Chapter 4 - Conditioned Place Preference', in *Methods of Behavior Analysis*

in Neuroscience.

Pudovkina, O. L. *et al.* (2001) 'The release of noradrenaline in the locus coeruleus and prefrontal cortex studied with dual-probe microdialysis', 906, pp. 38–45. doi: 10.1016/s0006-8993(01)02553-7.

Pudovkina, O. L., Cremers, T. I. F. H. and Westerink, B. H. C. (2002) 'The interaction between the locus coeruleus and dorsal raphe nucleus studied with dual-probe microdialysis', 445, pp. 37–42. doi: 10.1016/s0014-2999(02)01663-1.

Pudovkina, O. L., Cremers, T. I. F. H. and Westerink, B. H. C. (2003) 'Regulation of the release of serotonin in the dorsal raphe nucleus by α1 and α2 adrenoceptors', *Synapse*. doi: 10.1002/syn.10245.

Qi, J. *et al.* (2014) 'A glutamatergic reward input from the dorsal raphe to ventral tegmental area dopamine neurons', *Nature Communications*. Nature Publishing Group, 5, pp. 1–13. doi: 10.1038/ncomms6390.

Qian, H. *et al.* (2012) 'β2-adrenergic receptor supports prolonged theta tetanus-induced LTP', *Journal of Neurophysiology*, 107(10), pp. 2703–2712. doi: 10.1152/jn.00374.2011.

R. Wyrofsky, R., Reyes, B. A. S. and van Bockstaele, E. J. (2017) 'Co-localization of the cannabinoid type 1 receptor with corticotropin-releasing factor-containing afferents in the noradrenergic nucleus locus coeruleus: implications for the cognitive limb of the stress response', *Brain Structure and Function*. Springer Berlin Heidelberg, 222(7), pp. 3007–3023. doi: 10.1007/s00429-017-1381-7.

Rainbow, T. C., Parsons, B. and Wolfe, B. B. (1984) 'Quantitative autoradiography of beta 1- and beta 2-adrenergic receptors in rat brain.', *Proceedings of the National Academy of Sciences of the United States of America*, 81(5), pp. 1585–1589. doi: 10.1073/pnas.81.5.1585.

Ramos, B. P. and Arnsten, A. F. T. (2007) 'Adrenergic pharmacology and cognition: Focus on the prefrontal cortex', *Pharmacology and Therapeutics*, 113(3), pp. 523–536. doi: 10.1016/j.pharmthera.2006.11.006.

Rash, J. E. *et al.* (2007) 'Identification of connexin36 in gap junctions between neurons in rodent locus coeruleus', *Neuroscience*, 147(4), pp. 938–956. doi: 10.1016/j.neuroscience.2007.04.061.

Rassnick, S. *et al.* (1998) 'INJECTION OF CORTICOTROPIN-RELEASING HORMONE INTO THE LOCUS COERULEUS OR FOOT SHOCK INCREASES NEURONAL FOS EXPRESSION', *Neuroscience*, 85(1), pp. 259–268. doi: 10.1016/s0306-4522(97)00574-5.

Reichmann, F. and Holzer, P. (2016) 'Neuropeptide Y: A stressful review', *Neuropeptides*, (1), pp. 99–109. doi: 10.1016/j.npep.2015.09.008.Neuropeptide.

Remaury, A. *et al.* (1993) 'Coupling of the α2-adrenergic receptor to the inhibitory G-protein G(i) and adenylate cyclase in HT29 cells', *Biochemical Journal*, 292(1), pp. 283–288. doi: 10.1042/bj2920283.

Remy Simon, P. Y. and Rousseau, P.-F. (2017) 'Traitement des etats post-traumatiques par un antagoniste-1-adrenergique, la prazosine: Une revue des etudes d'evaluation', *The Canadian Journal of Psychiatry*, 62(3), pp. 186–198. doi: 10.1177/0706743716659275.

Reyes, B. A. S. *et al.* (2005) 'Hypothalamic projections to locus coeruleus neurons in rat brain', *European Journal of Neuroscience*, 22(1), pp. 93–106. doi: 10.1111/j.1460-9568.2005.04197.x.

Reyes, B. A. S. *et al.* (2006) 'Agonist-induced internalization of corticotropin-releasing factor receptors in noradrenergic neurons of the rat locus coeruleus', *European Journal of Neuroscience*, 23(11), pp. 2991–2998. doi: 10.1111/j.1460-9568.2006.04820.x.

Reyes, B. A. S., Drolet, G. and Van Bockstaele, E. J. (2008) 'Dynorphin and stress-related peptides in rat locus coeruleus: Contribution

of amygdalar efferents', *Journal of Comparative Neurology*, 508(4), pp. 663–675. doi: 10.1002/cne.21683.

Reynolds, J. N. J. and Wickens, J. R. (2002) 'Dopamine-dependent plasticity of corticostriatal synapses', *Neural Networks*, 15(4–6), pp. 507–5221. doi: 10.1016/S0893-6080(02)00045-X.

Ricardo, J. (1981) 'POSTSYNAPTIC LOCALIZATION OF a2-ADRENERGIC RECEPTORS IN RAT SUBMANDIBULAR GLAND', *The Journal of Neuroscience*, 1(9), pp. 1003–1007. doi: 10.1523/JNEUROSCI.01-09-01003.1981.

Robbins, T. W. (2002) 'The 5-choice serial reaction time task : behavioural pharmacology and functional neurochemistry', *Psychopharmacology*, 163, pp. 362–380. doi: 10.1007/s00213-002-1154-7.

Rodenkirch, C. *et al.* (2019) 'Feature selectivity via norepinephrine regulation of intrathalamic circuit dynamics', *Nature Neuroscience*. Springer US, 22, pp. 120–133. doi: 10.1038/s41593-018-0283-1.

Root, D. H. *et al.* (2014) 'Role of glutamatergic projections from ventral tegmental area to lateral Habenula in aversive conditioning', *Journal of Neuroscience*, 34(42), pp. 13906–13910. doi: 10.1523/JNEUROSCI.2029-14.2014.

Rossetti, Z. L. and Carboni, S. (2005) 'Noradrenaline and dopamine elevations in the rat prefrontal cortex in spatial working memory', *Journal of Neuroscience*, 25(9), pp. 2322–2329. doi: 10.1523/JNEUROSCI.3038-04.2005.

Ruchhoeft, M. L. *et al.* (1999) 'The Neuronal Architecture of Xenopus Retinal Ganglion Cells Is Sculpted by Rho-Family GTPases In Vivo', *The Journal of Neuroscience*, 19(19), pp. 8454–8463. doi: 10.1523/JNEUROSCI.19-19-08454.1999.

Sakaguchi, T. and Nakamura, S. (1987) 'Some in vivo electrophysiological properties of locus coeruleus neurones in fetal rats', *Experimental Brain Research*, 68, pp. 122–130. doi: 10.1007/bf00255239.

Saleeba, C. *et al.* (2019) 'A Student's Guide to Neural Circuit Tracing', *Frontiers in Neuroscience*, 13(August), pp. 1–19. doi: 10.3389/fnins.2019.00897.

Sanchez-Padilla, J. *et al.* (2014) 'Mitochondrial oxidant stress in locus coeruleus is regulated by activity and nitric oxide synthase', *Nature Neuroscience*. Nature Publishing Group, 17(6), pp. 832–840. doi: 10.1038/nn.3717.

Saponaro, A. *et al.* (2017) 'Fusicoccin activates KAT1 channels by stabilizing their interaction with 14-3-3 proteins', *Plant Cell*, 29(10), pp. 2570–2580. doi: 10.1105/tpc.17.00375.

Sara, S. J. (2009) 'The locus coeruleus and noradrenergic modulation of cognition', *Nature reviews neuroscience*, 10, pp. 211–223. doi: 10.1038/nrn2573.

Sara, S. J. and Bouret, S. (2012) 'Orienting and Reorienting: The Locus Coeruleus Mediates Cognition through Arousal', *Neuron*. Elsevier Inc., 76(1), pp. 130–141. doi: 10.1016/j.neuron.2012.09.011.

Sara, S. J. and Hervé-Minvielle, A. (1995) 'Inhibitory influence of frontal cortex on locus coeruleus neurons', *Proceedings of the National Academy of Sciences of the United States of America*, 92(13), pp. 6032–6036. doi: 10.1073/pnas.92.13.6032.

Sarti, F. *et al.* (2007) 'Acute cocaine exposure alters spine density and long-term potentiation in the ventral tegmental area', *European Journal of Neuroscience*, 26(3), pp. 749–756. doi: 10.1111/j.1460-9568.2007.05689.x.

Scavone, J. L. and Van Bockstaele, E. J. (2009) 'μ-opioid receptor redistribution in the locus coeruleus upon precipitation of withdrawal in opiate-dependent rats', *Anatomical Record*, 292(3), pp. 401–411. doi: 10.1002/ar.20860.

Scavone, J. L., Mackie, K. and Van Bockstaele, E. J. (2010) 'Characterization of cannabinoid-1 receptors in the locus coeruleus: Relationship with mu-opioid receptors', *Brain Research*, 1312, pp. 18–31. doi: 10.1016/j.brainres.2009.11.023.

Scheibner, J. *et al.* (2001) 'α2-adrenoceptors modulating neuronal serotonin release: A study in α2-adrenoceptor subtype-deficient mice', *British Journal of Pharmacology*, 132(4), pp. 925–933. doi: 10.1038/sj.bjp.0703882.

Scheiderer, C. L. *et al.* (2019) 'Novel Form of Long-Term Synaptic Depression in Rat Hippocampus Induced By Activation of Alpha-1 Adrenergic Receptors', *Journal of Neurophysiology*, 91, pp. 1071–1077. doi: 10.1152/jn.00420.2003.

Scheinin, M. *et al.* (1994) 'Distribution of α2-adrenergic receptor subtype gene expression in rat brain', *Molecular Brain Research*, 21(1–2), pp. 133–149. doi: 10.1016/0169-328X(94)90386-7.

Schiff, H. C. *et al.* (2017) 'β-Adrenergic Receptors Regulate the Acquisition and Consolidation Phases of Aversive Memory Formation Through Distinct, Temporally Regulated Signaling Pathways', *Neuropsychopharmacology*. Nature Publishing Group, 42(4), pp. 895–903. doi: 10.1038/npp.2016.238.

Schwarz, L. A. *et al.* (2015) 'Viral-genetic tracing of the input–output organization of a central noradrenaline circuit', *Nature*, 524(7563), pp. 88–92. doi: 10.1038/nature14600.

Schwarz, L. A. and Luo, L. (2015) 'Organization of the locus coeruleus-norepinephrine system', *Current Biology*, 25(21), pp. 1051–1056. doi: 10.1016/j.cub.2015.09.039.

Scofield, M. A., Deupree, J. D. and Bylund, D. B. (2002) 'Adrenergic Receptor Genes', *Molecular Biotechnology*, 21, pp. 171–197. doi: 10.1385/MB:21:2:171.

Segal, M. (1979) 'Serotonergic innervation of the Locus Coeruleus from the dorsal raphe and its action on responses to noxious stimuli', *Journal of Physiology*, 286, pp. 401–415. doi: 10.1113/jphysiol.1979.sp012628.

Seibenhener, M. L. and Wooten, M. C. (2015) 'Use of the Open Field Maze to Measure Locomotor and Anxiety-like Behavior in Mice', *Journal of Visualized Experiments*, 2015, pp. 1–6. doi: 10.3791/52434.

Semba, K. and Fibiger, H. C. (1992) 'Afferent connections of the laterodorsal and the pedunculopontine tegmental nuclei in the rat: A retro- and antero-grade transport and immunohistochemical study', *Journal of Comparative Neurology*, 323(3), pp. 387–410. doi: 10.1002/cne.903230307.

Shefner, S. A. and Osmanovic, S. S. (1991) 'GABA-A and GABA-B , receptors and the ionic mechanisms mediating their effects on locus coeruleus neurons', *Progress in Brain Research*, 88, pp. 187–195. doi: 10.1016/s0079-6123(08)63808-x.

Shipley, M. T. *et al.* (1996) 'Dendrites of Locus Coeruleus Neurons Extend Preferentially Into Two Pericoerulear Zones', *The Journal of Comparative Neurology*, 68, pp. 56–68. doi: 10.1002/(SICI)1096-9861(19960129)365:1<56::AID-CNE5>3.0.CO;2-I.

Shipley, M. T., Halloran, F. J. and De La Torre, J. (1985) 'Surprisingly rich projection from locus coeruleus to the olfactory bulb in the rat', *Brain Research*, 329, pp. 294–299. doi: 10.1016/0006-8993(85)90537-2.

Sievers, J. *et al.* (1981) 'Morphological and biochemical studies on the ontogenesis of the nucleus locus coeruleus.', *Bibliotheca anatomica*, (19), pp. 52–130.

Silva-Cruz, A. *et al.* (2017) 'Dual influence of endocannabinoids on long-term potentiation of synaptic transmission', *Frontiers in Pharmacology*, 8, pp. 1–13. doi: 10.3389/fphar.2017.00921.

Sjöström, P. J., Turrigiano, G. G. and Nelson, S. B. (2003) 'Neocortical LTD via coincident activation of presynaptic NMDA and cannabinoid receptors', *Neuron*, 39(4), pp. 652–654. doi: 10.1016/S0896-6273(03)00476-8.

Van Slooten, J. C. *et al.* (2018) 'How pupil responses track value-based decision-making during and after reinforcement learning',

PLoS Computational Biology, 14(11), pp. 1–24. doi: 10.1371/journal.pcbi.1006632.

Smith, D. M. and Bulkin, D. A. (2014) 'The Form and Function of Hippocampal Context Representations', *Neuroscience & Biobehavioral Reviews*, 40, pp. 52–61. doi: 10.1016/j.neubiorev.2014.01.005.The.

Soeder, K. J. *et al.* (1999) 'The β3-adrenergic receptor activates mitogen-activated protein kinase in adipocytes through a G(i)-dependent mechanism', *Journal of Biological Chemistry*, 274(17), pp. 12017–12022. doi: 10.1074/jbc.274.17.12017.

Soler-Llavina, G. J. and Sabatini, B. L. (2006) 'Synapse-specific plasticity and compartmentalized signaling in cerebellar stellate cells', *Nature Neuroscience*, 9(6), pp. 798–806. doi: 10.1038/nn1698.

Solopchuk, O. *et al.* (2018) 'Locus Coeruleus atrophy doesn't relate to fatigue in Parkinson's disease', *Scientific Reports*, 8(1), pp. 1–7. doi: 10.1038/s41598-018-30128-y.

Sonohata, M. *et al.* (2004) 'Actions of noradrenaline on substantia gelatinosa neurones in the rat spinal cord revealed by in vivo patch recording', *Journal of Physiology*, 555, pp. 515–526. doi: 10.1113/jphysiol.2003.054932.

Spreng, M., Cotecchia, S. and Schenk, F. (2001) 'A Behavioral Study of Alpha-1b Adrenergic Receptor Knockout Mice : Increased Reaction to Novelty and Selectively Reduced Learning Capacities', *Neurobiology of Learning and Memory*, 229, pp. 214–229. doi: 10.1006/nlme.2000.3965.

Stamatakis, A. M. and Stuber, G. D. (2013) 'Activation of lateral habenula inputs to the ventral midbrain promotes behavioral avoidance', *Nature Neuroscience*, 15(8), pp. 1105–1107. doi: 10.1038/nn.3145.Activation.

Starke, K. (1987) 'Presynaptic a-Autoreceptors', *Reviews of Physiology, Biochemistry and Pharmacology*, 107, pp. 73–146.

Steindler, D. A. (1981) 'Locus coerules neurons have axons that branch to the forebrain and cerebellum', *Brain Research*, 223(2), pp. 367–373. doi: 10.1016/0006-8993(81)91149-5.

Steininger, T. L. *et al.* (2001) 'Subregional organization of preoptic area/anterior hypothalamic projections to arousal-related monoaminergic cell groups', *Journal of Comparative Neurology*, 429(4), pp. 638–653. doi: 10.1002/1096-9861(20010122)429:4<638::AID-CNE10>3.0.CO;2-Y.

Stone, E. A. *et al.* (2007) 'Central a 1 -adrenergic system in behavioral activity and depression', *Biochemical Pharmacology*, 73, pp. 1063–1075. doi: 10.1016/j.bcp.2006.10.001.

Strosberg, A. D. (1993) 'Structure , function , and regulation of adrenergic receptors', *Protein Science*, 2, pp. 1198–1209. doi: 10.1002/pro.5560020802.

Sugiyama, D. *et al.* (2012) 'In vivo patch-clamp recording from locus coeruleus neurones in the rat brainstem.', *The Journal of physiology*, 590(Pt 10), pp. 2225–31. doi: 10.1113/jphysiol.2011.226407.

Sullivan, A. F., Dashwood, M. R. and Dickenson, A. H. (1987) 'α2-Adrenoceptor modulation of nociception in rat spinal cord: location, effects and interactions with morphine', *European Journal of Pharmacology*, 138(2), pp. 169–177. doi: 10.1016/0014-2999(87)90430-4.

Summers, R. J. *et al.* (1995) 'Expression of beta 3-adrenoceptor mRNA in rat brain.', *British journal of pharmacology*, 116(6), pp. 2547–8. doi: 10.1111/j.1476-5381.1995.tb17205.x.

Suto, T., Eisenach, J. C. and Hayashida, K. (2015) 'Peripheral nerve injury and gabapentin, but not their combinations impair attentional behavior via direct effects on noradrenergic signaling in the brain', *Pain*, 155(10), pp. 1935–1942. doi:

10.1016/j.pain.2014.05.014.Peripheral.

Svensson, T. H., Bunney, B. S. and Aghajanian, G. K. (1975) 'Inhibition of both noradrenergic and serotonergic neurons in brain by the α-adrenergic agonist clonidine', *Brain Research*, 92(2), pp. 291–306. doi: 10.1016/0006-8993(75)90276-0.

Svensson, T. H. and Usdin, T. (1978) 'Feedback inhibition of brain noradrenaline neurons by tricyclic antidepressants: α-receptor mediation', *Science*, 202(4372), pp. 1089–1091. doi: 10.1126/science.213833.

Swanson, L. W. (1982) 'The projections of the ventral tegmental area and adjacent regions: A combined fluorescent retrograde tracer and immunofluorescence study in the rat', *Brain Research Bulletin*, 9(1–6), pp. 321–353. doi: 10.1016/0361-9230(82)90145-9.

Swanson, L. W. and Hartman, B. K. (1975) 'The central adrenergic system. An immunofluorescence study of the location of cell bodies and their efferent connections in the rat utilizing dopamine-B-hydroxylase as a marker', *Journal of Comparative Neurology*, 163(4), pp. 467–505. doi: 10.1002/cne.901630406.

Swift, K. M. *et al.* (2018) 'Abnormal Locus Coeruleus Sleep Activity Alters Sleep Signatures of Memory Consolidation and Impairs Place Cell Stability and Spatial Memory', *Current Biology*. Elsevier Ltd., 28(22), pp. 3599–3609. doi: 10.1016/j.cub.2018.09.054.

Swinny, J. D. and Valentino, R. J. (2006) 'Corticotropin-releasing factor promotes growth of brain norepinephrine neuronal processes through Rho GTPase regulators of the actin cytoskeleton in rat', *European Journal of Neuroscience*, 24, pp. 2481–2490. doi: 10.1111/j.1460-9568.2006.05129.x.

Szabadi, E. (2013) 'Functional neuroanatomy of the central noradrenergic system', *Journal of Psychopharmacology*, 27(June), pp. 659–693. doi: 10.1177/0269881113490326.

Szymusiak, R. and McGinty, D. (2008) 'Hypothalamic regulation of sleep and arousal', *Annals of the New York Academy of Sciences*, 1129, pp. 275–286. doi: 10.1196/annals.1417.027.

Takahashi, K. *et al.* (2010) 'Locus Coeruleus neuronal activity during the sleep-waking cycle in mice', *Neuroscience*. Elsevier Inc., 169(3), pp. 1115–1126. doi: 10.1016/j.neuroscience.2010.06.009.

Takeuchi, T. *et al.* (2016) 'Locus coeruleus and dopaminergic consolidation of everyday memory', *Nature*, 537, pp. 357–362. doi: 10.1038/nature19325.

Teigen, K. H. (1994) 'Yerkes-Dodson: A Law for all Seasons', *Theory & Psychology*, 4(4), pp. 525–547. doi: 10.1177/0959354394044004.

Thomas, M. J. *et al.* (1996) 'Activity-dependent β-adrenergic modulation of low frequency stimulation induced LTP in the hippocampal CA1 region', *Neuron*, 17(3), pp. 475–482. doi: 10.1016/S0896-6273(00)80179-8.

Torres, G. E., Gainetdinov, R. R. and Caron, M. G. (2003) 'Plasma membrane monoamine transporters: Structure, regulation and function', *Nature Reviews Neuroscience*, 4(1), pp. 13–25. doi: 10.1038/nrn1008.

Totah, N. K. *et al.* (2018) 'The Locus Coeruleus Is a Complex and Differentiated Neuromodulatory System', *Neuron*. Elsevier Inc., 99(5), pp. 1055-1068.e6. doi: 10.1016/j.neuron.2018.07.037.

Travagli, A. R., Dunwiddie, T. V. and Williams, T. L. (1995) 'Opioid Inhibition in Locus Coeruleus', *Journal of Neurophysiology*, 74(2), pp. 519–528. doi: 10.1152/jn.1995.74.2.519.

Trendelenburg, U. (1991) 'The TiPS lecture: Functional aspects of the neuronal uptake of noradrenaline', *Trends in Pharmacological*

Sciences, 12(9), pp. 334–337. doi: 10.1016/0165-6147(91)90592-G.

Tully, K. *et al.* (2007) 'Norepinephrine enables the induction of associative long-term potentiation at thalamo-amygdala synapses', *Proceedings of the National Academy of Sciences*, 104(35). doi: 10.1073/pnas.0704621104.

Tully, K. and Bolshakov, V. Y. (2010) 'Emotional enhancement of memory: how norepinephrine enables synaptic plasticity.', *Molecular brain*, 3(15), pp. 1–9. doi: 10.1186/1756-6606-3-15.

Tye, K. M. *et al.* (2011) 'Amygdala circuitry mediating reversible and bidirectional control of anxiety', *Nature*. Nature Publishing Group, 471(7338), pp. 358–362. doi: 10.1038/nature09820.

Tye, K. M. (2018) 'Neural Circuit Motifs in Valence Processing', *Neuron*. Elsevier Inc., 100(2), pp. 436–452. doi: 10.1016/j.neuron.2018.10.001.

Tzounopoulos, T. *et al.* (2007) 'Coactivation of Pre- and Postsynaptic Signaling Mechanisms Determines Cell-Specific Spike-Timing-Dependent Plasticity', *Neuron*, 54(2), pp. 291–301. doi: 10.1016/j.neuron.2007.03.026.

Uematsu, A. *et al.* (2017) 'Modular organization of the brainstem noradrenaline system coordinates opposing learning states', *Nature Neuroscience*, 20(11), pp. 1602–1611. doi: 10.1038/nn.4642.

Ungerstedt, U. (1971) 'Stereotaxic Mapping of the Monoamine Pathways in the Rat Brain', *Acta Physiologica Scandinavica*, 367, pp. 1–48. doi: 10.1111/j.1365-201X.1971.tb10998.x.

Ungless, M. A. *et al.* (2001) 'Single cocaine exposure in vivo induces long-term potentiation in dopamine neurons', *Nature*, 411(6837), pp. 583–587. doi: 10.1038/35079077.

Unsworth, N. and Robison, M. K. (2017) 'A locus coeruleus-norepinephrine account of individual differences in working memory capacity and attention control', *Psychonomic Bulletin & Review*. Psychonomic Bulletin & Review, 24, pp. 1282–1311. doi: 10.3758/s13423-016-1220-5.

Valentino, R. J. *et al.* (1992) 'Corticotropin-releasing factor innervation of the locus coeruleus region: Distribution of fibers and sources of input', *Neuroscience*, 48(3), pp. 689–705. doi: 10.1016/0306-4522(92)90412-U.

Valentino, R. J., Bockstaele, E. Van and Van Bockstaele, E. (2008) 'Convergent Regulation of Locus Coeruleus activity as an adaptive Response to Stress', *European Journal of Pharmacology*, 583(2–3), pp. 194–203. doi: 10.1016/j.ejphar.2007.11.062.

Valentino, R. J. and Foote, L. (1987) 'Corticotropin-Releasing Hormone Increases Tonic but Not Sensory-Evoked Activity of Noradrenergic Locus Coeruleus Neurons in Unanesthetized Rats', *Journal of Neuroscience*, 8(3), pp. 1016–1025. doi: 10.1523/JNEUROSCI.08-03-01016.1988.

Valentino, R. J., Foote, S. L. and Aston-Jones, G. (1983) 'Corticotropin-releasing factor activates noradrenergic neurons of the locus coeruleus', *Brain Research*, 270(2), pp. 363–367. doi: 10.1016/0006-8993(83)90615-7.

Vazey, E. M., Moorman, D. E. and Aston-Jones, G. (2018) 'Phasic locus coeruleus activity regulates cortical encoding of salience information', *Proceedings of the National Academy of Sciences*, 115(40), pp. 9439–9448. doi: 10.1073/pnas.1803716115.

Velmurugan, B. K., Baskaran, R. and Huang, C. Y. (2019) 'Detailed insight on β-adrenoceptors as therapeutic targets', *Biomedicine and Pharmacotherapy*, 117, pp. 1–8. doi: 10.1016/j.biopha.2019.109039.

Vermeiren, Y. and De Deyn, P. P. (2017) 'Targeting the norepinephrinergic system in Parkinson's disease and related disorders: The locus coeruleus story', *Neurochemistry International*, 102, pp. 22–32. doi: 10.1016/j.neuint.2016.11.009.

Wallace, D. M., Magnuson, D. J. and Gray, T. S. (1989) 'The amygdalo-brainstem pathway: Selective innervation of dopaminergic, noradrenergic and adrenergic cells in the rat', *Neuroscience Letters*, 97(3), pp. 252–258. doi: 10.1016/0304-3940(89)90606-X.

Wamsteeker, J. I., Kuzmiski, J. B. and Bains, J. S. (2010) 'Repeated stress impairs endocannabinoid signaling in the paraventricular nucleus of the hypothalamus', *Journal of Neuroscience*, 30(33), pp. 11188–11196. doi: 10.1523/JNEUROSCI.1046-10.2010.

Wang, M. *et al.* (2007) 'α2A-Adrenoceptors Strengthen Working Memory Networks by Inhibiting cAMP-HCN Channel Signaling in Prefrontal Cortex', *Cell*, 129(2), pp. 397–410. doi: 10.1016/j.cell.2007.03.015.

Wang, W. *et al.* (2016) 'A Primary Cortical Input to Hippocampus Expresses a Pathway-Specific and Endocannabinoid-Dependent Form of Long-Term Potentiation', *eNeuro*, 3(4), pp. 1–17. doi: 10.1523/ENEURO.0160-16.2016.

Waskom, M. L. and Wagner, A. D. (2017) 'Distributed representation of context by intrinsic subnetworks in prefrontal cortex', *Proceedings of the National Academy of Sciences of the United States of America*, 114(8), pp. 2030–2035. doi: 10.1073/pnas.1615269114.

Waterhouse, B. D. *et al.* (1993) 'Topographic organization of rat locus coeruleus and dorsal raphe nuclei: Distribution of cells projecting to visual system structures', *Journal of Comparative Neurology*, 336(3), pp. 345–361. doi: 10.1002/cne.903360304.

Waterhouse, B. D. and Chandler, D. (2012) 'Evidence for broad versus segregated projections from cholinergic and noradrenergic nuclei to functionally and anatomically discrete subregions of prefrontal cortex', *Frontiers in Behavioral Neuroscience*, 6, pp. 1–9. doi: 10.3389/fnbeh.2012.00020.

Watson, M. and Mcelligott, J. G. (1984) 'Cerebellar Norepinephrine Depletion and Impaired Acquisition of Specific Locomotor Tasks in Rats', *Brain Research*, 296, pp. 129–138. doi: 10.1016/0006-8993(84)90518-3.

Weber, T. *et al.* (2011) 'Inducible Gene Manipulations in Brain Serotonergic Neurons of Transgenic Rats', *PLoS ONE*, 6(11), pp. 1–8. doi: 10.1371/journal.pone.0028283.

Weinshenker, D. (2018) 'Long Road to Ruin : Noradrenergic Dysfunction in Neurodegenerative Disease', *Trends in Neurosciences*. Elsevier Ltd, 41(4), pp. 211–223. doi: 10.1016/j.tins.2018.01.010.

Wellman, P. *et al.* (2002) 'Cocaine-induced hypophagia and hyperlocomotion in rats are attenuated by prazosin', *European Journal of Pharmacology*, 455(2–3), pp. 117–126. doi: 10.1016/S0014-2999(02)02616-X.

Werchan, D. M. and Amso, D. (2017) 'A Novel Ecological Account of Prefrontal Cortex Functional Development', *Psychological Review*, 124(6), pp. 720–739. doi: 10.1037/rev0000078.A.

Westlund, K. N. *et al.* (1991) 'Noradrenergic innervation of somatosensory thalamus and spinal cord', *Progress in Brain Research*, 88, pp. 77–88. doi: 10.1016/S0079-6123(08)63800-5.

Wiegert, J. S. *et al.* (2017) 'Silencing Neurons: Tools, Applications, and Experimental Constraints', *Neuron*. Elsevier Inc., 95(3), pp. 504–529. doi: 10.1016/j.neuron.2017.06.050.

Wilcox, G. L. *et al.* (1987) 'Mutual potentiation of antinociceptive effects of morphine and clonidine on motor and sensory responses in rat spinal cord', *Brain Research*, 405(1), pp. 84–93. doi: 10.1016/0006-8993(87)90992-9.

Williams, J. T. *et al.* (1984) 'Membrane properties of rat locus coeruleus neurones', *Neuroscience*, 13(1), pp. 137–156. doi: 10.1016/0306-4522(84)90265-3.

Wilson, R. S. *et al.* (2013) 'Neural reserve, neuronal density in the locus ceruleus, and cognitive decline', *Neurology*, 80(13), pp.

1202–1208. doi: 10.1212/WNL.0b013e3182897103.

Woo, S. and Gomez, T. M. (2006) 'Rac1 and RhoA Promote Neurite Outgrowth through Formation and Stabilization of Growth Cone Point Contacts', *The Journal of Neuroscience*, 26(5), pp. 1418–1428. doi: 10.1523/JNEUROSCI.4209-05.2006.

Wu, D. *et al.* (1992) 'Activation of phospholipase C by α1-adrenergic receptors is mediated by the α subunits of Gq family', *Journal of Biological Chemistry*, 267(36), pp. 25798–25802. Available at: http://www.jbc.org/content/267/36/25798.long.

Wu, Z. *et al.* (2014) 'Galanin neurons in the medial preoptic area govern parental behaviour', *Nature*. Nature Publishing Group, 509(7500), pp. 325–330. doi: 10.1038/nature13307.

Wyrofsky, R. R. *et al.* (2019) 'Neurobiology of Stress Endocannabinoids , stress signaling , and the locus coeruleus-norepinephrine system', *Neurobiology of Stress*. Elsevier, 11, p. 100176. doi: 10.1016/j.ynstr.2019.100176.

Xiao, R. P. (2001) 'Beta-adrenergic signaling in the heart: dual coupling of the beta2-adrenergic receptor to G(s) and G(i) proteins.', *Science's STKE : signal transduction knowledge environment*, 2001(104), p. re15. doi: 10.1126/stke.2001.104.re15.

Xu, H. *et al.* (2018) 'Dopamine–endocannabinoid interactions mediate spike-timing-dependent potentiation in the striatum', *Nature Communications*. Springer US, 9(1), pp. 1–18. doi: 10.1038/s41467-018-06409-5.

Xu, J.-Y., Zhang, J. and Chen, C. (2012) 'Long-lasting potentiation of hippocampal synaptic transmission by direct cortical input is mediated via endocannabinoids.', *The Journal of physiology*, 590(Pt 10), pp. 2305–2315. doi: 10.1113/jphysiol.2011.223511.

Xu, M. *et al.* (2015) 'Basal forebrain circuit for sleep-wake control', *Nature Neuroscience*. Nature Publishing Group, 18(11), pp. 1641–1647. doi: 10.1038/nn.4143.

Yamamoto, K. I., Shinba, T. and Yoshii, M. (2014) 'Psychiatric symptoms of noradrenergic dysfunction: A pathophysiological view', *Psychiatry and Clinical Neurosciences*, 68(1), pp. 1–20. doi: 10.1111/pcn.12126.

Yamawaki, N. *et al.* (2016) 'Combining optogenetics and electrophysiology to analyze projection neuron circuits', *Cold Spring Harbor Protocols*, 2016(10), pp. 840–846. doi: 10.1101/pdb.prot090084.Combining.

Yang, K. and Dani, J. A. (2014) 'Dopamine d1 and d5 receptors modulate spike timing-dependent plasticity at medial perforant path to dentate granule cell synapses', *Journal of Neuroscience*, 34(48), pp. 15888–15897. doi: 10.1523/JNEUROSCI.2400-14.2014.

Yerkes, R. M. and Dodson, J. D. (1908) 'The relation of strength of stimulus to rapidity of habit-formation', *Journal of Comparative Neurology and Psychology*, 18(5), pp. 459–482. doi: 10.1002/cne.920180503.

Young, W. S. and Kuhar, M. J. (1980) 'Noradrenergic α1 and α2 receptors: Light microscopic autoradiographic localization', *Proceedings of the National Academy of Sciences of the United States of America*, 77(3), pp. 1696–1700. doi: 10.1073/pnas.77.3.1696.

Zanettini, C. *et al.* (2011) 'Effects of endocannabinoid system modulation on cognitive and emotional behavior', *Frontiers in Behavioral Neuroscience*, 5, pp. 1–21. doi: 10.3389/fnbeh.2011.00057.

Zarow, C. *et al.* (2003) 'Neuronal loss is greater in the locus coeruleus than nucleus basalis and substantia nigra in Alzheimer and Parkinson diseases', *Archives of Neurology*, 60(3), pp. 337–341. doi: 10.1001/archneur.60.3.337.

Zerbi, V. *et al.* (2019) 'Rapid Reconfiguration of the Functional Connectome after Chemogenetic Locus Coeruleus Activation', *Neuron*. Elsevier Inc., 103(4), pp. 702-718.e5. doi: 10.1016/j.neuron.2019.05.034.

Zhang, C. *et al.* (1998) 'Locus coeruleus modulates thalamic nociceptive responses via adrenoceptors', *Brain Research*, 784(1–2),

pp. 116–122. doi: 10.1016/S0006-8993(97)01197-9.

Zhang, J., Muller, J. F. and Mcdonald, A. J. (2013) 'Noradrenergic innervation of Pyramidal cells in th rat basolateral amygdala', *Neuroscience*, 228, pp. 395–408. doi: 10.1016/j.neuroscience.2012.10.035.

Zhang, X. *et al.* (2010) 'Intrinsic membrane properties of locus coeruleus neurons in Mecp2 -null mice', *American Journal of Physiology Cell Physiology*, 30303, pp. 635–646. doi: 10.1152/ajpcell.00442.2009.

Zhang, X. Y. and Kosten, T. A. (2005) 'Prazosin, an α-1 adrenergic antagonist, reduces cocaine-induced reinstatement of drug-seeking', *Biological Psychiatry*, 57(10), pp. 1202–1204. doi: 10.1016/j.biopsych.2005.02.003.

Zhong, H. and Minneman, K. P. (1999) 'a1-Adrenoceptor subtypes', *European Journal of Neuroscience*, 375, pp. 261–276. doi: 10.1016/s0014-2999(99)00222-8.

Zhou, J. (2004) 'Norepinephrine transporter inhibitors and their therapeutic potential', *Drugs of the Future*, 29(12), pp. 1235–1244. doi: 10.1358/dof.2004.029.12.855246.

Zhu, F. *et al.* (2017) 'A single dose of cocaine potentiates glutamatergic synaptic transmission onto locus coeruleus neurons', *Cell Calcium*. Elsevier Ltd, 67, pp. 11–20. doi: 10.1016/j.ceca.2017.07.007.

Pubblications

1. Cavaccini, A., Gritti, M., Giorgi, A., **Locarno, A.**, Heck, N., Migliarini, S., … Tonini, R. (2018). Serotonergic Signaling Controls Input-Specific Synaptic Plasticity at Striatal Circuits. Neuron. https://doi.org/10.1016/j.neuron.2018.04.008

2. Alberio, L. & **Locarno, A.**, Saponaro, A., Romano, E., Bercier, V., Albadri, S., … Moroni, A. (2018). A light-gated potassium channel for sustained neuronal inhibition. Nature Methods. https://doi.org/10.1038/s41592-018-0186-9 (Co-first authorship)

Appendix

nature methods

ARTICLES

https://doi.org/10.1038/s41592-018-0186-9

A light-gated potassium channel for sustained neuronal inhibition

Laura Alberio[1,13], Andrea Locarno[2,13], Andrea Saponaro[1], Edoardo Romano[1], Valérie Bercier[3], Shahad Albadri[3], Federica Simeoni[1], Silvia Moleri[1], Silvia Pelucchi[4,5], Alessandro Porro[1], Elena Marcello[4], Noemi Barsotti[6], Kerri Kukovetz[7], Arjen J. Boender[2], Andrea Contestabile[8], Shizhen Luo[9], Aubin Moutal[9], Yingshi Ji[9], Giulia Romani[10], Monica Beltrame[1], Filippo Del Bene[3], Monica Di Luca[4], Rajesh Khanna[9], Henry M. Colecraft[11], Massimo Pasqualetti[6,12], Gerhard Thiel[7], Raffaella Tonini[2*] and Anna Moroni[1,10,11*]

Currently available inhibitory optogenetic tools provide short and transient silencing of neurons, but they cannot provide long-lasting inhibition because of the requirement for high light intensities. Here we present an optimized blue-light-sensitive synthetic potassium channel, BLINK2, which showed good expression in neurons in three species. The channel is activated by illumination with low doses of blue light, and in our experiments it remained active over (tens of) minutes in the dark after the illumination was stopped. This activation caused long periods of inhibition of neuronal firing in ex vivo recordings of mouse neurons and impaired motor neuron response in zebrafish in vivo. As a proof-of-concept application, we demonstrated that in a freely moving rat model of neuropathic pain, the activation of a small number of BLINK2 channels caused a long-lasting (>30 min) reduction in pain sensation.

Remote manipulation of ion channels by light is a powerful method to control neuronal activities. Light-gated proton (archaerhodopsin)[1] and chloride pumps (halorhodopsin)[2–4] and anion-selective channelrhodopsins (ACRs)[5–8] are established optogenetic tools for the inhibition of neuronal activity. Given their fast on and off kinetics, pumps are well suited for millisecond-precision applications[2,9,10], but they have limitations when long-lasting inhibition (for seconds to minutes) is required. Under prolonged activity, pumps substantially affect ion-concentration gradients across the plasma membrane[11,12] and eventually lead to paradoxical effects with activation instead of inactivation[13]. Longer inhibition can be achieved with ACRs that have a slow off kinetics[8,14]; however, their effectiveness depends directly on the chloride reversal potential (E_{Cl^-}), which can vary among neurons. Immature neurons[15] and axon initial segments[16] of mature neurons can have a positively shifted E_{Cl^-}, which will promote activation rather than inhibition after ACR channel opening.

Given the universal role of K^+ conductance in the termination of action potentials and its major contribution to the resting potential, there is interest in engineering light-gated K^+ channels. We previously engineered BLINK1, in which a LOV2[17,18] photoreceptor domain reversibly controls a K^+ channel (Kcv_{PBCV1})[19] in response to blue light (455 nm)[20]. BLINK1 has favorable properties for optogenetics: a low light requirement that avoids tissue heating and damage, a large unitary conductance (>100 pS) to counteract excitatory currents, and a lack of inactivation during prolonged illumination. In vivo experiments with zebrafish embryos highlighted the use of BLINK1 as an inhibitory tool. However, BLINK1 has low surface expression, which hampers its wider use. We present here an improved version of the channel, BLINK2, which showed higher surface expression in neurons compared with that of BLINK1, as well as efficient inhibition of firing in three animal models: zebrafish, rat and mouse. Unique to BLINK2 is its post-illumination activity, which lasts tens of minutes. This property is advantageous for achieving long neuronal inhibition without toxic exposure to prolonged illumination, for instance, in the case of neuropathic pain or in behavioral animal experiments. As proof of principle, we show that BLINK2 activation by light reduced pain for more than 30 min in a rat model and inhibited the touch-evoked escape response in zebrafish. This durable light-off activity of BLINK2 paves the way for optogenetic interventions in chronic applications.

Results

Improving surface expression of BLINK1. We improved BLINK1 trafficking to the plasma membrane by adding C-terminal signal sequences that promote forward trafficking in eukaryotic K^+ channels[21]. We tested, alone and in combination, the endoplasmic reticulum export motif and trafficking signals of Kir2.1[21] and the 14-3-3 binding sites of TASK1-3[22] and KAT1[23–25]. We coexpressed the constructs (Supplementary Table 1) with GFP in HEK293T cells and

[1]Department of Biosciences, University of Milan, Milan, Italy. [2]Neuromodulation of Cortical and Subcortical Circuits Laboratory, Neuroscience and Brain Technologies Department, Fondazione Istituto Italiano di Tecnologia, Genoa, Italy. [3]Institut Curie, PSL Research University, INSERM U934, CNRS UMR315, SU Sorbonne University, Paris, France. [4]Department of Pharmacological and Biomolecular Sciences, University of Milan, Milan, Italy. [5]Department of Neurosciences, Psychology, Drug Research and Child Health, Section of Pharmacology and Toxicology, University of Florence, Florence, Italy. [6]Department of Biology, University of Pisa, Pisa, Italy. [7]Department of Biology, Technische Universität-Darmstadt, Darmstadt, Germany. [8]Neuroscience and Brain Technologies Department, Fondazione Istituto Italiano di Tecnologia, Genoa, Italy. [9]Department of Pharmacology, University of Arizona, Tucson, AZ, USA. [10]Institute of Biophysics, Consiglio Nazionale delle Ricerche, Milan, Italy. [11]Department of Physiology and Cellular Biophysics, Columbia University, New York, NY, USA. [12]Center for Neuroscience and Cognitive Systems, Istituto Italiano di Tecnologia, Rovereto, Italy. [13]These authors contributed equally: Laura Alberio and Andrea Locarno. *e-mail: raffaella.tonini@iit.it; anna.moroni@unimi.it

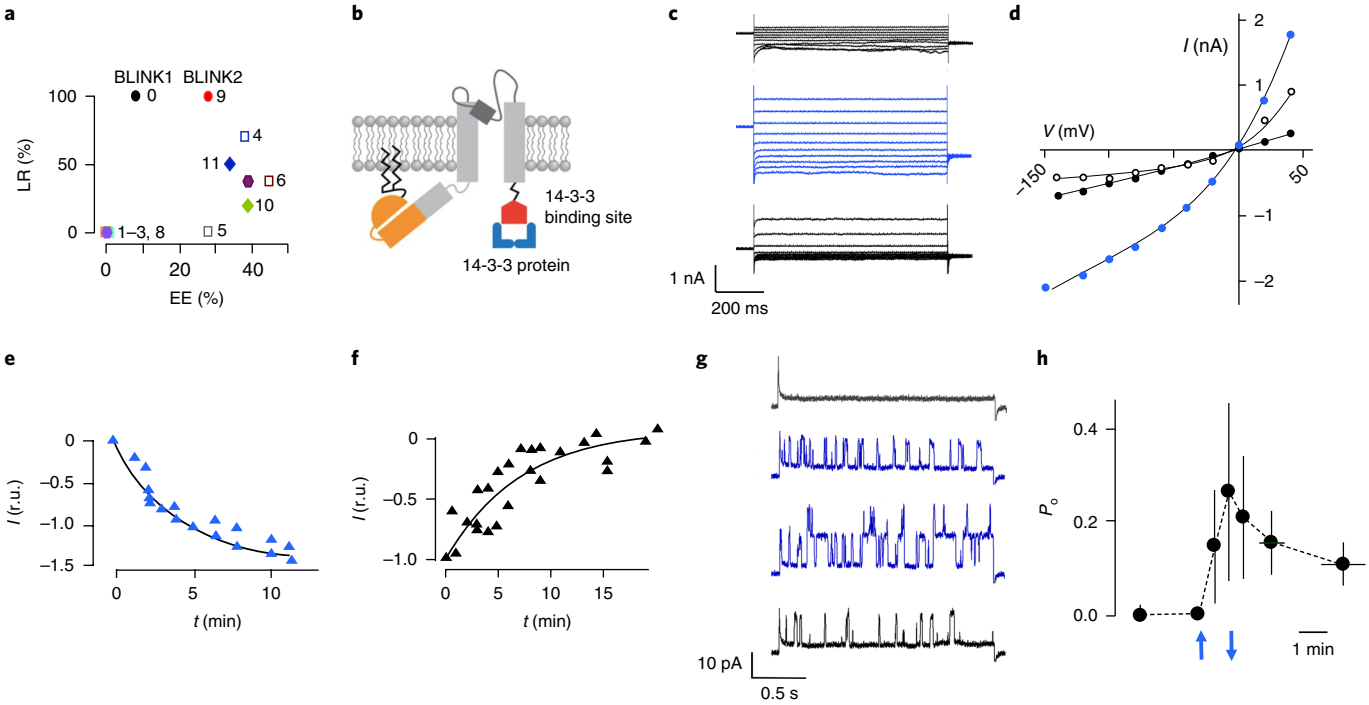

Fig. 1 | Engineering and characterization of BLINK2. a, Surface expression and light regulation of BLINK1 derivatives. Expression efficiency (EE) was defined as the percentage of cells with measurable BLINK1-like current. Light regulation (LR) represents the percentage of cells that did not show dark current. Clones are numbered according to Supplementary Table 1. **b**, Cartoon representation of BLINK2 showing the Kcv_{PBCV1} channel (gray), LOV2 domain (orange), N-terminal myristoylation and palmitoylation sites (zigzagging black lines) and a fragment of *Arabidopsis thaliana* KAT1 protein (GenBank AED95356.1) (red) for binding of 14-3-3 proteins (blue). **c**, Whole-cell recordings from a COS7 cell transfected with BLINK2 in response to voltage steps from +60 to −140 mV in the dark (top black traces), 5 min after the start of blue light illumination (blue traces) and 5 min after returning to darkness (bottom black traces). Similar results were obtained in $n = 9$ cells from 10 independent experiments. **d**, *I*/*V* relationship from measurements in **c** in the dark (black solid circles), in blue light (blue circles) and after a return to dark conditions (open black circles). **e**,**f**, Activation kinetics of BLINK2 current in blue light (**e**) and after deactivation in the dark (**f**). Currents were recorded at −100 mV and normalized to $t = 5$ and $t = 0$ min for activation and deactivation, respectively (r.u., relative units). Data were fitted with a single exponential (solid line). **g**, Single-channel recordings from cell-attached measurement of BLINK2 in COS7 cells. The traces show the current response to a voltage step from 0 mV to +40 mV in a dark-adapted cell (top black trace), after 1.5 and 2 min of blue light (blue traces) and 1 min after turning the light off (bottom black trace). Similar results were obtained in $n = 4$ cells from 4 independent experiments. **h**, Open probability (P_o) changes of BLINK2 single channels in response to dark/light transitions. Recordings were done at +40 mV in the cell-attached configuration. Blue arrows indicate the time of light on (upward-facing arrow) and light off (downward-facing arrow). Data shown are the mean ± s.d. of the time at which measurements were performed in 4 experiments. In all experiments reported in this figure, the blue light (455 nm) intensity was 90 μW/mm^2.

measured light-regulated currents by patch clamp. We evaluated two parameters: expression efficiency (the percentage of GFP^+ cells with a measurable BLINK1-like K^+ current) and light regulation (the percentage of cells with no K^+ current in the dark). Most clones showed an increase in expression efficiency to >25%, compared with 8% for BLINK1 (Fig. 1a). High expression efficiency, however, resulted in a loss of light regulation. In clone 4, for instance, the addition of Kir2.1 trafficking signal increased the expression efficiency to about 40% but decreased light regulation from 100% to ~70%, thus making the construct unsuitable as an optogenetic tool. Only clone 9, which we renamed BLINK2, showed improved expression efficiency (~28%) and 100% light regulation. BLINK2 (Fig. 1b) has the same topology as BLINK1 and the C terminus of KAT1 (amino acids 506–677, KAT1 numbering) (Supplementary Table 1). This KAT1 sequence ends with the binding motif ^{673}YFSDN^{677} for 14-3-3 proteins, a class of adaptors that promote KAT1 surface expression[25]. Figure 1c shows exemplary whole-cell recordings from a BLINK2-transfected COS7 cell in which dark/light transition activated a particularly high current, which is normally in the range of 200–500 pA. In the dark, we measured low currents in BLINK2-transfected cells that were similar to those in untransfected or GFP-transfected cells (Supplementary Fig. 1), indicating that the channel was closed. Inhibition by $BaCl_2$ showed that the dark current was an endogenous potassium conductance of COS7 cells. 3 min of blue light illumination (455 nm, 90 μW/mm^2) elicited a voltage-independent current increase, which reverted after 5 min of darkness (Fig. 1c,d). We estimated a t_{on} of 2.7 min ($n = 5$) and a t_{off} of 7.4 min ($n = 6$) (Fig. 1e,f).

BLINK2 is activated specifically by blue light (Supplementary Fig. 2). We measured BLINK2 single-channel currents in cell-attached recordings (Fig. 1g). Blue light gradually increased channel activity within 2 min. A return to darkness reduced channel activity after 1 min. The unitary conductance of the light-activated channel is about 130 pS (102 mM K^+_{out}). Comparison of the *i*/*V* relationship of BLINK2 with those of BLINK1 and Kcv_{PBCV1} (Supplementary Fig. 3) showed that BLINK2 retained a large unitary conductance (>100 pS in 100 mM K^+)[20,26].

We determined the dynamics of BLINK2 open probability (P_o) during light/dark transitions from cell-attached recordings (Fig. 1h; $n = 4$). An increase in P_o was measurable after only 30 s of light exposure and increased further during 60 s of illumination. Deactivation in the dark was slower and highly variable. For example, in one case

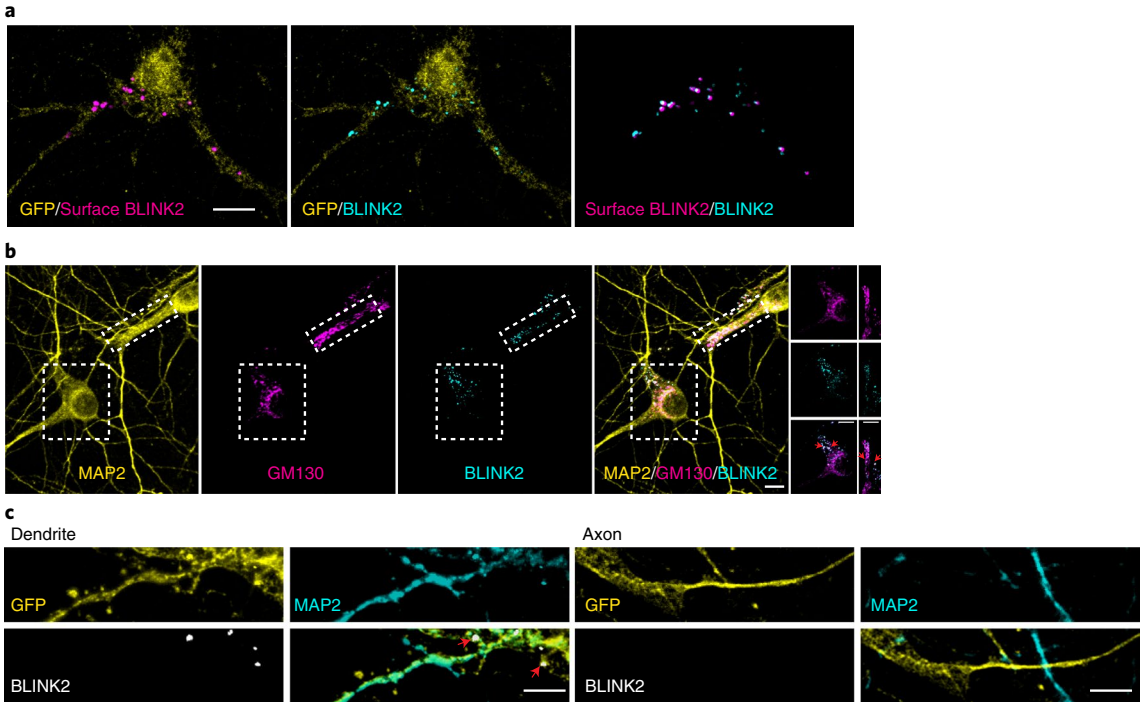

Fig. 2 | BLINK2 expression in rat hippocampal neurons. a, BLINK2 expression. Left, BLINK2 at the cell surface (magenta). Center, total BLINK2 (turquoise). Right, merged image. GFP is shown in yellow. Scale bar, 10 µm. Similar results were obtained in $n = 27$ cells from 3 independent experiments. **b**, From left to right, staining for MAP2, Golgi marker GM130 (magenta) and BLINK2 (turquoise), and merged images. The rightmost images are cropped views of the regions outlined by boxes in the other images in the row; red arrowheads indicate colocalization between BLINK2 and GM130. Scale bars, 10 µm. Similar results were obtained in $n = 15$ cells from 3 independent experiments. **c**, GFP (yellow), MAP2 (turquoise) and BLINK2 (white) in dendrites ($MAP2^+$) and axons ($MAP2^-$). Scale bars, 5 µm. Similar results were observed in $n = 16$ cells from 3 independent experiments. All images were acquired from cultured rat hippocampal neurons infected with AAV1/2-hSyn-BLINK2-IRES-eGFP. Neurons in **c** were also transfected with a GFP expression plasmid.

the current kept increasing over a short time window in the dark, and in another case we measured residual channel activity 20 min after the light was turned off. Single-channel data confirmed that the light-induced macroscopic current (Fig. 1c) was generated by the large conductance BLINK2 channel. The slow deactivation kinetics in the dark suggests that BLINK2 can be used as a tool for sustained inhibition after cessation of illumination.

BLINK2 localization in rat hippocampal primary neurons. We infected rat primary hippocampal neuronal cultures with an adeno-associated virus (AAV) expressing BLINK2 (AAV-hSyn-BLINK2-IRES-eGFP). An immunofluorescence-based antibody assay[27] showed that BLINK2 was expressed at the cell surface with a punctate staining pattern (Fig. 2a). We found no immunofluorescence for an intracellular protein (MAP2) in nonpermeabilized cells, which demonstrates the reliability of our assay and the specificity of BLINK2 membrane staining (Supplementary Fig. 4a). The percentage of cells surface-stained for BLINK2 versus the total number of GFP^+ cells ($n = 14$) was 66.14% ± 3.23% (all values are ± s.e.m. unless stated otherwise).

BLINK2 intracellularly colocalized with the Golgi marker GM130 in the soma and in dendritic Golgi outposts (Fig. 2b), which suggests that it is sorted along the secretory pathway. The average value for surface versus total staining was 32.73% ± 2.34% ($n = 27$). Thus, about one-third of BLINK2 protein expressed by a neuron reaches the plasma membrane. To determine the localization of BLINK2 in axonal and somatodendritic domains, we used the MAP2 marker. BLINK2 clusters were detectable in the dendritic compartment ($MAP2^+$) but not in the axon ($MAP2^-$) (Fig. 2c). We further assessed colocalization of BLINK2 clusters with the presynaptic marker Bassoon and the postsynaptic protein PSD-95. BLINK2 clusters partially colocalized with the synaptic markers Bassoon and PSD-95, indicating the presence of BLINK2 in some synapses (Supplementary Fig. 4b). The percentage of synapses in which BLINK2 localized was 26.35% ± 6.16% ($n = 8$ cells from two independent experiments) for Bassoon staining and 20.04% ± 2.98% ($n = 7$ cells from two independent experiments) for PSD-95 staining. In conclusion, our data show that BLINK2 is transported along the secretory pathway and expressed at the plasma membrane in hippocampal neurons, preferentially in the somatodendritic compartment.

Ex vivo recordings from mouse brain. To test neuronal silencing by BLINK2 in brain slices, we injected the AAV-hSyn-BLINK2-IRES-eGFP virus in the dorsal raphe nucleus (DRN) of the midbrain (Fig. 3a). BLINK2-expressing neurons (GFP^+) recorded at the soma in the dark showed basal tonic firing (0.2–7 Hz; Fig. 3a), similar to the activity in untransfected acute DRN slices[28–30]. After transfection with a control GFP-expressing virus (AAV1/2-hSyn-eGFP), none of the recorded cells ($n = 7$) showed inhibition of firing activity (Supplementary Fig. 5a,b). Passive and active properties of BLINK2-expressing cells were indistinguishable from those of controls in the dark (Supplementary Fig. 6a,b), which indicates that the channel is closed in the dark. Furthermore, the number of GFP^+ cells did not vary 2, 4 and 8 weeks after infection, thus indicating that BLINK2 expression does not interfere with cell viability (Supplementary Fig. 7).

After exposure to 60 s or 30 s of blue light (470 nm, 8.7 mW/mm^2), light-responsive neurons hyperpolarized and stopped firing within 2 min after the light was switched off (for 60-s exposure ($n = 11$), 1.32 ± 0.17 Hz $Before_{light}$ and 0.005 ± 0.003 Hz $After_{light\ 0\text{-}2'}$; for 30-s exposure ($n = 8$), 1.39 ± 0.2 Hz $Before_{light}$ and 0.016 ± 0.007 Hz $After_{light\ 0\text{-}2'}$) (Fig. 3b). Firing did not recover for at least 20–30 min

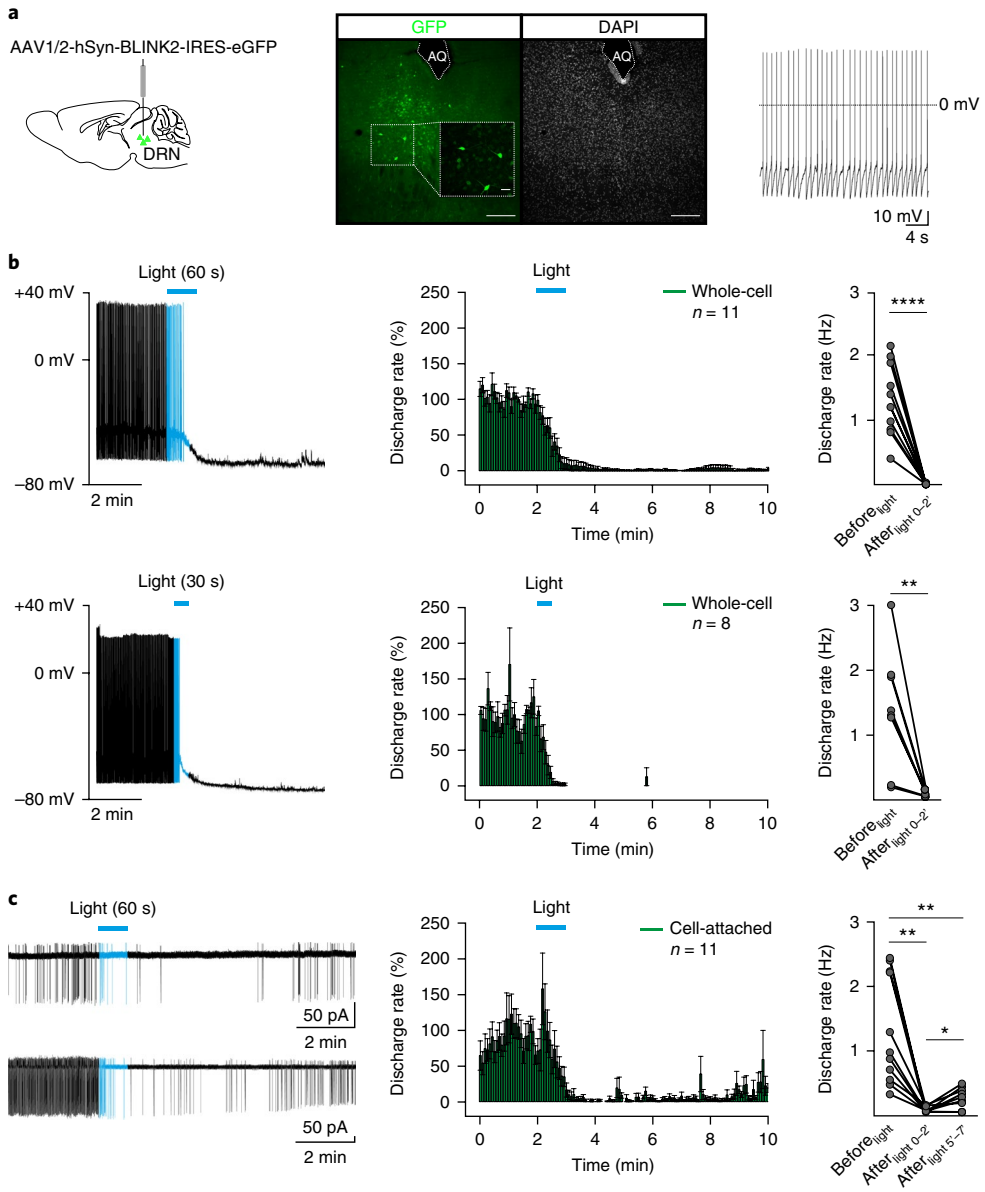

Fig. 3 | BLINK2-mediated silencing of tonic firing activity in mouse DRN neurons. a, Left, diagram indicating the virus injection site. Middle, sample confocal image showing expression of the AAV1/2-hSyn-BLINK2-IRES-eGFP virus in the mouse DRN (green, GFP; gray, DAPI). Scale bars, 200 µm or 40 µm (inset). AQ, aqueduct. $n = 21$ mice. Right, representative ($n = 19$ from 11 mice) current-clamp recording of tonic firing activity in DRN GFP$^+$ neurons. **b**, Left, representative whole-cell current-clamp recordings of the firing response before and after 60 s (top) and 30 s (bottom) of blue light stimulation (duration indicated by horizontal blue bars) (top, $n = 11$ independent recordings in 5 mice; bottom, $n = 8$ independent recordings in 6 mice). Middle, time course of the effect of 60 s (top) and 30 s (bottom) of blue light stimulation (blue bar) on the firing discharge rate (5-s binning). Right, summary plots indicating the mean firing discharge rate 2 min before light ($\text{Before}_{\text{light}}$; baseline) and 2 min after light-off ($\text{After}_{\text{light 0-2′}}$) (60 s, $\text{Before}_{\text{light}}$ versus $\text{After}_{\text{light 0-2′}}$, $n = 11$, $P < 0.0001$, $t = 7.9$, df = 10, two-sided paired t-test; 30 s, $\text{Before}_{\text{light}}$ versus $\text{After}_{\text{light 0-2′}}$, $n = 8$, $P = 0.004$, $t = 4.2$, df = 7, two-sided paired t-test). **c**, Left, representative cell-attached voltage-clamp recordings of firing responses before and after 60 s of blue light stimulation (blue bar) ($n = 11$ independent recordings; $n = 10$ mice). Middle, time course of the effect of 60 s of blue light stimulation (blue bar) on the firing discharge rate (5-s binning). Right, summary plot indicating the mean firing discharge rate 2 min before light ($\text{Before}_{\text{light}}$) and at 2 ($\text{After}_{\text{light 0-2′}}$) and 5 ($\text{After}_{\text{light 5′-7′}}$) min after the end of light exposure ($n = 11$; repeated measures one-way ANOVA, $F_{10,2} = 22$, $P = 0.0007$; post hoc, $\text{Before}_{\text{light}}$ versus $\text{After}_{\text{light 0-2′}}$, $P = 0.002$; $\text{Before}_{\text{light}}$ versus $\text{After}_{\text{light 5′-7′}}$, $P = 0.003$; $\text{After}_{\text{light 0-2′}}$ versus $\text{After}_{\text{light 5′-7′}}$, $P = 0.02$; multiple comparison and Tukey's P value correction) (*$P < 0.05$, **$P < 0.01$, ****$P < 0.0001$). Data in time course plots are presented as mean ± s.e.m. Blue light was delivered through the microscope objective (40× at 470 nm, 8.7 mW/mm^2).

after stimulation (data not shown). We reasoned that dialysis of intracellular constituents during whole-cell recordings might represent a caveat, and therefore we analyzed the discharge rate of tonically active GFP$^+$ neurons in a cell-attached configuration[28,31]. Although light stimulation (60 s) substantially reduced the firing discharge rate ($\text{Before}_{\text{light}}$, 1.3 ± 0.3 Hz; $\text{After}_{\text{light 0-2′}}$, 0.03 ± 0.01 Hz), we observed a slight recovery of activity ($\text{After}_{\text{light 5′-7′}}$, 0.18 ± 0.05 Hz) in 7 out of 11 cells in the dark ($n = 11$; repeated measures one-way ANOVA, $F_{10,2} = 22$, $P = 0.0007$; post hoc, $\text{Before}_{\text{light}}$ versus $\text{After}_{\text{light 0-2′}}$, $P = 0.002$; $\text{Before}_{\text{light}}$ versus $\text{After}_{\text{light 5′-7′}}$, $P = 0.003$; $\text{After}_{\text{light 0-2′}}$ versus $\text{After}_{\text{light 5′-7′}}$, $P = 0.02$; multiple comparison and Tukey's P value correction) (Fig. 3c).

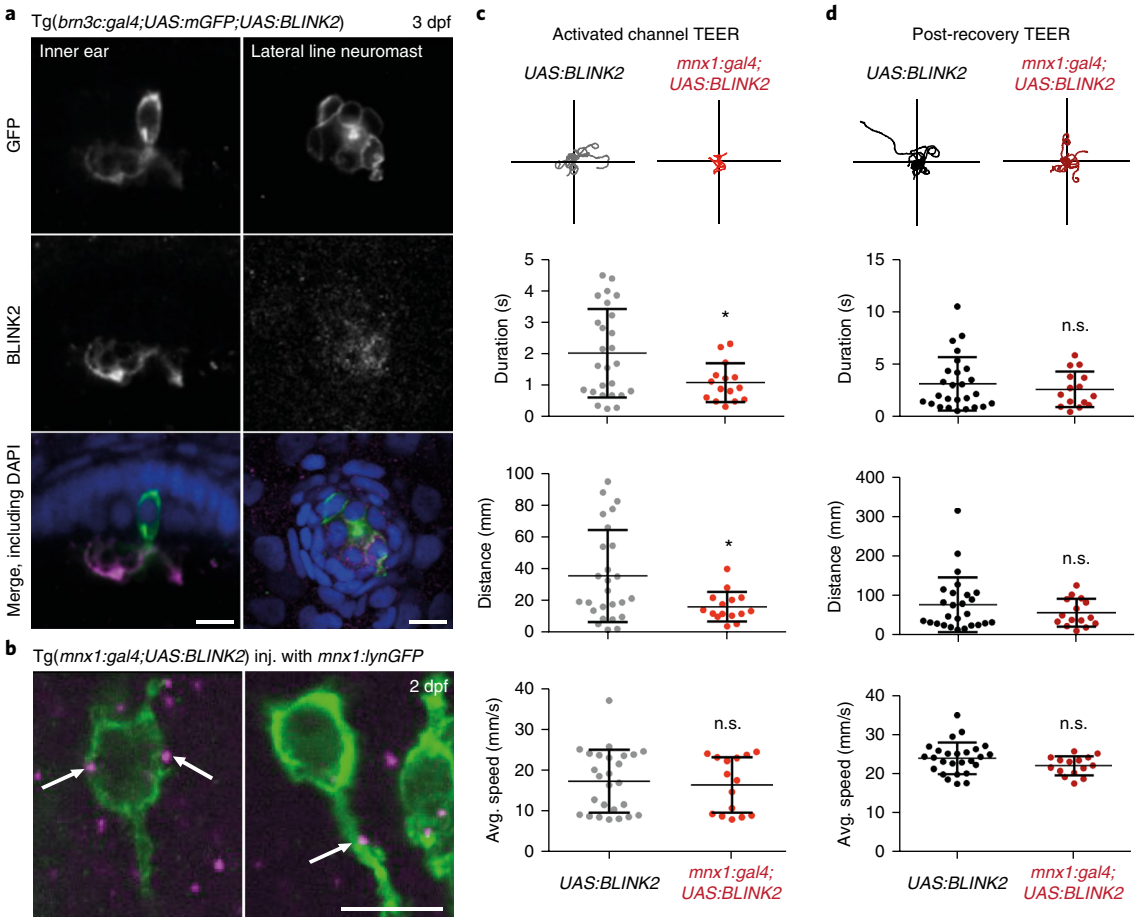

Fig. 4 | BLINK2 expression and functional silencing in zebrafish. a, Left, immunohistochemistry in 3-dpf (days post-fertilization) embryos, showing a hair cell of the inner ear labeled for membrane-targeted GFP (green in the merged image) and the BLINK2 channel (magenta in the merged image), both expressed under the control of *brn3c:gal4*. Right, neuromast cells from the same Tg(*brn3c:gal4;UAS:mGFP*) line labeled in the same way. Embryos were counterstained with DAPI (blue). Scale bars, 10 µm. Similar results were obtained in 3 independent experiments. **b**, Immunohistochemistry on whole 2-dpf embryos showing cell bodies and part of the axons of primary motor neurons stained by membrane-targeted GFP (green) and BLINK2 (magenta). White arrows indicate BLINK2 immunoreactivity at the plasma membrane and axonal tract. Genotypes are as indicated. GFP was expressed in subsets of motor neurons only. Scale bars, 10 µm. Similar results were obtained in 3 independent experiments. **c**, Touch-evoked escape response assay (TEER) in Tg(*mnx1:gal4;UAS:BLINK2*) and Tg(*UAS:BLINK2*) embryos. Embryos were assayed after a 20-min activation of the channel with blue light. Swim duration, distance and average speed were 2.03 ± 0.28 s, 35.80 ± 5.65 mm and 17.49 ± 1.50 mm/s, respectively, in control animals and 1.10 ± 0.16 s, 16.62 ± 2.38 mm and 16.60 ± 1.75 mm/s in BLINK2-expressing animals. Traces for 10 escape episodes are shown for each condition. $n = 26$ larvae for Tg(*UAS:BLINK2*) and $n = 15$ larvae for Tg(*mnx1:gal4;UAS:BLINK2*). Data are presented as the average (center line) ± s.d.; *P* values are, respectively, 0.019, 0.017 and 0.071. **d**, TEER assay in the same animals as in **c** after 1 h of rest in the dark. Swim duration, distance and average speed were 3.18 ± 0.50 s, 77.12 ± 13.42 mm and 24.03 ± 0.79 mm/s, respectively, in control animals and 2.67 ± 0.44 s, 57.03 ± 8.90 mm and 22.08 ± 0.63 mm/s in BLINK2-expressing animals. *P* values are, respectively, 0.48, 0.29 and 0.099. $^*P \leq 0.05$ (two-sided *t*-test). n.s., not significant.

To compare BLINK2 to the opsin-based chloride pump eNphR3.0, we coinjected AAV1-hsyn-Cre and AAV5-EF1α-DIO-eNpHR3.0-eYFP viruses into the DRN (Supplementary Fig. 8a). In YFP$^+$ cells, 60 s of yellow light (585 nm, 17 mW/mm^2) induced rapid (<5 s) silencing of firing activity (Supplementary Fig. 8b); this inhibitory effect faded within the illumination period. The firing rate returned to control levels within 2 min of dark onset (Before$_{light}$, 2.7 ± 0.8 Hz; Light, 1.3 ± 0.7 Hz; After$_{light\ 0\text{-}2'}$, 2.3 ± 0.9 Hz; Supplementary Fig. 8c). To provide a quantitative comparison between the eNpHR3.0-mediated and BLINK2-mediated effects, we calculated the duration of firing inhibition as the 'time below threshold' (a detailed definition is presented in the Methods section), which was 71 ± 28 s for eNpHR3.0 ($n = 9$) and 420 ± 148 s for BLINK2 ($n = 10$) (Supplementary Fig. 8d). Thus eNpHR3.0-induced inhibition was faster than that of BLINK2 and did not persist in the dark.

In vivo validation of BLINK2. Next we validated BLINK2 for in vivo application in a zebrafish model. In a touch-evoked escape-response assay, embryos are gently touched on the tail to elicit an escape-type swimming episode. We reasoned that BLINK2 photoactivation would prevent or impair this behavior. In blue light, 2-d-old larvae injected at the one-cell stage with BLINK2 RNA showed an altered escape response to touch compared with that of controls; we did not observe a significant difference between experimental and control specimens when we repeated the experiment in the dark (GFP dark, 4.2% ± 4.2%; BLINK2 dark, 10.4% ± 5.3%; GFP light, 7.2% ± 3.7%; BLINK2 light, 46.4% ± 5.2%) ($P = 0.028$ and 0.0023 for BLINK2 dark versus light and GFP light versus BLINK2 light, respectively). The percentage of affected larvae (Supplementary Fig. 9a) was similar to that reported for BLINK1[20], with the exception that a subpopulation of BLINK2 embryos (13 of 91 embryos) required more touches than

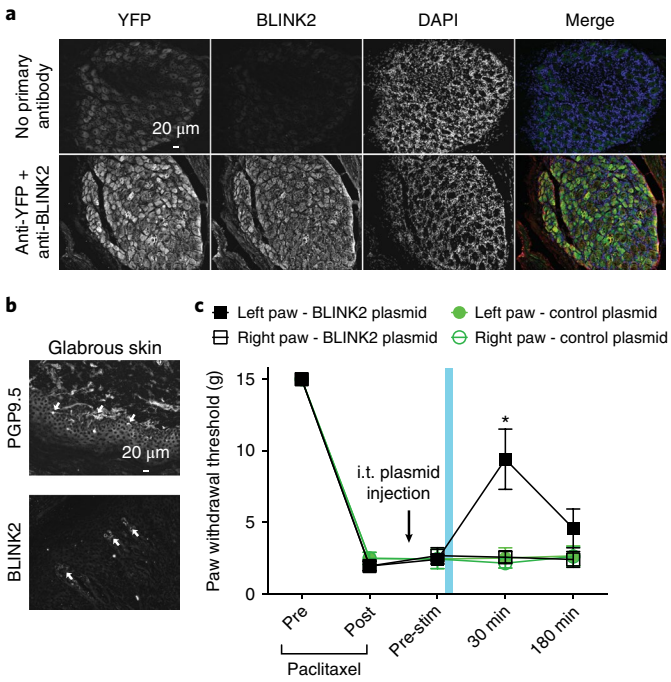

Fig. 5 | BLINK2-mediated reversal of chemotherapy-induced neuropathic pain in rats. a, Fluorescent micrographs of 12-µm sections of adult dorsal root ganglia from animals that received intrathecal (i.t.) injection of BLINK2–YFP expression plasmid, immunostained 24 h after injection for YFP and BLINK2 (bottom row). In the images in the top row, no primary antibody control was used to visualize YFP fluorescence. Presented data are from three independent animals that yielded similar results. **b**, Fluorescent micrographs of 12-µm sections of glabrous skin from animals that received i.t. injection of BLINK2–YFP expression plasmid, immunostained 24 h after injection for PGP9.5 (nerve terminals) or BLINK2. White arrows indicate the nerve terminals in the glabrous skin stained with PGP9.5 or BLINK2. Presented data are from three independent animals that yielded similar results. **c**, Paw withdrawal thresholds for rats with chemotherapy-induced neuropathic pain (paclitaxel) and i.t. injection of BLINK2 plasmid (4.5 µg per rat; $n = 6$). Blue light illumination was applied for 1 min to the left paw only. $^*P < 0.05$ for the left paw compared with the right paw. $P = 0.0001$ (two-way ANOVA with Student–Neuman–Kuels post hoc test). Data were analyzed by nonparametric two-way ANOVA, where time was the within-subject factor and treatment was the between-subjects factor. Data are presented as the average ± s.e.m.

BLINK1 embryos in order for an observable response to be elicited (Supplementary Fig. 9b). The light-driven effect on escape developed with a half-time of 15–20 min and reverted in the dark with a similar kinetics (Supplementary Fig. 9c). The mutation Q513D, which accelerates dark recovery in the isolated LOV2 domain[32], did not affect the kinetics of BLINK2 (Supplementary Fig. 9c).

Transgenic zebrafish line expressing BLINK2. Expression of BLINK2 under the control of UAS regulatory sequences in a transgenic zebrafish line allowed targeting of the channel in genetically defined populations of neurons through crossing with Gal4 reporter lines[33].

We expressed BLINK2, together with a membrane-bound fluorophore (mGFP), in hair cells of the zebrafish ear and lateral line neuromasts by crossing our specimens into the *brn3c:gal4* background (Tg(*brn3c:gal4*;*UAS:BLINK2;UAS:mGFP*)). Whole-mount immunohistochemistry with anti-BLINK2 showed expression of the channel preferentially at the level of the apical cilia in hair cells (Fig. 4a). Its expression in neuromasts seemed most prominent in the cell body in GFP$^+$ cells.

To express BLINK2 in primary motor neurons of the spinal cord, we crossed the *UAS:BLINK2* carrier zebrafish into the *mnx1:gal4* background[34] to obtain Tg(*mnx1:gal4*;*UAS:BLINK2*) embryos. We injected transgenic embryos from this cross with a construct containing the *mnx1* promoter[35] driving *lynGFP*, which encodes a membrane-bound fluorophore[36], in order to visualize cell membranes and allow localization of the channel in this cell type. Whole-mount immunohistochemistry revealed channel puncta at the level of the membrane in motor neuron cell bodies and at the axon (Fig. 4b).

To functionally test silencing of neurons by BLINK2, we exposed Tg(*mnx1:gal4*;*UAS:BLINK2*) embryos to light from a blue LED (447 nm, 80 µW/mm^2) for 20 min and then carried out the touch-evoked escape-response assay. The evoked behavior relies on spinal cord primary motor neurons and was affected by activation of the channel (Fig. 4c). We dissected the response into three parameters: duration, distance and average speed (Fig. 4c). Tg(*mnx1:gal4*;*UAS:BLINK2*) embryos exhibited a reduced escape duration and distance but a conserved instant maximum speed as compared with that of Tg(*UAS:BLINK2*) embryos, which indicates that BLINK2 did not inactivate muscles. We then left embryos for 1 h in the dark to allow BLINK2 channel-closing before we repeated the behavioral assay. The embryos with closed BLINK2 channels performed as the controls did, with no significant difference in their escape behavior ($P = 0.48$, 0.29 and 0.099 for duration, distance and average speed, respectively; two-sided *t*-tests) (Fig. 4d). This demonstrates that BLINK2 activation in this specific neuronal population was sufficient to reversibly impair function with a measurable behavioral defect.

BLINK2 stimulation relieves chemotherapy-induced neuropathic pain in a rat model. A property of BLINK2 is its prolonged activity after cessation of light exposure, which can last for several minutes (Figs. 1 and 3). Therefore BLINK2 is a candidate tool for optogenetic applications that require long-lasting inhibition, such as pain relief in peripheral neural circuits.

As proof of concept, we tested the effect of BLINK2 on neuropathic pain in rats. We expressed BLINK2 in dorsal root ganglia (containing the primary afferent neurons) by in vivo transfection via intrathecal injection. Twenty-four hours after injection, YFP and BLINK2 were expressed in sensory neurons in L4–L6 dorsal root ganglia (Fig. 5a) and nerve terminals of the glabrous skin (Fig. 5b). We then tested BLINK2-mediated silencing of nociceptive neurons in a preclinical model of chemotherapy-induced neuropathic pain. Rats injected with paclitaxel develop tactile allodynia (Fig. 5c), which is caused by ectopic firing of sensory neurons and increased nociceptive signal transmission[37]. Opening of a K$^+$ channel should hyperpolarize the nociceptive neurons and prevent firing of action potentials.

After inducing tactile allodynia, we injected rats intrathecally with a BLINK2 plasmid for in vivo transfection. We expected protein expression and physiological consequence to peak about 24 h after injection[38]. On the day after plasmid injection, we illuminated BLINK2 by exposing the left paw to blue light for 1 min. The right paw was not illuminated and was used as an internal control. Illumination of the left paw reduced nociception for at least 30 min, as indicated by an increased threshold for paw withdrawal after touch, which resolved after 3 h (Fig. 5c). We observed this effect only in the left paw; the right paw did not show an increased paw withdrawal threshold. This measured the force needed to elicit a response in the rats (Fig. 5c). Rats injected with an empty plasmid were insensitive to blue light (Fig. 5c). These experiments show that a specific effect of blue light is to trigger BLINK2 activation and silencing of ectopic nociceptive inputs in chemotherapy-induced neuropathic pain.

Discussion

We have shown that the light-gated K^+ channel BLINK2 is an inhibitory tool in long-lasting optogenetic experiments. Because BLINK2 is not activated by wavelengths greater than 500 nm, it can be combined with green-excitable labels and tools with minimal cross-talk.

Compared with BLINK1[20], BLINK2 shows slower activation and deactivation kinetics (on the order of minutes). The lasting inhibition is presumably due to the high channel conductance that prevents depolarizing inputs even if only a small number of channels remain active. We observed more severe inhibition in whole-cell experiments than in cell-attached experiments, which we presently do not understand and which may depend on the dilution of cytosolic factors during prolonged whole-cell measurements. However, the full recovery observed in our in vivo experiments indicates that the system is in principle reversible and does not cause severe stress to the cells. BLINK2 should have minimal effects on cells, as it exploits an inherent mechanism for hyperpolarization, namely, K^+ efflux. We expect that BLINK2 will provide inhibition in all cell types and in many model organisms. Moreover, the combination of large unitary conductance and prolonged light-off activity allows cellular inhibition in a time range inaccessible to other inhibitory tools, such as the opsin-based chloride pump eNpHR3.0. In our experimental conditions, eNpHR3.0 inhibited firing transiently for no longer than tens of seconds.

BLINK2 is suitable for in vivo experiments that require very long inhibition times. BLINK2 may be used to dissect the role of genetically defined neuronal populations in behavioral experiments or for silencing of neurons during the development of neural circuits, where it is necessary to silence neurons for hours or days. This may be achievable with BLINK2 by light pulses of low frequency and intensity, which should prevent the unwanted tissue heating often associated with prolonged inhibition by other optogenetic tools[39].

The slow post-illumination recovery of BLINK2 is a beneficial property for silencing peripheral neural circuits in the control of neuropathic pain. This is a high-priority issue in therapeutics because of inadequate responses to drug therapy[40]. In our hands, reduced pain sensation in a rodent model did not require constant light but was achieved with a brief transdermal light pulse and without the need for fiber-optic implantation. This avoids negative consequences of high-intensity illumination such as local tissue heating[41] and facilitates potential clinical translation.

Online content

Any methods, additional references, Nature Research reporting summaries, source data, statements of data availability and associated accession codes are available at https://doi.org/10.1038/s41592-018-0186-9.

Received: 23 January 2018; Accepted: 26 September 2018;
Published online: 30 October 2018

References

1. Han, X. & Boyden, E. S. Multiple-color optical activation, silencing, and desynchronization of neural activity, with single-spike temporal resolution. *PLoS One* **2**, e299 (2007).
2. Chow, B. Y. et al. High-performance genetically targetable optical neural silencing by light-driven proton pumps. *Nature* **463**, 98–102 (2010).
3. Zhang, F. et al. Multimodal fast optical interrogation of neural circuitry. *Nature* **446**, 633–639 (2007).
4. Chuong, A. S. et al. Noninvasive optical inhibition with a red-shifted microbial rhodopsin. *Nat. Neurosci.* **17**, 1123–1129 (2014).
5. Wietek, J. et al. Conversion of channelrhodopsin into a light-gated chloride channel. *Science* **344**, 409–412 (2014).
6. Berndt, A., Lee, S. Y., Ramakrishnan, C. & Deisseroth, K. Structure-guided transformation of channelrhodopsin into a light-activated chloride channel. *Science* **344**, 420–424 (2014).
7. Govorunova, E. G., Sineshchekov, O. A., Janz, R., Liu, X. & Spudich, J. L. Natural light-gated anion channels: a family of microbial rhodopsins for advanced optogenetics. *Science* **349**, 647–650 (2015).
8. Wietek, J. et al. An improved chloride-conducting channelrhodopsin for light-induced inhibition of neuronal activity in vivo. *Sci. Rep.* **5**, 14807 (2015).
9. Inoue, K., Kato, Y. & Kandori, H. Light-driven ion-translocating rhodopsins in marine bacteria. *Trends Microbiol.* **23**, 91–98 (2015).
10. Mattis, J. et al. Principles for applying optogenetic tools derived from direct comparative analysis of microbial opsins. *Nat. Methods* **9**, 159–172 (2011).
11. Alfonsa, H. et al. The contribution of raised intraneuronal chloride to epileptic network activity. *J. Neurosci.* **35**, 7715–7726 (2015).
12. Raimondo, J. V., Kay, L., Ellender, T. J. & Akerman, C. J. Optogenetic silencing strategies differ in their effects on inhibitory synaptic transmission. *Nat. Neurosci.* **15**, 1102–1104 (2012).
13. Mahn, M., Prigge, M., Ron, S., Levy, R. & Yizhar, O. Biophysical constraints of optogenetic inhibition at presynaptic terminals. *Nat. Neurosci.* **19**, 554–556 (2016).
14. Berndt, A. et al. Structural foundations of optogenetics: determinants of channelrhodopsin ion selectivity. *Proc. Natl. Acad. Sci. USA* **113**, 822–829 (2016).
15. Kaila, K., Price, T. J., Payne, J. A., Puskarjov, M. & Voipio, J. Cation-chloride cotransporters in neuronal development, plasticity and disease. *Nat. Rev. Neurosci.* **15**, 637–654 (2014).
16. Szabadics, J. et al. Excitatory effect of GABAergic axo-axonic cells in cortical microcircuits. *Science* **311**, 233–235 (2006).
17. Christie, J. M. Phototropin blue-light receptors. *Annu. Rev. Plant. Biol.* **58**, 21–45 (2007).
18. Christie, J. M., Gawthorne, J., Young, G., Fraser, N. J. & Roe, A. J. LOV to BLUF: flavoprotein contributions to the optogenetic toolkit. *Mol. Plant* **5**, 533–544 (2012).
19. Plugge, B. et al. A potassium channel protein encoded by chlorella virus PBCV-1. *Science* **287**, 1641–1644 (2000).
20. Cosentino, C. et al. Engineering of a light-gated potassium channel. *Science* **348**, 707–710 (2015).
21. Gradinaru, V. et al. Molecular and cellular approaches for diversifying and extending optogenetics. *Cell* **141**, 154–165 (2010).
22. Zuzarte, M. et al. Intracellular traffic of the K+ channels TASK-1 and TASK-3: role of N- and C-terminal sorting signals and interaction with 14-3-3 proteins. *J. Physiol. (Lond.)* **587**, 929–952 (2009).
23. Sottocornola, B. et al. The potassium channel KAT1 is activated by plant and animal 14-3-3 proteins. *J. Biol. Chem.* **281**, 35735–35741 (2006).
24. Sottocornola, B. et al. 14-3-3 proteins regulate the potassium channel KAT1 by dual modes. *Plant Biol. (Stuttg.)* **10**, 231–236 (2008).
25. Saponaro, A. et al. Fusicoccin activates KAT1 channels by stabilizing their interaction with 14-3-3 proteins. *Plant Cell* **29**, 2570–2580 (2017).
39. Wiegert, J. S., Mahn, M., Prigge, M., Printz, Y. & Yizhar, O. Silencing neurons: tools, applications, and experimental constraints. *Neuron* **95**, 504–529 (2017).
40. Finnerup, N. B. et al. Pharmacotherapy for neuropathic pain in adults: a systematic review and meta-analysis. *Lancet Neurol.* **14**, 162–173 (2015).
41. Stachniak, T. J., Ghosh, A. & Sternson, S. M. Chemogenetic synaptic silencing of neural circuits localizes a hypothalamus→midbrain pathway for feeding behavior. *Neuron* **82**, 797–808 (2014).

Acknowledgements

We thank S. Guazzi and M. Festa for technical help with cloning and zebrafish expression. We acknowledge M. Pesce and A. Gino for help with immunohistochemistry. pENN-AAV-hSyn-Cre-WPRE-hGH was a gift from J.M. Wilson (Perelman School of Medicine, University of Pennsylvania, Philadelphia, PA, USA). This work was supported by the 2016 Schaefer Research Scholars Program of Columbia University (to A. Moroni), MIUR PRIN (Programmi di Ricerca di Rilevante Interesse Nazionale; 494 2015, 2015795S5W to A. Moroni), the European Research Council (ERC; 2015 Advanced Grant 495 (AdG) n. 695078 noMAGIC to A. Moroni and G.T.), DFG priority program SPP1926 (to G.T.), the Fondazione Istituto Italiano di Tecnologia (to A.L., A.C., A.J.B. and R.T.), and AIRAlzh Onlus-COOP Italia (fellowship to S.P.).

Author contributions

L.A. designed and prepared channel constructs, performed whole-cell patch-clamp experiments in vitro and analyzed the data; A.S. contributed to the design of the final BLINK2 clone; A.P. conducted and analyzed some electrophysiological recordings in vitro; G.R. produced the anti-BLINK2 antibody; G.T. and H.M.C. performed the single-channel in vitro patch experiments and analyzed the data; S.P., E.M. and M.D.L. designed, conducted and analyzed the immunolocalization experiments in rat primary neurons; A.L. designed, performed and analyzed the ex vivo mouse patch-clamp experiments; A.J.B. and A.C. designed and produced the BLINK2 viral constructs; A.L., N.B. and A.J.B. performed intracerebral viral injections; N.B. and M.P. carried out immunofluorescence analysis; E.R., V.B., S.A., F.S., S.M., M.B. and F.D.B. designed,

performed and analyzed the zebrafish experiments; K.K. and G.T. designed, performed and analyzed the artificial bilayer measurements; S.L., A. Moutal, Y.J. and R.K. designed, performed and analyzed the pain experiments in rats; R.T. designed and supervised the electrophysiological ex vivo experiments and the production of BLINK2 and GFP-control viral constructs; A. Moroni conceived the study, coordinated research and wrote the manuscript; and G.T., F.D.B., E.M., M.B., R.K. and R.T. contributed to the writing.

Competing interests

The authors declare no competing interests

Additional information

Supplementary information is available for this paper at https://doi.org/10.1038/s41592-018-0186-9.

Correspondence and requests for materials should be addressed to R.T. or A.M.

Methods

Engineering of channel constructs. Constructs in Fig. 1a were prepared by overlapping PCR[42]. The IDs of the sequences used are as follow: AsPhototropin1 (*Avena sativa*), GeneBank AAC05083.1; mKir2.1 (*Mus musculus*), NCBI gene 16518; mTASK1 (*M. musculus*), NCBI gene 16527; mTASK3 (*M. musculus*), NCBI gene 223604; KAT1 (*Arabidopsis thaliana*), NCBI gene 834666.

QuikChange Lightning (Agilent Technologies) was used to introduce point mutations. BLINK2 used in all experiments except those in transgenic zebrafish contained the mutation Q513D in the LOV2 domain[32] (AsPhot1 numbering).

Electrophysiology in cell lines. *Cell culture and transfection protocol.* HEK293T or COS7 cells were cultured in Dulbecco's modified Eagle's medium (Euroclone) supplemented with 10% FBS (Euroclone), 100 IU/ml penicillin, 100 µg/ml streptomycin and stored in a 37 °C humidified incubator with 5% CO_2. Transfections were performed with TurboFect transfection reagent (Thermo Scientific) according to the supplier's protocol: BLINK2 inserted in pcDNA3.1+ was cotransfected with a plasmid encoding GFP and incubated in the dark. For viral infection we added the virus directly to the cell culture medium. Currents were recorded after 2–3 d in GFP^+ cells.

Patch-clamp recordings. One to two days after transfection, cells were dispersed by trypsin–EDTA treatment and seeded on 35-mm plastic petri dishes to allow single-cell measurements. GFP^+ cells were selected for patch-clamp measurements. Membrane currents were recorded in the whole-cell configuration with a Dagan 3900A amplifier and digitized with a Digidata 1322A controlled by pCLAMP 9.2. The pipette resistance was about 2 MΩ. The pipette solution contained 10 mM NaCl, 130 mM KCl, 2 mM ATP–magnesium salt, 1 mM EGTA and 5 mM HEPES–KOH buffer, pH 7.2. The extracellular bath solution contained 100 mM KCl, 80 mM D-mannitol, 1.8 mM $CaCl_2$, 1 mM $MgCl_2$ and 5 mM HEPES–KOH buffer, pH 7.4. K^+ concentrations were 101.7 mM for the extracellular solution and 133.7 mM for the pipette solution. The calculated Nernst reversal potential for K^+ is –6.89 mV. The voltage protocol consisted of 20-mV steps from +60 to –140 mV. For cell-attached measurements, the pipette resistance was 2 MΩ and the pipette solution was the same as the extracellular solution. Transfected cells were kept in the dark before the assays, and all preliminary operations were performed under red light illumination (MRH2060–20T, LUXEON Rebel LEDs Red-Orange (617 nm)). Blue light illumination was provided by an LED (Royal Blue, 455 nm, High-Power LED; Thorlabs) or monochromatic light from a 75-W Xenon Arc lamp (PTI DeltaRem X, Photon Technology International) delivered through the 60× objective of a fluorescent Nikon Eclipse Ti-U microscope with an oil-immersion lens. In both cases, the light intensity measured with a power meter (Thorlabs) at the position of the sample was about 90 µW/mm².

Statistical analysis. Significance was calculated by one-way ANOVA and Tukey post hoc test using GraphPad Prism for Windows (GraphPad Software, La Jolla, CA, USA; https://www.graphpad.com).

Viral expression of BLINK2. *Cloning of AAV plasmids.* BLINK2 cDNA was amplified from Q513D pGEMT-BLINK2 by PCR with primers containing BglII recognition sites (A^GATC). With the use of BglII restriction, pAAV1/2-hSyn-IRES-eGFP was linearized and BLINK2 cDNA was subsequently ligated into the linearized vector to produce pAAV1/2-hSyn-BLINK2-IRES-eGFP.

Virus production. HEK293T cells (ATCC, UK) were cultured in Iscove's modified Dulbecco's medium (Sigma-Aldrich, Germany) supplemented with 10% (v/v) FCS (Sigma-Aldrich) and penicillin–streptomycin–glutamine (Sigma-Aldrich) in 5×150 mm dishes. After 80% confluency was reached, cell were transfected in serum-free medium with the helper plasmids pRV1, pH21 and pDFΔ6 and pAAV1/2-hSyn-BLINK-IRES-eGFP or pAAV1/2-hSyn-IRES-eGFP at a molar ratio of 1:1 with $CaCl_2$. On the next day, the medium was replaced with serum-containing medium, and 48 h after transfection cells were harvested, pelleted and resuspended in lysis solution (150 mM NaCl, 20 mM Tris, pH 8). Next, cells were subjected to a freeze–thaw cycle, and after the addition of NaDOC (0.5% v/v), the solution was incubated with Benzonase (Sigma-Aldrich; 50 units/ml) for 60 min at 37 °C. After centrifugation (3,000*g* at 4 °C for 10 min), the supernatant was frozen. The next day, we carried out ion-exchange chromatography with 1-ml HiTrapQ columns (GE Healthcare, UK). Viral particles were washed and eluted with solutions of 20 mM Tris, pH 8, with increasing NaCl concentrations (100–500 mM NaCl). Eluate was transferred to an Amicon Ultra-4 filter (Millipore, USA) to concentrate the viral particles and exchange the buffer for PBS. The purified virus was then aliquoted and stored at −80 °C. The titer was determined by real-time quantitative PCR on a 7900HT Fast Real-Time PCR system (Applied Biosystems Inc., USA) using primers against GFP (forward, AAGCTGACCCTGAAGTTCATCTGC; reverse, CTTGTAGTTGCCGTCGTCCTTGAA) and the GoTaq RT-qPCR kit (Promega, USA).

BLINK2 immunolocalization in rat primary neurons. *Cell cultures and transfections.* Hippocampal neuronal primary cultures were prepared from embryonic day 18–19 (E18– E19) rat hippocampi as previously described[43]. All the experiments were approved by the Institutional Animal Care and Use Committee of University of Milan and by the Italian Ministry of Health (#326/2015). Neurons were transfected at 7 days in vitro (DIV7) via the calcium-phosphate precipitation method with 4 µg of plasmid DNA for GFP for the experiments assessing the axonal and dendritic distribution of BLINK2 reported in Fig. 2c. Neurons were infected with AAV1/2-hSyn-BLINK2-IRES-eGFP at DIV10 and fixed at DIV12 for the immunocytochemistry assays.

Immunocytochemistry. For colocalization experiments, cells were fixed with 4% paraformaldehyde (PFA)–4% sucrose in PBS solution at 4 °C and washed several times with PBS. Cells were permeabilized with 0.1% Triton X-100 in PBS for 15 min at room temperature and then blocked with 5% BSA in PBS for 45 min at room temperature. Cells were then labeled with antibodies for intracellular epitopes overnight at 4 °C. Cells were washed and incubated with secondary antibodies for 1 h at room temperature. Cells were washed in PBS and mounted on glass slides with Fluoromount mounting medium (Sigma-Aldrich, USA).

To evaluate surface and total staining of BLINK2, neurons were fixed with 4% PFA–4% sucrose in PBS solution at 4 °C, and then incubated with anti-BLINK2 8D6 custom-made monoclonal antibody. This antibody, originally raised against the potassium channel Kcv, recognizes BLINK channels too[20,44]. To visualize surface expression, we blocked cells with 5% BSA in PBS and incubated them with an Alexa Fluor 555–conjugated secondary antibody. Afterward, cells were permeabilized with 0.1% Triton X-100 for 10 min, and intracellular expression was determined after incubation with 8D6 antibody and labeling of the total receptor fraction with an Alexa Fluor 405–conjugated secondary antibody.

Fluorescence images were acquired with the Zeiss Confocal LSM510 Meta system with a sequential acquisition setting at 1,024×1,024 pixel resolution; for each image two to four 0.5-µm sections were acquired and a *z* projection was obtained[45]. Images were acquired with signals in a linear range and without any saturated pixel, for reliable quantification and appropriate comparison of all experimental conditions.

For quantification of surface and total expression intensities, images were acquired with the same settings. The average intensity of surface fluorescence staining was determined after cell tracing and was normalized to the total intensity to correct for differences in expression. We obtained surface ratios by dividing the background-subtracted fluorescence intensities.

Antibodies. We used antibodies to MAP2 (Millipore; AB5222), GM130 (BD Bioscience; 610822) and GFP (Millipore; AB16901). Alexa Fluor fluorescently labeled antibodies were purchased from Thermo Fisher.

Ex vivo electrophysiology. *Animals.* All procedures involving animals were carried out in accordance with the Italian Ministry of Health's directives (D.lgs 26/2014) regulating animal research. Animal experiments were designed in accordance with the ARRIVE (Animal Research: Reporting of In Vivo Experiments) guidelines, with a commitment to refinement, reduction and replacement, so as to minimize the number of mice used. C57BL/6J male mice were maintained in standard cages with food and water ad libitum at 22 ± 1 °C under an artificial 12/12-h light/dark cycle.

Stereotaxic injections. C57BL/6J male mice (4–6 weeks old) were anesthetized with a mixture of isoflurane (1–2%) and O_2. Mice were positioned in a stereotaxic frame (Kopf Instruments) and their body temperature was maintained at 37 °C. We injected 0.5 µl (titer 10^{13}) of AAV1/2-hSyn-Blink2-IRES-eGFP, AAV1/2-hSyn-eGFP or a 1:1 mixture of AAV1-hsyn-Cre (pENN.AAV.hSyn.Cre.WPRE.hGH, a gift from James M. Wilson (Perelman School of Medicine, University of Pennsylvania); Addgene viral prep # 105553-AAV1) and AAV5-EF1α-DIO-eNpHR3.0-eYFP (Stanford Virus Core) into the DRN (mediolateral, +1.15 mm, anteroposterior, –4.4 mm, dorsoventral, –3.6 mm under an angle of 20° from bregma; or mediolateral, +0.5 mm, anteroposterior, –4.36 mm, dorsoventral, –3 mm from bregma) at a speed of 0.1 µl/min. Ex vivo electrophysiology was performed at least 2 weeks after surgeries.

Immunofluorescence. Mice were killed 2, 4 or 8 weeks after the injection. Anesthetized mice were transcardially perfused with PBS followed by 4% PFA. Brains were dissected and post-fixed in 4% PFA overnight at 4 °C. 50-µm coronal sections were obtained with a vibratome (Leica Microsystems). Antigen retrieval was performed as follows: sections were incubated for 30 min at 80 °C in 50 mM sodium acetate solution. Then the slices were washed three times in a PBTriton 0.1% solution. Sections were incubated with chicken anti-GFP (Abcam; 1:500) primary antibody overnight at 4 °C and then rinsed in PBTriton 0.1%. Alexa Fluor 488–conjugated goat anti-chicken IgG (1:500; Life Technologies) was used overnight at 4 °C as the secondary antibody. The next day, sections were washed three times with PBTriton 0.1% solution and counterstained with DAPI. High-power confocal images in the injection site of the DRN region were obtained on a Nikon A1 confocal microscope with a 10× or 40× plan-apochromat.

Slice preparation. Mice were killed under isoflurane anesthesia, after which their brains were dissected out and transferred to ice-cold modified artificial cerebrospinal fluid (aCSF) containing 110 mM choline chloride, 2.5 mM KCl,

1.25 mM NaH_2PO_4, 7 mM $MgCl_2$, 0.5 mM $CaCl_2$, 25 mM $NaHCO_3$, 25 mM D-glucose and 11.6 mM ascorbic acid, saturated with 95% O_2 and 5% CO_2. Coronal slices containing the DRN (250-µm thickness) were prepared with a Vibratome 1000S slicer (Leica) and transferred to aCSF containing 115 mM NaCl, 3.5 mM KCl, 1.2 mM NaH_2PO_4, 1.3 mM $MgCl_2$, 2 mM $CaCl_2$, 25 mM $NaHCO_3$ and 25 mM D-glucose, aerated with 95% O_2 and 5% CO_2. After 20 min of incubation at 32 °C, slices were kept at 22–24 °C. During electrophysiological experiments, slices were continuously superfused with aCSF at a rate of 2 ml/min at 28 °C.

Electrophysiological recordings. Electrophysiology recordings were performed on coronal brain slices containing the DRN. The DRN was first visualized under infrared differential interference contrast to allow for subsequent identification of GFP^+ or YFP^+ neurons by epifluorescence microscopy. Patch pipettes (4–6 MΩ) were filled with a solution containing 135 mM NaCl, 10 mM HEPES, pH 7.2–7.3, for cell-attached recording or 130 mM $KMeSO_4$, 5 mM KCl, 5 mM NaCl, 10 mM HEPES, 2 mM $MgCl_2$, 0.1 mM EGTA, 0.05 mM $CaCl_2$, 2 mM Na_2ATP and 0.4 mM Na_3GTP, pH 7.2–7.3 (280–290 mOsm/kg), for whole-cell recordings. Cell-attached experiments were performed in the voltage clamp configuration with GFP^+ or YFP^+ neurons held at the potential that gave a holding current of 0 pA (ref. [31].), whereas whole-cell experiments were performed in the current-clamp configuration, without current injection. Light (470 nm for BLINK2 activation, 8.7 mW/mm^2; 585 nm for eNpHR3.0 activation, 17 mW/mm^2) emitted by an LED (CoolLED) was delivered to the specimen through the microscope objective (IR-ACHROPLAN 40×/0.8-NA (numerical aperture); Zeiss). Data were acquired with a Multiclamp 700B amplifier controlled by pClamp 10 software (Molecular Devices) filtered at 10 kHz and sampled at 50 kHz (current clamp and voltage clamp) (Digidata 1322; Molecular Devices). We generated time-course plots by averaging the discharge firing rate every 5 s; values were normalized to 1 min of baseline recording before light illumination. All data are reported without corrections for liquid junction potentials. Data where the access resistance (R_a) changed by >20% were excluded from further analyses.

To identify light-responsive cells, we applied a threshold-based criterion: the threshold (Th) was set as the mean discharge rate minus 2 s.d., and the mean firing rate was calculated on values (5-s binning) computed over 1 min prior to light illumination. Cells were considered light responsive when their mean discharge rate fell below Th, or to zero, in at least two consecutive 5-s bins. 'Time below threshold' ($Time_{th}$) was measured as the interval between the time point at which the discharge rate fell below Th in at least two consecutive 5-s bins and the time point at which the discharge rate increased above Th in at least two consecutive 5-s bins.

Statistics. Appropriate parametric statistics were used to test our hypothesis, unless data did not meet the assumptions of the intended parametric test (normality test). In that case, appropriate nonparametric tests were used. Power analysis assumptions were as follows: power, 0.9; alpha, 0.5; two-tailed and expected difference 50% greater than the observed s.d. Data were analyzed by one-way repeated measures ANOVA for comparisons within a group, and by one-way ANOVA for between-group comparisons (GraphPad Prism 6 software). Post hoc analysis (Tukey or Dunnet, as indicated) was performed only when ANOVA yielded a significant main effect. Two groups were tested for statistical significance by two-population *t*-test and Mann–Whitney *U* nonparametric test (GraphPad Prism 6 software). Statistical details of experiments are shown in the results, figures and figure legends. Data are reported as mean ± s.e.m., unless stated otherwise.

Zebrafish experiments. *Zebrafish husbandry.* The zebrafish were housed and maintained at 28.5 °C according to standard procedures[45]. Experiments were done in compliance with European and French animal welfare guidelines.

Microinjections. Zygotes were injected with *mnx1*:lynGFP constructs to label single primary motor neuron membranes in the spinal cord in the Tg(*mnx1*:GAL4;*UAS*:BLINK2) background.

Transgenic BLINK2 zebrafish generation. To express BLINK2 under the control of the Gal4 trans-activator in stable transgenic zebrafish, we cloned the *BLINK2* coding sequence in a *p10UAS* vector containing a *cmcl2:eGFP* cassette to visualize transgenic animals by heart GFP fluorescence using standard molecular biology techniques[46]. The plasmid also contained Tol2 flanking sites for efficient transgenesis in zebrafish and was named *p10UAS:BLINK2-tol2;cmcl2:eGFP*. This plasmid was injected at the one-cell stage with *tol2* mRNA via standard transgenesis protocols[47]. Transgenic F1 larvae were identified by heart GFP expression, and *BLINK2* gene insertion was verified by genomic PCR.

Whole-mount immunohistochemistry. Embryos at 48 h post-fertilization (hpf) were fixed overnight at 4 °C in 4% PFA diluted in PBS, then thoroughly rinsed in PBST (PBS with 0.1% Triton X-100). The fixed embryos were incubated with 1 mg/ml collagenase for 20 min, then rinsed in PBST before 1 h of incubation with block solution (PBS with 1% BSA, 2% normal goat serum, 1% DMSO, 0.1% Triton X-100). The embryos were then incubated sequentially with the primary antibodies (anti-GFP (1:300; Genetex), anti-RFP (1:200; AbCam), anti-BLINK2 (8D6) and DAPI (1:500; Life Technologies)) in fresh block solution, thoroughly rinsed in PBST and incubated with secondary antibodies (goat anti-rabbit Alexa Fluor 488 and goat anti-mouse Alexa Fluor 568 (both from Life Technologies)) also diluted in fresh blocking solution.

Microscopy. Embryos were embedded in 1% low-melting-point agarose in a glass-bottom tissue culture dish (Fluorodish; World Precision Instruments, USA).

Inner ear cells were imaged on an inverted laser scanning confocal microscope with spectral detection (LSM700; Zeiss) with a long-working-distance oil-immersion 25×/0.8-NA W GLY DIC LD LCI PL APO (UV) VIS-IR (420852-9870) lens. Acquisitions were done via the Zen software (Zeiss).

Spinal cord primary motor neurons were imaged on a Roper confocal spinning disk head mounted on a Zeiss upright microscope, using a long-working-distance water-immersion 40×/1-NA W DIC PL APO VIS-IR (421462-9900) lens. Acquisitions were done with a CoolSNAP HQ2 CCD (charge-coupled device) camera (Photometrics, USA) through the MetaMorph software (Molecular Devices, USA).

Touch-evoked escape response assay. Embryos at 48 hpf were staged, dechorionated and exposed to a blue LED light (Royal-Blue LED, λ 447 ± 10 nm, LUXEON Rebel LED) for 20 min ($\lambda = 447$, 80 µW/mm²) to activate the BLINK2 channel. The embryos were then placed in the center of an open petri dish filled with embryo medium. The escape response was elicited by a light touch on the tail with blunt forceps, and the resulting swimming episode was recorded with an Olympus FE-5000 camera at 30 Hz. The embryos were then left in the dark for 1 h to allow the inactivation of BLINK2, and the assay was subsequently performed again to test for recovery of locomotion. The videos were analyzed in ImageJ (NIH) using the Manual Tracking plugin (Fabrice Cordelières, Institut Curie-Orsay, France).

Statistics. Data were compiled in GraphPad Prism (Windows version 6.01) and *t*-tests were run to determine significance, set at $P \leq 0.05$.

Rat pain model and intrathecal injection of BLINK2. *Animals.* Pathogen-free adult male and female Sprague Dawley rats (150–200 g; Envigo) were housed in temperature-controlled (23 ± 3 °C) and light-controlled (12-h light/12-h dark cycle; lights on 07:00–19:00) rooms with standard rodent chow and water available ad libitum. The Institutional Animal Care and Use Committee of the College of Medicine at the University of Arizona approved all experiments. All procedures were conducted in accordance with the Guide for Care and Use of Laboratory Animals published by the National Institutes of Health and the ethical guidelines of the International Association for the Study of Pain. Animals were randomly assigned to treatment or control groups for the behavioral experiments. Animals were initially housed three per cage but were individually housed after the intrathecal cannulation on a 12-h light-dark cycle with food and water ad libitum. All behavioral experiments were performed by experimenters who were blinded to the experimental groups and treatments

Paclitaxel-induced neuropathy model. Rats were given paclitaxel (P-925-1; Goldbio) based on the protocol described by Polomano et al.[48]. In brief, pharmaceutical-grade paclitaxel (Taxol) was resuspended at a concentration of 2 mg/ml in 30% 1:1 Cremophor EL:ethanol, 70% saline and given to the rats at 2 mg/kg intraperitoneally every other day for a total of four injections (days 0, 2, 4 and 6), resulting in a final cumulative dose of 8 mg/kg. No abnormal spontaneous behavioral changes in the rats were noted during or after the treatment. Animals developed mechanical hyperalgesia within 10 d after the first paclitaxel injection.

Implantation of intrathecal catheter. For intrathecal drug administration, rats were chronically implanted with catheters as described[49]. Rats were anesthetized with halothane and placed in a stereotactic head holder. The occipital muscles were separated from their occipital insertion and retracted caudally to expose the cisternal membrane at the base of the skull. Polyethylene tubing was passed caudally from the cisterna magna to the level of the lumbar enlargement. Animals were allowed to recover and were examined for evidence of neurologic injury. Animals with evidence of neuromuscular deficits were excluded.

In vivo transfection of BLINK2 plasmid. For in vivo transfection, the BLINK2 plasmid was diluted to 0.3 µg/µl in 5% sterile glucose solution as done previously[38]. Then, Turbofect in vivo transfection reagent (R0541; Thermo Fisher Scientific, Waltham, MA) was added according to the manufacturer's instructions. Finally, 15 µl of the plasmid complexes were injected intrathecally in Sprague Dawley rats.

Testing of allodynia. The assessment of tactile allodynia (i.e., a decreased threshold for paw withdrawal after probing with normally innocuous mechanical stimuli) consisted of testing the withdrawal threshold of the paw in response to probing with a series of calibrated fine (von Frey) filaments. Each filament was applied perpendicularly to the plantar surface of the paw of rats held in suspended wire mesh cages. We determined the withdrawal threshold by sequentially increasing and decreasing the stimulus strength (the 'up and down' method), and we analyzed

data using the nonparametric method of Dixon, as described by Chaplan et al.[50], with results expressed as the mean withdrawal threshold.

Illumination of the paw was performed with blue LED light (Royal-Blue LED, λ 455 ± 9 nm, LUXEON Rebel LED) for 1 min (35.6 μW/mm²). The light was measured at a distance of 1–1.5 cm from the paw.

Immunohistofluorescence and epifluorescence imaging. L4–L6 dorsal root ganglia were dissected from adult rats and then fixed with 4% PFA overnight at 4 °C. Dorsal root ganglia were next transferred into a 30% sucrose solution and left at 4 °C until sinking of the tissues could be observed (~3 d). Tissues were cut at 12-μm thickness with a Bright OTF 5000 microtome cryostat (Hacker Instruments and Industries, Inc.), fixed onto charged glass slides and kept at −20 °C until use. Prior to antibody staining, slides were dried at room temperature for 30 min and rehydrated in PBS for 5 min. For glabrous skin staining, slides were incubated in ice-cold methanol for 5 min and left to dry at room temperature. The slices were permeabilized and saturated with PBS containing 3% BSA, 0.3% Triton X-100 solution for 30 min at room temperature, and then antibodies diluted in PBS, 3% BSA were added overnight at room temperature. Primary antibodies used were anti-GFP (AB3080; Millipore), anti-PGP9.5 (NB600-1160; Novus Biologicals) and anti-Blink2 8D6. The slices were then washed three times in PBS and incubated with PBS, 3% BSA containing secondary antibodies (Alexa Fluor 488 goat anti-rabbit or Alexa Fluor 594 goat anti-mouse secondary antibodies (Life Technologies)) for at least 3 h at room temperature. After three washes (PBS, 10 min, room temperature), DAPI was used to stain the nuclei of cells. Slides were mounted and stored at 4 °C until analysis. Immunofluorescent micrographs were acquired on a Nikon Eclipse Ti-U (Nikon Instruments Inc.) with a Plan Apo 10×/0.45-NA objective controlled by NIS Elements software (version 4.51; Nikon Instruments). The freeware image-analysis program ImageJ (https://imagej.nih.gov/ij/) was used to remove background and generate merged images. All images were obtained with identical acquisition parameters by individuals blinded to the staining conditions.

Statistical analyses. Behavioral threshold values were statistically analyzed for each foot separately, and the significance of differences was assessed between the averages of at least two pre-injection tests and the mean obtained for each post-injection test. In all tests, baseline data were obtained before and after paclitaxel treatment. Within each treatment group, post-administration means were compared with the contralateral values by nonparametric two-way ANOVA, where time was the within-subjects factor and treatment was the between-subjects factor, followed by post hoc pairwise comparisons (Student–Newman–Keuls method). A P value of <0.05 indicated statistical significance between treatment and nontreatment groups. Data were analyzed and plotted with Graphpad Prism 7.

Reporting Summary. Further details on research design are available in the Nature Research Reporting Summary linked to this article.

Data availability

Raw data generated and analyzed during the current study are available from the corresponding author on reasonable request. Data have been deposited under the following accession codes: AddGene 117075; GenBank submission MH937726. Source data for Fig. 1 and Supplementary Fig. 9 are available online.

References

26. Pagliuca, C. et al. Molecular properties of Kcv, a virus encoded K^+ channel. *Biochemistry* **46**, 1079–1090 (2007).
27. Marcello, E., Gardoni, F., Di Luca, M. & Pérez-Otaño, I. An arginine stretch limits ADAM10 exit from the endoplasmic reticulum. *J. Biol. Chem.* **285**, 10376–10384 (2010).
28. Zhao, S. et al. Cell type–specific channelrhodopsin-2 transgenic mice for optogenetic dissection of neural circuitry function. *Nat. Methods* **8**, 745–752 (2011).
29. Giorgi, A. et al. Brain-wide mapping of endogenous serotonergic transmission via chemogenetic fMRI. *Cell Rep.* **21**, 910–918 (2017).
30. Mlinar, B., Montalbano, A., Piszczek, L., Gross, C. & Corradetti, R. Firing properties of genetically identified dorsal raphe serotonergic neurons in brain slices. *Front. Cell. Neurosci.* **10**, 195 (2016).
31. Perkins, K. L. Cell-attached voltage-clamp and current-clamp recording and stimulation techniques in brain slices. *J. Neurosci. Methods* **154**, 1–18 (2006).
32. Pudasaini, A., El-Arab, K. K. & Zoltowski, B. D. LOV-based optogenetic devices: light-driven modules to impart photoregulated control of cellular signaling. *Front. Mol. Biosci.* **2**, 18 (2015).
33. Baier, H. & Scott, E. K. Genetic and optical targeting of neural circuits and behavior—zebrafish in the spotlight. *Curr. Opin. Neurobiol.* **19**, 553–560 (2009).
34. Böhm, U. L. et al. CSF-contacting neurons regulate locomotion by relaying mechanical stimuli to spinal circuits. *Nat. Commun.* **7**, 10866 (2016).
35. Flanagan-Steet, H., Fox, M. A., Meyer, D. & Sanes, J. R. Neuromuscular synapses can form in vivo by incorporation of initially aneural postsynaptic specializations. *Development* **132**, 4471–4481 (2005).
36. Yoo, S. K., Starnes, T. W., Deng, Q. & Huttenlocher, A. Lyn is a redox sensor that mediates leukocyte wound attraction in vivo. *Nature* **480**, 109–112 (2011).
37. Li, Y. et al. Dorsal root ganglion neurons become hyperexcitable and increase expression of voltage-gated T-type calcium channels (Cav3.2) in paclitaxel-induced peripheral neuropathy. *Pain* **158**, 417–429 (2017).
38. Moutal, A. et al. Blocking CRMP2 SUMOylation reverses neuropathic pain. *Mol. Psychiatry* https://doi.org/10.1038/mp.2017.117 (2017).
42. Bryksin, A. V. & Matsumura, I. Overlap extension PCR cloning: a simple and reliable way to create recombinant plasmids. *Biotechniques* **48**, 463–465 (2010).
43. Piccoli, G. et al. Proteomic analysis of activity-dependent synaptic plasticity in hippocampal neurons. *J. Proteome Res.* **6**, 3203–3215 (2007).
44. Romani, G. et al. A virus-encoded potassium ion channel is a structural protein in the chlorovirus *Paramecium bursaria* chlorella virus 1 virion. *J. Gen. Virol.* **94**, 2549–2556 (2013).
45. Westerfield, M. *The Zebrafish Book: A Guide for the Laboratory Use of Zebrafish (Danio rerio)* 4th ed. (Univ. of Oregon Press, Eugene, OR, 2000).
46. Malinverno, M. et al. Synaptic localization and activity of ADAM10 regulate excitatory synapses through N-cadherin cleavage. *J. Neurosci.* **30**, 16343–16355 (2010).
47. Suster, M. L., Sumiyama, K. & Kawakami, K. Transposon-mediated BAC transgenesis in zebrafish and mice. *BMC Genomics* **10**, 477 (2009).
48. Polomano, R. C., Mannes, A. J., Clark, U. S. & Bennett, G. J. A painful peripheral neuropathy in the rat produced by the chemotherapeutic drug, paclitaxel. *Pain* **94**, 293–304 (2001).
49. Yaksh, T. L. & Rudy, T. A. Chronic catheterization of the spinal subarachnoid space. *Physiol. Behav.* **17**, 1031–1036 (1976).
50. Chaplan, S. R., Bach, F. W., Pogrel, J. W., Chung, J. M. & Yaksh, T. L. Quantitative assessment of tactile allodynia in the rat paw. *J. Neurosci. Methods* **53**, 55–63 (1994).

nature research

Corresponding author(s): Anna Moroni, Raffaella Tonini

Reporting Summary

Nature Research wishes to improve the reproducibility of the work that we publish. This form provides structure for consistency and transparency in reporting. For further information on Nature Research policies, see Authors & Referees and the Editorial Policy Checklist.

Statistical parameters

When statistical analyses are reported, confirm that the following items are present in the relevant location (e.g. figure legend, table legend, main text, or Methods section).

n/a	Confirmed	
☐	☒	The exact sample size (*n*) for each experimental group/condition, given as a discrete number and unit of measurement
☐	☒	An indication of whether measurements were taken from distinct samples or whether the same sample was measured repeatedly
☐	☒	The statistical test(s) used AND whether they are one- or two-sided *Only common tests should be described solely by name; describe more complex techniques in the Methods section.*
☐	☒	A description of all covariates tested
☐	☒	A description of any assumptions or corrections, such as tests of normality and adjustment for multiple comparisons
☐	☒	A full description of the statistics including central tendency (e.g. means) or other basic estimates (e.g. regression coefficient) AND variation (e.g. standard deviation) or associated estimates of uncertainty (e.g. confidence intervals)
☐	☒	For null hypothesis testing, the test statistic (e.g. *F*, *t*, *r*) with confidence intervals, effect sizes, degrees of freedom and *P* value noted *Give P values as exact values whenever suitable.*
☒	☐	For Bayesian analysis, information on the choice of priors and Markov chain Monte Carlo settings
☒	☐	For hierarchical and complex designs, identification of the appropriate level for tests and full reporting of outcomes
☒	☐	Estimates of effect sizes (e.g. Cohen's *d*, Pearson's *r*), indicating how they were calculated
☐	☒	Clearly defined error bars *State explicitly what error bars represent (e.g. SD, SE, CI)*

Our web collection on statistics for biologists may be useful.

Software and code

Policy information about availability of computer code

Data collection	Figure 1: data analysis was performed with Axon pCLAMP 10 Software Suite | Molecular Devices Figure 3, Supplementary figures 5-7: data collection was performed with Axon pCLAMP 10 Software Suite Figure 3, Supplementary figure 5,7: images collection was performed with LAS AF 2.7
Data analysis	Figure 1: Clampfit 10, Molecular Devices and Origin 7 Figure 2: LSM510 Meta system and the images were analyzed and prepared using ImageJ software. Figure 3, Supplementary figures 5-7: data analysis was performed with Axon pCLAMP 10 Software Suite | Molecular Devices, Origin9.1 | OriginLab and GraphPad Prism7 SFig.8: GraphPad PRISM version 5.0, GraphPad, San Diego, CA

For manuscripts utilizing custom algorithms or software that are central to the research but not yet described in published literature, software must be made available to editors/reviewers upon request. We strongly encourage code deposition in a community repository (e.g. GitHub). See the Nature Research guidelines for submitting code & software for further information.

Data

Policy information about availability of data

All manuscripts must include a data availability statement. This statement should provide the following information, where applicable:

- Accession codes, unique identifiers, or web links for publicly available datasets
- A list of figures that have associated raw data
- A description of any restrictions on data availability

The data that support the findings of this study are available from the corresponding author upon reasonable request.

Field-specific reporting

Please select the best fit for your research. If you are not sure, read the appropriate sections before making your selection.

☒ Life sciences ☐ Behavioural & social sciences ☐ Ecological, evolutionary & environmental sciences

For a reference copy of the document with all sections, see nature.com/authors/policies/ReportingSummary-flat.pdf

Life sciences study design

All studies must disclose on these points even when the disclosure is negative.

Sample size	Figure 1- Patch clamp on cell cultures: we use as a sample size, usually between 6-10 cells for patch experiments. These numbers are adequate for the kind of measurements, based on the fact that the signal to noise ratio is very high (at least >4). Figure 2 ans Suppl. Figure 2: Staining of hippocampal primary cultures: No statistical analyses have been performed. With regards to the quantitative analysis of surface/total staining, cells were chosen randomly from four to eight different coverslips (two to three independent experiments) and representative images are shown. Figure 3, Supplementary Figures 5-7: Patch clamp experiments in DRN brain slices- Sample size is chosen according to the "sample size calculator" implemented in the software Sigma-plot 12.0 taking into account the minimal detectable difference in means, the expected standard deviation, the desired power (0.80), the alpha value (0.05) and the statistic test applied (t-student test or 1WAY ANOVA). Estimated values used in the calculator were taken from a previous study on pharmacogenetic manipulations of serotonergic neurons: "D.J. Urban et al. Neuropsychopharmacology (2016) doi:10.1038/npp.2015.293" Figure 4: Sample size is chosen according to our experience with behavioral experiments. Because genotyping was not known before behavioral testing we tested enough larvae to have at least n>10 for each condition. Figure 5: For in vivo pain studies, We used n=6 samples based on power analysis and previous experience. Supplementary Figure 8: In each experiment, fertilized eggs were collected and randomly distributed into several subgroups, to be injected with either GFP RNA or wt and mutated forms of BLINK RNAs. Sample size was thus varying depending on clutches of eggs (usually 30-60 per group). Sample size was defined based on our experience in order to have statistically relevant numbers of embryos, but also to avoid overcrowded Petri dishes for escape response assays in order to better detect individual responses.
Data exclusions	Figure 1: Patch experiments on cell cultures: The criteria for discarding cells was if seal resistance remained > 1 gigaOhm throughout the experiment or not. Figure 2: Staining of hippocampal primary cultures: we have excluded dead neuronal cells and cells showing a certain suffering due to the transfection. Figure 3, Supplementary figures 5-7: cells were excluded based when the access resistance changed >20%, as described in the "Materials and Methods" or when defined as statistical outliers according to the "Identify Outliers" implemented in Prism7.0 using the ROUT method. Figure 4, 5: No data exclusion Supplementary Figure 8: Embryos showing grossly abnormal morphology, due to unspecific developmental problems/poor egg quality were excluded from touch-response assays. GFP-injected embryos were used as a control for unspecific developmental problems: when control embryos were massively not responding to mechanical stimuli, the entire experiment was discarded.
Replication	Figure 1: Patch experiments on cell cultures were performed once or twice in a week, cells were patched 12-24h after (transient) transfection. Each condition/protocol was tested at least in 3 independent experiments, each time the number of cells tested was > 5, usually 10-15.

Staining of hippocampal primary cultures: not relevant to our study

Figure 3, Supplementary figures 5-7: data were collected from 3 to 8 animals for each condition to ensure biological reproducibility.

Figure 4: data were reproduced in three independent experiments giving always comparable results. Results of one experiments are reported.

Supplementary Figure 8: In vitro transcribed RNAs from each construct were injected several times in independent clutches of eggs. Inhibitory effect of blue light exposure on touch-evoked escape response of BLINK-injected embryos, as well as reversibility in the dark, were thus verified in several individuals derived from several clutches of eggs, injected with several batches of in vitro transcribed RNAs.

Randomization

Figure 1: Patch clamp experiments on cell cultures: not relevant as the operator cannot influence the outcome of the measurement
Figure 3, Supplementary figures 5-7: not relevant
Figure 4: not relevant to our study
Figure 5: For in vivo pain studies, rats were ramdomly assigned to treatments and groups

Supplementary Figure 8: Fertilized eggs were randomly distributed into groups prior to microinjection

Blinding

Figure 1:Patch clamp experiments on cell cultures: not relevant as the operator cannot influence the outcome of the measurement
Figure 2:Staining of hippocampal primary cultures: not relevant to our study
Figure 3, Supplementary figures 5-7: not relevant
Figure 4: The genotyping of each larva was determined after behavioral response was recorded. Genotyping and beahvioral recording were performed by two independent investigators
Figure 5: For in vivo pain studies, experimenter was blinded to the groups and treatments.

Supplementary Figure 8: Investigators were not blinded to group allocation. Assays were always performed first on control group (GFP-injected embryos), to monitor the quality of the clutches.

Reporting for specific materials, systems and methods

Materials & experimental systems

n/a	Involved in the study
☒	☐ Unique biological materials
☐	☒ Antibodies
☐	☒ Eukaryotic cell lines
☒	☐ Palaeontology
☐	☒ Animals and other organisms
☒	☐ Human research participants

Methods

n/a	Involved in the study
☒	☐ ChIP-seq
☒	☐ Flow cytometry
☒	☐ MRI-based neuroimaging

Antibodies

Antibodies used

Figure 2-5: anti-BLINK2: 8D6, custom made monoclonal antibody
Figure3, Supplementary figure 5,7, anti-eGFP: antibody name ab13970, chicken polyclonal antibody anti eGFP
Figure 5: anti-GFP (Cat# AB3080, Millipore, Billerica, MA), anti-PGP9.5 (Cat# NB600-1160, Novus Biologicals, Littleton, CO)

Validation

8D6 was validated for the Kcv channel expressed in several organisms and on the native Kcv in the PBCV-1 virus (Romani et al, 2013 J Gen Virol. 2013 Nov; 94(Pt 11): 2549–2556. doi: 10.1099/vir.0.055251-0); 8D6 was further validated against BLINK1 expressed in HEK 293T cells (Cosentino et al., 2015, Science 348(6235):707-10. doi: 10.1126/science.aaa2787).
Other primary antibodies used in Fig.2 are commercial antibodies frequently used in the literature (e.g. GM130 see Saraceno et al. 2014, PSD-95 see Marcello et al., 2007)

anti-eGFP: commonly used antibody, used in more than 1000 published scientific journals (https://www.abcam.com/gfp-antibody-ab13970-references.html).

Anti-GFP and anti PGP9.5 were validated by the company and widely used in the litterature.

Eukaryotic cell lines

Policy information about cell lines

Cell line source(s)

HEK 293 T: obtained from ATCC (RRID:CVCL_0063)

Cell line source(s)	COS7, obtained from Gerhard Thiel lab, TU-Darmstadt, originally bought by ATCC
Authentication	both lines were authenticated by ATCC
Mycoplasma contamination	HEK 293T : Tested negative for mycoplasma COS7: not tested
Commonly misidentified lines (See ICLAC register)	HEK293 cells (but not HEK293T) are listed in the ICLAC database for possible contamination by HeLa cells. We think that for our purposes, i.e. virus amplification and heterologous expression of a synthetic light-activated channel conductance, such a contamination should not matter.

Animals and other organisms

Policy information about studies involving animals; ARRIVE guidelines recommended for reporting animal research

Laboratory animals	Figure 2: E18 embryos from Sprague–Dawley rats for primary hippocampal neuron cultures were used. All the experiments were approved by the Institutional Animal Care and Use Committee of University of Milan and by the Italian Ministry of Health (#326/2015). Figure 3, Supplementary figures 5-7: Mus Musculus, C57BL/6J, males, P45-P70 Figure 4: Experiments with zebrafish embryos/larvae were conducted within the first 5 days post fertilization, when zebrafish are not considered as animals yet and are thus not subject to the European or local directives on animal research. Figure 5: adult male Sprague–Dawley rats (250 g; Envigo)
Wild animals	No wild animals were used in this study
Field-collected samples	No field-collected samplese were used in this study